Durability Evaluation of Florida's Fiber-Reinforced Polymer (FRP) Composite Reinforcement for Concrete Structures

Final Report   **March 2017**

Principal investigator:
H. R. Hamilton

Consultant:
Jeff Brown

Research assistants:
Jovan Tatar
Mark Lisek
Natassia R. Brenkus

Department of Civil and Coastal Engineering
University of Florida
P.O. Box 116580
Gainesville, Florida 32611
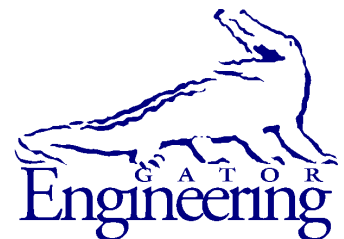
University of Florida
Engineering School of Sustainable Infrastructure and Environment
Department of Civil and Coastal Engineering

Disclaimer

The opinions, findings, and conclusions expressed in this publication are those of the authors and not necessarily those of the State of Florida Department of Transportation.

Unit of Measurement Conversions

SI* (MODERN METRIC) CONVERSION FACTORS
APPROXIMATE CONVERSIONS TO SI UNITS

SYMBOL	WHEN YOU KNOW	MULTIPLY BY	TO FIND	SYMBOL
LENGTH				
in	inches	25.4	millimeters	mm
ft	feet	0.305	meters	m
yd	yards	0.914	meters	m
mi	miles	1.61	kilometers	km
AREA				
in²	square inches	645.2	square millimeters	mm²
ft²	square feet	0.093	square meters	m²
yd²	square yard	0.836	square meters	m²
ac	acres	0.405	hectares	ha
mi²	square miles	2.59	square kilometers	km²
VOLUME				
fl oz	fluid ounces	29.57	milliliters	mL
gal	gallons	3.785	liters	L
ft³	cubic feet	0.028	cubic meters	m³
yd³	cubic yards	0.765	cubic meters	m³
NOTE: volumes greater than 1000 L shall be shown in m³				
MASS				
oz	ounces	28.35	grams	g
lb	pounds	0.454	kilograms	kg
T	short tons (2000 lb)	0.907	megagrams	Mg (or "t")
TEMPERATURE (exact degrees)				
°F	Fahrenheit	5(F-32)/9 or (F-32)/1.8	Celsius	°C
ILLUMINATION				
fc	foot-candles	10.76	lux	lx
fl	foot-Lamberts	3.426	candela/m²	cd/m²
FORCE and PRESSURE or STRESS				
kip	1000 pound force	4.45	kilonewtons	kN
lbf	pound force	4.45	newtons	N
lbf/in²	pound force per square	6.89	kilopascals	kPa

*SI is the symbol for the International System of Units. Appropriate rounding should be made to comply with Section 4 of ASTM E380.

SI* (MODERN METRIC) CONVERSION FACTORS
APPROXIMATE CONVERSIONS *FROM* SI UNITS

SYMBOL	WHEN YOU KNOW	MULTIPLY BY	TO FIND	SYMBOL
LENGTH				
mm	millimeters	0.039	inches	in
m	meters	3.28	feet	ft
m	meters	1.09	yards	yd
km	kilometers	0.621	miles	mi
AREA				
mm²	square millimeters	0.0016	square inches	in^2
m²	square meters	10.764	square feet	ft^2
m²	square meters	1.195	square yards	yd^2
ha	hectares	2.47	acres	ac
km²	square kilometers	0.386	square miles	mi^2
VOLUME				
mL	milliliters	0.034	fluid ounces	fl oz
L	liters	0.264	gallons	gal
m³	cubic meters	35.314	cubic feet	ft^3
m³	cubic meters	1.307	cubic yards	yd^3
MASS				
g	grams	0.035	ounces	oz
kg	kilograms	2.202	pounds	lb
Mg (or "t")	megagrams (or "metric	1.103	short tons (2000 lb)	T
TEMPERATURE (exact degrees)				
°C	Celsius	1.8C+32	Fahrenheit	°F
ILLUMINATION				
lx	lux	0.0929	foot-candles	fc
cd/m²	candela/m^2	0.2919	foot-Lamberts	fl
FORCE and PRESSURE or STRESS				
kN	kilonewtons	0.225	1000 pound force	kip
N	newtons	0.225	pound force	lbf
kPa	kilopascals	0.145	pound force per square inch	lbf/in^2

*SI is the symbol for the International System of Units. Appropriate rounding should be made to comply with Section 4 of ASTM E380.

1. Report No.	2. Government Accession No.	3. Recipient's Catalog No.

4. Title and Subtitle	5. Report Date
Durability Evaluation of Florida's Fiber-Reinforced Polymer (FRP) Composite Reinforcement for Concrete Structures	March 2017
	6. Performing Organization Code

7. Author(s)	8. Performing Organization Report No.
Tatar, J., Lisek, M., Brenkus, N., Brown, J., and Hamilton, H. R.	

9. Performing Organization Name and Address	10. Work Unit No. (TRAIS)
University of Florida Department of Civil & Coastal Engineering P.O. Box 116580 Gainesville, FL 32611-6580	
	11. Contract or Grant No. BDV31-977-01

12. Sponsoring Agency Name and Address	13. Type of Report and Period Covered
Florida Department of Transportation 605 Suwannee Street, MS 30 Tallahassee, FL 32399	Final Report Feb. 2013-Feb. 2017
	14. Sponsoring Agency Code

15. Supplementary Notes

16. Abstract

Externally bonded fiber-reinforced polymer (FRP) composites are an effective method to increase the strength and stiffness of bridge superstructures. They have also been touted as a method to prevent or mitigate corrosion of steel reinforcement by reducing the diffusion of chlorides into concrete. Composite durability is generally evaluated using accelerated methods. Real-time exposure data, however, are not readily available either in the form of testing recovered structural elements or in visual examination of existing FRP systems. In this research, the effectiveness of FRP repairs used on a number of bridges exposed to field conditions in real time were evaluated. Several girders from FRP-repaired bridges in Florida were taken out of service and tested in four-point bending. Infrared (IR) thermography inspections and pull-off tests were conducted to measure and assess the condition of adhesive bond between FRP and concrete. In addition, chloride contents were evaluated to quantify the effects of FRP on the reduction in chloride ion diffusion. The ultimate strength measured during the test agreed well with theoretically computed values, indicating that the system had maintained its strength over the duration of its service life. Further testing also provided evidence that the intrusion of chloride ions were reduced on regions repaired with externally bonded FRP, which may result in a positive impact. The findings from this study will inform future decisions related to design, installation, and maintenance of FRP systems in concrete structures.

17. Key Words Fiber-reinforced polymer composites, wet layup, repair, corrosion, concrete, reinforcement	18. Distribution Statement No restrictions

19. Security Classif. (of this report) Unclassified	20. Security Classif. (of this page) Unclassified	21. No. of Pages 273	22. Price

Form DOT F 1700.7 (8-72)   Reproduction of completed page authorized

Acknowledgments

Executive Summary

Bonded fiber-reinforced polymer (FRP) composite systems have been used to reinforce deteriorated piles and beams, repair impact-damaged girders, strengthen bents, and confine anchorage of sign structures. The purpose of this research project is to evaluate the durability of the FRP repairs used on a number of bridges exposed to field conditions over longer periods (10 to 15 years). While composite durability has been evaluated using accelerated methods, real-time environmental exposure data are not readily available. A comprehensive literature review is also provided, which focused primarily on: (1) durability of carbon fiber-reinforced polymer (CFRP) composites bonded to concrete for shear or flexural reinforcement; (2) field studies of FRP-repaired bridge girders and the service life of repairs; and (3) protection provided by FRP for underlying steel reinforcement from marine salt.

Several girders from three FRP-repaired bridges in Florida were taken out of service and tested in four-point bending. A durability evaluation was conducted in the laboratory on CFRP in the form of either a wet layup or precured strips, as well as a spray-up glass fiber-reinforced polymer (GFRP). Infrared (IR) thermography inspections and direct tension pull-off tests were conducted to measure and assess the condition of adhesive bond between FRP and concrete. In addition, chloride content of concrete was evaluated to quantify the effects of FRP on the reduction in chloride ion diffusion.

Structural testing revealed improvement in the total flexural capacity of FRP strengthened bridge girders of up to 19% from their residual strength. Additionally, tensile strengths of each type of FRP were within the design strength values specified by the manufacturers. For the laboratory evaluations on one bridge, direct tension pull-off tests showed that the majority of samples, over 82%, met the specified pull-off bond strength requirement of 200 psi; however, over 35% experienced an adhesive or mixed failure mode, indicating either installation issues or that some bond degradation may have occurred.

Overall, the FRP repairs for that case performed satisfactorily throughout their nine-year service life. Also, after an 18-month period for one of the field evaluations, adhesive failure mode characteristics increased at the location without the UV coating, indicating that UV radiation may be a significant contributing factor to the bond degradation as well. Degradation of bond between FRP and concrete, however, may be a concern in externally bonded FRP repairs designed for longer service lives.

The ultimate strength measured during the four-point bending test agreed well with theoretically computed values, indicating that the system had maintained its strength over the duration of its service life. Further testing also provided evidence that intrusion of chloride ions was reduced on regions repaired with externally bonded FRP, which may result in a positive impact. For the same case, no signs of significant corrosion had occurred following the CFRP repair after 14 years.

Table of Contents

List of Figures

xiv

List of Tables

1   Introduction

FDOT has elected to use fiber-reinforced polymer (FRP) reinforcement for concrete in a number of configurations. Bonded systems have been used to reinforce deteriorated piles and beams, repair impact-damaged girders, strengthen bents, and confine anchorage of sign structures. Near surface mounted (NSM) bars have been used to strengthen bridge decks.

FRP composites provide a potentially cost-effective manner in which to lengthen the life span of an existing structure that is functionally or structurally deficient in lieu of the more costly replacement option. While the structural efficacy of FRP composites is well-proven, their long-term performance is yet unclear. FRP composites are generally regarded as durable systems in aerospace and industrial applications, but their efficacy in the harsh environment to which civil infrastructure is subjected is still under study. Further complicating this understanding is the very long life (greater than 100 years) that is expected of bridges.

Because of the long service life required, composite durability is generally evaluated using accelerated methods. Real-time exposure data, however, are not readily available either in the form of testing recovered structural elements or in visual examination of existing FRP systems. This report covers research focused on the documentation of performance over the last 20 years of FRP composite repair systems.

2   Research Approach

The research covered in this report is different from the usual research in that it includes several activities that are common but not necessarily related. As such, this chapter attempts to describe the approach used for this research including the organization of this report to provide the reader a roadmap of the report.

In Chapter 3 a comprehensive literature review is presented that focused primarily on: (1) bond durability of CFRP composites bonded to concrete for shear or flexural reinforcement; (2) field studies of FRP-repaired bridge girders and the service life of repairs; and (3) protection provided by FRP for underlying steel reinforcement from marine salt.

Chapter 4 reports on a survey conducted of FDOT districts and other local transportation agencies regarding the use of FRP composites. The survey also requested the level of use and age of FRP composites located in bridges around the state. Also included in this chapter are reports of several site visits to selected bridges with CFRP repairs. Some of these visits involved only visual observations and in some of them pull-off tests were conducted and cores for chloride testing were taken.

The following three chapters (Chapters 5, 6, and 7) cover testing of girders salvaged from three different bridges that were undergoing upgrading or replacement: University Blvd. in Jacksonville; Indian River Causeway near Melbourne; and Chaffee Road – I-10 overpass near Jacksonville. Each bridge had been repaired in some form using FRP composites. These bridges were chosen based on their availability as well as their diverse array of exposure conditions and configurations. Each of these chapters reports on the history, girder salvaging, materials testing, structural testing, and analysis. Each chapter contains a separate Findings section that reports the salient outcomes of each set of testing.

Finally, overall outcomes are presented in Chapter 8 followed by suggested future research in Chapter 9.

3 Literature Review

Multiple authors have studied the behavior of bond between FRP and concrete under a variety of environmental conditioning such as moisture (Au and Buyukozturk, 2006), dry heat (Leone et al. 2009), freeze–thaw cycles (Green et al., 2006), alkaline (Cromwell et al., 2011), salt and moisture (Silva and Biscaia, 2008), UV radiation (Dolan et al., 2010), etc. Different levels of bond degradation were observed depending on the conditioning protocol; most researchers, however, agree that moisture is the most critical environment for an FRP–concrete bond. Consequently, the focus of this literature review is on the durability of bond between the FRP composite and concrete in surface bonded systems.

Several mechanisms are possible when considering the failure of the bond between concrete and FRP composites (Figure 1). Structurally, the most desirable failure mode is cohesive, in which the fracture surface passes through the concrete substrate. This type of failure mode is the strongest and most reliable of the possible failure modes and has been the primary focus of structural research in bonded FRP composites. Failure modes corresponding to adhesive decohesion or adhesive failure between FRP and adhesive are typically not experienced (Figure 1). FRP decohesion (Figure 1) is usually not an issue and may occur in under-reinforced members, due to development of high interlaminar stresses, or due to exposure to aggressive environments. Exposure to moisture, however, may result in a failure mode shift to the interface between concrete substrate and adhesive. This failure mode is termed adhesive failure mode and will be detailed further in the literature review.
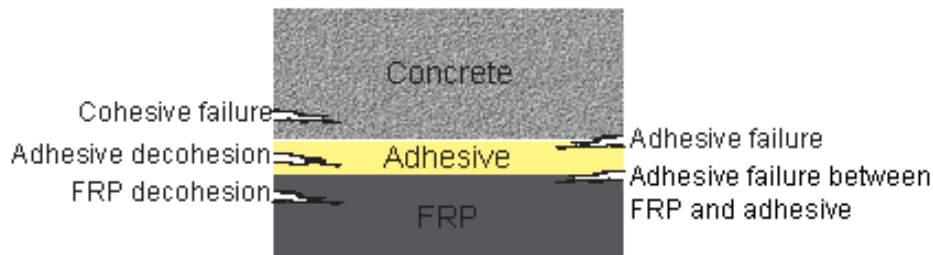
Figure 1—Possible failure modes in FRP-concrete bond system

3.1 Adhesive Bond of FRP Composites to Concrete

The adhesive bond has been shown to be a combination of chemical bond and mechanical interlock as illustrated in Figure 2. Due to the changing mechanical properties of adhesives (loss of stiffness) and their adhesion properties (loss of chemical bonds), when exposed to bond critical environments, the reliability of the FRP strengthening/repair scheme is compromised. Environmental exposure, primarily moisture, will affect the integrity of epoxy–concrete bond. In dry ambient conditions, external load is completely transferred into the concrete substrate, allowing for distribution of damage in the substrate at critical loading. When stiffness of epoxy and chemical bonding are adversely affected by the presence of moisture, however, full bond capacity cannot be attained, as the bond fails prematurely along the epoxy–concrete interface.
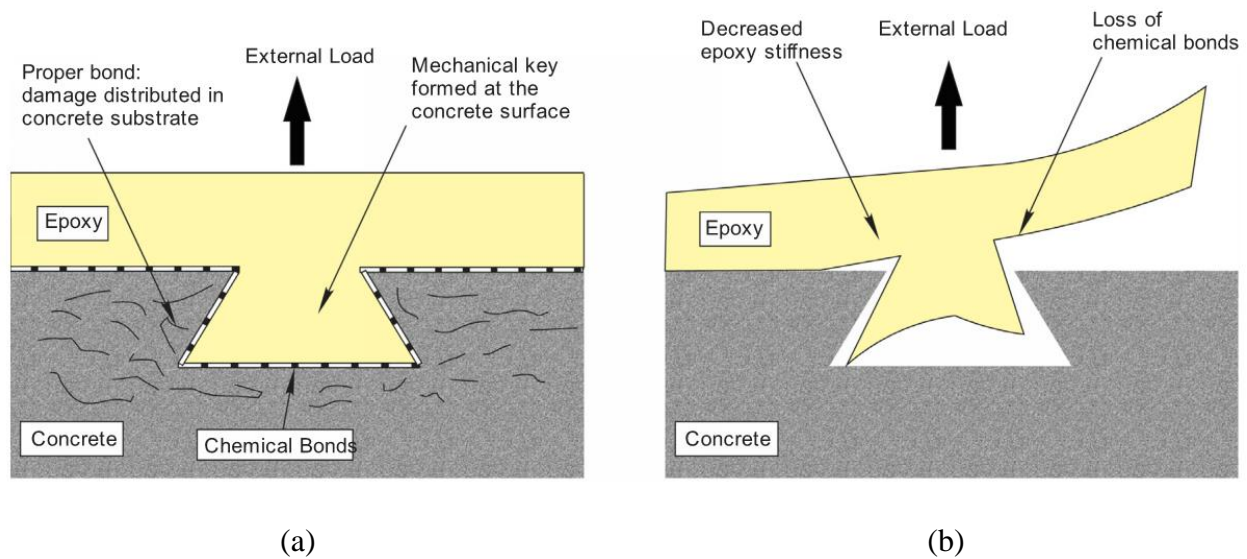
Figure 2—Graphical representation of (a) chemical and mechanical bond mechanisms for adhesively bonded FRP composites and (b) loss of bond due to loss of individual bond mechanisms (Blackburn et al., 2015)

Mechanical interlock is established by flow of epoxy into the holes, crevices and pores of concrete substrate. After it cures, epoxy bonds mechanically to the surface. Plasticization caused by exposure to moisture or water may cause weakening of this mechanical bond. Plasticization is a change in the thermal and mechanical properties of a given polymer that results in reduction of rigidity at room temperature; reduction of temperature at which substantial deformations can be affected with minimal forces; increase in elongation to rupture at room temperature; and increase of the toughness (impact strength) down to the lowest temperature of serviceability (Immergut and Mark, 1965).

Epoxy mechanical properties (and thus mechanical interlock) are also adversely affected when exposed to temperatures higher than T_g (glass transition temperature), which causes epoxy to lose stiffness due to increased chain mobility. In an amorphous polymer, or amorphous regions of a partially crystalline polymer, T_g is the approximate midpoint of the temperature range over which reversible change to a rubbery or viscous condition from a glassy or hard condition occurs (ISO 22768:2006).

Chemical bond is established through hydrogen bonding. Hydrogen bonds form because of interaction between positively charged hydrogen atoms and highly negatively charged atoms such as oxygen or nitrogen. In general, hydrogen bonds represent a combination of electrostatic, covalent, and Van der Waals interaction, and should not be confused with covalent bonds. In the case of bond to concrete, hydrogen bonds are established through oxygen atoms on the concrete surface and hydrogen atoms of epoxy hydroxyl groups. If sufficient moisture is present after the bond has formed, then hydrogen bonds are replaced by water molecules causing chemical bond to degrade.

3.2   Bond Test Methods

The importance of FRP-concrete bond has led to the development of a number of test methods that are intended to provide a measure of the behavior and bond capacity. These tests can generally be separated into two groups. The first group is made up of direct bond tests in which the FRP is subjected to a controlled load (Figure 3):

- Direct pull-off
- Direct torsion
- Direct shear pull-off
- Peel test
- Mixed-mode test

The second group is made up of indirect bond tests that utilize a flexural test setup to evaluate the bond performance:

- Three-point bending beam tests
- Four-point bending beam tests

(a)   (b)
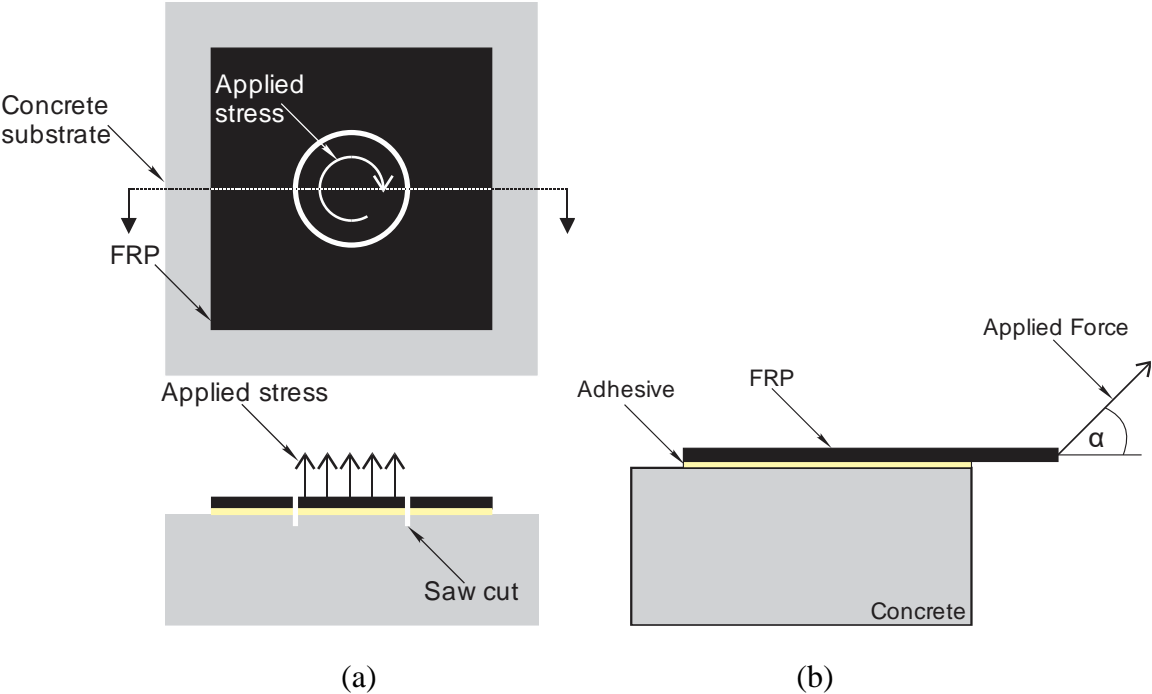
Figure 3—(a) Direct pull-off (bottom) and direct torsion (top) test; and (b) direct shear (α=0˚), peel ($\alpha = 90$˚) and mixed-mode (0˚ $< \alpha < 180$˚) test

3.3   Durability of Bond

There is no widely accepted general definition of durability in the context of engineering materials. There are different interpretations of the term depending on the specific material's properties. Concrete durability is generally thought of as the ability to withstand deterioration

caused by weather exposure, chemical exposure, or surface abrasion. For the purpose of this study, by bond durability of FRP-to-concrete, its long-term resistance to aggressive environmental conditions is implied (e.g. high temperature, high moisture levels, UV, alkali, etc.). The following sections present findings from the literature related to the durability of FRP-to-concrete bond.

3.3.1 Strength Retention

Durability of bonded FRP reinforcement is typically considered in terms of the strength remaining after the system has been exposed to the environment (Tatar and Hamilton 2016). There is some original or basic strength available in the original system (Q_n). Bonded FRP reinforcement can be applied to improve the strength to (Q_{nf}). The strengthening ratio (SR), then quantitatively defines the strength added by the FRP composite reinforcement as:

$$SR = \frac{Q_{nf}}{Q_n} 100 \ (\%)$$

Eq. 1

To avoid undue reliance on FRP reinforcement for strength, the design recommendations typically limit the amount of strengthening allowed. Excessive FRP will cause a larger portion of applied load to be dependent on the integrity of FRP system, particularly the bond that has shown to be the most critical component of the bonded system.

FRP-concrete bond, as it will be shown later in this report, may be susceptible to degradation due to environmental impacts, as depicted in Figure 4a and Figure 4b. Such environmental effects may or may not result in degradation of the original beam strength. Consequently, to ensure consistency when comparing research results, it is necessary to define strength retention as it relates to both the original strength (Q_n) and the improved strength (Q_{nf}). In this report, strength retention is the quantitative measure of the specimen's strength (expressed as failure load, ultimate stress, or fracture energy) after exposure to a specific environmental conditioning (Q_{nfc}), when compared to the strength of control specimens stored in benign laboratory conditions (Q_{nf}). Quantitatively, strength retention (R_n) is represented as:

$$R_n = \frac{Q_{nfc}}{Q_{nf}} 100 \ (\%)$$

Eq. 2

R_n necessarily includes environmental effect on the strengthened system, which includes the steel reinforcement and concrete, and not just the FRP-concrete bond. To distinguish research in which it is desirable to evaluate the bond only, then the original strength (Q_n) should be subtracted when computing the effect of environment on bond. Only that portion of the system strength above the dotted line in Figure 4a and Figure 4b should be compared, as they represent the contribution of FRP. Therefore, bond strength retention, R_b, is defined as:

$$R_b = \frac{Q_{nfc} - Q_n}{Q_{nf} - Q_n} 100 \ (\%)$$

Eq. 3

This approach assumes that residual strength is determined from an unexposed specimen. For plain concrete flexural specimens (Figure 4a, Figure 4b), the assumption is that its resistance to

tensile stresses is due to FRP only (concrete contribution is neglected: $Q_n = 0$). Therefore, specimen strength is assumed to be representative of FRP-concrete bond strength.
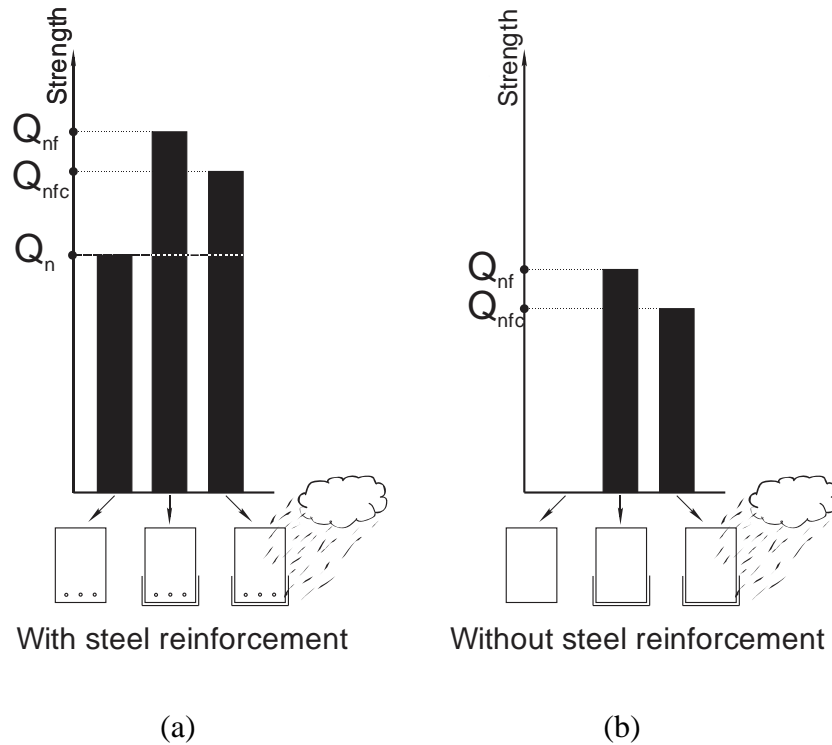
Figure 4—Residual strength of (a) steel reinforced and (b) plain concrete beams exposed to accelerated conditioning (Tatar and Hamilton, 2016)

3.3.2 Effects of High Temperature, Moisture, UV, Alkaline Environment and Cycling

One of the first times that the issue of long-term performance of the composite-to-concrete bond was mentioned in the literature was in paper by Saadatmanesh and Ehsani (1990). They found that FRP would increase the strength of concrete members; however, they raised the question of its long-term durability. Amongst the first attempts to conduct tests that included environmental considerations was by Xie et al. (1995). They subjected multiple reinforced concrete specimens, with an addition of CFRP laminates at the beam soffit to both accelerated and long-term environmental tests (Figure 5). The exposure conditions were as follows: (1) 2 weeks of water immersion at room temperature followed by 10 days of drying at room conditions; and (2) heating in oven at 40°C for a week followed by refrigeration at -23°C for a week, for a total of two months. Authors found that specimens exposed to water experienced a slight increase in strength (about 2%), which they credited to increased fracture toughness of epoxy due to plasticization. On the other hand, specimens that were exposed to hot-cold cycles experienced a decrease in strength of about 10% (BSR = 90%).
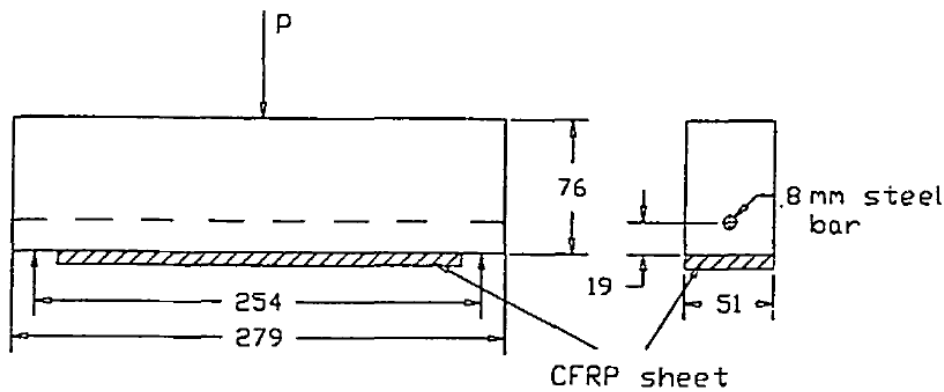
Figure 5—Three-point bending test setup (Xie et al., 1995)

Chajes et al. (1995) studied the influence of aggressive environmental conditioning on durability of bond between FRP and concrete. The concrete test specimens measuring 1.5 in. × 1.1 in. × 13 in. (38.1 mm × 28.6 mm × 330 mm) were reinforced with one threaded steel bar placed 0.75 in. (19.1 mm) from the compression face of the beam (Figure 6). A graphite FRP strip, the same width as the test specimen, was adhered to the beam. Beams were first covered with a calcium chloride solution and then conditioned at (a) 50 and 100 freeze/thaw cycles as per ASTM C672-84 (freezing at -17°C for 16 h, followed by thawing at room temperature for 8 h); and (b) 50 and 100 wet/dry cycles (immersion in calcium chloride solution for 16 h, followed by drying at room temperature for 8 h). After conditioning, beams were loaded until total failure in four-point bending test setup. A BSR of approximately 87% resulted from 100 wet/dry cycles.
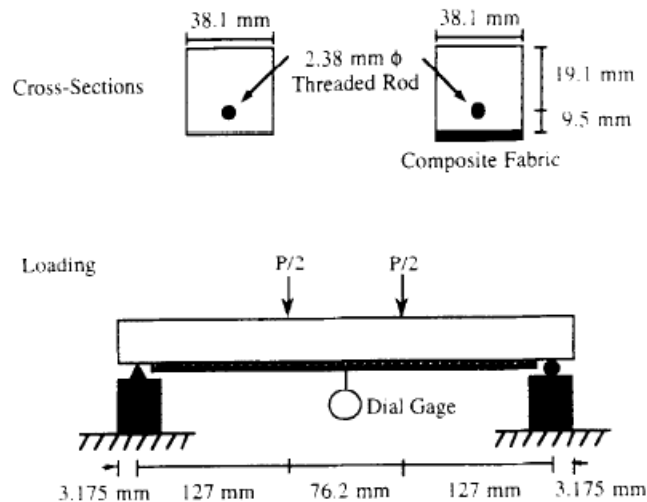
Figure 6—Four-point bending test setup (Chajes et al., 1995)

Further work in addressing long-term performance of FRP-concrete bond was undertaken by Karbhari and Engineer (1996). They tested small concrete beams (measuring 2 in. × 1 in. × 13 in. or 50.8 mm × 25.4 mm× 330.2 mm) reinforced with different FRP materials (GFRP and CFRP) in four-point bending tests. All beams were exposed to the following environments for a

period of 60 days before testing: (1) immersion in water at 20˚C; (2) immersion in synthetic seawater at 20˚C; (3) freezing at -15.5˚C; and (4) Freeze-thaw cycling (-15.5˚C for 24 hours followed by 50˚C for 24 hours). Control samples were kept in ambient conditions at 20˚C. Test results showed the lowest BSR in beams immersed in fresh and seawater was about 65%. The minimum overall change was observed for specimens exposed to freezing at -15.5˚C. According to the authors, the degradation in bond in moisture was due to epoxy's susceptibility to plasticization and increase in compliance caused by the water absorption. Moreover, a significant drop in glass transition temperature (T_g) of resins was noticed after exposure to continuous water ingress. According to the authors, the reduction in T_g due to water absorption signifies a degradation in epoxy matrix properties which may lead to decreased bond capacity.

In a separate study, Karbhari et al. (1997) subjected specimens exposed to the same environmental conditions to a controlled mixed mode test (Figure 7). They measured interfacial fracture energy for each exposure condition as a function of phase angle ψ (mode mixity parameter - $\psi = \tan^{-1} \dfrac{K_{II}}{K_I}$) and the angle at which is the peel force applied. It should be noted that the phase angle ψ=0˚ corresponds to a pure Mode I condition, and ψ=90˚ relates to pure Mode II loading. They observed a clear difference in interfacial fracture energy magnitudes between the systems exposed to water immersion and freeze/freeze-thaw cycles, with the former set of specimens having higher values of interfacial fracture energy.
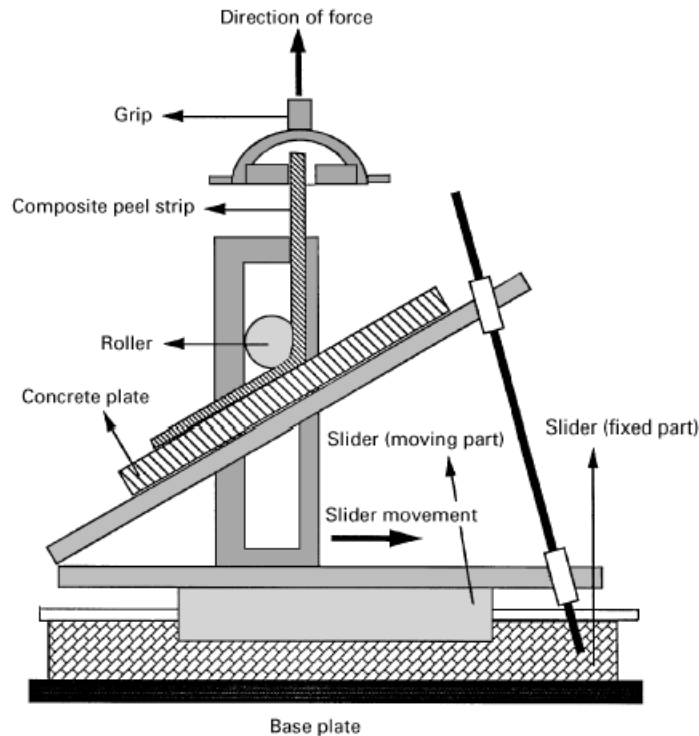
Figure 7—Mixed mode peel test setup (Karbhari and Engineer, 1996)

This difference was not as apparent in specimens reinforced with carbon fiber as it was in specimens with glass fibers. Additionally, specimens reinforced with carbon fibers showed

almost no change in interfacial fracture energy in respect to phase angle. On the other hand, an increase in fracture energy of up to 300% (from Mode I to Mode II) was observed for specimens with glass fibers. Analysis of dependency of peel force, Mode I fracture energy (G_I), Mode II fracture energy (G_{II}), and total fracture energy ($G=G_I+G_{II}$) to the peel angle showed that exposure to water resulted in a decrease of peel force and interfacial fracture energy. In addition, it also causes a shift in overall trends – variation of G_{II} in respect to peel angle changes from exponential (for ambient conditions) to linear dependency (after exposure to water). According to the authors, this indicates a change in mechanisms during peel due to exposure to water. In addition to this, authors observed a change in failure mode from cohesive to adhesive. Specimens exposed to freezing and freeze-thaw conditions showed an increase in peel force and interfacial fracture energy when compared to control specimens.

Another study pertaining to long-term durability of concrete bonded with external FRP in marine environments was performed by Toutanji and Gomez (1997). The test specimen consisted of small concrete beam, measuring 2 in. × 2 in ($51 mm × 51 mm$) with a total length of 14.4 in (365 mm), reinforced with either a CFRP or a GFRP laminate over the full length of the beam (Figure 8). Three different adhesives were used to bond FRP sheets to concrete. The test method consisted of loading the specimens in four-point bending at a constant crosshead displacement rate until failure. Specimens were exposed to 300 wet and dry cycles (hot air at 35˚C average and 90% relative humidity) in a salt environment (35 g of salt per 1 liter of water). Control specimens were kept in standard room conditions. Test results showed that BSR ranged from 67 to 97% depending on the type of fibers and epoxy used. The low BSR was attributed to degradation of epoxy.
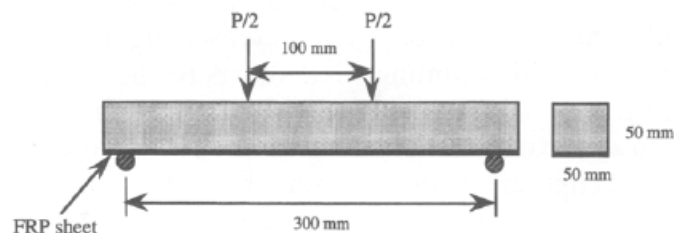
Figure 8—Four-point bending test setup (Toutanji and Gomez, 1997)

Beaudoin et al. (1998) performed a durability study on reinforced concrete beams with external FRP. Beams measured 3.9 in. × 5.9 in. × 47.2 in. ($100 mm × 150 mm × 1200 mm$) and were reinforced with two 0.26 in. (6.5 mm) diameter steel bars ($0.1 in^2$ or $65 mm^2$) in addition to stirrups that were placed to improve shear strength (Figure 9). Beams were further reinforced with Mitsubishi Replak 20 or Sika CarboDur CFRP laminates. Control specimens were kept in dry laboratory conditions, while the rest of the samples were exposed to 13 wet-dry cycles. Cycles consisted of immersion in water at 70 ˚F (21˚C) for five days, followed by drying for two days at 81˚C (27˚C). After conditioning beams were subjected to four-point bending tests. Test results showed that beams reinforced with Replak 20 had SR of around 90%, while beams strengthened with CarboDur experienced an increase in SR of approximately 10% (BSR≈110%). The loss in BSR was around 80% for Replak 20. CarboDur samples had an increase of 15% in BSR on average (BSR≈115%).
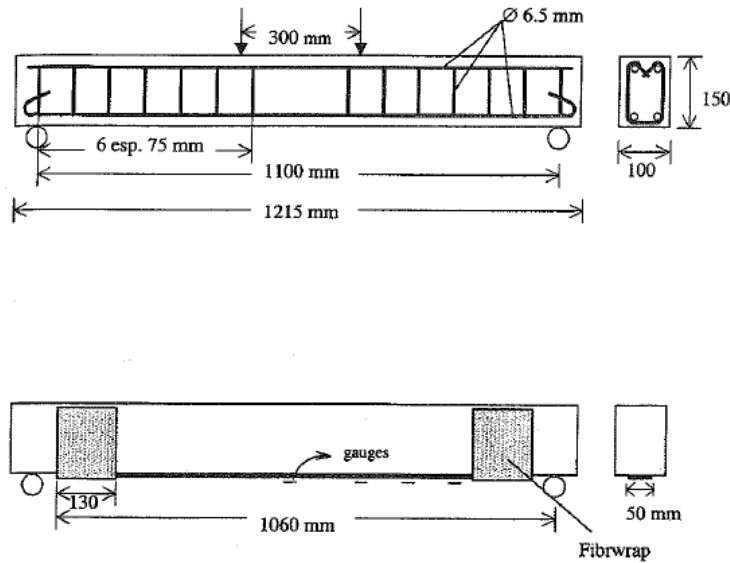
Figure 9—Four-point bending test setup (Beaudoin et al., 1998)

Sen et al. (1999) studied durability of FRP-concrete bond in marine environments. Test specimens were prepared by bonding two types of carbon fibers (either bidirectional woven fabric or unidirectional carbon fiber procured laminate) to a concrete slab using five different epoxy systems. Concrete slabs were each 17.9 in. × 17.9 in. (455 mm × 455 mm) with the thickness varying between 2.95 in. and 3.74 in. (75 mm and 95 mm). Four different exposure conditions were investigated: (1) combined wet/dry cycles and hot/cold cycles in 5% salt water for 17 months; (2) wet/dry cycles in 15% salt water for 17 months; (3) outdoor conditions for 23 months; and (4) air conditioned laboratory conditions (control) for 23 months. To measure the bond strength, destructive direct pull-off or direct torsion tests were performed (Figure 10). Test results showed that bond degradation was least under outdoor exposure and greatest under wet/dry cycles. Authors concluded that moisture absorption is potentially more damaging to bond durability than other environmental factors. Test results indicated that direct pull-off tests generally produced bond failures at lower stresses than direct torsion tests. As stated by the authors, direct torsion test is, therefore, more appropriate for identifying bond degradation in flexural applications.

<div align="center">(a)   (b)</div>
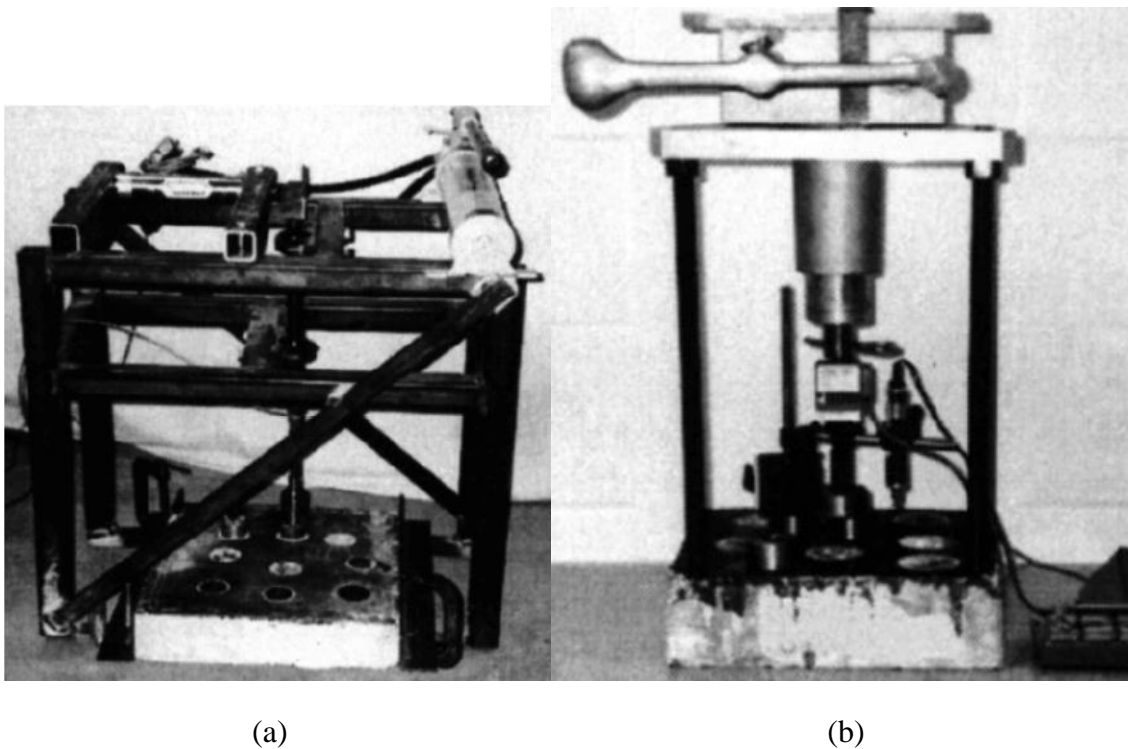
Figure 10—Sen et al. (1999): (a) torsion test setup; (b) pull-off test setup

Leung et al. (2001) evaluated environmental impacts on the flexural behavior of reinforced concrete beams strengthened with CFRP. Beams were made of concrete and had the following dimensions: 2.95 in. × 2.95 in. × 11.8 in. (75 mm × 75 mm × 300 mm). Test beams were subjected to three-point bending until the failure. The following four exposure conditions were introduced: (1) water immersion at 27˚C; (2) Wetting/drying cycle (water immersion at 27˚C for half a week, followed by storage in a control room for half a week – 25±2˚C and RH 65±2%); (3) constant moisture condition (25±2˚C and RH 65±2%); and (4) heating/cooling cycle (oven at 60˚C for half a week, followed by storage in a control room for half a week). Authors found that exposure to the aforementioned environments caused changes in the concrete and the adhesive. Generally, plain concrete specimens had higher failure loads with a decrease in moisture contents. Also, longer exposure to the moist environments resulted in an increase in strength of plain concrete beams. Finally, authors concluded that long-term exposure of CFRP reinforced beams to highly moist environments affects the adhesive and leads to decreased BSR and midspan deflection. Observed failure mode for beams reinforced with CFRP was "shear failure with plate peel-off."

Myers and Ekenel (2005) conducted a study that investigated the effects of moisture and temperature of the concrete surface at time of installation on FRP-concrete bond strength. Direct pull-off and direct torsion tests were performed in order to identify the critical surface moisture content and relative humidity of concrete (Figure 11). Additionally, flexural tests were performed on precracked reinforced concrete beams to determine the effects of temperature at installation on the performance of bond between FRP and concrete. Authors found that specimens that were constructed with at a high surface moisture content exhibited poor bond performance. Furthermore, it was found that specimens that were strengthened at a relative

humidity higher than 82% may have lower bond quality. When it comes to the effects of temperature, it was concluded that the extremely low temperatures affected the bond adversely. However, installation of FRP in high temperatures did not prove to affect the bond behavior.

(a)

(b)

(c)
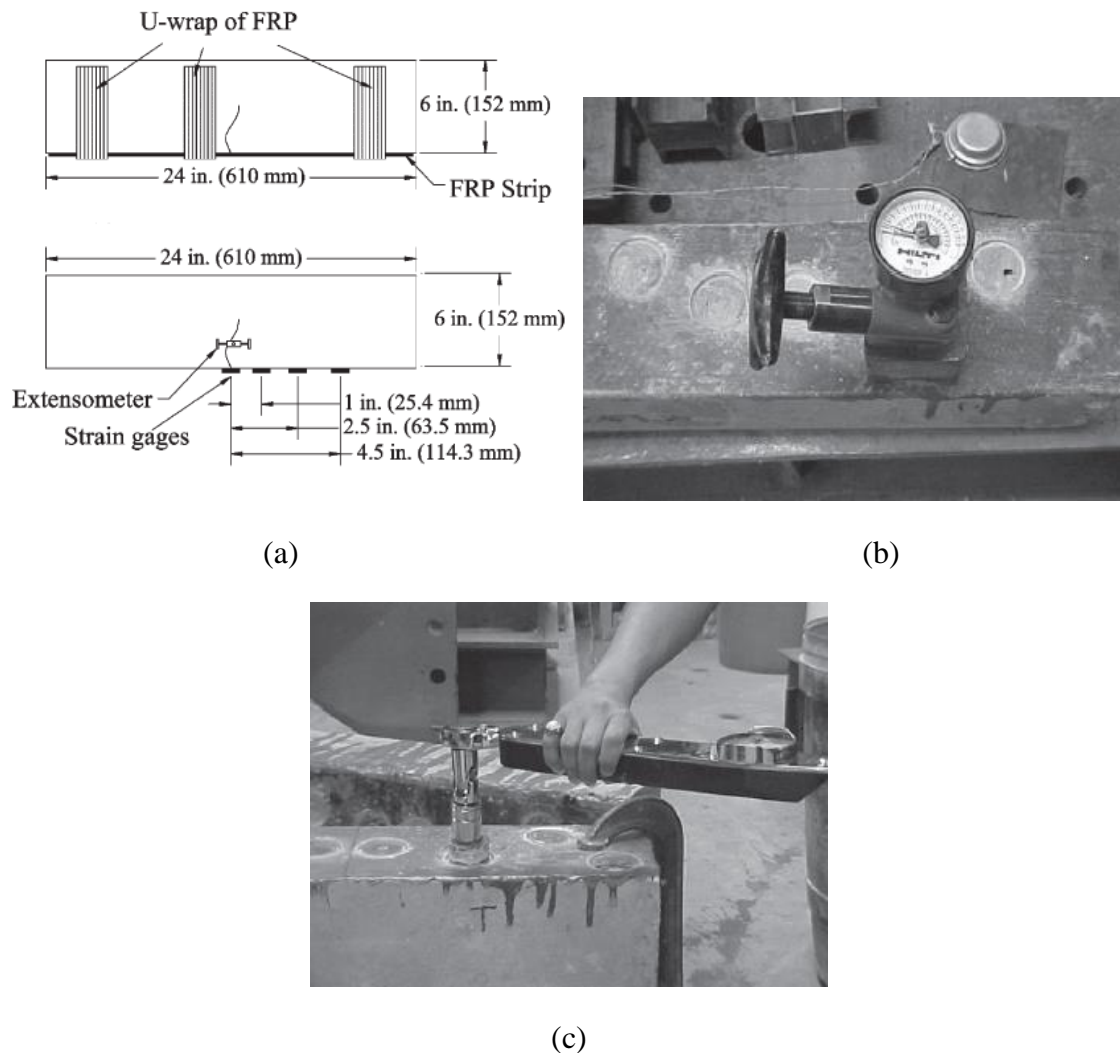
Figure 11—Myers and Ekenel (2005): (a) flexural specimens; (b) direct pull-off test setup; (c) direct torsion test setup

Grace and Singh (2005) explored the effects of various environmental conditions on the performance of reinforced concrete beams externally strengthened with CFRP laminates and fabrics. Reinforced concrete beams specimens used in this study measured 6 in. × 10 in. (152.4 mm × 254 mm) in cross-sectional dimensions and were 108 in. (2743 mm) long (Figure 12). Specimens were exposed to the following environmental conditions: (a) 100% humidity; (b) dry heat; (c) saltwater solution; (d) alkaline solution; (e) freeze-thaw cycles; and (f) thermal expansion. Beams were then tested in four-point bending by loading and unloading in two stages until the complete failure. All beams failed either due to debonding of FRP or "onset of delamination (shear-tension failure)." Again, the lowest BSR (of around 70%) was observed in beams that were exposed to highly moist environments. Beams experienced either a smaller decrease in SR or a decrease in strength due to exposure to other environmental conditions.

Authors noted that CFRP laminates are more susceptible to aggressive environmental conditions than wet layup CFRP fabric. Furthermore, they observed that duration of exposure for the beams exposed to humidity and saltwater solution had no significant influence on beams that were reinforced with CFRP fabric, while beams strengthened with CFRP laminates experienced further deterioration in strength due to the prolonged exposure.
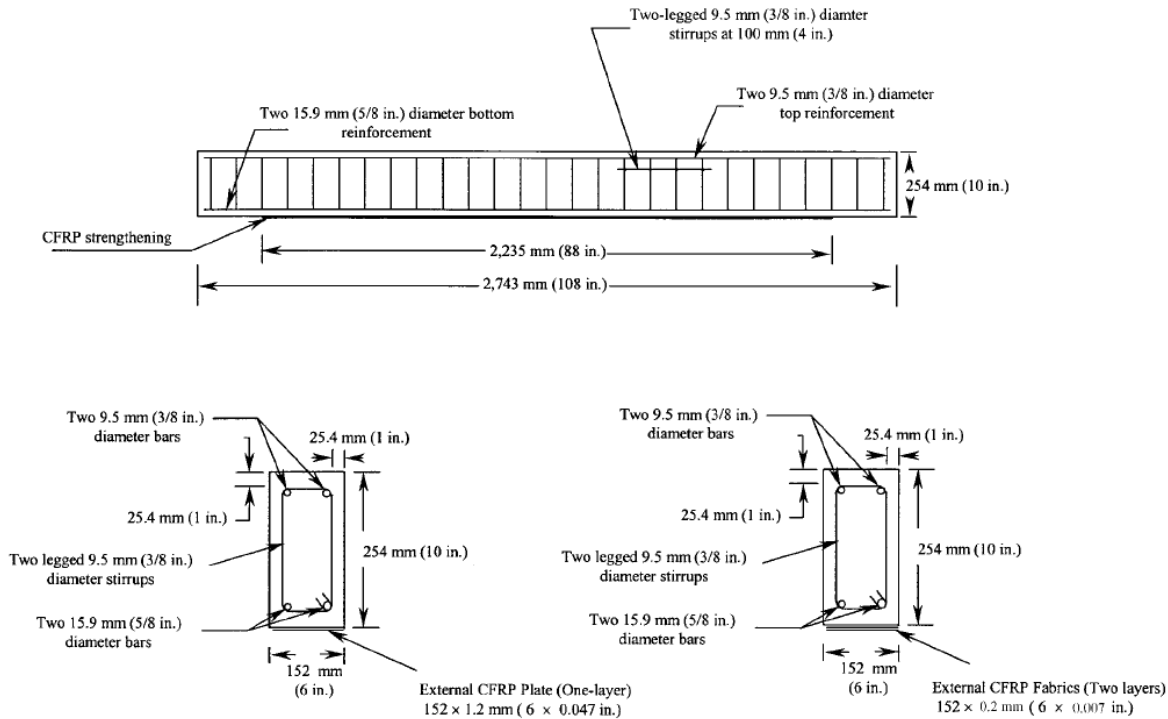
Figure 12—Drawings of test specimen (Grace and Singh, 2005)

Attempt in determining the influence of temperature only on the bond performance of concrete externally strengthened with FRP was undertaken by Klamer et al. (2005). They conducted both shear-lap tests and three-point bending tests at different environmental temperatures (Figure 13). Concrete specimens were strengthened with CFRP laminate and paste epoxy (Adhesive B in this report) with a glass transition temperature $T_g = 62°C$. Change in the failure mode, from cohesive to adhesive, was observed for temperatures higher than 50°C. In shear-lap specimens, an increase in temperature (below the T_g) produced an increase in the bond capacity. Authors concluded that the bond capacity is affected by the increase in temperature due to the decrease in adhesive stiffness and reduction in adhesive strength (especially for temperatures above the T_g). It should be regarded that the measured force in CFRP was lower and the displacement was higher at higher temperatures in the three-point bending test, which ultimately resulted in a higher specimen capacity. Authors explained this by effects introduced by the test setup.
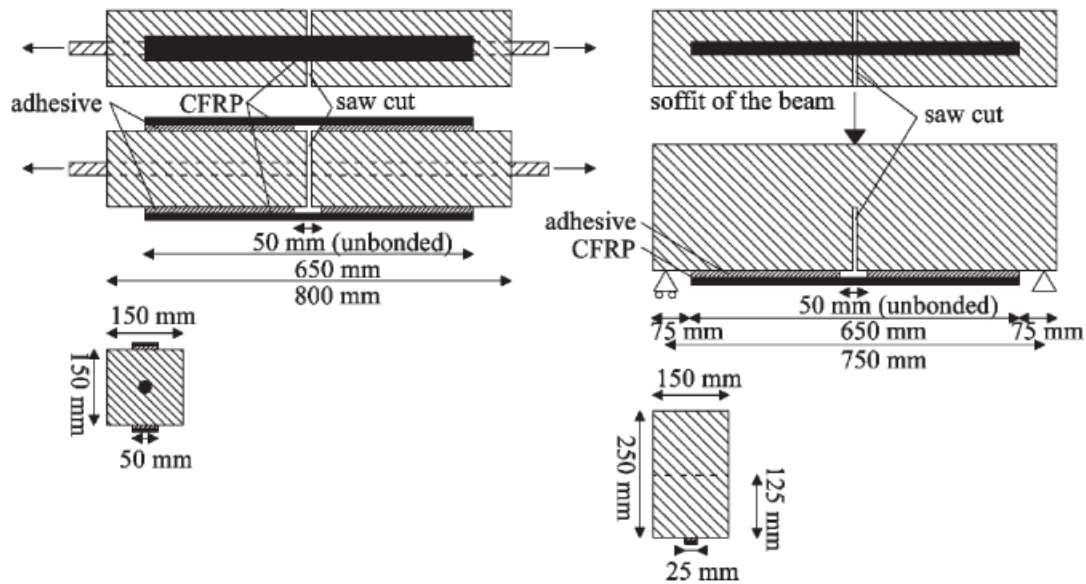
Figure 13—Double lap shear test setup (left); and three-point bending test setup (right) (Klamer et al., 2005)

Au and Buyukozturk (2006) performed a study on influence of moisture on the bond behavior in peel (Mode I) and shear (Mode II) test configurations (Figure 14). Pre-cracked peel and direct shear fracture specimens were conditioned at: (a) RH=100% at 23˚C; and (b) RH=100% at 50˚C. Specimens were conditioned for 2, 4 and 8 weeks. Control samples were kept in dry conditions. Results from these tests were presented in terms of specialized fracture energy release rate, based on the tri-layer fracture model developed by Au and Buyukozturk (2006). Under the peel conditions, exposed specimens experienced a sudden drop in bond fracture energy of around 60%. Shear fracture specimens, however, experienced a more gradual drop in fracture energy peaking at around 50% loss. Higher temperature did not significantly affect the peel properties of test specimens, whereas shear fracture specimens achieved lower capacities at higher conditioning temperature. Additionally, Tuakta and Buyukozturk (2010) extended this study to include specimens conditioned by immersion in water at same temperatures and wet-dry cycling. They also explored the influence of drying before testing the specimens (referred to as moisture reversal tests). They noted that the decrease in fracture energy of FRP-concrete bond may be up to 70%. Furthermore, they concluded that bond properties were not fully restored after drying or successive wet-dry cycles. Authors observed a shift in failure mode from cohesive to adhesive in all conditioned samples.

Study on assessment of quality of bond between FRP and concrete with the presence of water at the time of installation was undertaken by Wan et al. (2006). They used the modified double cantilever beam (MDCB) test to obtain the energy release rate of FRP debonding when subjected to mixed mode loading conditions (Figure 15). Details on the test setup and analytical model may be found in the referenced journal article. To simulate the presence of water at time of installation of wet layup CFRP, four different surface moisture conditions were introduced: (a) dry; (b) saturated surface dry 1 (SSD1); (c) saturated surface dry 2 (SSD2); and (d) wet. For dry surface condition, specimens were left in ambient conditions to cure before and after priming. For SSD1 condition specimens were submerged in water for 3 days, followed by drying the

surface with a paper towel and then applying the primer. Additionally, specimens were submerged in water after priming with the water level below the concrete surface. For SSD2 condition, the same procedure was followed, however, specimens were left in ambient conditions after priming. For the wet condition, primer was applied to the wet concrete surface directly. Specimens were then submerged in water again. Based on the test data authors concluded that the bond capacity decreases with the amount of water present at the surface. Namely, loss in measured energy release rate for SSD2, SSD1, and wet specimens was 58, 38, and 8% of the specimens kept in dry conditions, respectively. The prevailing failure mode for all conditioned specimens was mixed or adhesive. In addition to the previously described test program, authors performed a series of tests to investigate the influence of water on bond after FRP cures. The specimens were conditioned in water for 3, 6, and 8 weeks and then subjected to MDCB tests. Results showed that FRP-concrete bond degrades with respect to time, with a loss of up to about 75% in ultimate energy release rate when compared to results for specimens kept in dry conditions.
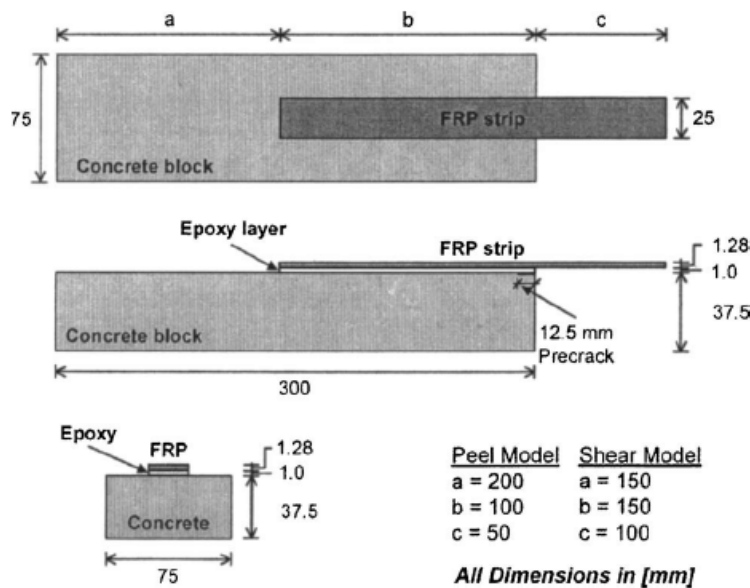
Figure 14—Direct shear/peel test specimen (Au and Buyukozturk, 2006)
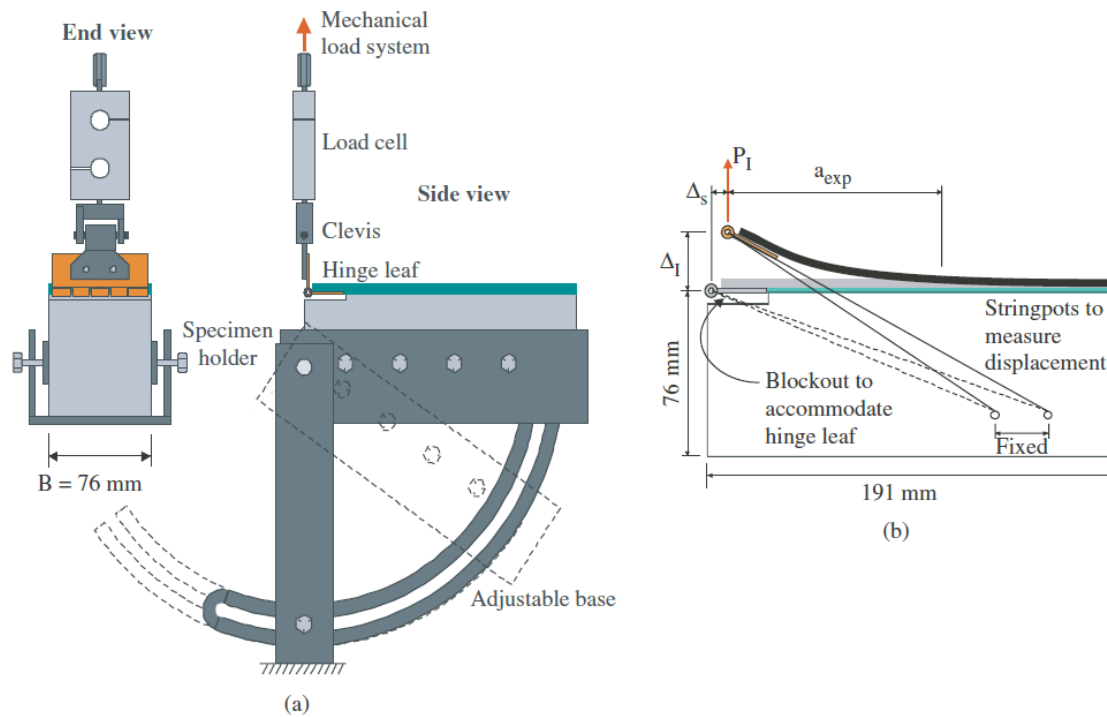
Figure 15—Mixed mode peel test setup (Wan et al., 2006)

Alfar (2006) studied the durability of CFRP strengthened reinforced concrete members subjected to real-time exposure in environments typical for Amman city (at Building Research Center of the Royal Scientific Society of Jordan), Dead Sea region (salt extracting plant), and Aqaba region (splash and tidal zone) in Jordan. According to the authors, the latter two locations provided exposure to some of the most severe marine environments. Salinity of Dead Sea is close to 34% (340 parts per thousand) compared to only around 3.5% (35 parts per thousand) that is the salinity of North Atlantic Ocean. Specimens were also subjected to high temperatures ranging from 37 to 49.5°C in the summer and RH = 80%. Additionally, some samples were exposed to artificially created laboratory conditions that included: (a) wetting specimens with chloride solution (9.6% NaCl) and storing them at RH = 65% at 20°C; and (b) RH = 65% at 20°C (control). Specimens consisted of reinforced concrete slabs measuring 63 in. × 19.7 in. × 4.7 in. (1600 mm × 500 mm × 120 mm) and concrete prisms measuring 5.9 in. × 5.9 in. × 17.7 in. (150 mm × 150 mm × 450 mm) in nominal dimensions.

Slab specimens were notched on both sides, at 200 mm and 300 mm from the midspan. After curing, each pair of slabs was tied together with a sustained load applied in excess of the theoretical cracking load to produce cracking. Then, pairs of slab specimens were conditioned in previously described environments. After four months of exposure, specimens were repaired with CFRP laminates and three types of epoxies. Then, sustained load was increased by 20%, and specimens were conditioned for an additional 12 months. Eventually, slab specimens were tested in three-point bending. Authors noted the lowest BSR was recorded for specimens conditioned in Dead Sea environment of about 88%. Most of the specimens failed by debonding of CFRP laminate caused by an intermediate flexural crack. Moreover, a shift from cohesive to adhesive failure mode was observed in all specimens after conditioning in severe environments.

Concrete prism specimens were used to perform direct shear test, and were subjected to the same conditioning and repair protocol as slab specimens. Results from direct shear tests showed that exposure to severe environments did not have detrimental effect on FRP-concrete bond.

Frigione et al. (2006) studied the efficiency of bond in concrete joints adhered by epoxy when affected by moisture. The slant shear tests were performed based on ASTM C882-91 (Figure 16) using two different concrete mixes (25 MPa and 50 MPa) and three different epoxy adhesives. Test results for only one of the epoxies were included here, as that was the only one that was used to bond CFRP to concrete. Adhesive thickness in concrete-concrete joint was varied at 0.5 mm, 2 mm, and 5 mm. Shear slant specimens were conditioned in distilled water at 23±1˚C for 2, 7, 14, and 28 days before testing. Test results indicated that the bond strength decay plateaus after 14 days of exposure, peaking at around 35%. This loss in bond capacity of concrete-concrete joint produces a BSR of 65%. Relatively slight decreases in bond strength were observed as the epoxy thickness was increased.
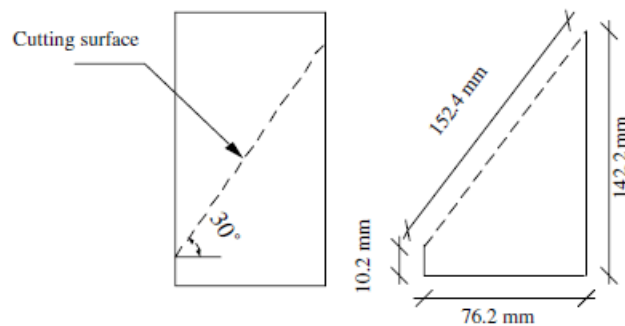
Figure 16—Slant shear test specimen (Frigione et al., 2006)

Fava et al. (2007) used the direct shear test in Mode II loading to assess the performance of FRP-concrete bond after conditioning in multiple environments. The test setup was similar to those used by Taljsten (1996) and Au and Buyukozturk (2006) (Figure 17). Test specimens were exposed to: (a) standard conditions – at 20˚C and RH = 60%; and (b) one month of salt spray fog at 50˚C. Authors noted an increase in BSR of around 30% (BSR≈130%) in specimens conditioned in salt fog environment when compared to the specimens kept in standard conditions. They attributed this rise in bond capacity to "beneficial effects on epoxy resin of high humidity level" as found by Wu et al. (2004).
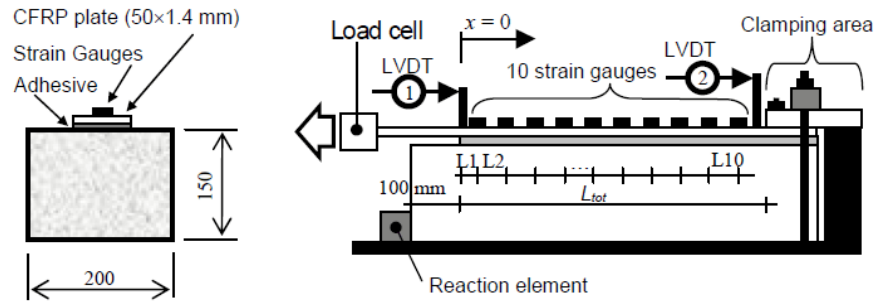
Figure 17—Direct shear test setup (Fava et al., 2007)

Soudki et al. (2007) tested 11 reinforced concrete beams repaired with CFRP laminate or wet layup. Eight beams were precracked before repairing, while the remaining three beams were kept intact as a control. Each beam was 5.9 in. (150 mm) wide, 9.8 in. (250 mm) deep and 94.5 in. (2,400 mm) long (Figure 18). Beams were lightly reinforced, with a reinforcing ratio of 0.6%. Control beams were kept at a room temperature, while the rest of the beams were conditioned in 100, 200 and 300 wet/dry cycles with a 3% solution of NaCl. One wet/dry cycle lasted two days – one day of wetting followed by one day of drying. This conditioning protocol was established to achieve active corrosion of reinforcing steel in a reasonable time. After exposure, specimens were tested in four-point bending. In addition, corrosion rates of reinforcing steel, and chloride contents at different depths were measured. Authors noted that all specimens failed by debonding of FRP followed by a minimum BSR of 89 and 72% for wet layup sheets and laminates, respectively. Furthermore, CFRP and the resin system seemed to decrease the corrosion rate of the reinforcing steel.
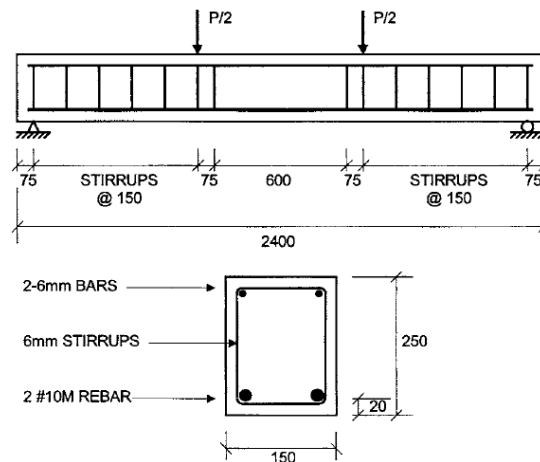
Figure 18—Four-point bending test beam design (Soudki et al., 2007)

Silva and Biscaia (2008) developed an experimental program to evaluate the degradation of bond between FRP and concrete (Figure 19). They tested hinged concrete specimens in four-point bending. Specimens were conditioned as follows: (a) salt fog cycles at 35°C – 16 h dry followed

by 8 h of fog; and (b) moisture cycles – RH = 20% for 12 h, followed by RH=90% for 12 h. Specimens from the first group were conditioned for 3000 and 6000 h, while the specimens in the second group were exposed for 1000, 5000 and 10,000 h. Authors noted that failure mode was affected by the exposure environment. They observed cohesive failure mode in specimens exposed to moisture cycles, while the specimens conditioned in salt fog cycles experienced adhesive failure along the interface. Both groups of specimens, however, had almost the same BSR of about 80%.
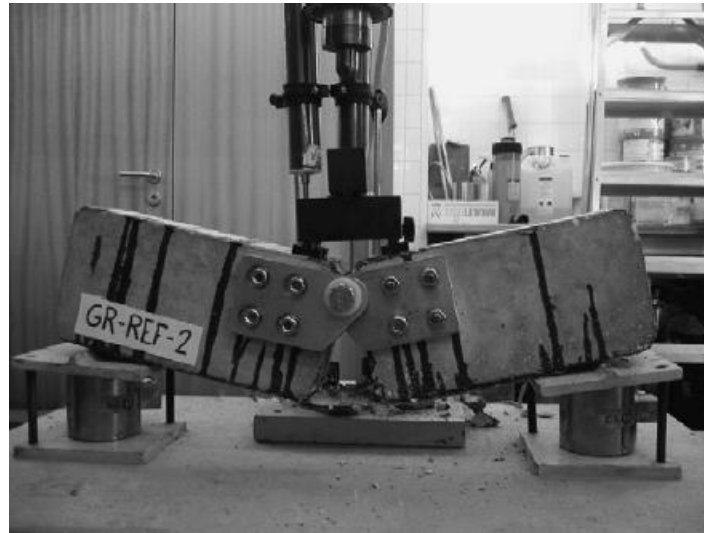
Figure 19—Hinged beam specimen (Silva and Biscaia, 2008)

Garmage et al. (2009) performed a durability study of FRP-concrete bond using a 3 in. × 3 in. × 10 in. (75 mm × 75 mm × 250 mm) concrete specimen reinforced with wet layup CFRP sheets. All specimens were conditioned at temperature cycles ranging from 20˚C to 50˚C within a 4.5-hour period, with 1.25 hours soaking time at minimum and maximum temperatures. Relative humidity was kept constant at 90%. Some of the conditioned specimens were subjected to different levels of sustained loading. As this study is not concerned with effect of sustained loading on bond performance, findings related to those samples will be omitted in the literature review. Control samples were not conditioned. Specimens were tested in a single lap shear test setup after 175, 325, 1250, and 2400 hours of conditioning and reported a BSR of close to 70%.

To determine the sensitivity of FRP-concrete bond to chloride content Pan et al. (2010) performed direct shear tests (Figure 20) on specimens conditioned in water solutions with the following concentrations of NaCl: (a) 3%, (b) 6%; (c) 10%; and (d) 15%. Specimens were conditioned for 15, 30, 60, 90, and 120 days. Authors concluded that concrete compressive strength significantly increases with the immersion time in NaCl solution. The chloride concentration, however, did not have significant effect on the compressive strength of concrete. Furthermore, authors noted a slight decrease in initial and ultimate debonding loads after 15 and 30 days of conditioning. Specimens that were conditioned longer, however, experienced a slight increase in bond strength when compared to unconditioned samples. Moreover, there was no apparent correlation between the bond strength and the chloride concentration of the water solution.
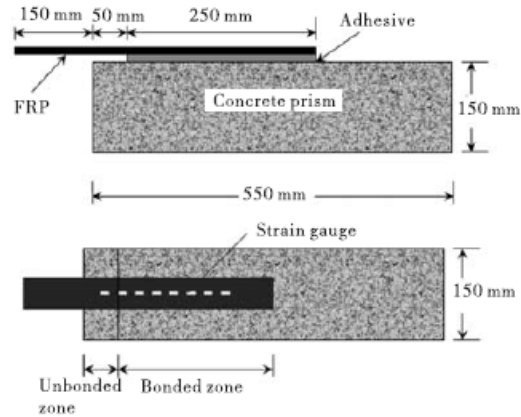
Figure 20—Direct shear test specimen (Pan et al., 2010)

Dai et al. (2010) performed a study on influence of moisture on concrete surface during the application of FRP, and in service moisture on performance of FRP-concrete bond. Authors utilized direct pull-off and bending tests (Figure 21) to assess the bond performance after conditioning for 8, 14 and 24 months in wet-dry cycles consisting of four days of immersion in 60˚C followed by drying for three days in standard laboratory conditions. Additional variables were: (1) curing conditions after repair (RH = 48% vs. RH = 90%); (2) wet vs. dry substrate at the time of repair; (3) normal vs. hydrophilic primer; and (4) normal vs. ductile adhesive. It should be noted that for the purpose of this research a special form of CFRP, called carbon-stranded sheet (CSS), was used. The CSS consists of 1 to 2 mm in diameter circular carbon microbars, formed by pultruding dry carbon fibers with epoxy. In pull-off test specimens, the minimum BSR was about 50%, while the minimum BSR in bending specimens was approximately 60%. Based on the results of the experimental program authors concluded the following:

1. Different curing conditions were not of critical importance on the bond capacity.
2. Wet concrete substrate at time of installation detrimentally affected the bond performance, however, only when the normal primer was used.
3. Wet-dry cycling caused shift of failure mode from cohesive to adhesive (between primer and concrete). This may be due to microcracks observed by microscope that formed at the primer-to-concrete interface that formed after wet-dry cycling.
4. No general trend was observed in bond capacity in respect to duration of wet-dry cycling. Bending specimens experienced both increase and decrease in capacity over time of conditioning.
5. Pull-off tests are not indicative of the overall bond condition, because they rather capture the local weaknesses at the interface. Pull-off test, however, was considered sufficient to provide a conservative estimate of durability of the FRP-concrete bond capacity.
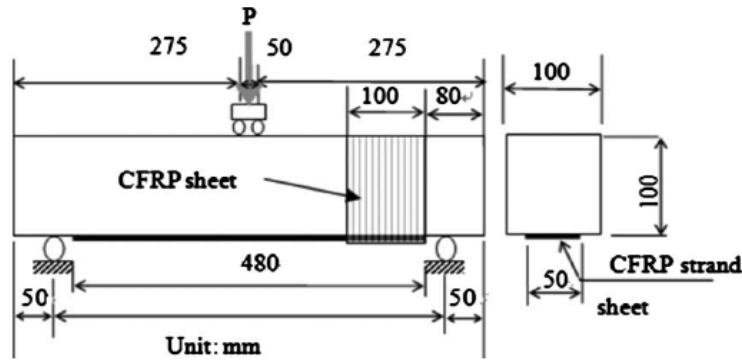
Figure 21—Three-point bending test setup (Dai et al., 2010)

Cromwell et al. (2011) investigated influence of multiple aggressive environments on performance of FRP reinforcement in concrete structures. Authors used two types of CFRP in their test program: a laminate and a wet layup system. Test program included three different types of specimens: (1) tension coupon specimens – prepared as per ASTM D3039; (2) bond specimens – "two 2 in. (51 mm) concrete cubes spaced 1 in. (25 mm) apart and bonded together using 0.75 in. (19 mm) wide by 5 in. (127 mm) long FRP strips on opposing faces" (Figure 22); (3) beam flexure (three-point bending) specimens – concrete beams reinforced with two #3 bars at top and bottom and U shaped stirrups W2.9 spaced at 5.98 in. (152 mm) on center, and the following dimensions D:W:L=6.1:8:96.1 in (154:203:2440 mm); reinforced with CFRP at the soffit (Figure 23). Specimens were conditioned in the following environments: (a) water – RH=100% at 38°C for 1000, 3000, and 10,000 as per ASTM D2247; (b) salt water solution - prepared as per ASTM D1141, for 1000. 3000, and 10,000 h at 22°C; (c) alkaline (CaCO$_3$ solution) – at 22°C for 1000 h, 3000 h, and 10,000 h; (d) dry heat - 60°C in a forced-draft circulation-air furnace as per ASTM D3045, for 1000 h and 3000 h; (e) diesel fuel – immersion in diesel fuel at 22°C for 4 h as per ASTM C581; (f) weathering – UV340 light at 63°C for 2 h, followed by RH = 100% at 22°C for 2 h, for the total of 2000 h (1000 cycles); (g) freeze-heat – cycling between -18°C for 15 h, and RH=100% at 38°C for 15 h (20 cycles in total), following the exposure to RH = 100% at 38°C for 500 h and drying for 48 h; (h) freeze-thaw cycling – 360 cycles as follows: "(1) 70 min at -18°C at RH = 30%; (2) 20 min ramp up to 4.5°C (resulting in 90% RH); (3) 70 min at 4.5°C at 50% RH with UV lights on; and (4) UV lights off and 80 min ramp down to -18°C (resulting in 40% RH)".

Control specimens were conditioned in standard laboratory relative humidity and temperature. It should be noted that only beam flexure specimens were exposed to freeze-thaw cycling. Tension and bond specimens were conditioned in all other aforementioned environments. Results from tension coupon tests showed that properties of both CFRP laminate and fabric are not significantly affected by exposure to aggressive environments. In any of the conditioning environments, modulus of elasticity and ultimate did not fall below 95% and 90% for CFRP laminate and fabric, respectively. Bond specimens showed a much greater variation in results as well as a higher level of sensitivity to aggressive environmental conditions. Specimens with bonded CFRP laminate reinforcement showed the greatest reduction in bond capacity (BSR=80%) after exposure in salt water for 10,000 h, and dry heat for 1000 h. On the other hand, specimens reinforced with CFRP fabric proved to be mostly affected by dry heat condition

where they showed a BSR of close to 60% of control bond strength. Beam flexure specimens experienced very low reductions in strength. Therefore, authors concluded that the "intermediate-crack (IC) debonding" is unaffected by freeze-thaw cycling.
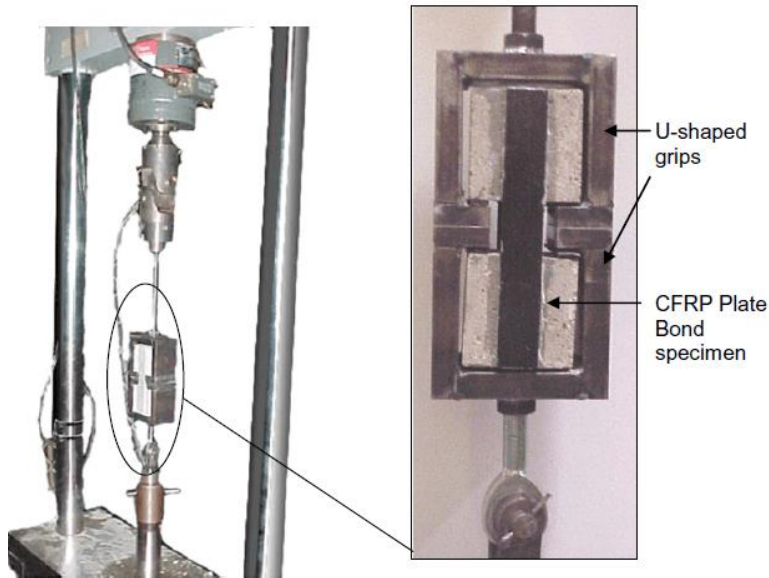
Figure 22—Bond test setup
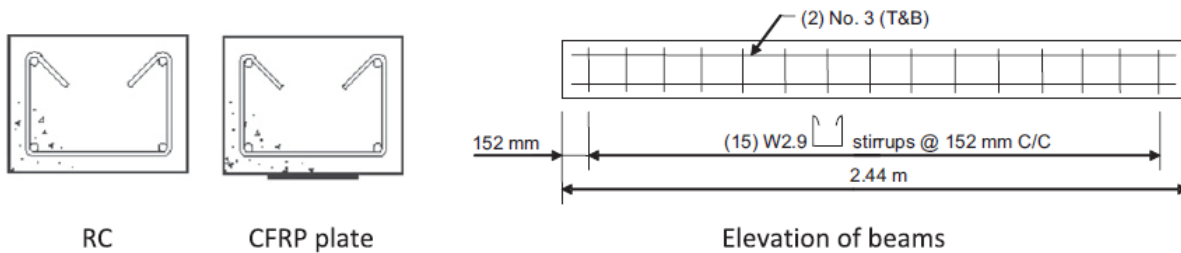
Figure 23—Beam flexure specimen (Cromwell et al., 2011)

Lai et al. (2009) performed a series of direct shear tests to determine effects of high temperature and water ingress on durability of FRP-concrete bond (Figure 24). Specimens were immersed for 5, 15 and 30 weeks in water at the following temperatures: (a) 25°C; (b) 40°C; and (c) 60°C. By digitally processing the visual images of FRP strips, authors identified three distinguishing failure modes:

- Failure in concrete
- Failure at FRP-epoxy interface
- Failure within adhesive bonding layer

Aside from a decrease in ultimate failure load (of up to 30%), authors observed increase in average delamination (flaws in adhesive layer that form due to exposure to aggressive environments) sizes in the 40 °C and 60°C specimens, when compared to control. In addition to

that, they observed a shift from failure mode A in control and the 25˚C specimens, to predominantly failure modes B and C in specimens exposed to 40 and 60˚C, as presented in Table 1.
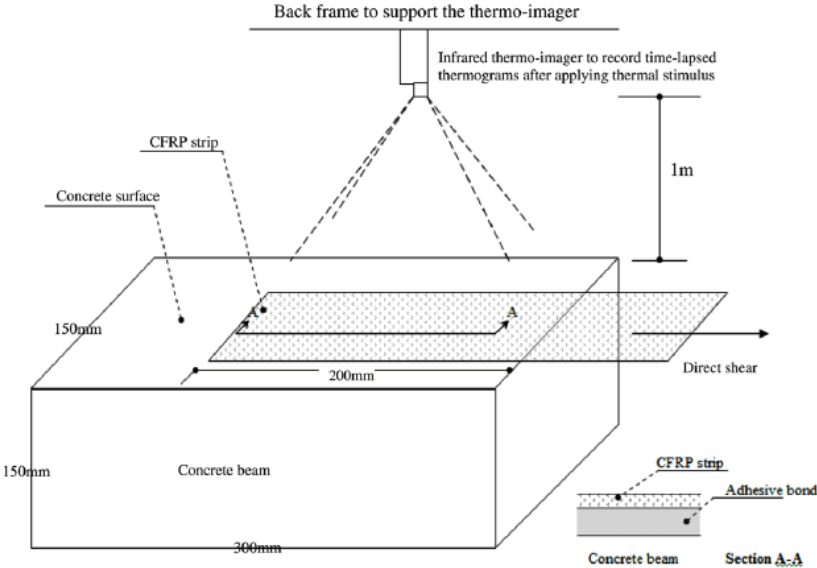
Figure 24—Direct shear test setup (Lai et al., 2009)

Table 1—Distribution of failure modes (Lai et al., 2009)

Exposure temperature (˚C)	Average failure mode (%)		
	Mode A	Mode B	Mode C
Control	75.3	24.7	0
25	63.8	33.3	2.8
40	58.1	17.4	24.5
60	41.3	32.7	26

In a different study on durability of FRP-concrete bond when conditioned in water with elevated temperatures, Lai et al. (2013) used infrared thermography in conjunction with direct shear test.

Based on the thermographs, three distinguishing stages in debonding process can be identified (Smith and Teng 2002, Colombi et al. 2010):

1. "Elastic stage (no interfacial softening or rupture can be found over the entire interface)";
2. "Elastic-softening stage (local softening starts at the loaded end and some parts of the interfacial bonds become softened while the portion near the fixed end, remains elastic)";
3. "Elastic-softening-debonding stage and softening-debonding stage (local rupture of the bond layers happens and propagates from the loaded to the fixed ends)"

From the results of durability study authors noted an early occurrence of the softening-ruptured state for all specimens that were conditioned at 60°C. For the control, 25°C, 40°C specimens, the debonding process commenced with elastic-softening stage. The degradation due to exposure caused a drop in BSR from control to specimens exposed at 60°C to about 70%.

Srestha et al. (2013) examined influence of water on FRP-concrete bond in high strength concrete by utilizing direct shear pull-off test. They tested specimens made of normal strength concrete for comparison purposes. Specimens (Figure 25) were immersed in water at 20°C for up to 12 months. Two types of epoxy (Epoxy E: combination of Bisphenol-A and Bisphenol-F epoxy resins; and Epoxy F: Bisphenol-A epoxy resin), and one CFRP fabric were used in the study. Linear dependency of ultimate bond strength in respect to exposure time was observed, with ultimate values recorded in Table 2. Better performance of bond in lower strength concrete was explained by differences in surface properties between the two. Namely, high strength concrete is tightly packed and due to lack of pores and voids does not have much available surface for transfer of frictional forces, whereas this is not the case in normal strength concrete. As evidence to support this claim, authors compared the failure surfaces, which revealed that less concrete debris was found on CFRP that debonded from concrete surface (Figure 26 and Figure 27).

Table 2—BSR after 12 months of exposure (Srestha et al., 2013)

Epoxy Type	Normal Strength Concrete	High Strength Concrete
Epoxy E	≈140%	≈68%
Epoxy F	≈100%	≈70%
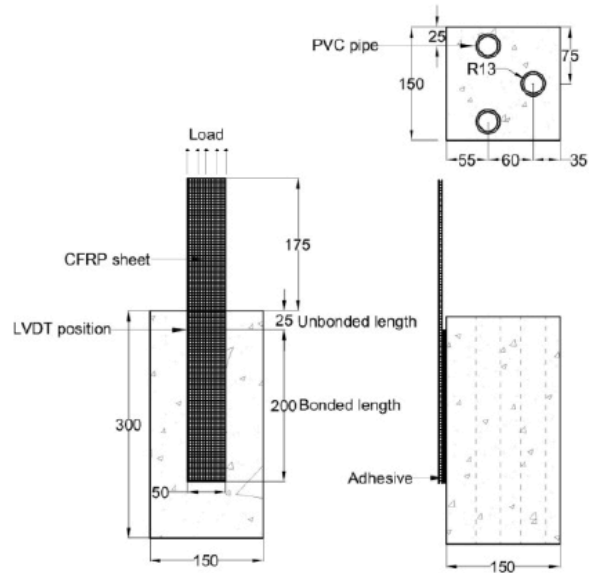
Figure 25—Direct shear test specimen (Srestha et al., 2013)

Figure 26—Failure surfaces for normal strength concrete (Srestha et al., 2013)

Exposure time	Type E	Type F
0 month	Mixed failure	Mixed failure
3 month	Adhesive failure	Adhesive failure
6 month	Adhesive failure	Adhesive failure
12 month	Adhesive failure	Adhesive failure
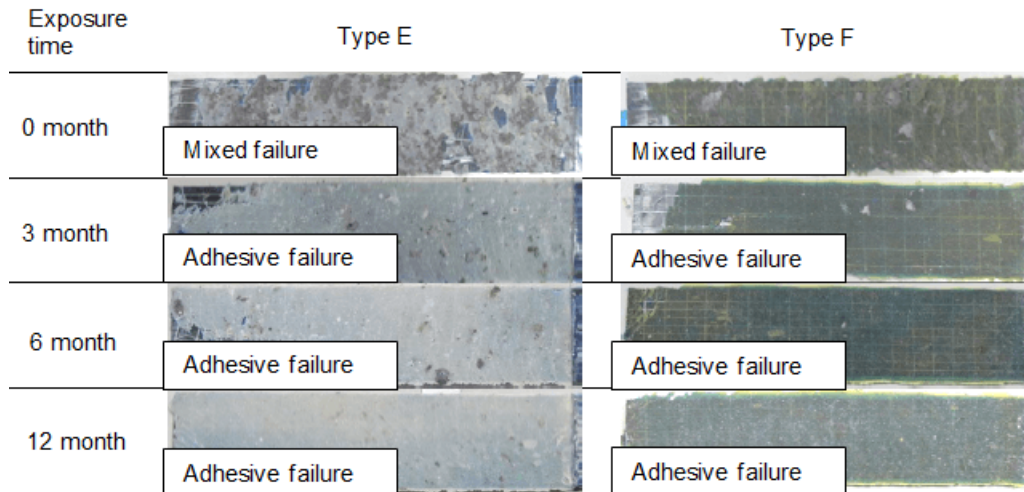
Figure 27—Failure surfaces for high strength concrete (Srestha et al., 2013)

3.4 FRP-Concrete Bond Durability Database

Based on the performed literature review, all data from the publications was compiled into a single database using the following guidelines:

- Control samples were chosen from specimens that were kept in standard laboratory conditions
- Results for CFRP wet layup composites (WTL) and CFRP laminate (P) composites were included.
- Physical values that were compared: ultimate load or ultimate stress. Fracture energy data was not included since the current ACI 440-08 design guidelines are strength based.
- Test setups included direct pull-off (DP), direct torsion (DT), direct shear pull-off (DSP), peel test (PT), three-point bending (TPB), and four-point bending (FPB).
- Results from both small-scale (SS) and large-scale (LS) tests were included. Large-scale specimens were considered beam and slab specimens of a minimum span length of 5 ft. All other tests were considered small scale.
- Test result values were used to calculate the BSR for each test. In the literature review, BSR data were expressed as a percentage. For computational convenience, the data are analyzed and presented here in decimal form.
- Included test results correspond to monotonic loading condition.

BSR data distributions for both small-scale and large-scale specimens are presented in Figure 28 and Figure 29. The data tend to be normally distributed and were treated as such when computing the statistical parameters. High variability in data from the literature was expected due to variations in materials, test setups, test methods, etc. Closer examination of the data indicated that the distribution of data improved when the laminate and wet layup systems were treated separately as shown in Figure 30 and summarized in Table 3. Distribution properties for small-scale and large-scale wet layup results appear to be in good agreement. Distribution properties differ, however, when comparing small-scale and large-scale test results for CFRP

laminate results. This may indicate that scale effects have influence on behavior of CFRP laminate.
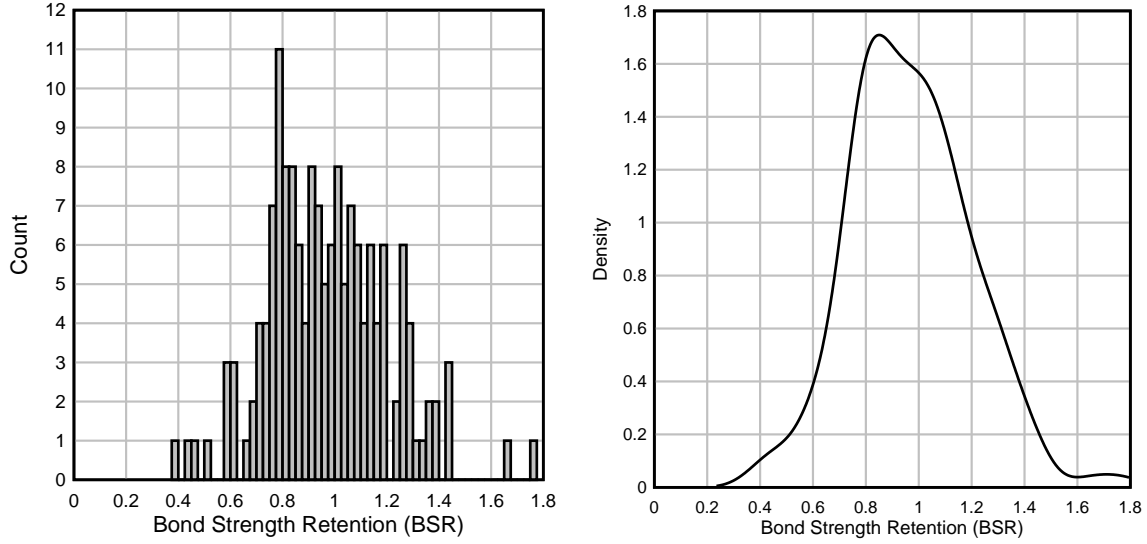
Figure 28—Small-scale data distribution (literature)
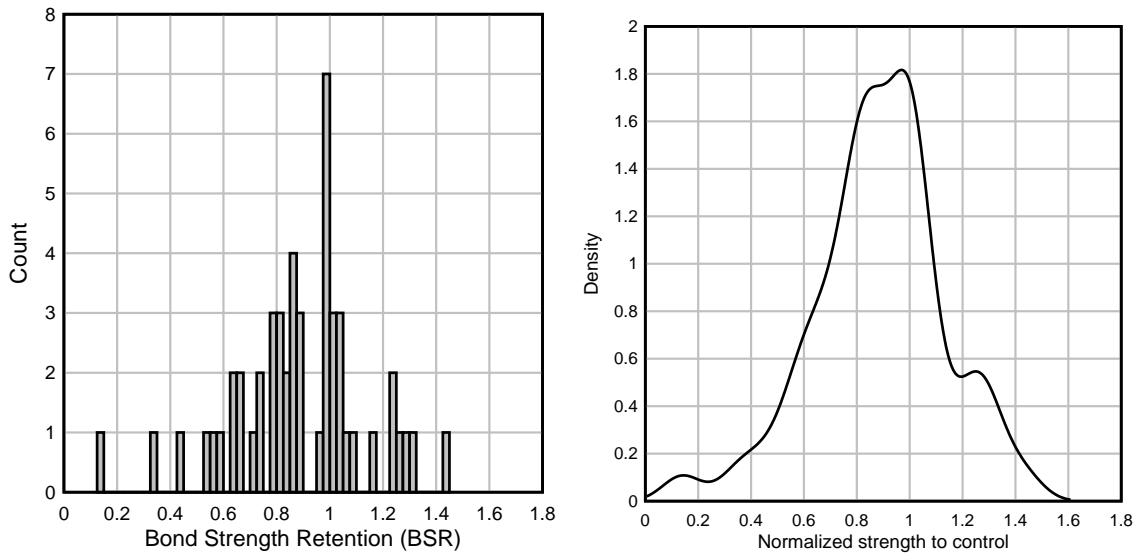
Figure 29—Large-scale data distribution (literature)
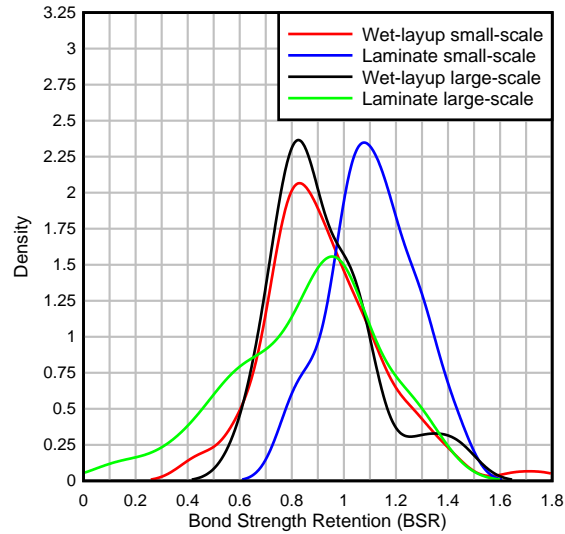
Figure 30—Comparison of distributions for different groups of data from literature

Table 3—Theoretical normal distribution parameters for different groups of data from literature

Category	Population size	Mean	COV (%)
Wet layup small scale	121	0.92	25
Laminate small-scale	39	1.04	15.4
Wet layup large-scale	20	0.92	20.65
Laminate large-scale	31	0.86	32.6

3.5   Summary of Findings from Database

Based on the presented literature review it was concluded that presence of moisture has the most severe effect on bond performance between FRP and concrete. Hypothesis is that effect of water is twofold: (a) saturation of bond by water molecules diminishes the established chemical bonds at the interface and (b) saturation with water produces plasticization of epoxy matrix (loss of stiffness). Evidence from literature further suggests that high temperature combined with moisture has adverse effect on bond performance. This is probably because: (a) rate of moisture diffusion is proportional to increase in temperature and (b) epoxy matrix turns into a rubbery state at temperatures near Tg.

3.6   CFRP Protection of Steel Reinforcement

The following table presents findings from literature related to the effects of FRP wraps on corrosion properties of internal steel reinforcement, primarily the corrosion rate and steel mass loss. Figures related to each reference are placed in the Appendix A. The general finding is that CFRP and GFRP wraps decrease the rate of corrosion, with some studies finding that GFRP had superior properties in that respect.

Table 4—Findings from literature

Author	Specimen	Accelerated conditioning	Findings
Bae and Belarbi (2009)	30 Small scale and 4 midscale RC columns wrapped with CFRP; Destructive test method: axially loaded to failure	Wet-dry cycles with 5% saline with applied electric potential of 6V between the anode and cathode	Decreased corrosion rate in CFRP wrapped columns Swelling of concrete due to corrosion caused straining of CFRP wraps
Gadve et al. (2009)	Cylindrical RC specimen wrapped with CFRP and GFRP; Destructive test method: bar pull-out test.	3.5% NaCl solution Constant 100 mA current between cathode and anode	Wrapping slows down the rate of corrosion; Increase in pull-out strength, decrease in mass loss and increase in corrosion current in wrapped specimens; GFRP may provide better protection from corrosion than CFRP.
Green et al. (2006)	Small-scale RC cylinders (152 mm $\times$ 305 mm), and larger-scale circular RC columns (300 mm $\times$ 1200 mm) Destructive test method: axially loaded to failure	3% saline solution at 40°C	Rate of corrosion was reduced after wrapping.
Halstead et al. (2000)	Field tests on New York Court Street Bridge near Binghamton, NY	N/A	Evidence that measured corrosion rates follow ambient temperature fluctuations.
Maaddawy et al. (2006)	Cylindrical R/C specimens (103 mm in diameter and 204 mm high) wrapped with CFRP	Application of low-voltage (15 V) and high-voltage (60 V) between cathode and anode	Measured current in wrapped specimens was on average 36% lower; the steel mass loss in wrapped specimens was on average 30% lower; CFRP wraps impeded the cathodic reaction; steel mass loss increased with increase in bar diameter and applied potential; unwrapped cylinders experienced about three times larger circumferential expansion due to corrosion.

Author	Specimen	Accelerated conditioning	Findings
Masoud and Soudki (2006)	Large-scale R/C beam specimens (152x254x3200 mm) Destructive test method: four-point bending until failure	Application of current density of 140 μA/cm^2 through main reinforcing Wet-dry cycles for some of the specimens	Application of FRP reduced the mass loss by about 16% after 152 days of corrosion; GFRP had effect on corrosion activity; CFRP sheets had no significant effect on corrosion.
Nossoni and Harichandran (2010)	R/C prism specimens (305x152x152 mm) wrapped with GFRP	Soaking specimens for 1 h in each 12 h period in 3.5% NaCl solution Constant voltage of 12 V impressed across the reinforcing bars	Addition of GFRP delays cracking and changes the cracking pattern; Rate of corrosion is reduced in samples with GFRP patches
Pantazopoulou et al. (2001)	R/C columns (150 mm in diameter and 30 mm high)	Applied fixed potential of 6 V between the anode and the cathode Immersion in 2% Cl- solution, at initial stages	GFRP wraps improved corrosion resistance of test samples.
Lee et al. (2000)	R/C columns wrapped with CFRP	Applied fixed potential to induce corrosion Continuous and cycled immersion in 3% NaCl solution	Wrapping impeded the rate of corrosion by about 50%.
Spainhour and Wootton (2008)	R/C cylinders measuring 2 in. in diameter and 4 in. in height	Immersion in a 5% NaCl solution at a room temperature (24°C); Impressed current so that reinforcing bars are anodic	CFRP was effective in delaying onset of corrosion, and reducing rate of corrosion mass loss; Type of epoxy used to saturate the fibers had effect on the corrosion; With one type of epoxy increasing the number of CFRP layers improved the sample's performance.

3.7 Field Assessment of FRP Repairs

Banthia et al. (2010) performed a series of infrared thermography measurements and pull-off tests on four concrete bridges in Canada that were repaired with FRP materials. The following bridges were included in the study:

- St. Etienne de Bolton Bridge near Sherbrooke, QC, exposed to temperatures ranging from -18 to 24˚C, notable amounts of deicing salts, and physical impact during snow cleaning

- Leslie Street Bridge in Toronto, ON, exposed to varying temperatures (from -10˚C to 27˚C) with multiple freezing and thawing cycles

- Maryland Bridge in Winnipeg, MB, exposed to a relatively dry climate with temperatures between -23 and 6˚C

Authors noted that debonded areas determined from thermographs corresponded to areas with reduced bond strength. Furthermore, they observed that cohesive failures were related to pull-off strengths higher than 330 psi. Relatively low bond strengths were observed on one particular bridge "probably because the geometry of the girders allowed for the infiltration of water behind the FRP layer". Authors also reported that, aside from water infiltration, it was not clear why many of the bond strengths were low. They suspected that the low values were related to general deterioration; however, this could not be proven, as the initial bond strength data was not obtained.

Davalos et al. (2012) performed field tests of concrete T-beams before and after repair with FRP for bridge 49-4012-0250-1032, located near Sunbury, Northumberland County, Pennsylvania. Authors also conducted laboratory tests to evaluate strengthening effects by the use of FRP.

Two full-deck core samples at mid-span and quarter point of span were used for the field assessment of the unrepaired bridge. Several tests and analyses were performed on material samples extracted from the bridge, including the core sample compression test, concrete carbonation test, scanning electron microscopy (SEM) and energy dispersive X-ray (EDX) analyses, chemical analysis of concrete powder samples, and steel tension test. It was found that concrete in the deck experienced carbonation to the depth of 1 in. to 1.5 in. Furthermore, chemical analysis along with SEM/EDX analysis showed that leaching of C-S-H and calcium hydroxide had occurred in the beam due to severe carbonation and chloride attack. The chloride contents of core samples ranged from 0.19% to 1.6%, which exceeded the prescribed limits (ACI 318).

Prior to repair, a load test with tandem trucks was conducted on the bridge to determine the deflections and the natural frequency. A finite element model was prepared for the bridge to compare field and computational results, which were found to be in good agreement. FEM calculated natural frequency was about 10% lower than the field test result.

After repair, quality control bond strength between old and new concrete was evaluated by pull-off test method. Compression and splitting tension tests [ASTM C496 (2004c)] of the concrete repairing materials were conducted in the lab. Direct pull-off testing was also performed to assess the quality of bond between FRP and concrete. The FRP was attached both as single and

double layers. A comparison showed that double-layer FRP interface was stronger than single layer in pull-off tests. Post construction load tests were carried out on the bridge after repair, and the finite element model was modified to account for repair by FRP strips. It is noted by the authors that the stiffness of the repaired bridge did not change much. However, there was effect of FRP repair on increase in flexural and shear strength.

Additionally, a laboratory study was conducted to evaluate the effects of different concrete substrate repair methods such as replacing contaminated and damaged concrete with polymer-modified concrete (PMC) or injecting with crack-fill-only epoxy (CFO). The focus was to evaluate the post-repair corrosion. Beams measuring 6 in. × 8 in. × 108 in. were tested in four-point bending, as per Figure 31. Beams underwent one corrosion cycle before, and another one after the repair. Beams that utilized CFO performed better after the first corrosion cycle; however, PMC outperformed the CFO after the second cycle. Authors concluded that overall PMC repair performed better; it produced a more ductile failure and better durability of the test specimen.
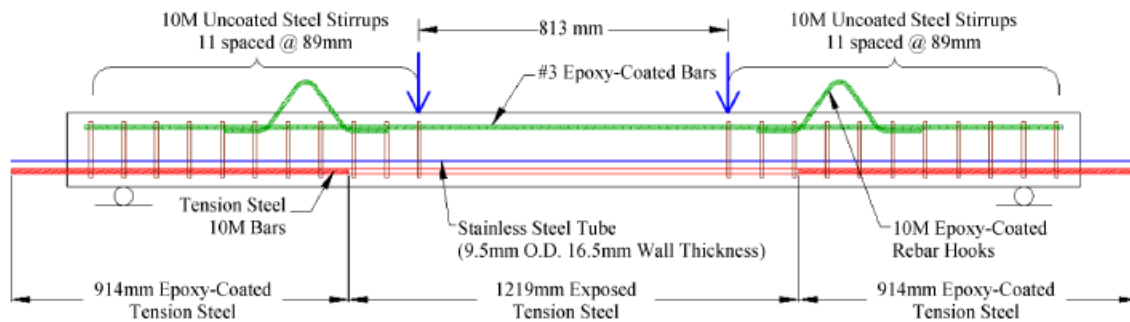
Figure 31—Substrate repair method study test specimen (Davalos et al., 2012)

Moreover, performance of three different FRP anchorage schemes (Figure 33 through Figure 35) was examined under both static and fatigue loading conditions in four-point bending (Figure 32). Beams measuring 6 in. × 8 in. × 78 in. were subjected to the similar accelerated corrosion cycles prior to testing. Authors found that anchorage scheme had insignificant effect on newly repaired beams; however, they noted that more anchorage would be beneficial to the long-term durability, as the FRP-concrete bond is deteriorating over time. Based on the laboratory study authors recommended the repair procedure that consists of: (1) removal of deteriorated cover level concrete; (2) cleaning of steel reinforcement; (3) application of "epoxy scrub coat" treatment with corrosion inhibitor; (4) replacement of cover with PMC with corrosion inhibitors; (5) installation of FRP sheets; and (6) application of a minimum of two CFRP U-wrap anchors.
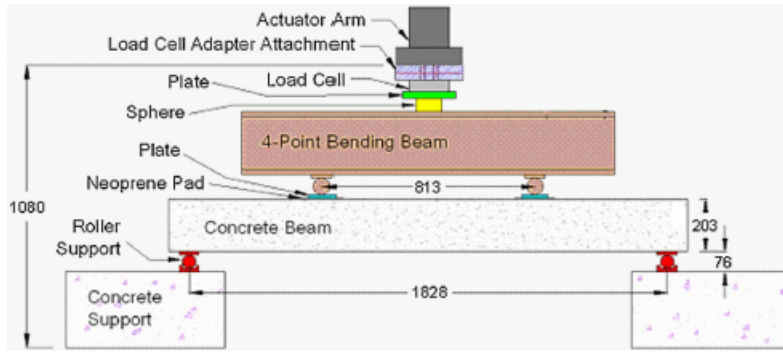
Figure 32—Anchorage scheme method study test specimen (Davalos et al., 2012)
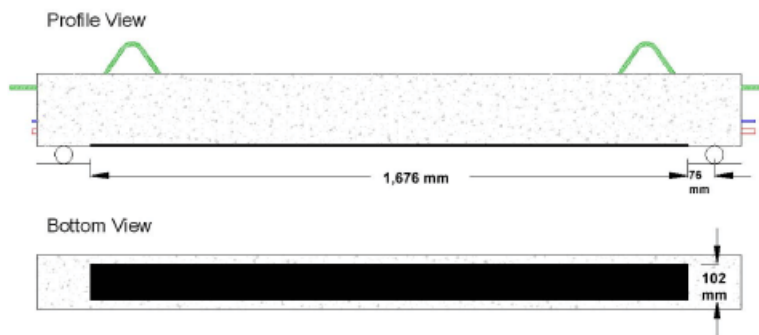
Figure 33—Wrapping scheme 1 (Davalos et al., 2012)
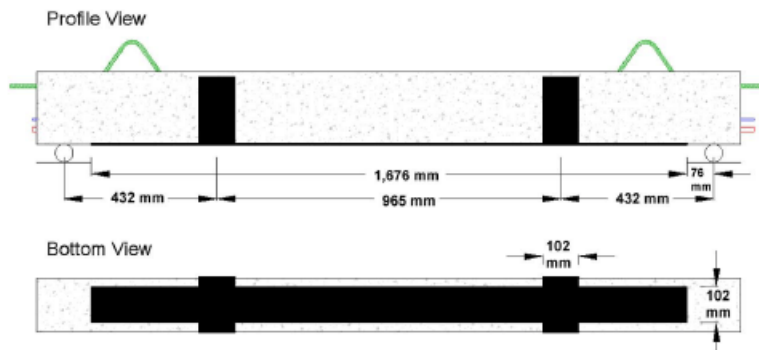
Figure 34—Wrapping scheme 2 (Davalos et al., 2012)
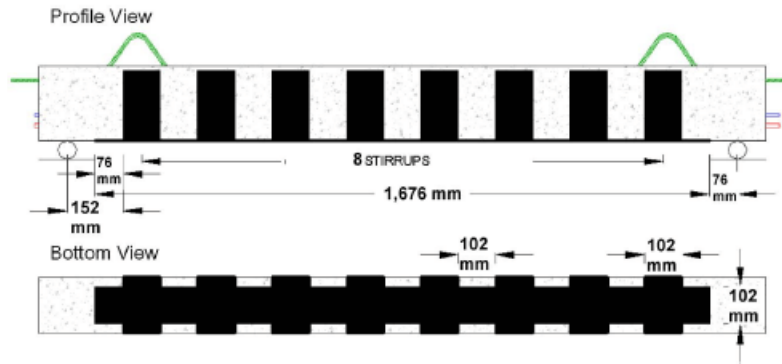
Figure 35—Wrapping scheme 3 (Davalos et al., 2012)

Atadero et al., (2013) conducted field assessment over a span of 8 years (2003-2011) on the prestressed concrete Castlewood Canyon Bridge, Colorado. The existing arches of the bridge were repaired with CFRP in 2003. The field assessment included void detection between concrete and FRP using acoustic sounding and thermographic imaging. Direct tension pull-off tests were used to check bond strength (Figure 36). Direct pull-off test showed weaker bond strengths in comparison to design values. Authors noted that results appeared consistent with material degradation. However, detail regarding which material was deteriorating (substrate, filler resin, or FRP) giving considerable contribution to degradation was not found. Tensile test were conducted on the CFRP removed from the field. Specimens 1 in. (2.5 cm.) wide and 8.5 in. (21.6 cm.) long were used. Specimens were tested in direct tension using universal testing machine promptly after returning from field in accordance with ACI 440.3R-04 (2004). Authors noted the ultimate strength and modulus of elasticity for each test and found that there is reduction in tensile strength significantly lower than the design value without considerable change in the modulus of elasticity. The study reported that number and size of voids underwent considerable increase over the inspection period. Direct pull-off test failure modes had a distribution with more failures occurring in the concrete layer. The study provided recommendations to improve quality of information gained from future field assessments. It appeared from the field assessment that some degradation had occurred over the eight-year service life; however, interpretation of data could not be validated due to lack of documentation and missing baseline values. Moreover, relative contribution of the material (substrate, filler resin or FRP) towards degradation also needs to be quantified.

Maaddawy et al. (2006) conducted full scale bending tests of concrete lighting poles repaired using E-glass and CFRP in wet layup with lateral confining wraps (unidirectional) as well as additional longitudinal flexure sheets (bidirectional) (Figure 37). Their approach included the development of a retrofit method for the repair of deteriorated reinforced concrete lighting poles. Test specimens used were 4 damaged poles with repair and 1 undamaged pole: (1) GFRP with lateral confining (unidirectional) (2) CFRP with lateral confining (unidirectional) (3) GFRP (bidirectional) (4) CFRP (bidirectional) and (5) undamaged. Wet layup FRP application was carried out on the damaged poles by preparing the surface, injecting cracks and damaged areas with epoxy resin, and impregnating of E-glass or carbon fiber textiles. After 7 days of curing, specimens were tested in cantilever bending according to CAN/CSA-A14-00 specification (CSA International 2000). The test results suggested that pole with bidirectional GFRP showed best performance in terms of obtained maximum load and tip deflection. The study reports that the

bidirectional FRP repaired poles exhibited superior flexural response in terms of the loading capacity, stiffness, deflection at failure, and increased ductility compared to the unidirectional FRP repaired and undamaged poles. The FRP repair introduced a change in failure mode from compressive flexure to tensile flexure.
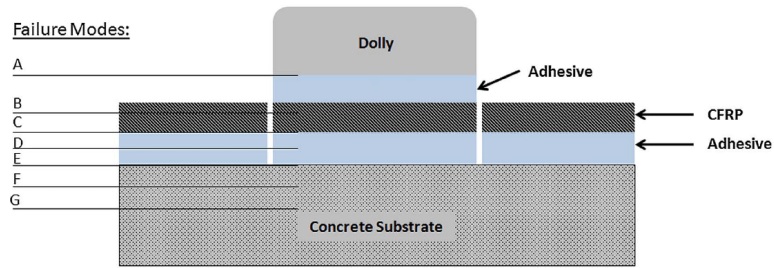
(a)
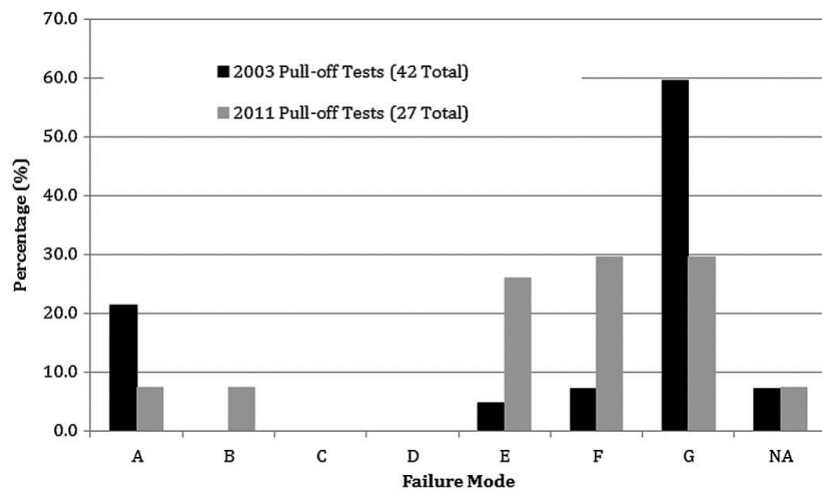
(b)

Figure 36—(a) Possible failure modes as per ASTM D7522-09 (b) distribution of failure modes (Atadero et al., 2012)
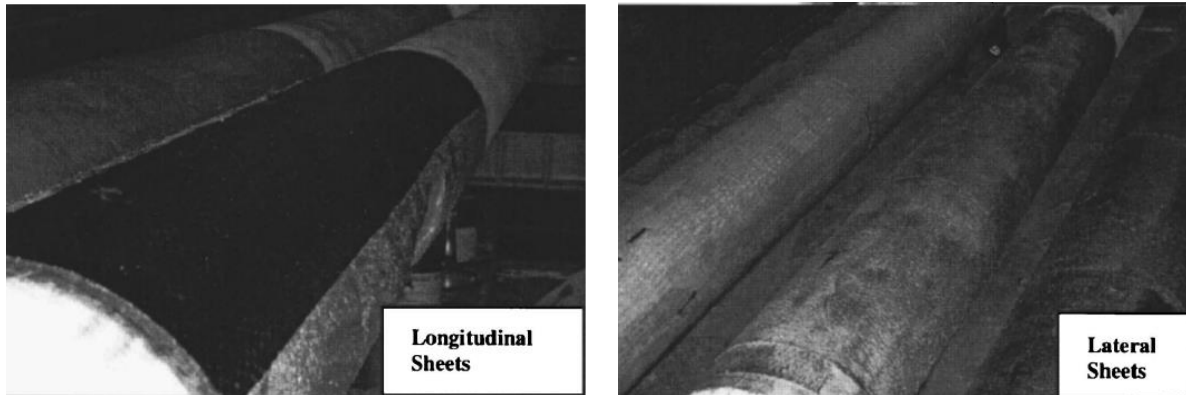
Figure 37—Longitudinal flexure sheets and lateral confinement sheets application (Maaddawy et al., 2006)

Labossiere et al. (2000) evaluated the possibility of utilizing FRP reinforcement in bridges in Quebec. The candidate bridge was chosen based on the live load rating factor LLRF of 0.94. The Sainte-Emelie –de-l'Energie is a single span bridge with four parallel reinforced concrete beams that form a T-section with the slab (Figure 38). Based on the analysis of the bridge, a 35% (strengthening ratio of 135%) increase in flexural strength and a 20% increase (strengthening ratio of 120%) in its shear strength were deemed required. Prior to FRP strengthening a laboratory study was conducted on scaled-down concrete beams (about 3 times) to examine the benefits of different FRP materials and strengthening configurations on the performance of repair, which confirmed the potential of utilizing FRP as a repair method (increase of up to 50% in ultimate strength was observed). Consequently, the bridge was strengthened with FRP, and electrical resistance strain gages along with Bragg Grating fiber optic strain gages were installed on the bridge to evaluate the efficiency of the strengthening procedure. Static and dynamic load tests were performed using three four-axle trucks each weighing 33 tons. A difference of up to 30% was observed between the same measurements made by fiber optic strain gages and electrical resistance strain gages; this was accredited to the sensitivity of fiber optic demodulating system to temperature changes. Load tests confirmed that behavior of FRP strengthened members was in line with design assumptions (plane sections remain plane; bond between concrete, steel, and composite is perfect; shear strain can be neglected; a proper anchorage is ensured to prevent premature debonding of the FRP) that were made.

Shahrooz and Boy (2004) conducted a series of load tests on a three-span reinforced concrete slab bridge (CLI-380-0032) that was repaired with different CFRP systems (Table 5 and Figure 39). Strain in the FRP was measured at three locations (Figure 40); concrete strain and slab vertical deflection was measured at 20 different locations. Load tests were performed before the repair, shortly after the repair, and after one year of service. Although the bridge was likely located in Ohio, neither the exact location nor the environmental conditions were specified. The environmental conditions Two standard Oregon Department of Transportation (FDOT) two-axle loaded dump truck, each weighing around 132 kN was used. Seven positioning schemes were chosen for the trucks to produce maximum positive moments in each span, and maximum negative moments in each pier. Truck loads were different up to 9% between different tests; consequently, measured values were normalized to account for it. Test results are presented in Figure 41.
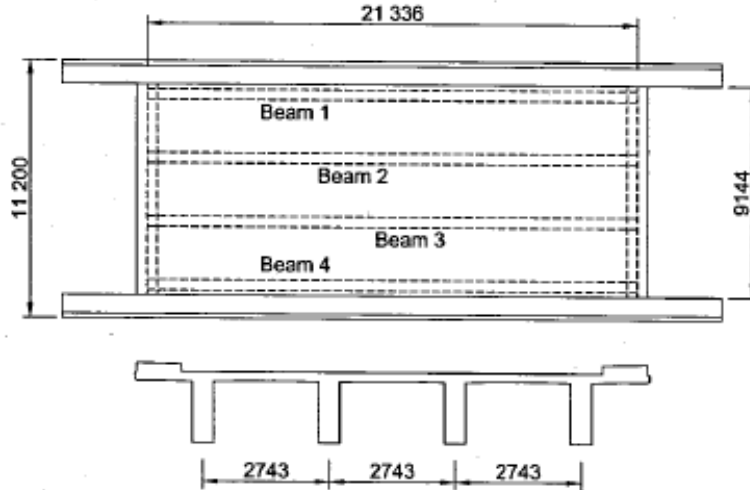
Figure 38—Sainte-Emelie-de-l'Energie bridge (Labossiere et al., 2000)

Authors noted that, based on the test results, FRP reinforcement did not have a significant influence on the overall stiffness of the bridge spans (maximum increase was 2.5%). Furthermore, it was concluded that test results suggest that the bonded FRP reinforcement showed no detectable degradation after 1 year of service. Visual inspection combined with sounding showed no signs of debonding or deterioration of FRP systems installed. The load rating factors of the repaired bridge were higher. Moreover, it was determined that the FRP strengthening provided an overall BSR of 122%. Also, authors noted that ACI 440 provisions for design of externally bonded FRP systems were somewhat conservative in the estimate of T-beam capacity, when compared to the measured experimental data (Figure 42).

Table 5—Properties of FRP systems used in the study (Shahrooz and Boy, 2004)

CFRP system	Thickness (mm)	σ_u (MPa)	E (MPa)	Fracture strain (%)
Type A and B: 76.2-mm wide plate	1.33	2,289	155,052	1.48
Type C: 127-mm wide plate	1.9	1,117	116,514	0.96
Type D: 305-mm wide carbon fabric	n/a	0.547 kN/mm	58.5 kN/mm	0.93
Type E: 102-mm wide bolted plate	4.83	585	53,095	1.10

Type A: 76.2 mm x 5.49 m CFRP Plates @ 305 mm O.C. (32 Plates)
Type B: 76.2 mm x 7.16m CFRP Plates @ 305 O.C (16 Plates)
Type C: 127 mm x 7.16 m CFRP Plates @ 457 mm O.C. (10 Plates)
Type D: 305 mm x 5.49 m CFRP Fabric @ 305 mm O.C. (16 Fabric Pieces)
Type E: 102 mm x 5.49 m CFRP Bolted Plates @ 305 mm O.C. (16 Plates)
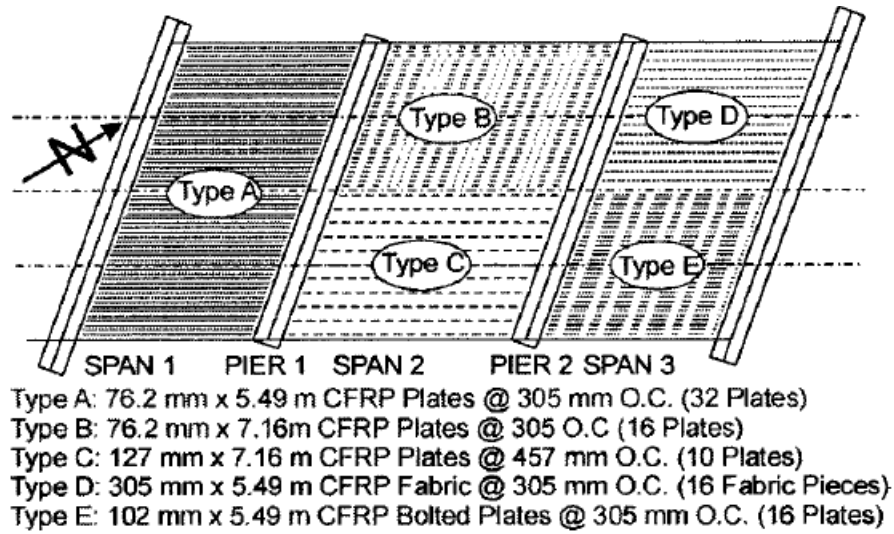
Figure 39—Locations of FRP repair systems (Shahrooz and Boy, 2004)

FRP Systems are shown partially.
SG21, SG22, & SG23: on FRP systems.
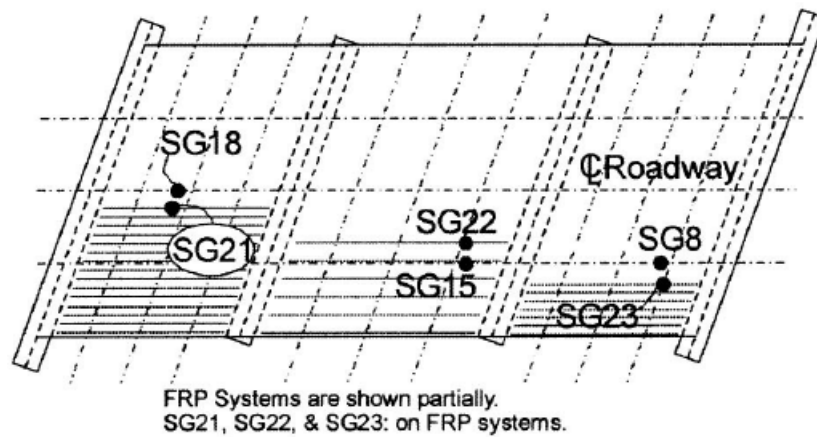
Figure 40—Locations of some of the strain gages: (1) on FRP (SG21, SG22, SG23); and (2) on concrete (SG8, SG15, SG18); Shahrooz and Boy (2004)
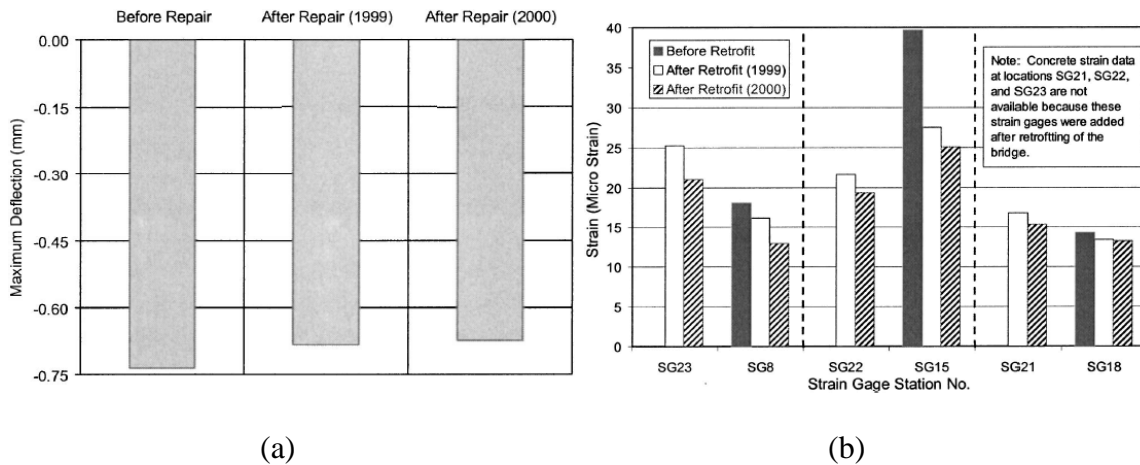
Figure 41—(a) Maximum slab deflection (b) maximum strains in slab and FRP (Shahrooz and Boy, 2004)
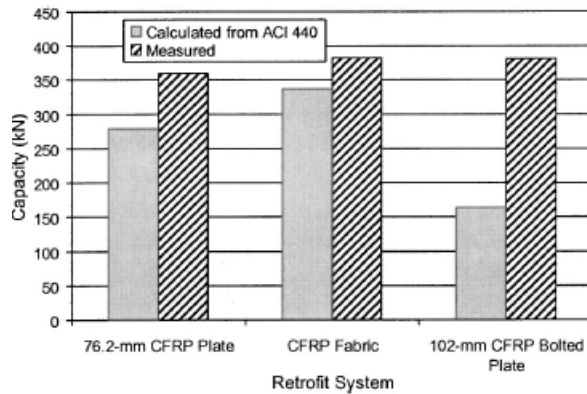
Figure 42—Comparison between measured and calculated capacity as per ACI 440

A similar study was performed by Sim et al. (2006) on a bridge built in 1938 in mid-south part of Korea peninsula (Figure 43 and Figure 44). The bridge consisted of one continuous reinforced concrete T-girder with three spans, one simply supported reinforced concrete T-girder, and two simply supported steel I girders. For the purpose of the study, the continuous T-girder was cut into three simple spans and each was strengthened with a different type of FRP: Carbon FRP sheet (CFRP), Glass FRP sheet (GFRP), and Aramid FRP (AFRP). To evaluate the effectiveness of strengthening designed as per ACI 440 (Figure 45), load tests were performed on each span with the concrete weight blocks of 2.9 kip and 5.7 kip. Blocks were added such that the load was 95% of the design flexural strength. Vertical deflections, steel reinforcement strain, and FRP reinforcement strain measurements were taken at the locations shown in Figure 46. Span 2 was tested both before and after strengthening. Authors concluded that all repair materials provided increase in flexural strength of repaired girders. No material delamination or debonding was observed. AFRP, however, experienced localized small-scale ruptures on the surface.
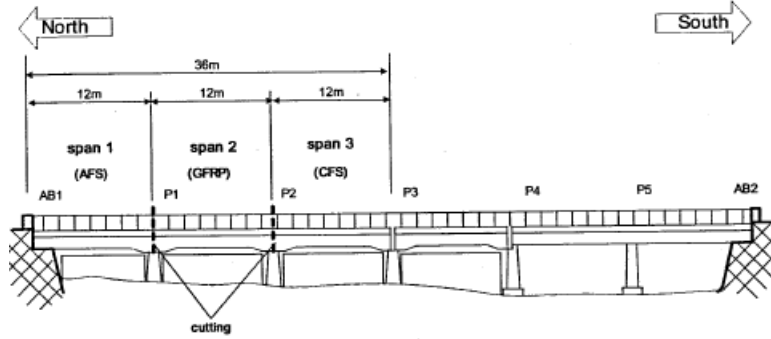
Figure 43—Bridge elevation view (Sim et al., 2006)
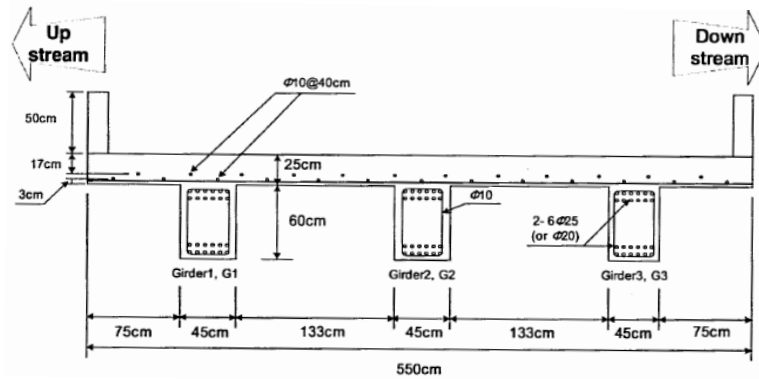
Figure 44—Cross-section view of test bridge girders (Sim et al., 2006)
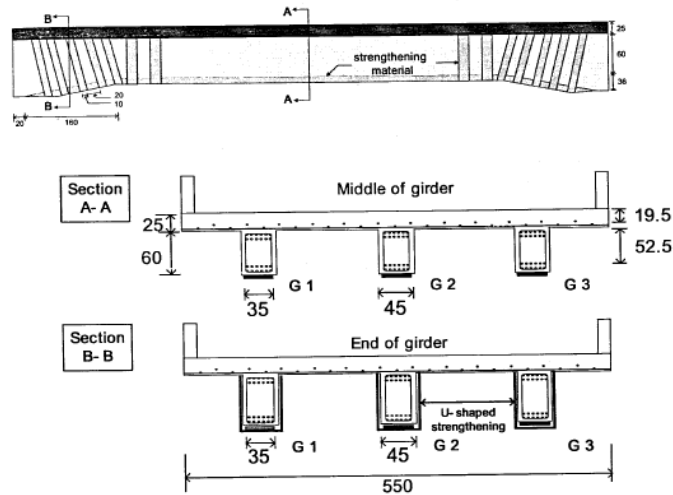
Figure 45—FRP strengthening details (Sim et al., 2006)
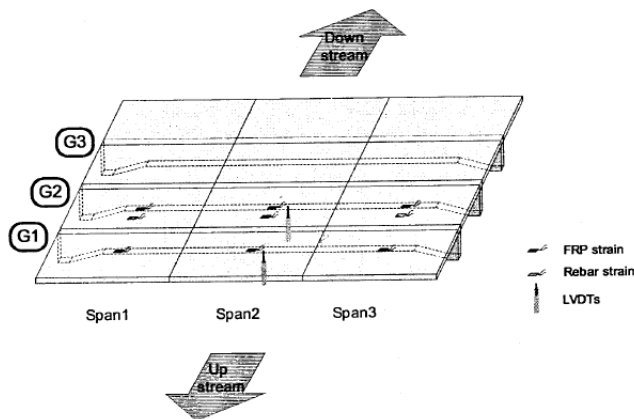
Figure 46—Location of instrumentation (Sim et al., 2006)

Myers et al.(2008) conducted load tests on five different bridges strengthened with bonded FRP reinforcement. This report is Volume 1 of 5 issued by the Missouri Department of Transportation (MoDOT). The following bridges were tested:

- Bridge X-596 in Morgan County, MO (strengthened with CFRP NSM bars for flexure and wet layup FRP for flexure and shear);
- Bridge T-530 in Crawford County, MO (strengthened with CFRP wet layup and CFRP laminates on the deck and girders);
- Bridge X-495 in Iron County, MO (strengthened with CFRP NSM bars and wet layup FRP);
- Bridge P-962 in Dallas County, MO (strengthened with CFRP NSM bars, wet layup FRP and steel reinforced polymer (SRP));
- Bridge Y-298 in Pulaski County, MO (strengthened with wet layup CFRP and mechanically fastened CFRP laminates in flexure).

The FRP strengthening of the tested spans for each bridge is summarized in Table 6.

Each bridge was loaded with dump trucks and displacements of the test span members were measured with a method utilizing survey equipment to facilitate the process of collecting the data. Multiple tests were performed in a time span of about 5 years. Bridges T-530 and P-962 experienced an increase in stiffness due to FRP strengthening, while for bridges X-495 and X-596 it was unfeasible to quantify the change in stiffness due to FRP strengthening. Authors noted, however, a decrease in stiffness of FRP strengthened members in bridges T-530 and P-962 over time, which was accredited to softening of the FRP materials, the deterioration of other bridge components, and softening of the adhesive due to thermal effects. To better show this finding, results for bridges P-962 and T-530 were presented in terms of percent change in deflection when compared to unstrengthened concrete member in respect to time (Figure 47).

Table 6—Summary of FRP strengthening on tested spans

Bridge & Tested Span	Girder	Flexural Reinforcement Description	Analytical Strengthening Ratio
X-596 Span 2	Interior	Wet layup FRP: 4 plies 20 in. wide; (4) CFRP NSM bars	142%
	Exterior	None	N/A
T-530 Span 2	Interior	1 CFRP laminate: 12 in. wide	129%
	Exterior	1 CFRP laminate: 12 in. wide	115%
X-495 Span 2	Interior	Wet layup CFRP: 5 plies 20 in. wide	140%
	Exterior	None	N/A
P-962 Span 1 & 2	Interior	Wet layup CFRP: 5 ploes16 in. wide; (4) CFRP NSM bars	156%
	Exterior	Wet layup CFRP: 3 plies 16 in. wide	125%
P-962 Span 3	Interior	SRP: 3 plies 16 in. wide	154%
	Exterior	SRP: 3 plies 16 in wide	149%

(a) (b)
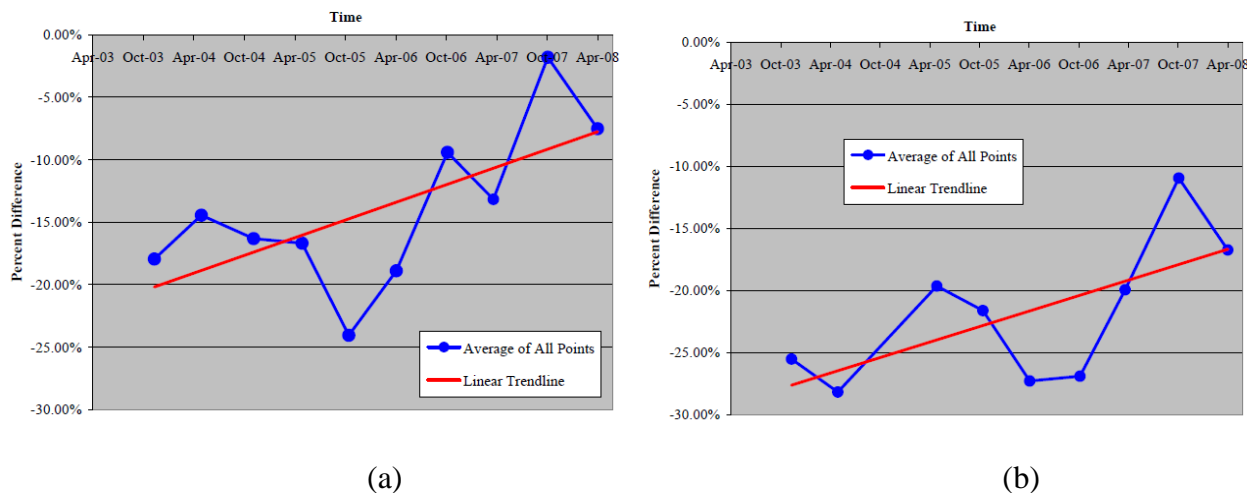
Figure 47—Average deflection percent difference for bridge: (a) P-962 and (b) T-530

The study included examination of normalized load distribution of each tested span to determine if FRP strengthening had affected it. It was found that in bridge P-962, FRP strengthened exterior girders took more load as the testing progressed. Furthermore, the distribution coefficients were increasing with time. Researchers explained this by the inconsistencies in installation of FRP system, as well as possible misalignments of the truck during testing.

Volume 2 of the MoDOT report, written by Kharkovsky et al. (2008), also presented the development of a near-field microwave nondestructive testing method with some examples. Volume 3 of the report (Watkins, 2008) describes the application of Fabry-Perot interferometric (EFPI) strain sensors in monitoring of FRP strengthened bridge. Volume 4 of the report, written by Maerz and Galecki, (2008), covers application of a laser profilometer and use of direct pull-off and direct torsion tests for quality control. Finally, volume 5 of the report, written by Myers

and Sawant (2008), discusses one possible analytical strength degradation approach to determine the life expectancy of FRP-strengthened bridges. The final four volumes are not discussed here, as they do not pertain to the purpose of this literature review.

Riggs et al. (2004) conducted a study to determine the applicability of FRP in repair of historic bridges in Hawaii by conducting a state-of-the-art literature review and experimental testing of FRP-repaired prestressed concrete girders. This study was later extended by Stockdale et al. (2012), who explored the application of Fiber-Bragg grating (FBG) sensors in a bridge that was externally repaired with FRP. Both authors found that FBG sensors could be applied to monitor strains in the FRP.

Stallings et al. (2000) performed a study on performance of FRP repair (CFRP laminate applied at the tension face with or without GFRP laminate on the sides of the girder) of a bridge on Alabama Highway 110 by comparing the results from pre-repair and post-repair static and dynamic load tests. Test results showed that measured strains in reinforcement were lower after the repair for both static (4% to 12% reduction) and dynamic loading condition (4% to 9% reduction). In addition, FRP repaired members experienced higher flexural stiffness for static (2% to 12% reduction) and dynamic test (8% to 12% reduction). Authors noted that addition of GFRP laminates on the sides of the repaired girders improved the performance of the repair (lower steel strains and smaller deflections when compared to girders with CFRP laminate at the tension face only).

Similarly, Carmichael and Barnes (2005) reported the repair with CFRP and results of pre- and post-repair (soon after installation of CFRP and twice about six months after the repair) load tests on the fifty-year-old War Memorial (Uphapee Creek) Bridge located in Alabama. The bridge was loaded with tri-axle trucks, and the strains in FRP and steel along with deflection data were collected. Authors found that the overall reduction in steel strain was around 5%. There was no significant difference between tests conducted soon after and six months after repair. As a part of the study, the integrity of bond was examined by coin-tap test method, and no serious delaminations were observed.

Similar findings were observed in a series of load tests conducted in New York State on FRP repaired bridges. After repair, these tests were performed by Hag-Elsafi et al. (2001) and Hag-Elsafi et al. (2002). FRP repairs caused shift of neutral axis downwards, lowering the strains in the steel, and increasing the stiffness. Furthermore, in a comparative study on the bond two years after repair, the authors concluded that no degradation in bond was observed.

3.7.1   Laboratory Studies

Kachlakev and McCurry (2000) evaluated the FRP repair design for Horsetail Creek Bridge near Portland, OR by conducting a laboratory study on bridge girder replicates. Four beams were constructed (control, flexure-only, shear-only, and shear & flexure) that followed the design presented in Figure 48 and Figure 49. CFRP was used for flexure, while GFRP was used as shear reinforcement. All beams were tested in four-point bending, with maximum applied force limited to 160 kip. Direct current displacement transducers and electrical resistance and fiber optic strain gages were placed at locations indicated in Figure 50 through Figure 52.

Control and flexure-only specimens both failed due to diagonal tension cracks (shear failure). In shear only specimens, tension steel yielded followed by crushing of concrete in compression. Shear & flexure specimen showed no signs of failure, even after being reloaded.

Flexure-only and shear-only beams both had an increase in strength of about 45% (strengthening ratio of 145%). The first test on the shear and flexure beam showed an increase of at least 50% in beam's strength (strengthening ratio of 150%), while the second test revealed a 99% increase in strength (strengthening ratio of 199%). All beams had an increase of around 30% in post cracking stiffness. Authors noted that the addition of GFRP in place of stirrups was successful in forcing the beam to fail by steel yielding, increasing the deflections at ultimate load by 200% compared to the control beam.
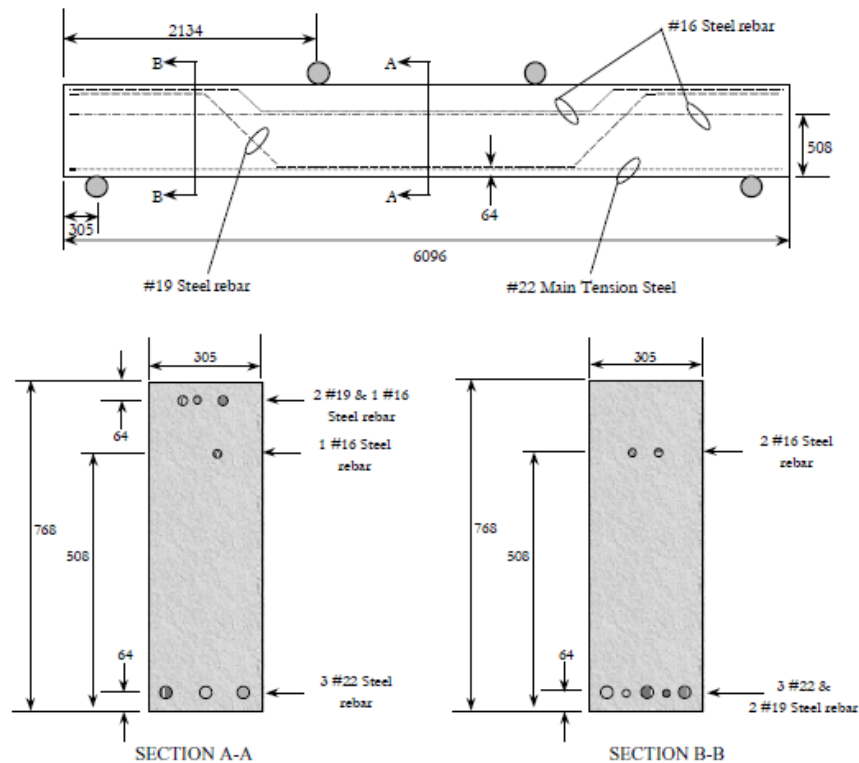
Figure 48—Reinforced concrete control specimen design (Kachlakev and McCurry, 2000)
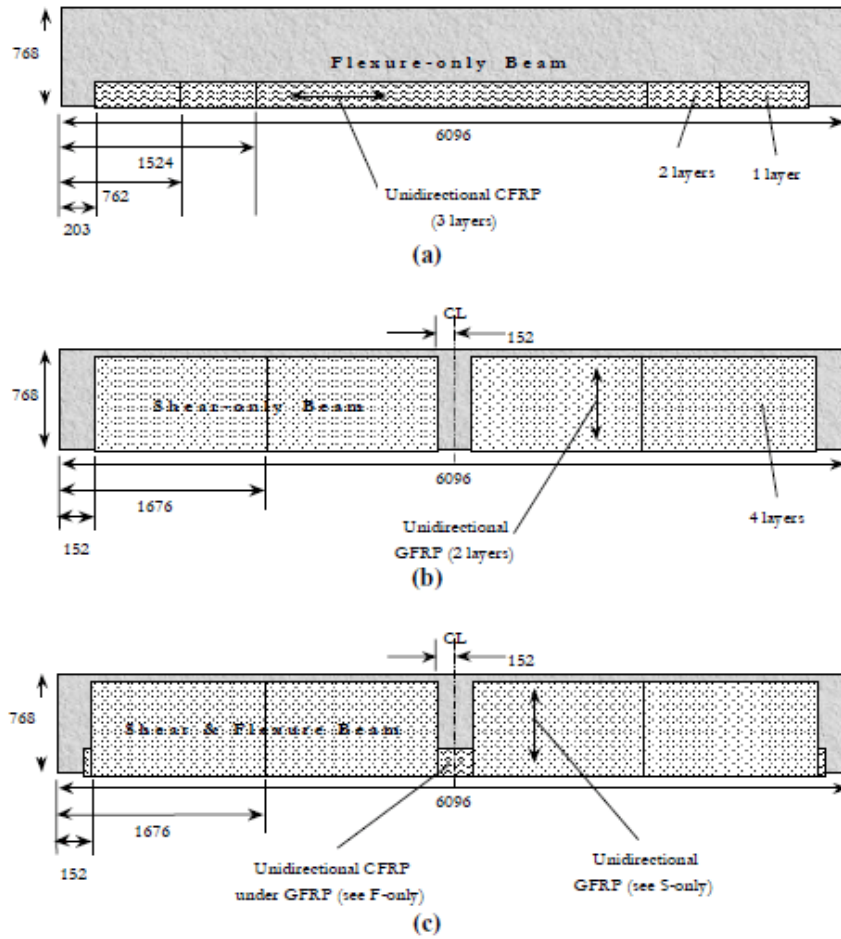
Figure 49—FRP strengthened girder: (a) flexure-only beam (b) shear-only beam; and (c) shear and flexure beam (Kachlakev and McCurry, 2000)
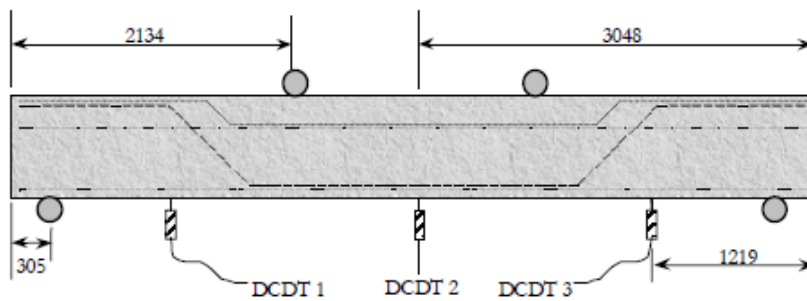
Figure 50—Location of displacement transducers (Kachlakev and McCurry, 2000)
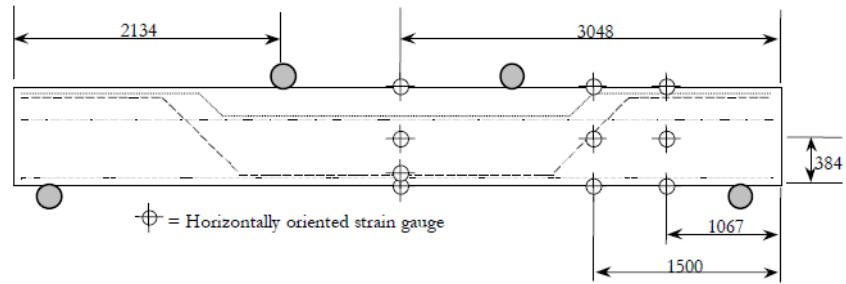
Figure 51—Location of electrical resistance strain gages (Kachlakev and McCurry, 2000)
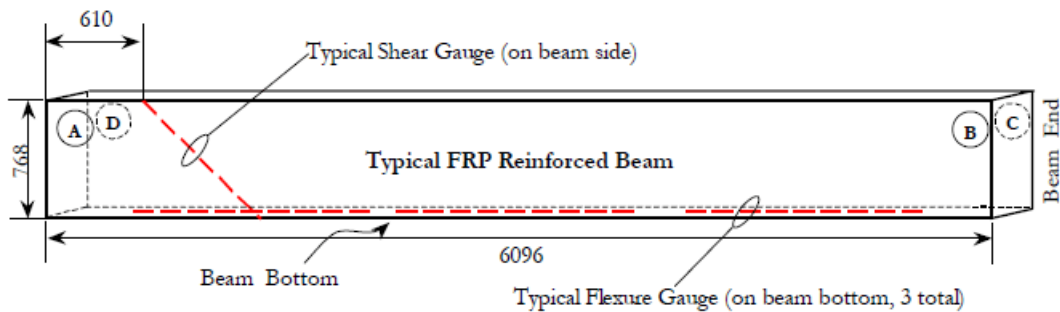
Figure 52—Location of fiber optic strain gages (Kachlakev and McCurry, 2000)

Reay and Pantelides (2006) performed a non-destructive evaluation of the CFRP repair on the State Bridge on Interstate 80 in Utah. A laboratory study followed on samples that were exposed to the field conditions on the bridge that included CFRP material load tests, load testing of confined concrete cylinders and direct tension pull-off bond testing to assess the quality of bond. The typical repair scheme is presented in Figure 53. The testing was performed after 6, 12 and 36 months after the repair.

Infrared thermography images revealed only a small number of voids. Authors found that UV coating had increased the resistance of the CFRP composite to environmental degradation. Destructive load tests (tensile coupon test, and direct pull-off bond test) revealed that specimens stored in the laboratory had 3 to 16% higher strength than the specimens stored on the bridge. Strength of confined concrete cylinders has decreased by 3% in laboratory specimens, and 8% in specimens conditioned in the field.
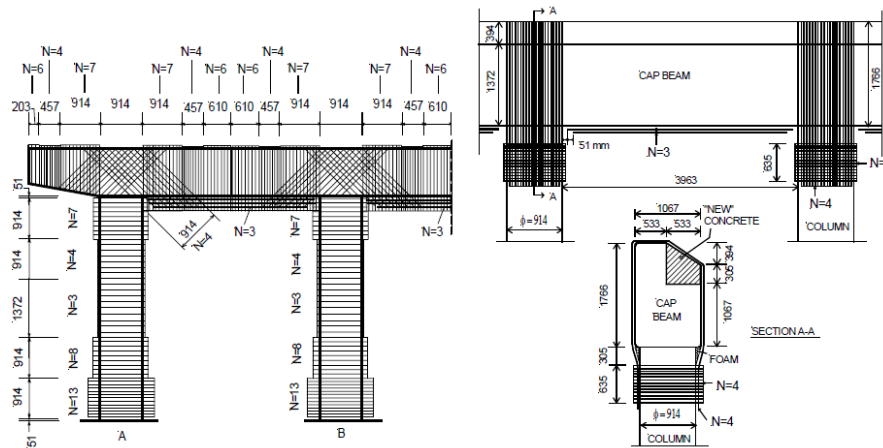
Figure 53—Typical bent CFRP strengthening scheme; N = number of CFRP layers (Pantelides et al., 2006)

Pantelides et al. (2011) conducted a durability study on FRP confined reinforced concrete columns. The study included medium sized laboratory specimens, and concentric and eccentric load tests under 2,000 kip on FRP-repaired bridge columns that were in service for 40 years (9 years rehabilitated) to determine the performance of FRP repair. Laboratory specimens were reinforced with steel rebar and spiral only, steel in longitudinal direction with a GFRP spiral (hybrid), and GFRP bars and spiral only. Before FRP wrapping, the laboratory specimens were conditioned in a 5% saltwater solution with a 6 V current impressed voltage to accelerate the corrosion process of internal steel reinforcement. Specimens were conditioned for a total of 11 weeks. Columns were then confined with CFRP and GFRP. Control specimens were not corroded. Specimens were finally tested in compression. As in previous studies, it was found that FRP wrapping slowed the corrosion process in hybrid specimens and there was no detrimental effects of corrosion noted. Hybrid columns also experienced a higher ductility. It was found that GFRP spiral prevented cracking due to tensile stresses caused by corrosion of steel. Less cracking helped lower the rate of corrosion to 1/3 of that observed in all-steel columns.

Two FRP repaired columns (12 ft. tall and 3 ft. in diameter) taken out of service were tested in compression (Figure 54). The column was instrumented with LVDT's and electrical resistance strain gages (Figure 55). Each column was tested using ten half-cycles: two half-cycles at each 400 kip increment up to 2000 kip. After the initial concentric and eccentric tests on the columns, two 1/8 in. slits were cut on compression and tension face of the column. The testing revealed the following findings:

1. CFRP jacket did not have adequate bond, which resulted in adhesive failure. Authors credited this to installation related issues.
2. A small amount of corrosion occurred in the column reinforcement after CFRP wrapping. The expansion from corrosion caused prestressing of CFRP confinement.
3. In general, columns performed well under a 2000 kip load in both concentric and eccentric test before the CFRP confinement was manually cut.

Figure 54—Column test setup (Pantelides et al., 2011)
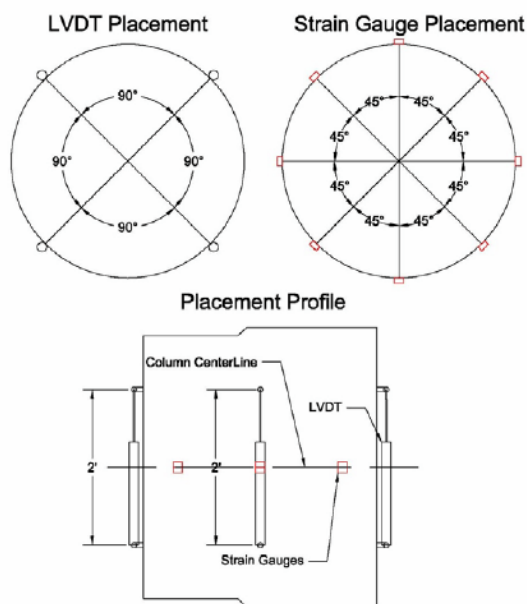
Figure 55—Instrumentation plan (Pantelides et al., 2011)

Higgins et al. (2009) performed a study on full-scale girders that were designed to resemble the 1950's proportions and detailing for conventionally reinforced concrete deck girders in highway bridges. The typical T and inverted T-beams (IT) are shown in Figure 56. The test matrix consisted of 6 T and 4 IT beams. Prior to FRP repair, the girders were cracked in flexure. All girders were then conditioned in freeze-thaw (one-hour soak at -16˚C, 30 minute ramp to 16˚C, a one-hour soak at 16˚C, and a 30 minute ramp back to -16˚C) or moisture conditions (submerged in an outside water tub). Testing was conducted in a four-point bending test setup. Prior to

testing, each beam was instrumented according to Figure 57. Testing was performed in multiple load cycles, each consisting of a 50 kip increase in load. Between loading cycles, cracking and debonding was identified by coin tap method and IR thermography.

It was found that CFRP increased the strength of all specimens. Using CFRP for shear reinforcement did not affect the flexural stiffness. Both exposure to moisture and freeze-thaw caused reduction in CFRP shear contribution. Freeze-thaw exposure caused a change in behavior of the shear reinforcement (decrease in stiffness). Authors explained this by the increase in debonded areas due to conditioning. Results indicated that the SR for T-beams ranged from 91 to 98% and 84 to 102% for IT beams.

IT Specimen (Typical)

T Specimen (Typical)

T Specimen (Typical)

Inverted T Specimen (Typical)
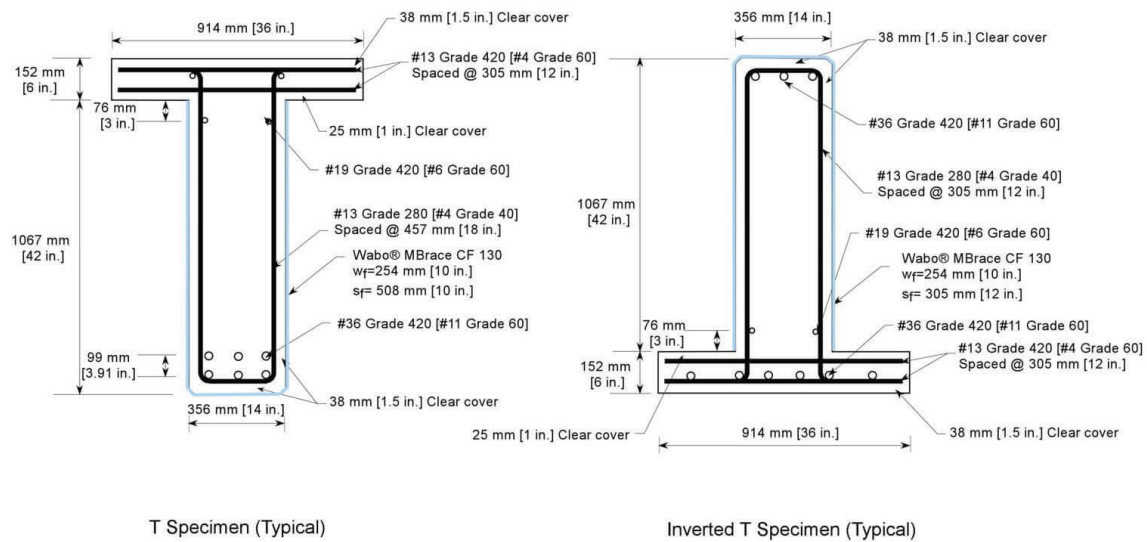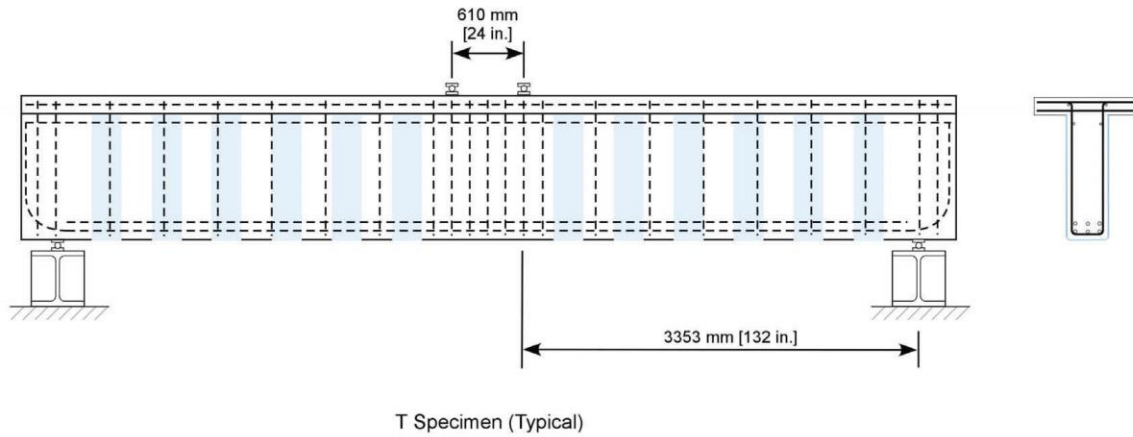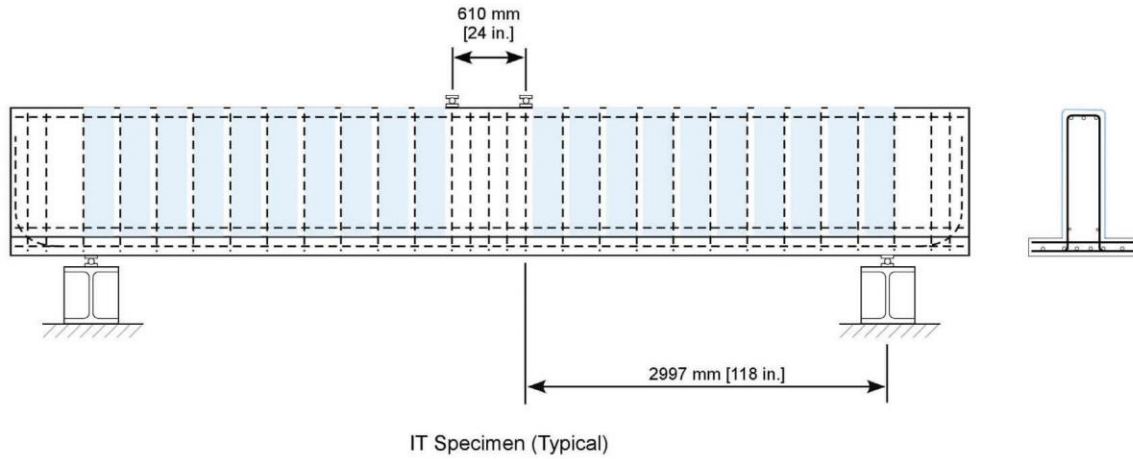
Figure 56—Typical T and inverted-T specimen design (Higgins et al., 2009)
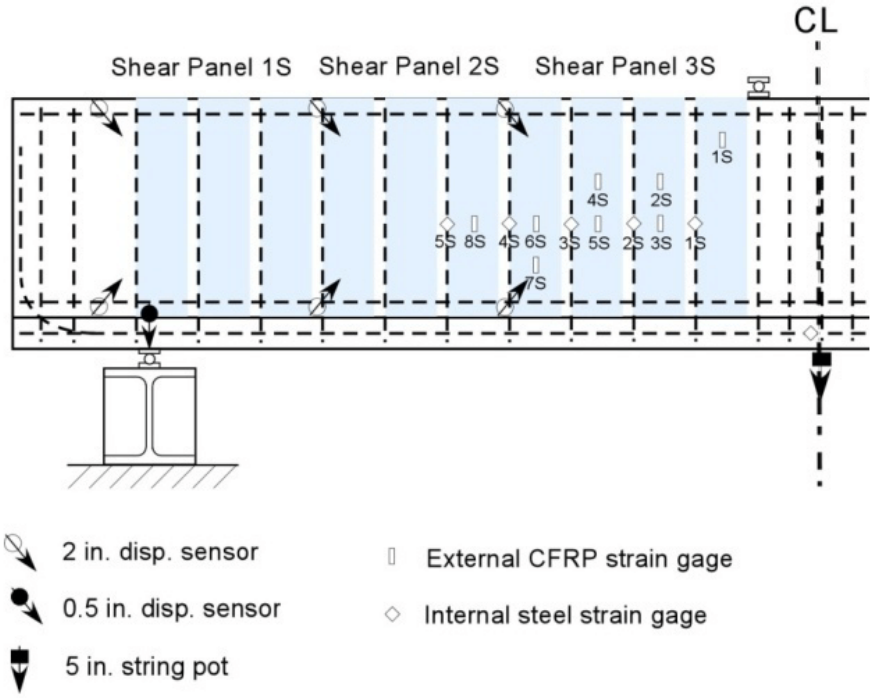
Figure 57—Typical instrumentation plan (Higgins et al., 2009)

4 Survey and Site Visits

4.1 Introduction

A survey was conducted to determine the extent of utilization of FRP reinforcement in Florida's bridges. Districts and municipalities statewide were contacted to gather information pertaining to FRP design documentation, availability of inspection reports before and after the repair, and reports from the load tests.

Site visits were also conducted on selected bridges to document the condition of FRP installations around the State. Documentation from multiple such visits are documented in this report. **Observations documented in this report as part of the site visits were for the purposes of this research project and should not be construed to represent a structural evaluation or rating of the bridge capacity.**

4.2 Survey

A formal survey (questionnaire in Appendix C) was conducted to form a database of bridges in Florida that contained externally bonded FRPs. Of special interest in the survey was the location of the bridge, age of repair, details about FRP materials used, and the availability of design documentation, inspection reports, and load test data. This information from the collected survey data is summarized in Table 7.

Table 7—Summary of survey responses

Bridge No.	Location	Repair Date	FRP	FRP source	Inspection reports?	Load test?
790035	Volusia County	2007	Wet layup CFRP	Unknown	Y	Y
570017	District 3	2015	Wet layup CFRP	Unknown	Y	N
570018	District 3	2015	Wet layup CFRP	Unknown	Y	N
110070	SR 91 NB over CR 561	2009	Wet layup CFRP	TREX Wrap TEC3-10U	Y	N
110074	Bridges Road over SR 91	2005	Wet layup CFRP	MAS-2000	Y	N
920027	CR 530 WB over SR 91	2010	Wet layup CFRP	TREX Wrap TEC3-10U	Y	N
920075	Ramp A over SR 91	2005	Wet layup CFRP	MAS-2000	Y	N
930144	45th Street over SR 91	2007	Wet layup CFRP	TREX Wrap TEC3-20C	Y	N
930144	45th Street over SR 91	2004	Wet layup CFRP	BASF MBrace CF160	Y	Y
930148	PGA Blvd Ramp over SR 91	2004	Wet layup CFRP	BASF MBrace CF160	Y	Y
104320	Phillips Lane, Hillsborough County	2001	Wet layup CFRP	Unknown	Y	Y
104323	Dickman Road, Hillsborough County	2014	Wet layup CFRP	Mapei	Y	N
104422	Durant Road, Hillsborough County	2013	Wet layup CFRP	Mapei MapeWrap C Bi-Ax 230	Y	N

4.3 Site Visits

4.3.1 Grenada Bridge

Initial visit to Grenada Bridge in Ormond Beach, FL (Figure 58a) occurred on Monday, September 29, 2014 to observe FRP repairs on the crash wall of Pier 8. On Monday, November 3, 2014, an additional trip was taken by personnel from FDOT State Materials Office (SMO) Corrosion Lab and eUniversity of Florida to perform coring for chloride content testing and

direct-tension pull-off bond tests on the crash wall of Pier 8 (Figure 58b). Additionally, control core specimens were taken from the middle foundation of Pier 7 and crash wall of Pier 9.

(a)   (b)

Figure 58—(a) Grenada Bridge (b) crash wall of Pier 8

Chloride penetration testing was conducted on 2-in. diameter cores collected from the aforementioned elements. Core lengths ranged from 3-5 in., depending on the concrete cover thickness at cored locations. The cored locations were repaired with a grout filler material normally used for this purpose by the FDOT SMO Corrosion Lab technical specialists. Chloride content tests were conducted by SMO Corrosion Lab.

Pull-off testing was performed in accordance with ASTM D7522 (Figure 59b) to assess the bond capacity of the bonded FRP composite. On Monday, November 3, 2014, pull-off locations were scored and test disks were attached. On the following day (November 4, 2014), pull-off tests were conducted.

FRP-concrete bond was evaluated by coin-tap method during the initial visit; based on the results it was concluded that the bond was in good condition. Pull-off testing, however, revealed that bond strength was less than 200 psi (Table 8), which is recommended by ACI 440.2R-08 and NCHRP (2010) specification. In addition, the failure modes (Figure 60) were typically adhesive and not cohesive; cohesive failure mode in which the failure plane passed through the concrete is preferred. The adhesive failure modes for the majority of the performed tests may indicate a degradation in bond over the service life or perhaps initial installation problems. This could only be confirmed if pull-off tests were conducted immediately following installation of the CFRP composite for comparison purposes. Exact locations of pull-off tests are included in Appendix B.

<center>(a)</center> <center>(b)</center>

<center>Figure 59—(a) Coring (b) direct tension pull-off test apparatus</center>

<center>Table 8—Summary of direct tension pull-off test results</center>

Test No.	Failure stress (psi)	ASTM D7522 failure mode
PN1	336	Failure mode F
PN2	200	Failure mode F
PS1	164	Failure mode G
PS2	0*	Failure mode E*
PN3	0*	Failure mode C*
PS3	111	Mixed mode D and mode E

*bond failed during coring prior to testing

Based on the review of available documentation, the original intent of the repair was not clear. Furthermore, it is not clear if the design of FRP repair was intended to be bond critical or contact critical. If the FRP wrapping was supposed to function as a bond critical application, then the state of FRP bond (based on the available results from pull-off tests) is not satisfactory and the repair may not perform as intended. However, if the anticipated function of FRP was contact critical, the FRP wrap may perform well (only minor debonding was observed during coin-tap).
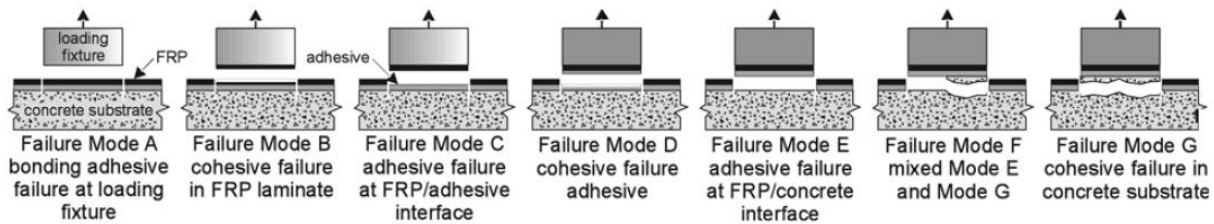
Figure 60—Failure modes for pull-off test (ASTM D7522)

Chloride concentrations (coring locations and test results summarized in Appendix B) reveal that the standard industry threshold for chloride concentration of 1.2 lb/yd^3 (ACI 222R) was exceeded at coring locations below the high tide water line, while all locations above the high tide water line, on the FRP wrapped crash wall, had significantly lower concentrations of chlorides. Concrete jacket repair on Pier 9 had low chloride concentrations both below and above the high tide water line. The highest chloride concentrations were observed on the foundation of Pier 7; this may be accredited to the foundation geometry, as well as the lack of FRP wrapping. Based on the available data, it is not clear if FRP had any contribution in preventing the diffusion of chlorides into concrete.

4.3.2   Hillsborough County Bridges

On Monday May 4, 2015, UF met with the Hillsborough County Public Works (Nils Olsson, Senior Professional Engineer and Rodney Phillips, Engineering Technician)) and performed site visits to FRP-repaired bridges in the area. Currently, there are multiple concrete bridges in the Tampa area with FRP repairs:

1. Berth 21 at Port of Tampa – I girders wrapped with CFRP
2. Phillips Lane - Bridge #104320 – double T bridge girders wrapped with CFRP in 2001
3. Dickman Road – Bridges #104323 – multiple piles wrapped with CFRP in Dec, 2014
4. Durant Road – Bridge #104422 – single exterior column wrapped with FRP in 2013 (impact damage)
5. Friendship Trail Bridge – Bridge #100068 – former interstate 275 bridge that was converted to a pedestrian bridge – multiple piles wrapped with FRP

Additionally, pedestrian park wooden bridges were repaired with FRP:

1. Alderman's Ford Regional Park – three glulam bridges repaired with FRP
2. Upper Tampa Bay Trail – three timber columns were wrapped with CFRP, a few pile caps were wrapped with GFRP

Details from the site visits are summarized in Figure 61.
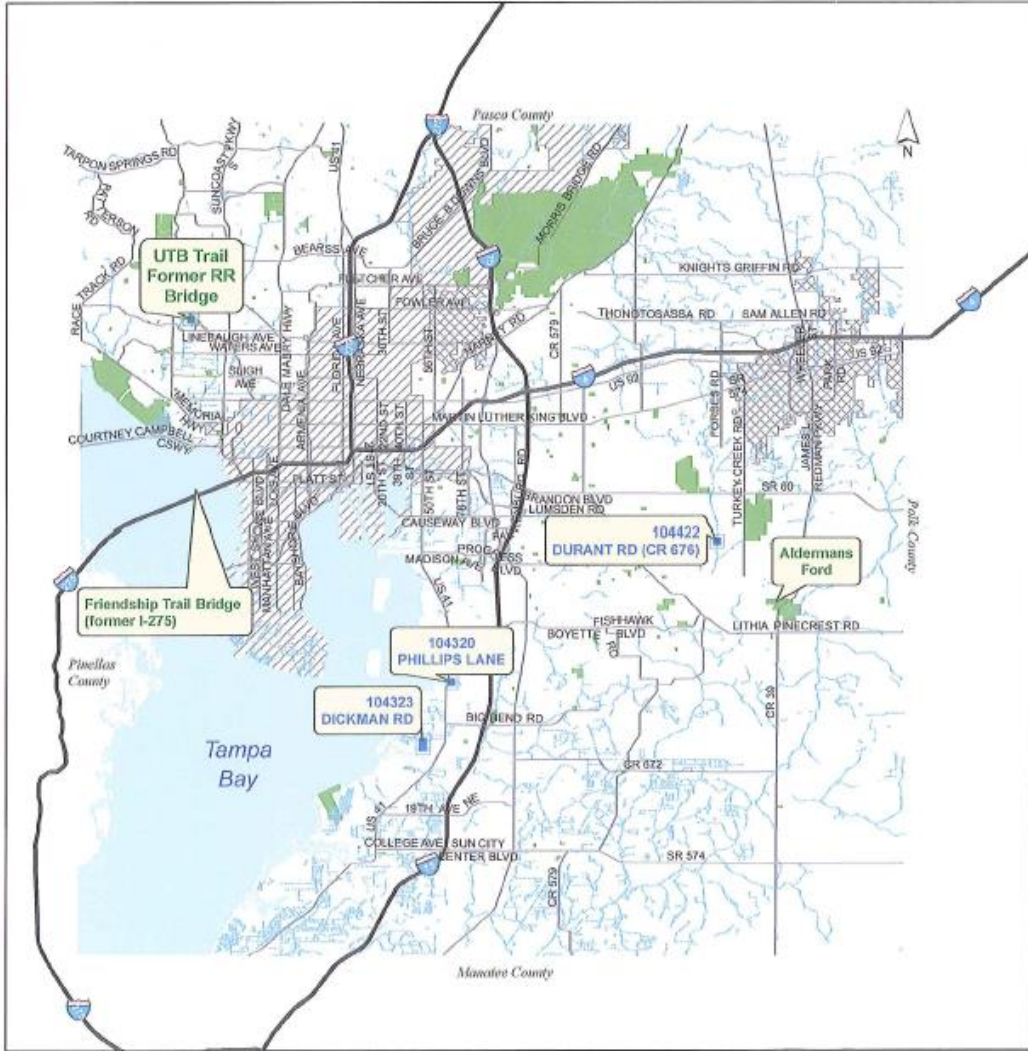
Figure 61—Locations of bridges with external FRP in Hillsborough County

4.3.3   Hillsborough County Bridges: Berth 21 at Port of Tampa

Berth 21 at Port of Tampa was repaired in 2011 with FRP wraps by Premier Corrosion Protection. The span adjacent to the abutment experienced significant spalling due to corrosion, which affected the load-carrying capacity of the span. Two precured CFRP laminate strips were applied at the tension face, and then the girders were wrapped. No significant debonding was noted when the FRP was sounded with coin tap. CFRP installation photos and site conditions are shown in Figure 62 and Figure 63. A coating, most likely to match the finish of the concrete material and serve as a UV protection, was applied on the surface of the CFRP wrap.

Figure 62—CFRP laminate strip installation at Port of Tampa Berth 21

Figure 63—Site conditions at Port of Tampa Berth 21

4.3.4 Hillsborough County Bridges: Phillips Lane Bridge

Phillips Lane bridge experienced significant corrosion damage (brackish water environment), and was repaired with CFRP wraps in 2001. No significant deterioration of the composite wrap was observed (Figure 64), with an exception of one girder where an entire side of the wrap was debonded as observed during the visual inspection (Figure 65) based on visual inspection. The debonded CFRP was located on one of the vertical faces of the concrete channel girder; close proximity of adjacent webs would have made accessing the concrete for surface preparation and CFRP installation difficult. Observation of multiple pull-off test locations (performed in the past) revealed rust staining and adhesive failure modes (Figure 66). The inspection was performed in 2015.

Figure 64—Girders with external FRP on Phillips Lane Bridge

Figure 65—Debonded FRP wrap on a double tee girder

Figure 66—Pull-off test locations on Phillips Lane Bridge indicate adhesive failure modes. It is not known when these pull-off tests were conducted

4.3.5 Hillsborough County Bridges: Dickman Road Bridge

Two piles were repaired by wrapping with CFRP (Figure 67 and Figure 68). Coin tap sounding revealed minor debonding in both piles. Decay of the coating was apparent in the exterior pile, most likely due to exposure to sunshine.

Figure 67—Repaired piles on Dickman Road Bridge

Figure 68—FRP-confined piles on Dickman Road Bridge

4.3.6 Hillsborough County Bridges: Durant Road Bridge

An impact damaged pile (Figure 69) on Durant Road Bridge was confined with CFRP. Coin tap sounding revealed two debonded regions shown in Figure 70. The middle section of the superstructure was also repaired with CFRP (Figure 71), presumably to offset the damage due to a longitudinal crack in the deck crossing multiple spans.

Figure 69—Cracking at the base of pile due to impact

Figure 70—FRP-confined pile on Durant Road Bridge

Figure 71—Repaired superstructure on Durant Road Bridge

4.3.7 Sunshine Skyway

Portions of the approach spans in the Sunshine Skyway Bridge, located in Tampa, FL, were recently repaired using a wet layup CFRP system. To alleviate the effects of cracking in shear-critical regions (near the supports), multiple locations were wrapped with CFRP composite strips (Figure 72a). At the time of the repair, researchers from University of Florida installed 4 test patches (24 in. × 24 in.) at the approach span girders of the north abutment of the bridge for the purpose of determining the durability of bond between the composite and concrete substrate by means of direct pull-off testing (ASTM D7522). Tests were performed after 6 and 18 months of exposure.

Test locations were first sandblasted by the contractor. Two patches installed on the interior girder and one patch on the exterior girder were installed as per manufacturer's instructions; all three components of the system were used (primer, putty, and CFRP). One patch on the exterior girder was installed without the putty layer to determine the effects of putty on bond durability. Twenty-four hours after installation one-half of each patch was coated with a UV protective coating. Patches were divided vertically for coating to account for possible effects of rainfall on the bond durability (Figure 72b, Figure 72c). Interior and exterior girder locations were chosen to minimize/maximize (respectively) influence of UV irradiance, rainfall, diurnal temperature fluctuations, etc. on the bonded system.

(a)   (b)   (c)
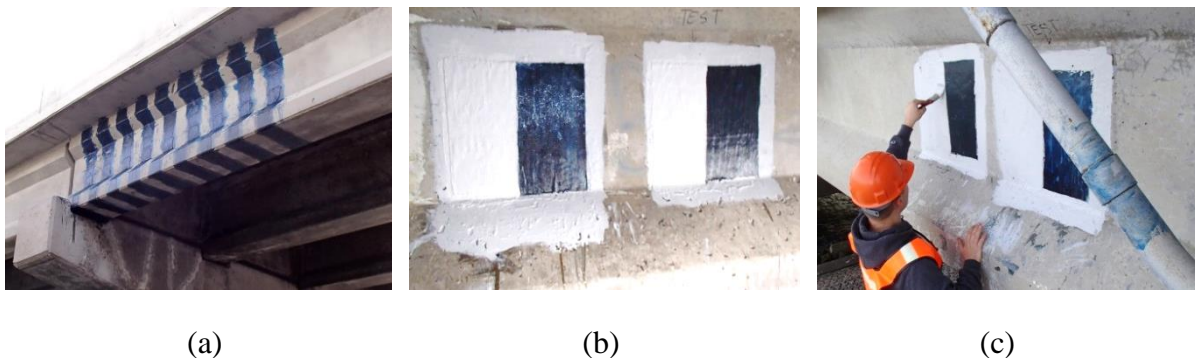
Figure 72—(a) Repair of Sunshine Skyway Bridge (b) interior girder test patches and (c) exterior girder test patches

Testing on the girder FRP patches was conducted after 18 months of exposure. At each time interval, four direct tension pull-off tests were performed per patch (two from an area with UV coating and two from an area without UV coating), making it a total of 16 tests. Test locations were prepared by first coring the desired location to approximately 0.25 in. deep, and adhering a dolly. The pull-off testing was conducted 24 hours following the preparation of testing locations, to assure proper cure of the adhesive used to bond the dollies to the test patch. The pull-off test data is summarized in Table 9. Failure modes were recorded as a percent of surface that failed adhesively. Percentages were expressed in increments of 5% based on visual observation (Figure 73).

<div align="center">(a)   (b)   (c)</div>
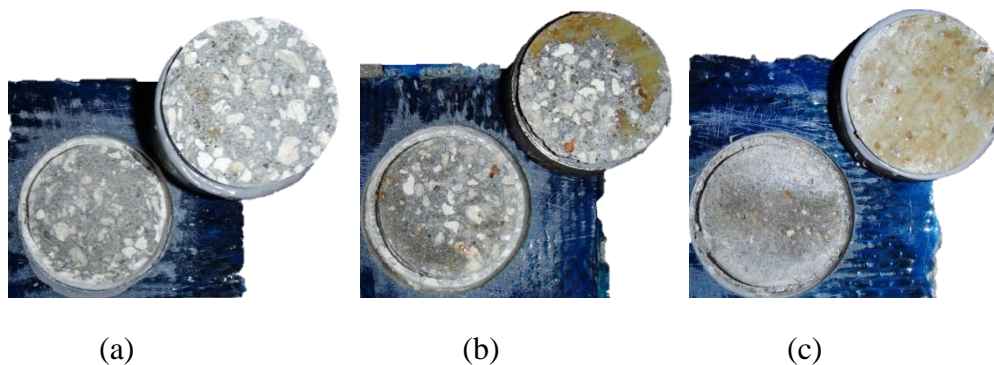
Figure 73—Typical failure modes in direct tension pull-off test: (a) cohesive (0% adhesive) (b) 30% adhesive and (c) 100% adhesive

Twenty-four control tests were conducted by the contractor, within a 24 to 48-hour time window following the installation of the FRP repair. The mean of all tests was 322 psi with a COV of 7.8%, with six of the total tests having a cohesive failure mode, while five exhibited the undesired failure mode through dolly-adhesive interface (failure mode C, as per ASTM D7522). All normalized strength values in Table 9 were calculated relative to the obtained mean value of control tests.

As per ACI 440.2R, for a test to be considered passing, the stress at failure should be a minimum of 200 psi, followed by a cohesive failure. Other failure modes, such as adhesive failure mode are not explicitly discussed in the design guidelines; they are rather left up to a "licensed design professional for evaluation and acceptance". Direct pull-off test results suggest that all tests satisfied the strength criterion (Table 9).

A more compelling evidence of higher degradation of FRP-concrete bond in the exterior girder is observed when comparing the failure mode data between the two girders. The presented results in Figure 74a show an increase in adhesive failure mode characteristics from interior to exterior girder, with the difference being apparent for the 18-month tests; typical failure modes that were observed on the interior and exterior girder are shown in Figure 75 and Figure 76. A comparison of test data obtained from locations with UV coating to those without it, on the exterior girder (at 18 months of exposure), reveals the existence of correlation between the presence of UV coating and the failure mode. As shown in Figure 74b, adhesive failure mode characteristics increased at the location without the UV coating, indicating that UV radiation may be a significant contributing factor to the bond degradation. Effects of radiation were observed on the surface of CFRP composite without UV coating in the form of scaling and change in color of the saturating

resin; the interior girder patch locations without UV coating maintained the same color and glossy finish that was obtained following the initial cure of the composite.

Table 9—Summary of field direct pull-off test

Location	UV coating?	18 months		
		Stress at failure (psi)	Normalized	Failure mode (% adhesive)
1 – Interior #1	Y	477.5	1.485	0
2 – Interior #1	Y	416.3	1.295	0
3 – Interior #1	N	533.5	1.659	15
4 – Interior #1	N	404.3	1.257	5
5 – Interior #2	Y	567.2	1.764	10
6 – Interior #2	Y	571.4	1.777	0
7 – Interior #2	N	344.4	1.071	0
8 – Interior #2	N	335.5	1.043	0
9 – Exterior #1	Y	251.8	0.783	10
10 – Exterior #1	Y	359.7	1.119	0
11 – Exterior #1	N	397.3	1.235	40
12 – Exterior #1	N	212.6	0.661	70
13 – Exterior #2	Y	441.2	1.372	15
14 – Exterior #2	Y	403.9	1.256	50
15 – Exterior #2	N	470.8	1.464	90
16 – Exterior #2	N	248.9	0.774	10
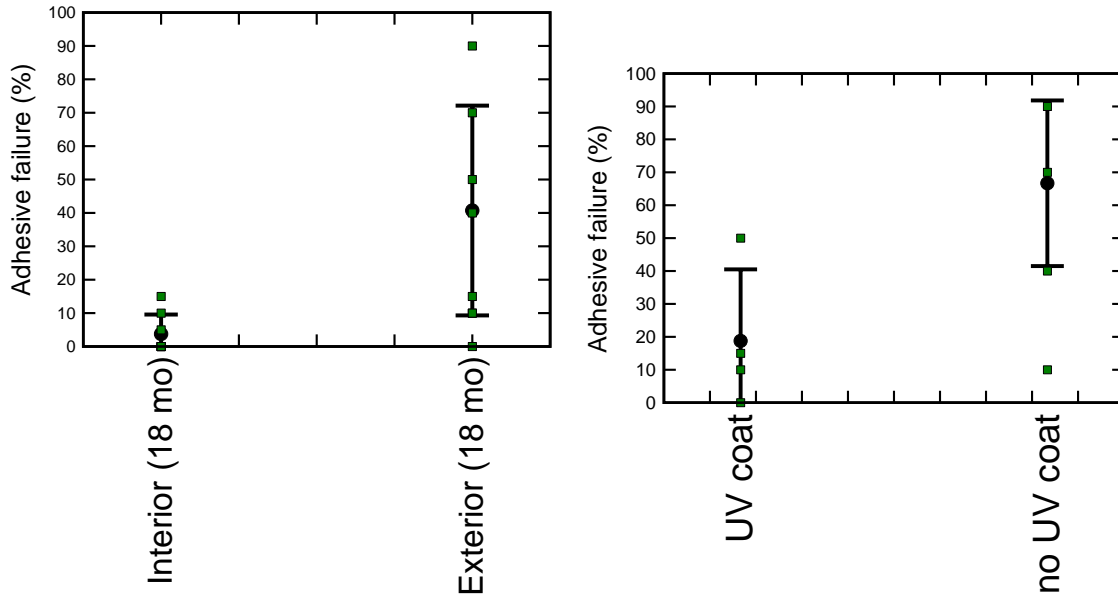
(a)   (b)

Figure 74—(a) Distribution of adhesive failure modes amongst the test groups (b) distribution of
adhesive failure mode characteristics on exterior girder

(a)   (b)

Figure 75—(a) Typical cohesive failure mode (b) typical mixed failure mode

(a)   (b)

Figure 76—(a) Typical adhesive failure mode (system with putty) (b) typical adhesive failure
mode (system without putty)

5   Indian River

5.1   Bridge History

The Indian River Bridge is located at the east end of the Melbourne causeway and connects the cities of Melbourne, Florida and Indialantic, Florida (bridge # 700037). The bridge is a part of the Melbourne causeway, which is approximately 1.25 miles (2 km) long and carries State Road 500 across the Indian River Lagoon in Brevard County. It was originally constructed in 1948 and was widened in 1969. The two test girders used in this study were collected from the widened portion of the bridge span, marked in Figure 77. The girders were salvaged from the bridge in 2010.

Figure 77—Indian River Bridge plan view

The exact locations of the test girders are specified in Figure 78 and Figure 79. The bridge was a cast-in-place slab and girder bridge that was typical of short span construction in Florida in the 1950's and 1960's. The girders were simply supported for a span of 36 ft. (11 m) from pier to pier with expansion joints at every pier. The bridge contained six spans. The girders were supported by direct concrete bearing against the top of the pier cap. It was typical of this form of construction to use asphalt-saturated paper under the girder bearing.
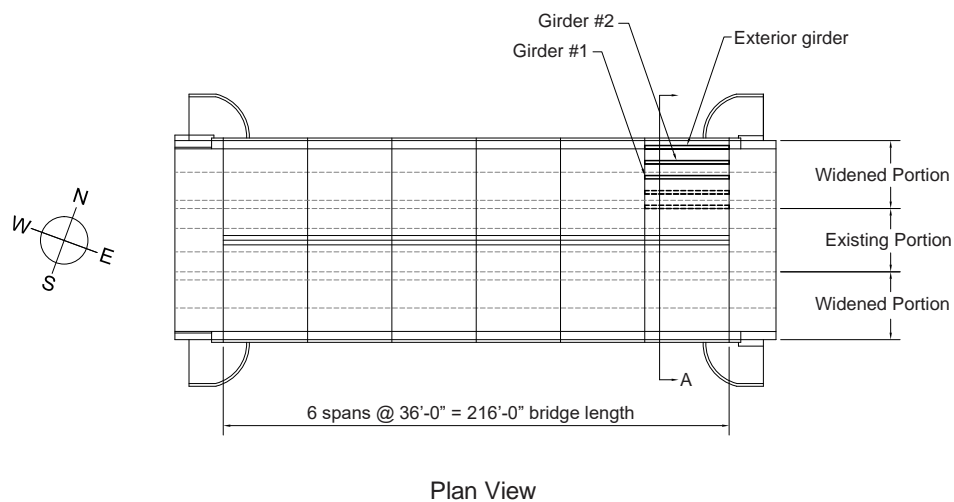
Plan View

Figure 78—Plan view of Indian River Bridge
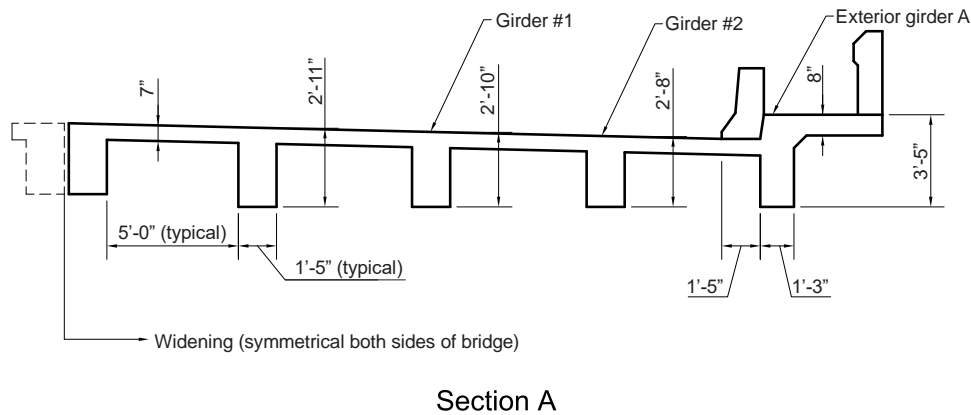
Section A

Figure 79—Cross-section view of widened portion of Indian River Bridge

In the early 1990's, the girders had shown signs of corrosion, which was particularly severe in the span adjacent to the abutment (Figure 80). Tidal fluctuations put the water level within 3 to 5 ft (1 to 1.5 m) of the bottom of the girders. Near the abutment, wind-driven waves splashed salt water onto the underside of the girders and accelerated the corrosion. Little is known about the repair other than the system was a commercially available system. Florida Department of Transportation (FDOT) records indicate that both wet layup and precured laminate bonded reinforcement were applied to the girders. The repaired span was at the east end of the bridge with one end supported on the abutment (Figure 81). The first FRP repair on the bridge apparently had degraded and was reapplied in 1999. Neither the details of the first repair nor the characteristics of the degradation are known. The repair material was a wet layup CFRP system composed of bi-directional (0-90 deg.) carbon sheets (Figure 82).

Figure 80—Indian River Bridge – corrosion damage

Figure 81—North elevation view of Indian River Bridge

Figure 82—Exterior Indian River Bridge girder wrapped with bidirectional CFRP

Girders were extracted from the bridge by saw-cutting the north side of the deck, while the south side was hammer-jacked. Cross-sections of the girders with steel reinforcement are shown in Figure 83; the hammer-jacked side of the deck is represented by irregular lines. Axisymmetric view of east end (abutment) of a typical girder is shown in Figure 84. The coordinate system shown in Figure 84 was adopted throughout this report.

(a)   (b)
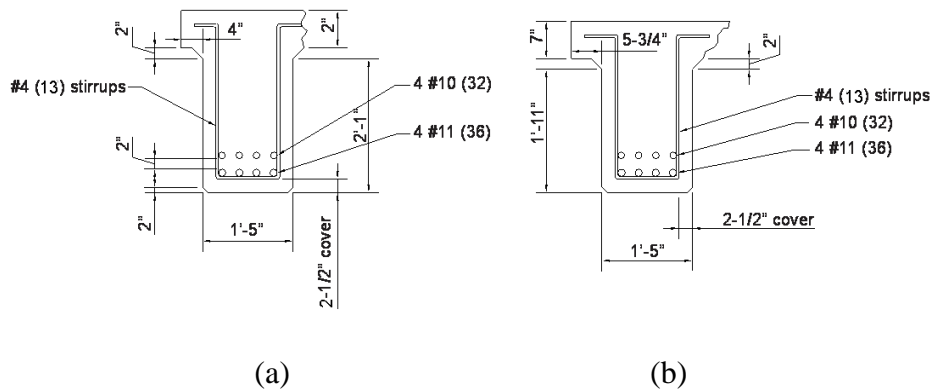
Figure 83—Cross-section of (a) Girder #1, and (b) Girder #2
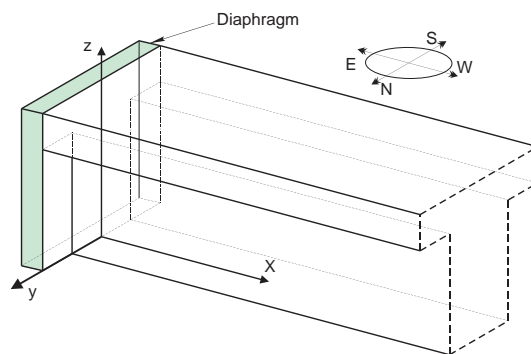
Figure 84—Axisymmetric view of east end of typical girder with specified coordinate system location

5.2   IR Scanning

5.2.1   IR Scanning Procedures

Infrared (IR) Thermography inspections were performed on both girders. Complete scans of the bottom, north, and south faces prior to and after the structural testing were collected. Additionally, scans were taken on Girder #2 during the loading and unloading phase of the structural test (in the service loads range). These scans were confined to a small area near midspan due to time constraints.

For the purpose of IR scanning, areas of CFRP on each girder were divided into multiple zones. The size of each zone was dictated by the resolution of the IR camera and the size of the area that could be heated effectively with eight halogen lamps (Figure 85).
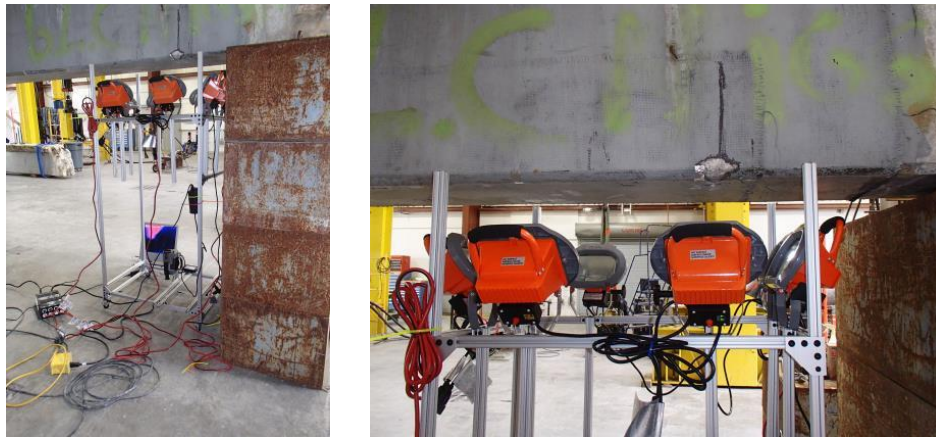
Figure 85—Heating of CFRP surface with halogen lamps

The heating profile that was applied to each zone consisted of four, single-cycle sinusoids with the following periods of 5, 10, 20, and 40 s, resulting in total heating and acquisition time for each zone of 75 seconds.

The IR scans prior to the structural test were completed using a FLIR PM695 IR camera. The image size was 240×320 pixels and the image save rate was one frame per second. Scanning following the load tests was completed using the FLIR A655sc, which has an image size of 480×640 pixels; images were saved at a rate of three frames per second.

The series of images obtained for each of the four periods in the time domain was processed using a least-squares sinusoidal curve fit to obtain the corresponding phase shift for each pixel. This resulted in four images (one for each period) for each zone. Once processing was complete for all of the zones on a given side (north, south, or bottom), the images for each period were stitched together to form a composite phase image of each side (Figure 86 through Figure 91).
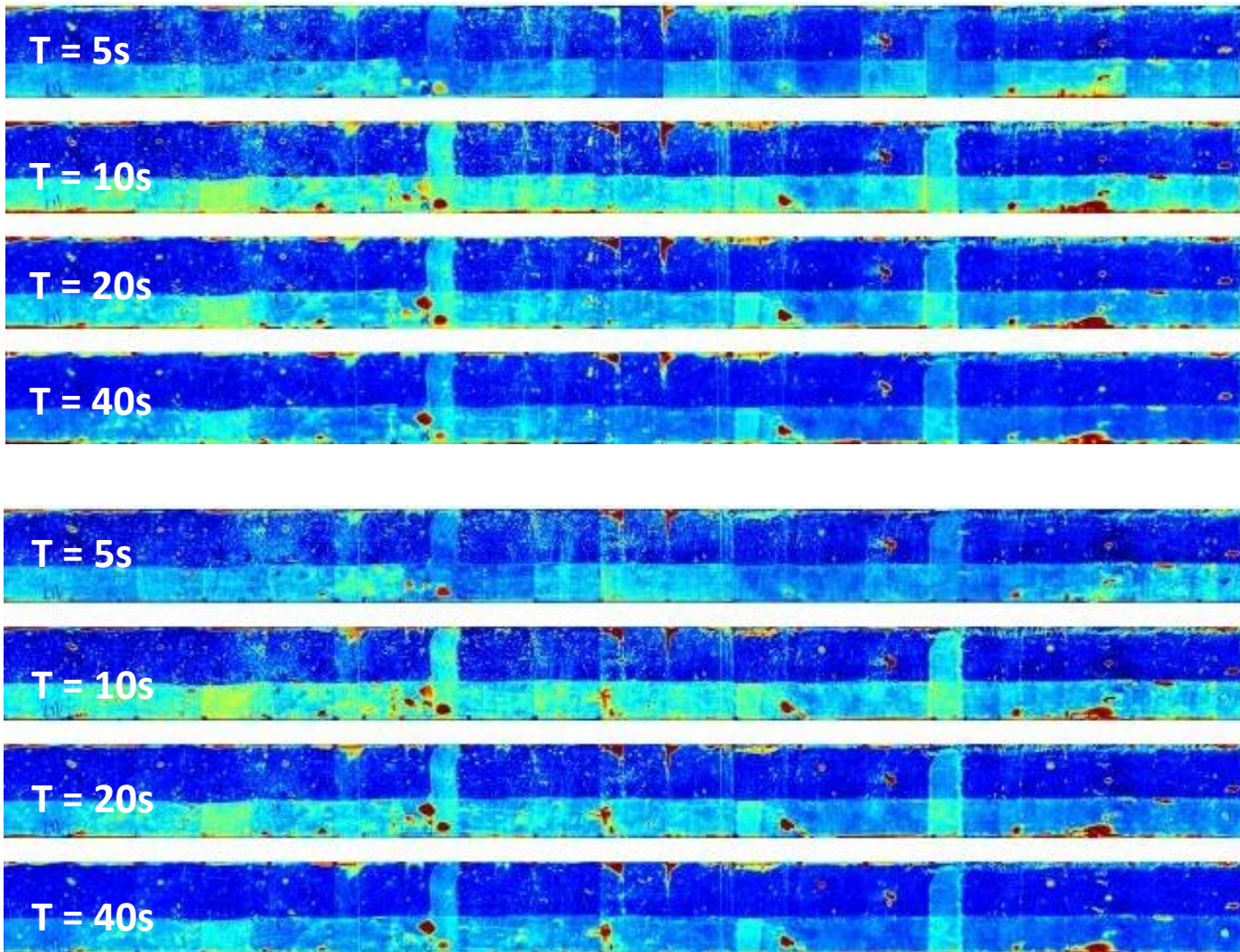
Figure 86—Girder #1 – south face: prior to structural test (top), and after structural test (bottom)
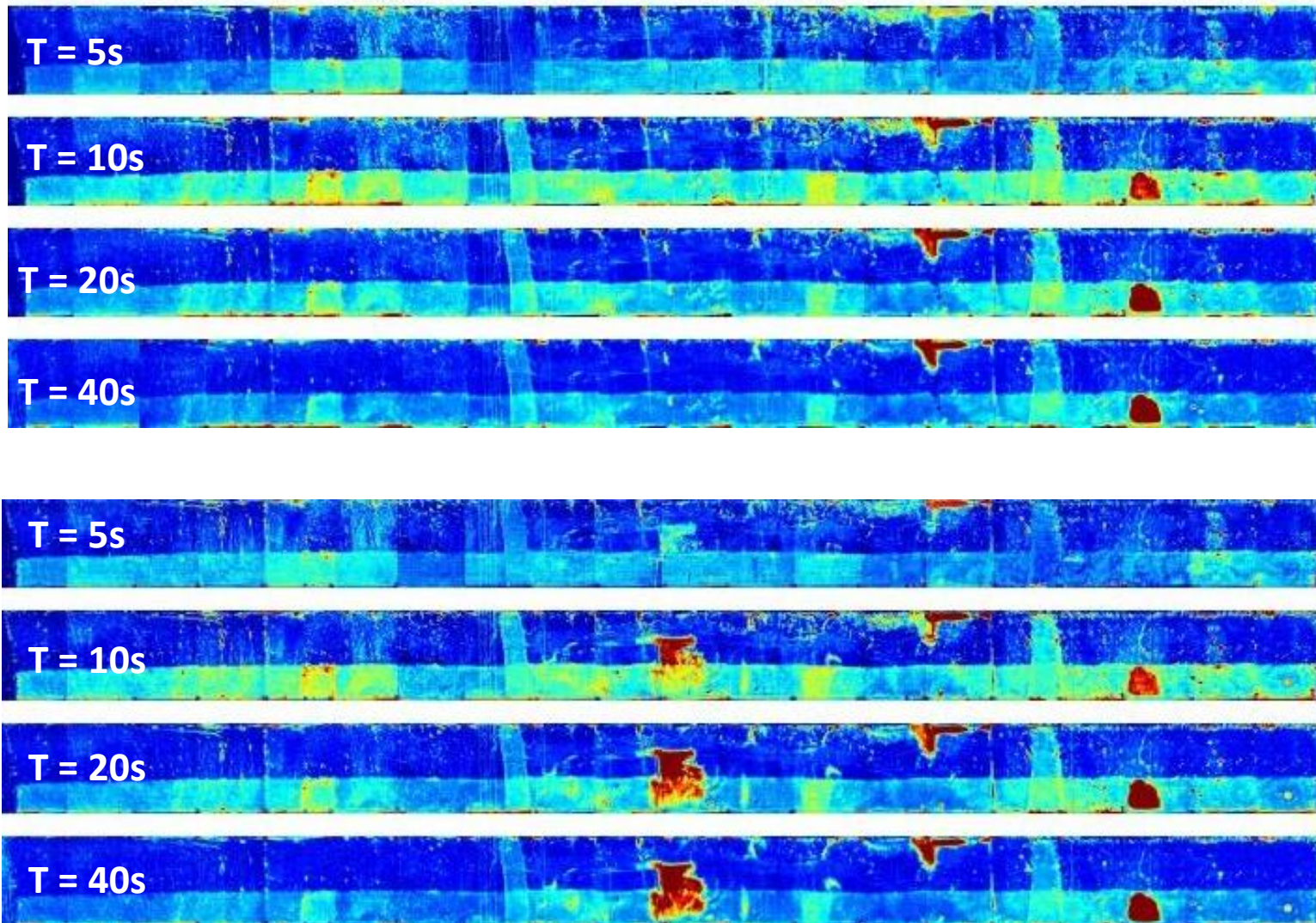
Figure 87—Girder #1 – north face: prior to structural test (top), and after structural test (bottom)
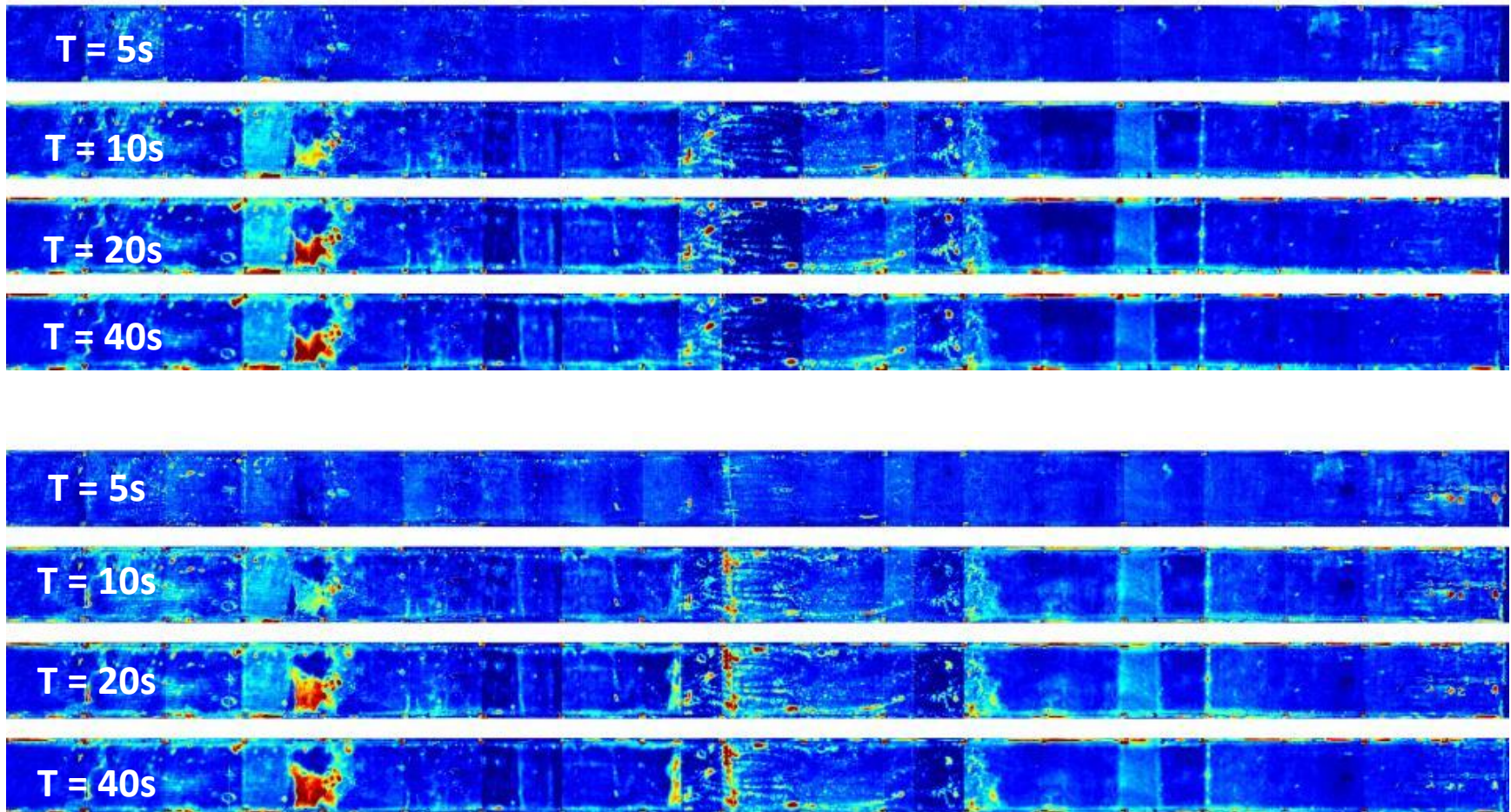
Figure 88—Girder #1 – bottom: prior to structural test (top), and after structural test (bottom)
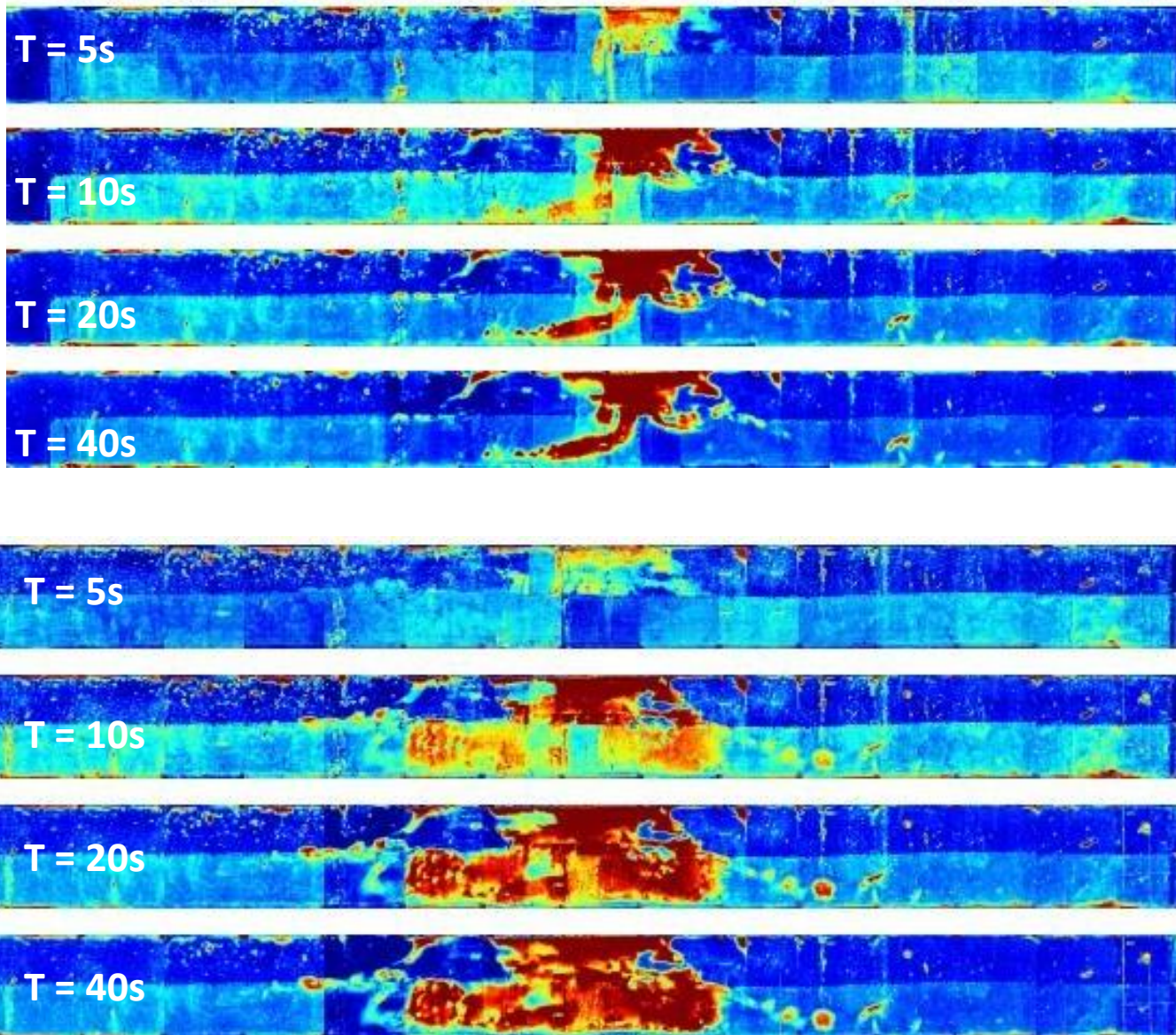
Figure 89—Girder #2 – south face: prior to structural test (top), and after structural test (bottom)
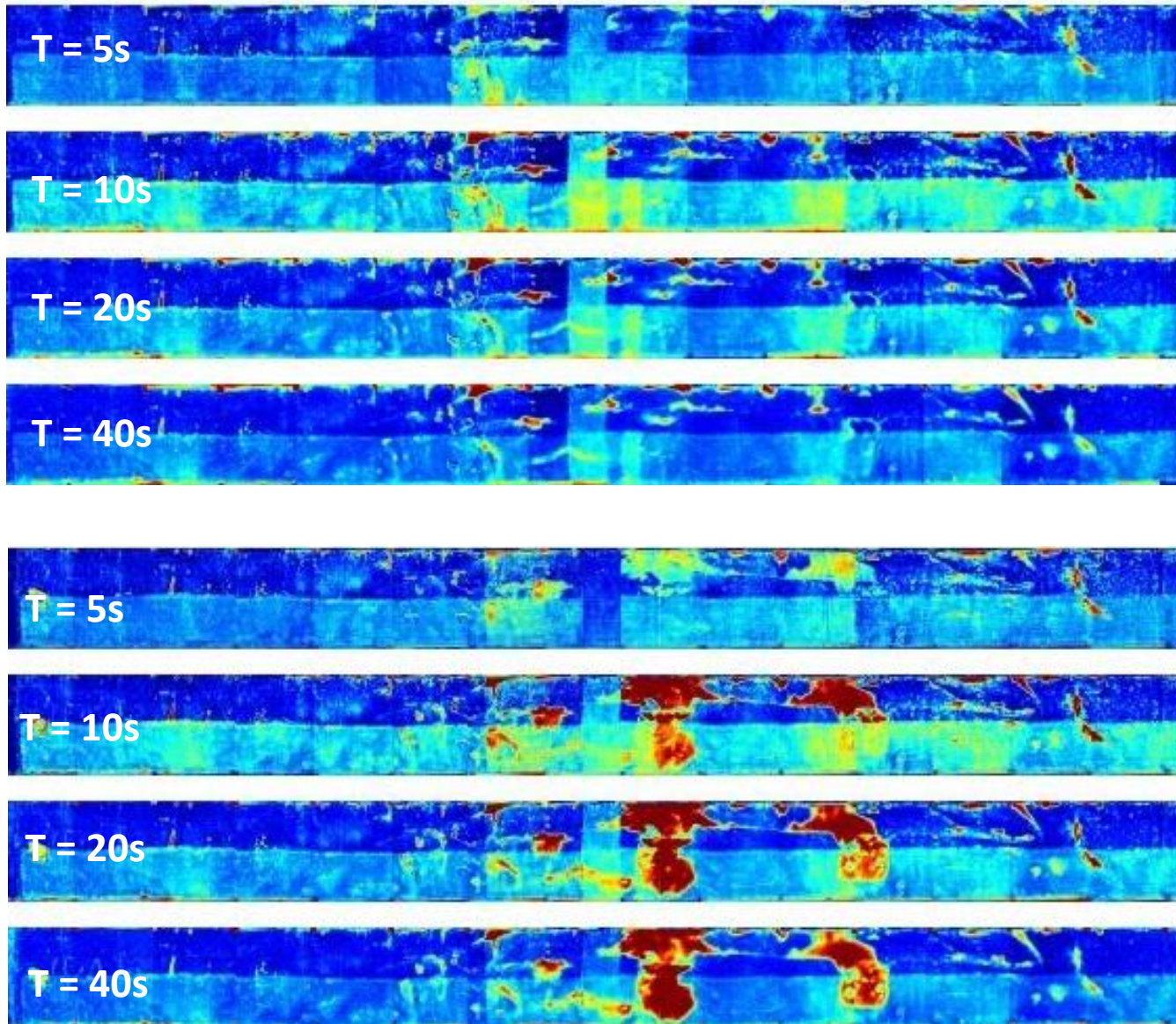
Figure 90—Girder #2 – north face: prior to structural test (top), and after structural test (bottom)
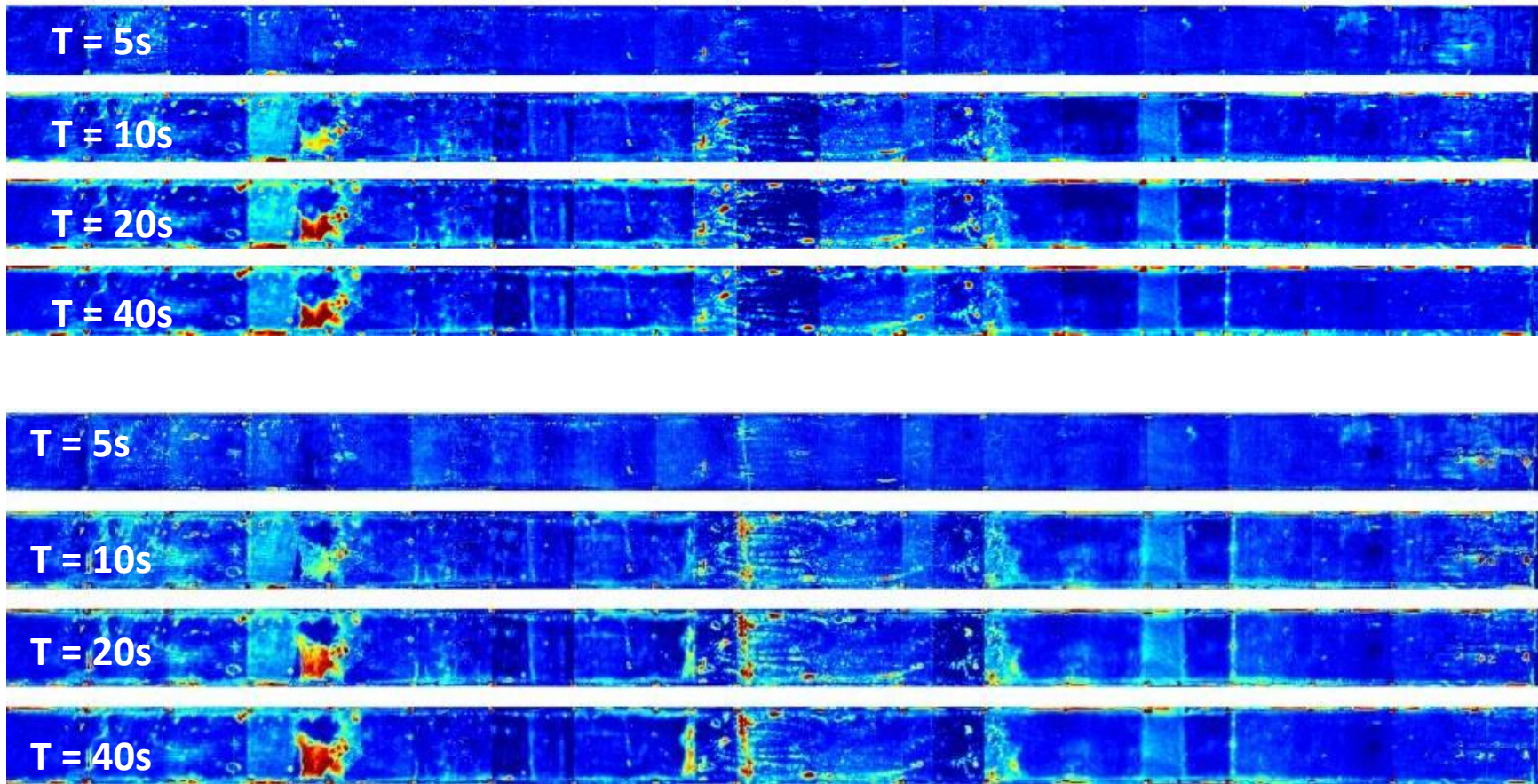
Figure 91—Girder #2 – bottom: prior to structural test (top), and after structural test (bottom)

5.3 Material Properties

Multiple tests were conducted to determine the properties of materials used in the girders. The tests can be generally separated into four categories:

1. Concrete;
2. Steel reinforcement;
3. CFRP; and
4. CFRP-concrete bond.

5.3.1 Concrete: Compressive Strength

Concrete cores for compression test were taken from locations near the supports that did not experience severe cracking due to the structural test (Figure 92). Care was taken to inspect each core and make sure their quality and size conformed to ASTM C42/AASHTO T24. Three satisfactory cores per girder were obtained.

Figure 92—Coring of bridge girders

The collected concrete cores were tested for compressive strength at FDOT State Materials Office (SMO) in Gainesville, FL (ASTM C39). Ends of each core were ground to a smooth finish. Results from the tests are summarized in Table 10; failure modes were recorded in accordance with ASTM C39.

The in-place strength of concrete at each core location was determined as per ACI 214.4R. Strength correction factors were computed assuming dried conditions; results are summarized in Table 11. Specified compressive design strengths for each girder were determined based on tolerance factor method (Hindo and Bergstrom, 1985), as 10% fractile with 75% confidence.

Measured values of modulus of elasticity (MOE) were significantly lower than $57,000\sqrt{f'_c}$; the cause was likely the disturbance near the surface of the core, produced by the drilling process.

Table 10—Summary of compression test results

Girder	Core	x (in.)	y (in.)	z (in.)	Strength (psi)	Failure mode (ASTM C39)	Average strength (psi)	MOE (ksi)
1	1	324	8.5	14	5,540	Type 1	5,660	-
	2	291	8.5	13	5,940	Type 4		-
	3	269	8.5	14	5,500	Type 4		3,090
2	1	332	-8.5	12	5,610	Type 1	5,350	-
	2	280	-8.5	14	5,200	Type 1		-
	3	304	-8.5	14	5,230	Type 4		2,890

Table 11—Actual in-place concrete strength and design properties

Girder	Core	In-place Strength (psi)	Average strength (psi)	Specified Strength (psi)	MOE (ksi)
1	1	5,633	5,760	5,120	4,080
	2	6,043			
	3	5,596			
2	1	5,704	5,440	4,840	3,970
	2	5,287			
	3	5,322			

5.3.2 Concrete: Chloride Content

Six cores for chloride ion penetration, measuring 2-in. in diameter and min. 4-in. in length, were taken from each girder, prior to structural testing. Coring locations were chosen to examine the effects of CFRP wrapping on Cl^- contents (Figure 93). Cores were taken 1-2 in. above the top layer of bottom flexural reinforcement, from the north face of each girder (more severely exposed to splashing).

Chloride ion concentrations were determined by FDOT SMO, as per AASHTO T260. Chloride ion concentrations were measured in 0.5 in. thick samples taken 2 in. away from the concrete surface; results are summarized in Table 12.

Figure 93—Approximate coring locations for Cl^- penetration profile cores on each girder

Table 12—Cl⁻ penetration cores locations and contents in pounds per cubic yard (pcy)

Location Number	Description	Cl⁻ Content – Girder #1 (pcy)	Cl⁻ Content – Girder #2 (pcy)
1	Splash zone – no coating	0.802	6.010
2	Splash zone – primer coated	1.748	5.325
3	Splash zone – under CFRP	3.824	4.479
4	End of CFRP	0.090	0.479
5	Concrete – primer coated	0.105	0.525
6	Concrete – no coating	0.622	1.096

Cored locations were filled with a commercially available polymerized mortar mix to minimize the effects of coring on the results of structural test (Figure 94a). Following the initial cure, repaired locations were moist cured, to alleviate the effects of shrinkage of the repair material (Figure 94b).

(a)   (b)

Figure 94—(a) Repair of cored locations (b) moist cure of repaired locations

5.3.3   Concrete: Carbonation

Following the compression testing of concrete cores, freshly fractured concrete surfaces were sprayed with a solution of 1% phenolphthalein in 70% ethyl alcohol to determine the extent of carbonation near the concrete surface that was in contact with air (Figure 95). Measurements of depth of carbonation were performed as per Rilem CPC-18 recommendation: both average (d_k) and maximum (d_{max}) depths of carbonation were measured (Table 13). Cores tested in compression were ground on each end so the carbonation results are slightly lower because of the concrete lost to grinding. The thickness of ground layer, however, is typically small (approximately 0.10 in.) compared to the measured depth. One core from each girder was not subjected to compression test, and therefore, no grinding was performed on those.

Higher (on average) depths of carbonation were noted in specimens with no CFRP, or epoxy only on the exterior surface compared to specimens with bonded CFRP (Figure 95). At this point, however, no conclusive evidence exists regarding the possible correlation between the CFRP wrapping and progression of carbonation.

Figure 95—Concrete carbonation examined on a concrete cylinder following the compression test

Table 13—Average and maximum carbonation depths

Girder	Core	Compression test?	Surface	d_k (in)	d_{max} (in)
1	1	Y	CFRP	0.48	0.88
	2	Y	CFRP	0	0
	3	Y	CFRP	0	0
	4	N	CFRP	0.44	0.85
2	1	Y	Concrete	0.54	0.72
	2	Y	CFRP	0.16	0.45
	3	Y	Epoxy	0.66	1.30
	4	N	CFRP	2.57	3.26
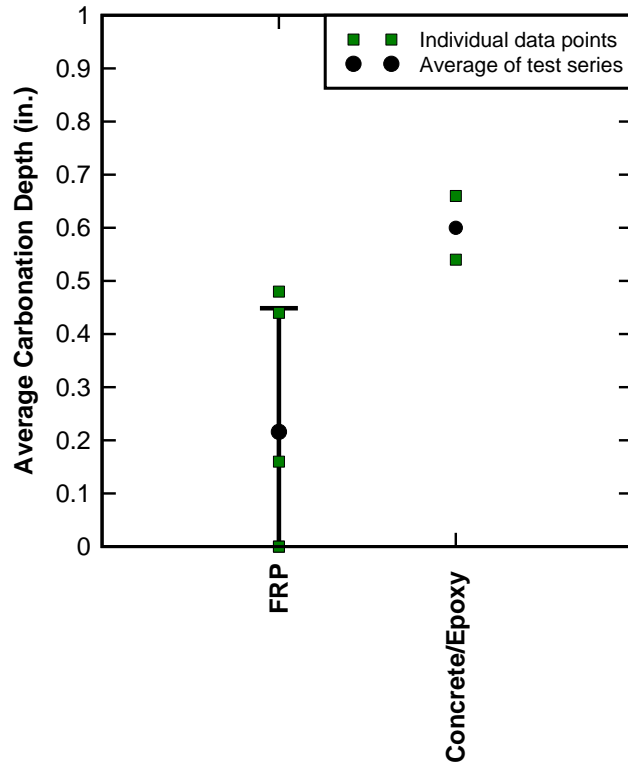
Figure 96—Carbonation depth measurements (error bars represent one standard deviation)

5.3.4 Steel Reinforcement

Steel reinforcement samples, for the purpose of tension testing, were taken from the corroded and uncorroded regions along the span (Figure 97). Steel reinforcement most severely affected by corrosion was located near the repaired portion of girder span, while uncorroded steel reinforcement was situated towards the west end of the girder in the area under old concrete. Less corrosion was observed in the repaired region of Girder #1 than in that of Girder #2. Steel bars measuring approximately 45 in. were collected using an acetylene torch (Figure 97). Four specimens were collected from repaired regions of both Girder #1 and #2, two of which were #11 bars and two #10 bars. Four bars (two #10 and two #11) were taken from the uncorroded region of Girder #2, in addition to two #11 bars from Girder #2.

Steel reinforcement specimens were tension tested at FDOT SMO, as per ASTM A370. To obtain yield and ultimate tensile strength all data were normalized to the nominal bar areas according to ASTM A615 (Table 14). Bar dimensions were measured near the corroded portion of each bar to determine the section loss; additionally, weight loss for each bar was calculated prior to testing by submerging the samples in muriatic acid with a 33% HCl concentration for 24 hours to remove corrosion for a more accurate weight of the steel. Measurement of the cross-sectional dimension on uncorroded and lightly corroded regions of each bar were performed with a caliper so that the rib thickness was not included in the measurement; more severely corroded sections were elliptical in shape, so the measurements were taken along both major and minor axes. Section loss was calculated by normalizing the cross-sectional area of corroded

reinforcement to an average cross-sectional area of uncorroded reinforcement. Good correlation was observed between yield/ultimate strength, and weight/section loss (Figure 98; Figure 99).

(a)   (b)

Figure 97—Steel reinforcement: (a) corroded (b) uncorroded

Table 14—Results of tests on steel reinforcement

Girder	Location	Bar #	Yield Strength (ksi)	Tensile Strength (ksi)	Elongation (%)	Section loss (%)	Weight loss (%)
#1	Corroded	11	46	72	9[*]	14+	9
		11	45	78	16	2	3
		10	47	77	9[*]	0	4
		10	46	80	13	2	3
	Uncorroded	11	47	79	14	0	3
		11	45	77	18	0	3
#2	Corroded	11	37	60	6[a]	17+	26
		11	34	58	12	19+	24
		10	36	60	14	10+	16
		10	44	74	15	0	6
	Uncorroded	11	52	83	19	0	3
		11	45	74	14	3	5
		10	45	75	26	0	2
		10	46	80	22	1	2

*specimen failed outside the gage region
+elliptical shape assumed
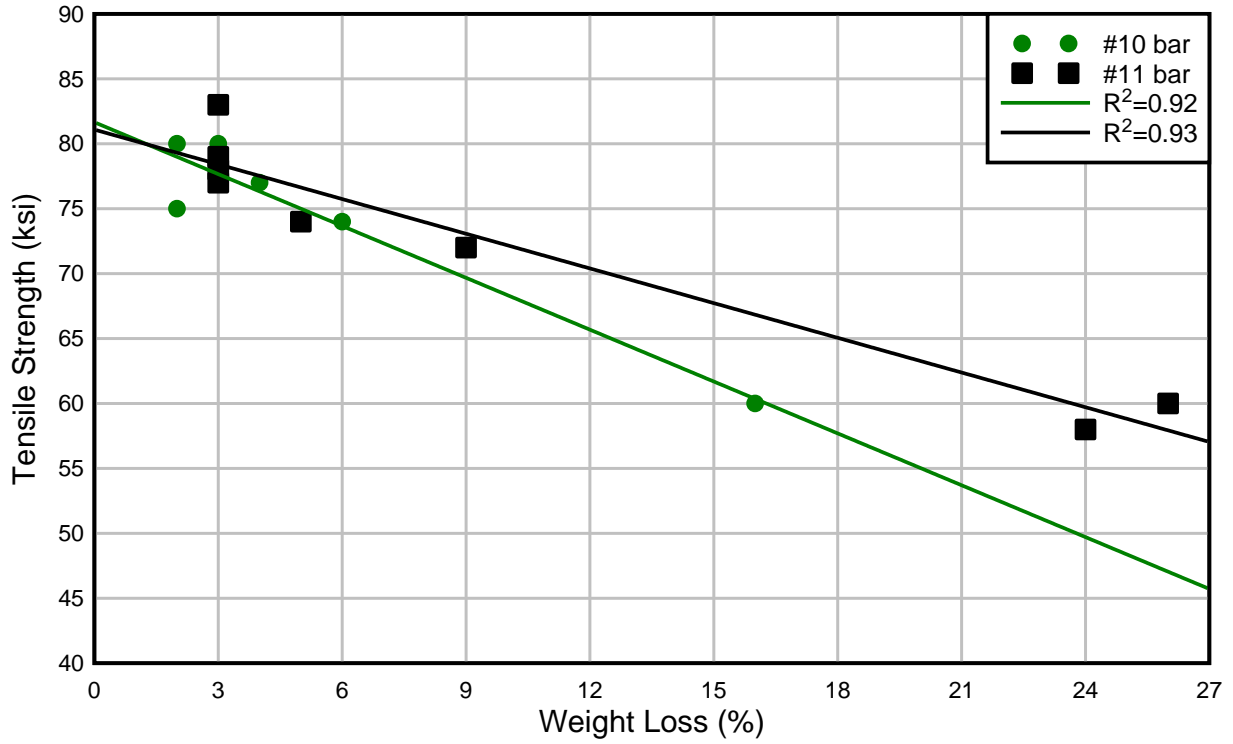
Figure 98—Correlation between tensile strength and measured weight loss
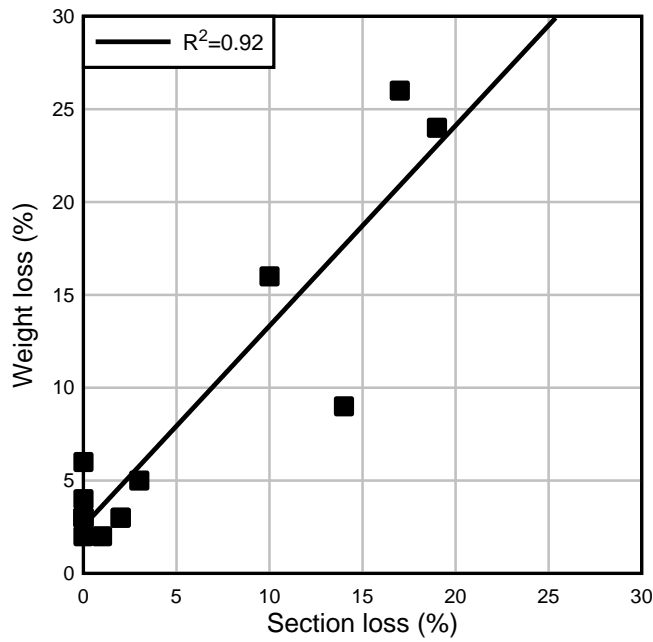
Figure 99—Correlation between weight loss and section loss

5.3.5 CFRP Reinforcement

To determine the mechanical properties of the CFRP material, 10 tensile tests were performed on single-ply CFRP coupons that were cut out of the CFRP wrap that was in service. The CFRP surface of four samples was prepared for strain gage bonding by sanding; two specimens were sanded more vigorously to determine the effects of introduced damage on the material properties. Tab installation procedures are in Appendix C. The tests were performed on Instron universal testing machine, as per ASTM D3039. Test setup is shown in Figure 100a. Load data were acquired by the testing machine built-in 33.75 kip load cell, and the displacement data was collected with an Instron 2360 clip-on extensometer with a gage length of one in. Typical failure mode of the test coupon is shown in Figure 100b.

Tensile properties were determined according to ASTM D7565 (Table 15). In interpretation of test results, it should be noted that the composite had experienced significant stress prior to tensile testing - during the structural test, and due to the removal of CFRP from the concrete surface. Such manipulation of the test samples, prior to testing, could have initiated damage within the carbon fibers, microcracking within the composite matrix, and debonding at the fiber/matrix interface. The aforementioned factors could have resulted in lower measured mechanical properties of the composite, particularly the modulus of elasticity/tensile stiffness; it was shown by performing light sanding on the specimen surface that slight damaging of the composite can have significant detrimental effects on its tensile stiffness. This would also explain the large coefficients of variation of the composite's mechanical properties.

(a)   (b)

Figure 100—(a) CFRP coupon tension test setup (b) typical failure mode of test coupon

Table 15—CFRP coupon tension test results

Specimen No.	Surface preparation	Stiffness (kip/in)	Elongation	Tensile strength (lbf/in)
A1	Sanded	71,500*	0.008*	548*
A2	Sanded	74,400*	0.009*	687*
1P1	Lightly sanded	79,600*	0.011*	943*
1P2	Lightly sanded	77,800*	0.012*	896*
1P7	None	109,000*	0.005*	554*
1P8	None	117,700	0.008	1043.
1P9	None	94,300	0.012	1055
1P10	None	90,300	0.012	1097
1P11	None	87,200	0.011	918
1P12	None	92,300	0.010	999
	Average:	96,400	0.0106	1,022
	COV:	0.13	0.16	0.07

*=excluded from average values of CFRP-concrete bond

5.3.6 CFRP Reinforcement: Pull-off Tests

Direct pull-off test is one of the most commonly utilized standardized tests for the quality control of externally bonded CFRP repairs (Figure 101). Three tests were performed on each girder (two tests near each end of CFRP and one test along the span) in a single ply region, to avoid the possibility of interlaminar failure where more than one ply was used. Tests were conducted as per ASTM D7522. Passing tests have a cohesive failure mode (Figure 102) with a tensile pull-off strength of over 200 psi, according to ACI 440.2R and NCHRP (2010).

Figure 101—Direct pull-off test setup

Figure 102—Failure mode: (a) cohesive and (b) adhesive

Direct pull-off test results are summarized in Table 16. All tests passed the tensile pull-off strength criterion. An adhesive and a mixed failure mode on each girder, however, were observed, which may signify bond degradation and/or inadequate surface preparation.

5.3.7 CFRP Reinforcement: Materials Testing of Bond Specimens

Circular (2 in. diameter) samples of CFRP were taken from debonded regions with a core sample of concrete underneath. Care was taken to ensure that cores were at least 1 in. long. Both the surface of debonded CFRP and the corresponding concrete surface were inspected with Phenom Pro X scanning electron microscope (SEM) at housed in the Department of Materials Science and Engineering at the University of Florida.

Table 16—Summary of direct pull-off test results

Girder	x (in.)	z (in.)	Pull-off Tensile Strength (psi)	Failure Mode
	18	288	318	Adhesive Failure
1	19	255	436	Cohesive Failure
	20	20	286	Cohesive Failure
	22	18	522	Cohesive Failure
2	20	252	414	Mixed Failure
	19	313	465	Cohesive Failure

Two concrete cores (measuring at least 1-in. long) were taken from locations with a sound bond (as determined from IR scans). These samples were sliced with a wafer saw longitudinally and used to study the interface cross-section under the SEM (Figure 103). Table 17 shows samples that were collected from regions with intact CFRP-concrete bond, as well as regions with adhesive failures or that were already delaminated prior to the load test. These samples were later subjected to a rigorous micro-scale evaluation under SEM.
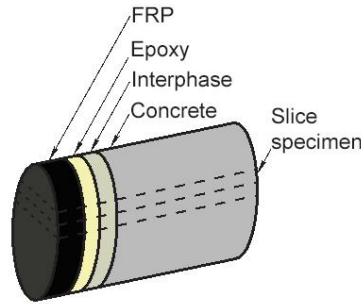
Figure 103—CFRP bond core specimen

Table 17—Summary of bond samples

Sample ID	Sample Description	No. of samples
DFRP	Core sample of CFRP and underlying concrete substrate (min. 1 in. deep) from a debonded region	2
AFRP	Core sample of CFRP and underlying concrete substrate (min. 1 in. deep) from an adhesively failed region	2
FRPC	Core sample of CFRP and underlying concrete substrate (min. 1 in. deep) from a region with healthy bond.	2

5.3.8 SEM Results

Specimens were polished to a near-mirror finish using a series of abrasives (silicon carbide polishing paper and diamond suspension). They were then coated with a thin layer of carbon and imaged in the SEM. Images were collected at the adhesive-concrete interface and in the CFRP. To differentiate between different material phases (concrete substrate, the adhesive and fibers), backscatter electron images were collected.

Collected images showed defects within the FRP composite (Figure 104). Voids within the matrix were likely a result of inadequate impregnation of dry carbon-fiber fabric in the field. At higher magnifications, microcracks located at the fiber-matrix interface were observed. These fibers could be due to manipulation of the samples during the extraction, or due to the environmental degradation. Larger microcracks were also present in the epoxy-concrete interfacial region, as shown in Figure 105. Sustained loading, combined with fatigue and environmental impacts could have been the cause of these microcracks. While further research is necessary to understand the source of cracking near the interface, these observed microcracks might result in early onset of debonding once they reach their critical length.
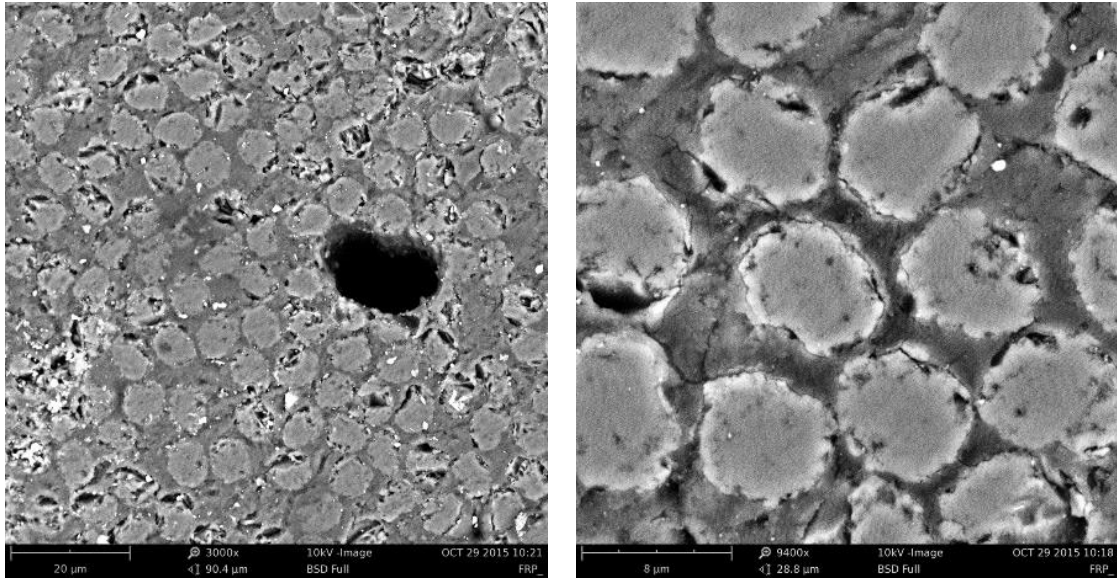
(a)   (b)

Figure 104—SEM images of defects present within the CFRP composite including
(a) voids and (b) epoxy microcracking
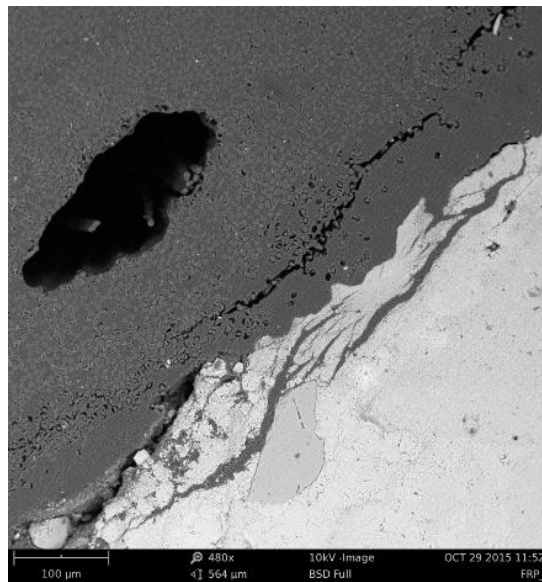
Figure 105—Large void and initiation of debonding of CFRP near CFRP-concrete interface

5.4   Flexural Test Setup and Instrumentation

Both Indian River Bridge girders were tested in flexure using a four-point bending test setup; the intended failure mode was flexural. To transfer the load from the actuator to the deck, a 9-ft. spreader beam was used, with 8 ft. center-to-center distance between the supports. The beam was supported by neoprene pads placed on top of cast-in-place grout pads. Girder ends were supported on 1.5-in. neoprene pads measuring 9 in. × 24 in. at the base. The pads were placed on

heavy steel sections stabilized to the strong floor with a cast-in-place grout pad. A 600-kip load cell was used to measure the applied load.

Laser displacement transducers (LDT) were used to measure the vertical deflection. Displacements were measured above the supports, at the midspan and at 3.5 ft. intervals starting from the midspan towards each end of the girder. LDT locations are shown in Figure 106 and Figure 107.

Electrical resistance strain gages with a grid length of 60 mm were used to measure strain in CFRP ("FSG") and concrete ("CSG"). Strain gage locations are shown in Figure 108 and Figure 109. Gage line 2 was placed to match the one from the in situ load test, for the purpose of comparison of the strain data within the service load levels between the two tests. Gage line 3 was placed at the midspan, while Gage line 1 toward the east support of the girder to capture strain development away from the constant moment region, should the failure mode change unexpectedly. A complete test setup is shown in Figure 110.

Top View

6x12x2 in. bearing pad

9'-0"

$9\frac{1}{8}$"

LDT6   LDT8   LDT10

LDT1   LDT2   LDT3   LDT4   LDT11   LDT12   LDT13   LDT14

East   West

X

Y

LDT5   LDT7   LDT9

$9\frac{1}{8}$"

Spreader beam - W12x45

North Elevation

2'-6"   3'-6"   3'-6"   3'-6"   3'-6"   3'-6"   3'-6"   3'-6"   3'-6"   2'-6"

8'-0" span length

East   West

z

$2'-4\frac{7}{8}$"

x

9x24 in. Bearing pad   Midspan   FRP

30'-8"

33'-0" Support to support
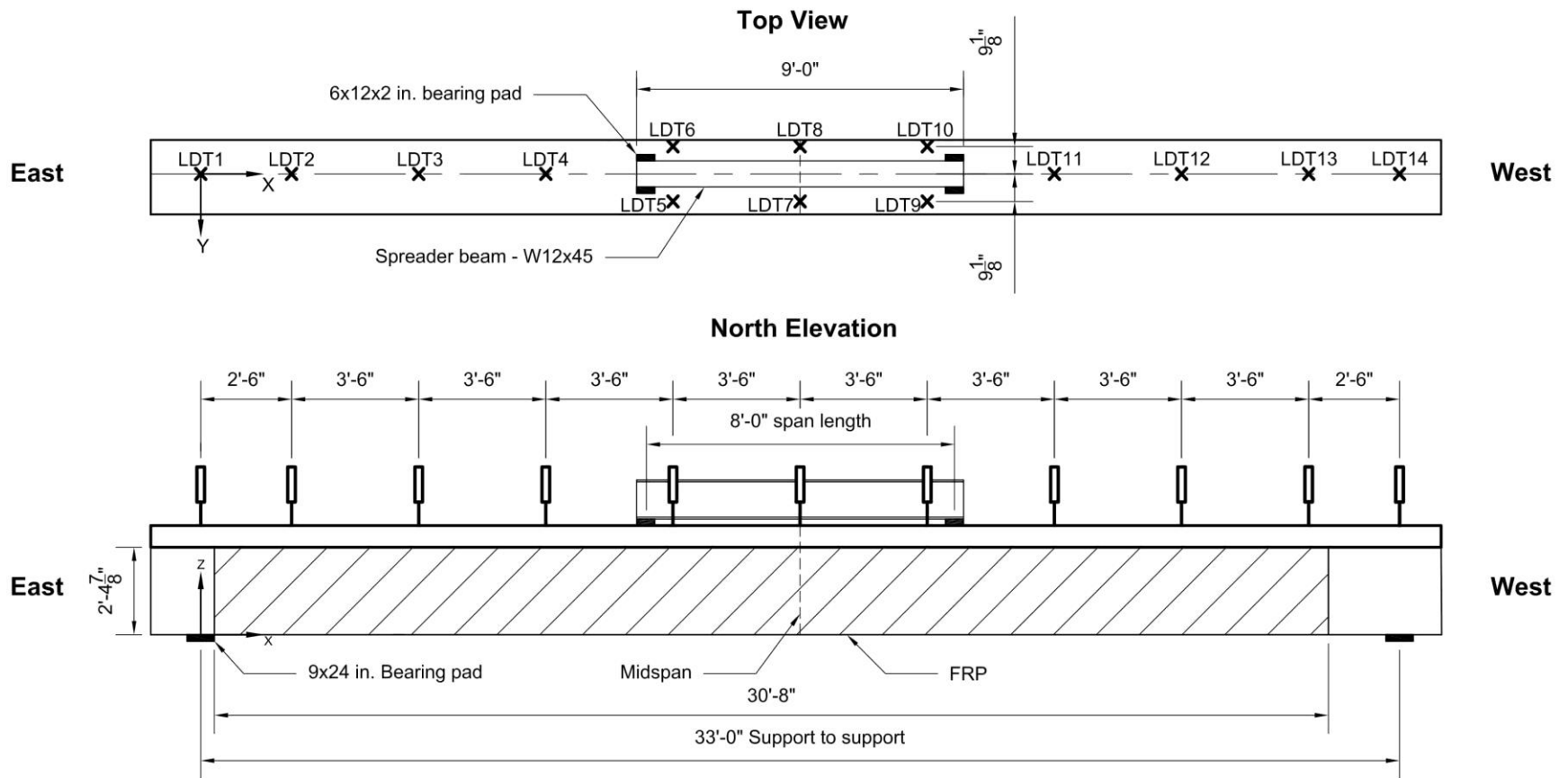
Figure 106—Girder #1 – Instrumentation plan representing the locations for laser displacement transducers
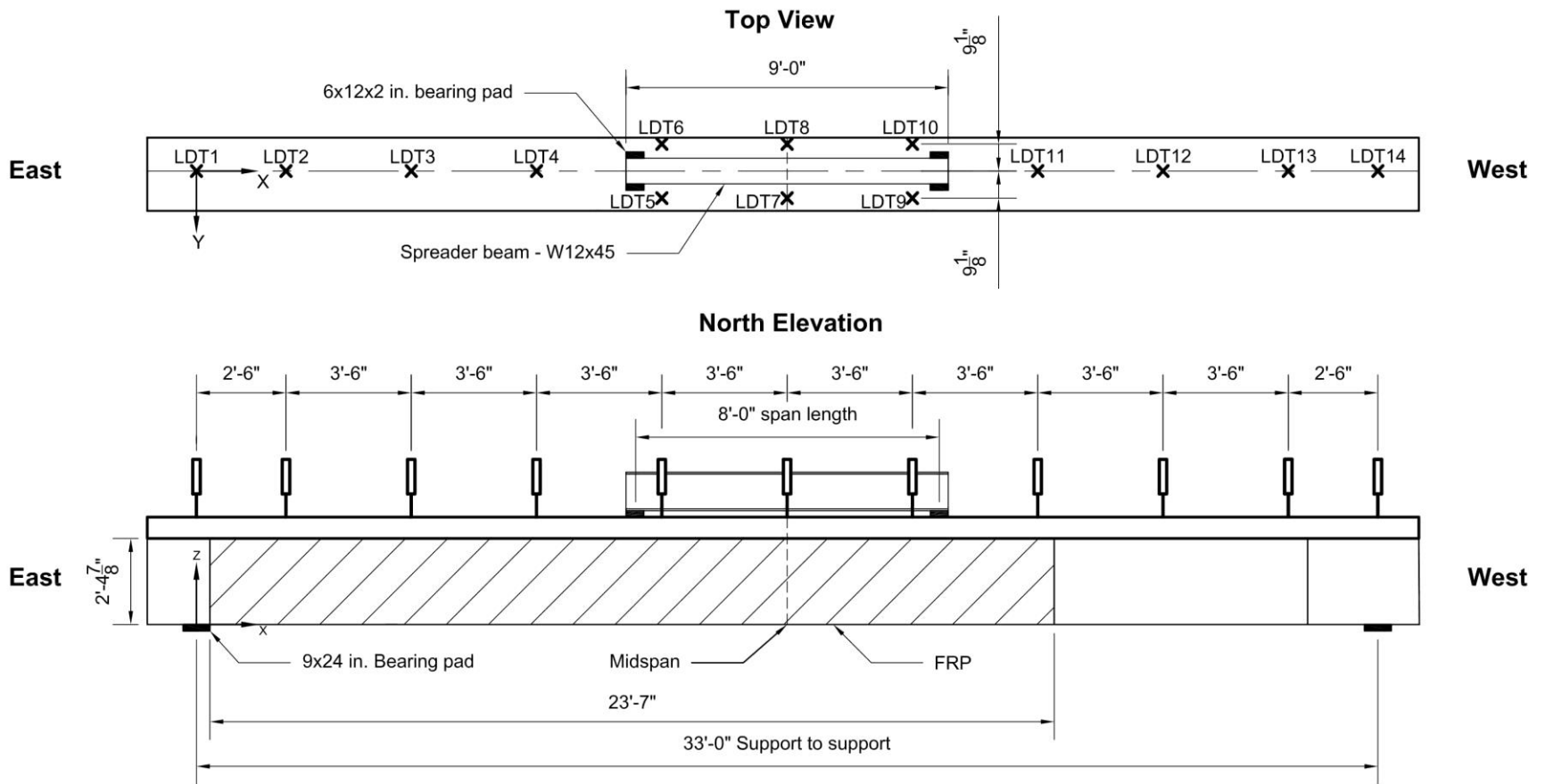
Figure 107—Girder #2 – Instrumentation plan representing the locations for the laser displacement transducers
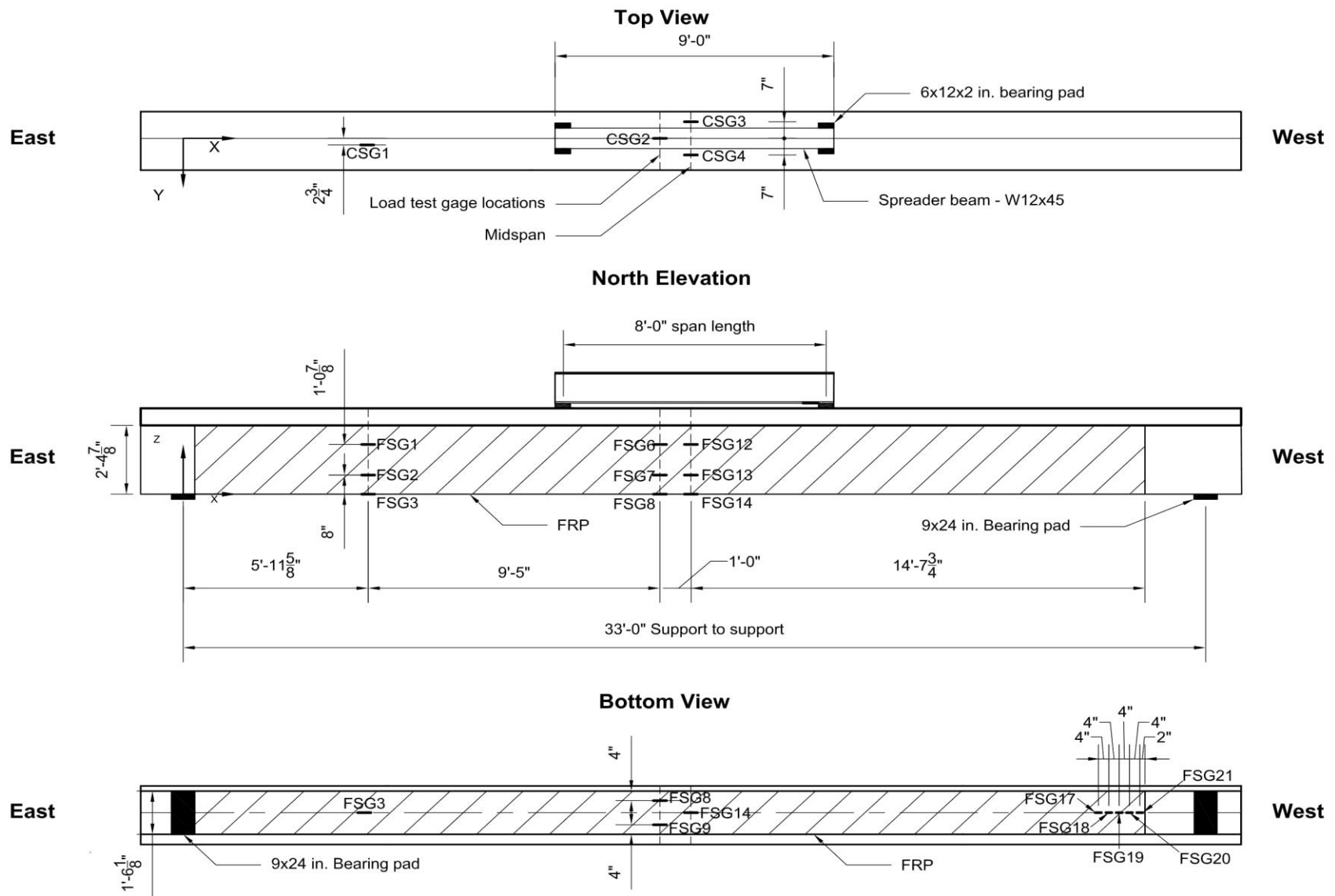
Figure 108—Girder #1 – Instrumentation plan representing the locations for the strain gages
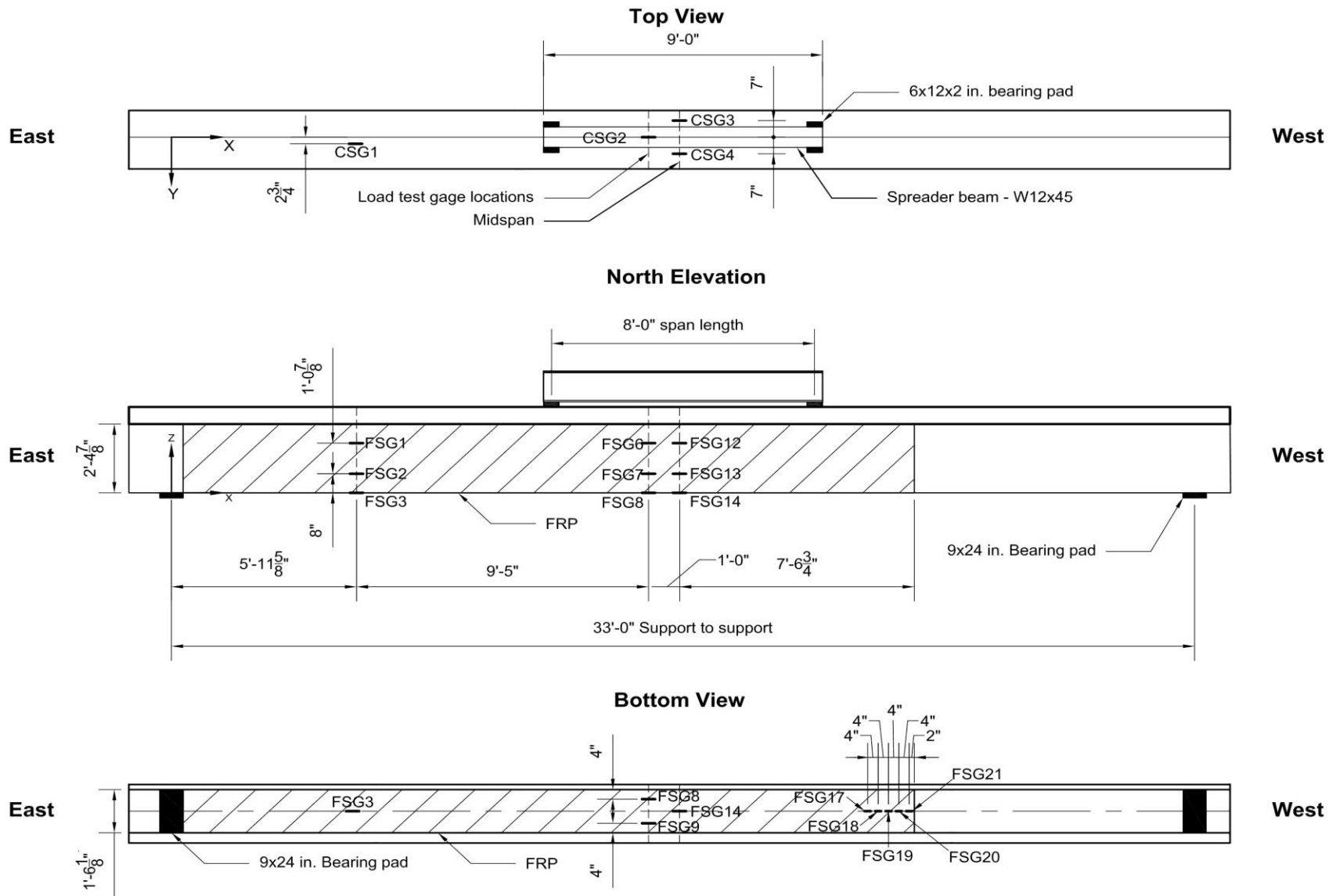
Figure 109—Girder #2 – Instrumentation plan representing the locations for the strain gages

Figure 110—Girder loaded in test frame

5.5 Flexural Test Procedures

Girders were loaded monotonically to the incremental service load levels shown in Table 18 for five cycles. Each load increment was followed by unloading and IR scanning of the CFRP composite. The final cycle consisted of monotonic loading up to the full flexural strength. Load increments within the service loads, corresponding to cycles 1-5, were selected to be equivalent to truck loads from the in situ load test.

Each increment was defined by the load that would produce the same strain in steel of the test girder that was produced by the truck load (from the load test) in the same girder while it was a part of the bridge structure. The corresponding calculations were performed based on the typical assumptions made in section analysis of reinforced concrete structures. Cracked section properties were calculated for both the in situ bridge girder (by assuming the full effective flange width as per ACI 318) and the laboratory girder. Based on the calculated section properties, strains in steel reinforcement for in situ bridge girders were estimated for selected truck loads. By assuming the equal strain in steel, corresponding loads in the laboratory girder were back calculated. This approach allowed a direct comparison of the laboratory load test to that of the in situ load test. It should be noted that in Girder #1 structural test, steps 3 and 4 were excluded from the loading procedures, as it was determined from IR scans taken on Girder #2 that no progression of debonding occurred under the service load levels.

Table 18—Girder loading scheme

Cycle	Step	Description
1	1	Load to 25 kip
	2	Hold to mark cracks/cointap
	3	Unload
	4	Take an IR image
2	1	Load to 35 kip
	2	Hold to mark cracks/cointap
	3	Unload
	4	Take an IR image
3	1	Load to 40 kip
	2	Hold to mark cracks/cointap
	3	Unload
	4	Take an IR image
4	1	Load to 50 kip
	2	Hold to mark cracks/cointap
	3	Unload
	4	Take an IR image
5	1	Load to 65 kip
	2	Unload
	3	Take an IR image
6	n/a	Load to full strength capacity

5.6 Flexural Test Results and Discussion

Load-displacement plots for the girders are presented in Figure 111. Both girders exhibited similar behavior in the laboratory test. No significant change in stiffness was noted up until approximately 160 kip in Girder #1, and approximately 150 kip in Girder #2. Loss of initial stiffness occurred at a lower load in Girder #2, likely due to the generally more degraded state of the girder, as it was observed during the CFRP-concrete bond evaluation. Moreover, more severe corrosion of internal steel reinforcement could have been an additional contributing factor to this difference between the two girders. Kinks in the lower-stiffness region of Girder #2 (marked with arrows in Figure 111), prior to failure, correspond to occurrence of flexural cracking and localized debonding of CFRP that was audible during the test; in Girder #1 such behavior was not observed, probably due to better bond between CFRP and concrete (as observed in IR thermographs). At ultimate strength, both girders experienced rupture of CFRP; crushing of concrete was also observed in both girders (Figure 112). In Girder #1, initial crushing of concrete (Figure 113a – sudden drop in load prior to ultimate) was followed by the CFRP rupture, while in Girder #2 these two events occurred simultaneously. In Girder #2, rupture of CFRP was accompanied by debonding on the sides of the girder in the rupture region. This was documented in IR thermographs acquired post-mortem.
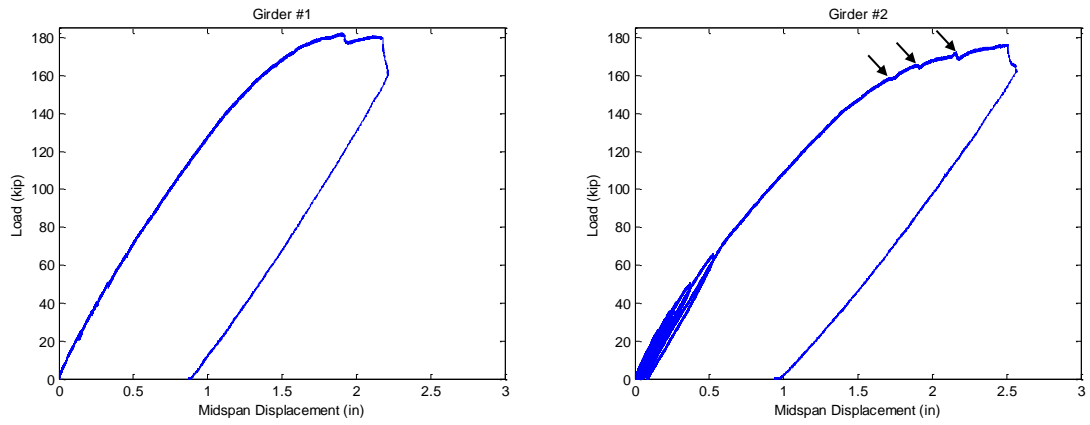
Figure 111—Load-midspan displacement of test girders
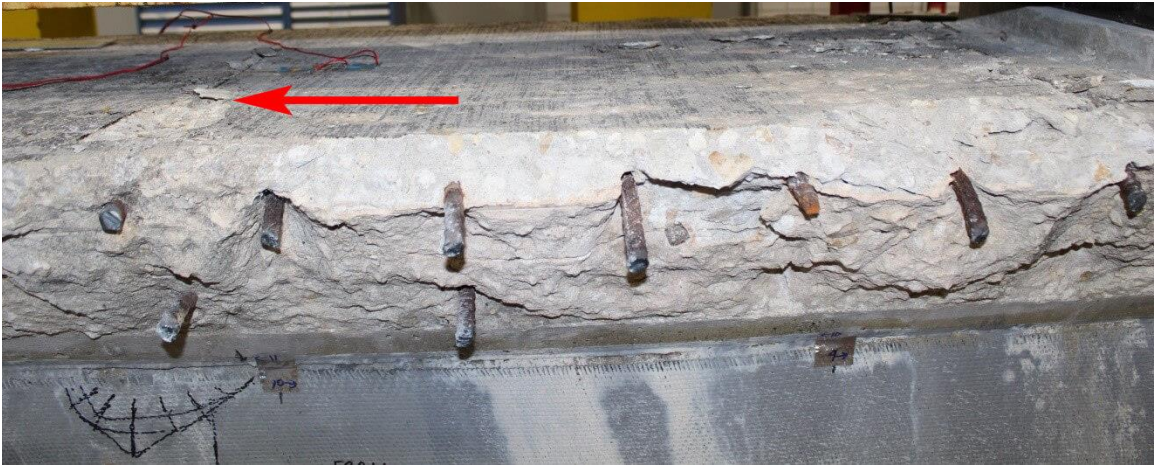
Figure 112—Failure of concrete in compression indicated by red arrow

Figure 113—Rupture of CFRP near midspan

Evolution of strains over the girder depth during loading was analyzed on both girders. All gage lines followed linear strain distribution across the depth of the girder (Figure 114). Exemplary plots, that confirm this behavior, are shown in Figure 115 - high R^2 values (in the range 0.8-1.0) show that first order polynomial is a satisfactory fit for the strain distribution in each girder.
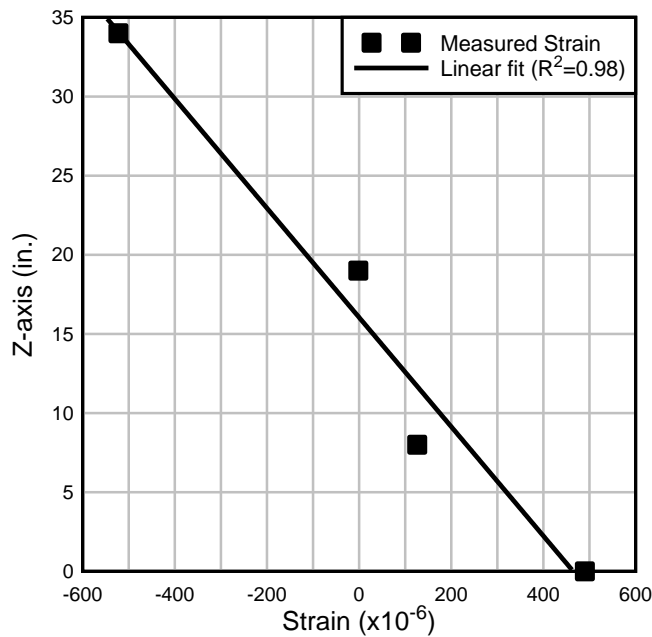
Figure 114—Typical strain profile along the girder depth

(a)   (b)
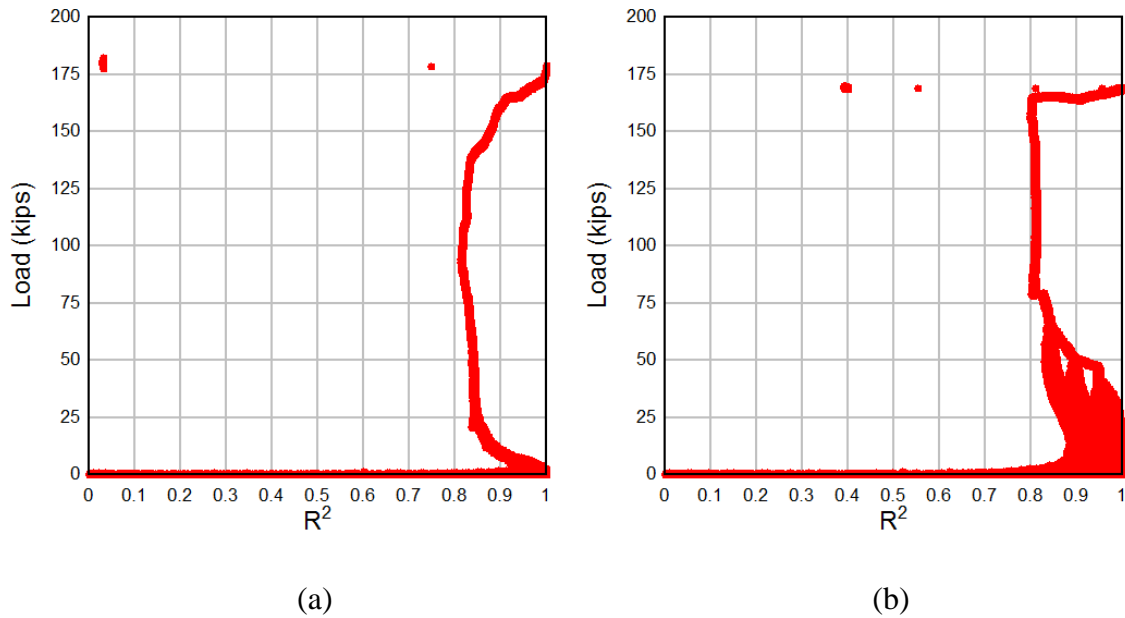
Figure 115—Goodness of linear fit with respect to applied load for gage line 2 on (a) Girder #1, and (b) Girder #2

Strain in CFRP, at the bottom of each girder, in the constant moment region is plotted in Figure 116. In Girder #1 an apparent discrepancy exists between the two measurement locations; this is due to rupture of CFRP taking place within the gage length of strain gages placed at the girder soffit (Figure 117); both strain measurements show excellent agreement in Girder #2 (rupture of CFRP occurred outside the constant moment region near the spreader girder support). The maximum measured strains in CFRP in both girders are well below the CFRP rupture strains reported in Table 15, with an exception of Gage Line 2 location on Girder #1 that registered strain levels approaching those measured in the tensile test. This behavior is further discussed in the following section of the report. Changes in slope of strain plots in Figure 116 agree well with changes in stiffness of the test girders (Figure 111).

5.7 Moment Curvature Analysis

Displacement was monitored along each girder throughout the loading cycles. Girder curvature at the midspan was determined by fitting a 3rd order polynomial through the experimental data points, along the span. Such treatment of the collected data allowed the curvature at midspan to be determined. For comparison, girder curvature at midspan was calculated from a linear fit through the strain profile (Gage Line 3).

For comparison purposes, a theoretical moment curvature analysis was performed for each girder using the numerical model developed by Consolazio et al. (2004). Concrete compressive strength of 6,000 psi was assumed based on the compressive strength data for these girders (Table 10). Concrete in compression was modeled according to Collins and Mitchel (1991); concrete in tension was assumed to follow the stress-strain relationship proposed by Belarbi and Hsu (1994). Steel reinforcement was modeled as linear elastic perfectly plastic material with yield strength of 45 ksi and modulus of elasticity of 29,000 ksi. CFRP was assumed to act as a

linear elastic material until ultimate strain was reached; CFRP material properties obtained from tensile tests (Table 15) were used in the analysis.

(a)   (b)
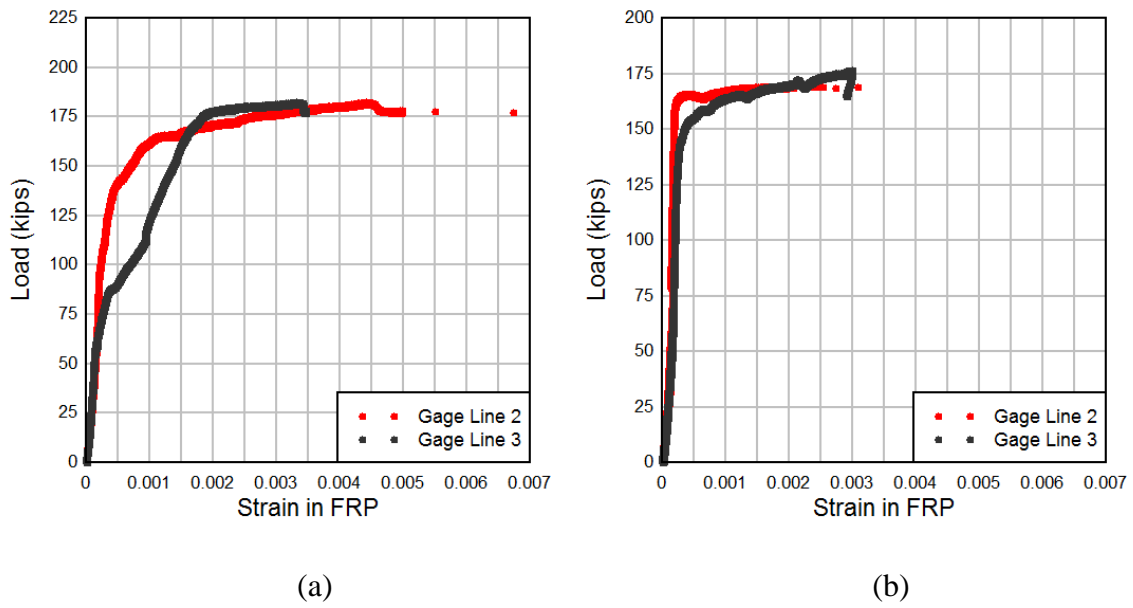
Figure 116—Development of strain in CFRP at the bottom of (a) Girder #1, and (b) Girder #2

Figure 117—CFRP rupture relative to Gage Line 2 on Girder #1

Figure 118 shows excellent agreement between experimental and theoretical moment curvatures. In Girder #2, a slight difference between the two experimental moment curvature diagrams was observed. Debonding that took place prior to rupture of CFRP could have affected the strain measurement, causing discrepancy between the two curves. Moment curvature obtained from the displacement profile is deemed more representative of the actual girder behavior as the accuracy of the displacement measurement was not affected by debonding of CFRP.

In theoretical moment curvatures, ultimate strain in CFRP was adjusted to match the CFRP failure observed in experimental moment curvatures. The assumed ultimate strain of 0.003 corresponds to only 28% of measured (Table 15) elongation at rupture of CFRP. This behavior is explained primarily by the development of localized strains in FRP that occur at the flexural cracks; Pessiki et al. (2001) discussed this behavior in detail in the case of FRP-confined columns. Other contributing factors could be associated with fiber misalignment (Yang et al., 2002), and size effects.

The fact that only about 28% of CFRP rupture strain was utilized indicates the need for further investigation of this phenomenon, and possibly its incorporation in the design where FRP rupture limit state governs the ultimate strength. Current design guidelines for externally bonded FRP (ACI 440.2R) recommend an efficiency factor (κ_ε) of 0.55 to be applied to ultimate FRP strain to account for the difference between the rupture strain from tensile tests to that observed in FRP-confined columns. By adjusting the measured rupture strain of 0.0106 (Table 15) by the proposed efficiency factor, estimated ultimate strain in CFRP would be 0.006, which is twice as much as the strain assumed in moment-curvature analysis. Additional research is required to determine the appropriate efficiency factors for CFRP U-wraps used in flexural applications. It should be noted that, if used in the design, this factor would be only applicable to FRP rupture limit state, and would not apply to debonding failure mode.
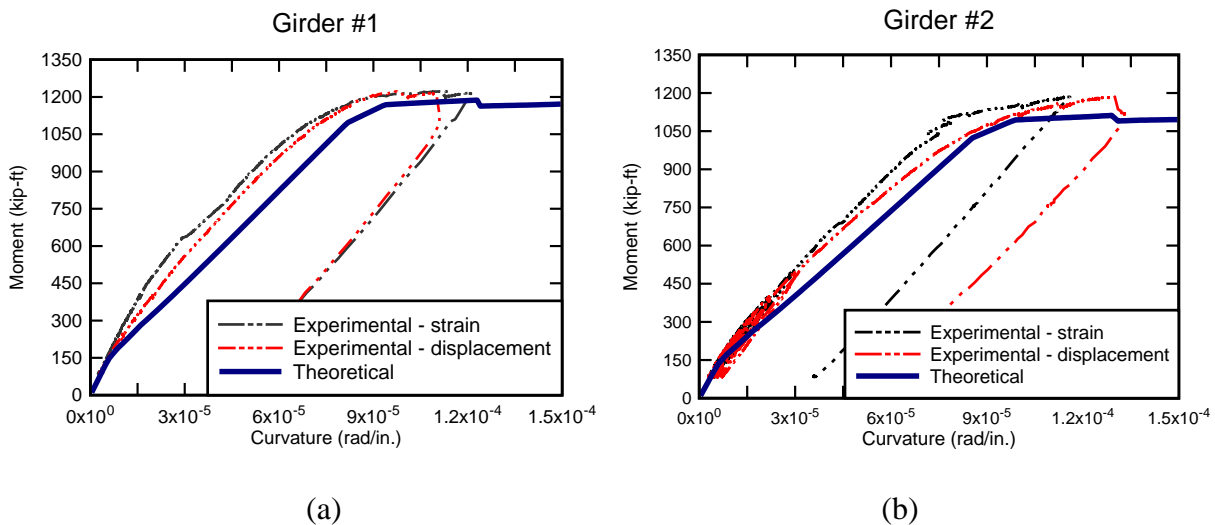
Figure 118—Moment curvature for: (a) Girder #1 and (b) Girder #2

5.8 Girder Dissection

Following the structural test, an autopsy was performed on both Indian River Bridge girders. After CFRP was removed, the girders were placed upside-down to allow cover concrete to be removed for inspection of the steel reinforcement at desired locations (Figure 119).

Figure 119—Test girder in inverted position

5.8.1 CFRP Condition

CFRP was removed by either pulling off by hand or using a scraping tool. This process revealed the variation in surface condition on each girder. Figure 120 shows marks from plywood grains on the surface indicating that the surface was not prepared. Such regions were observed intermittently on the sides of the girders. Approximately 30-40% of the total surface area of the sides on each girder did not appear to have been sandblasted.

(a)   (b)
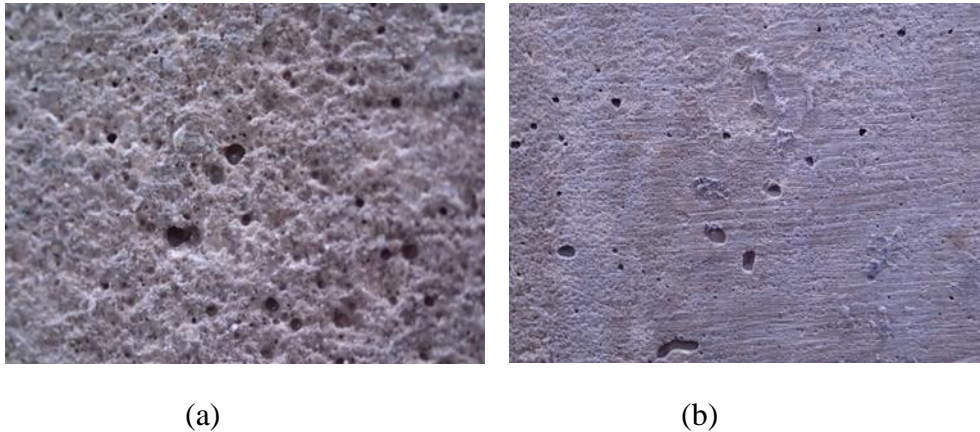
Figure 120—Difference between: (a) sandblasted concrete surface and (b) concrete surface without surface preparation

Removal of CFRP also revealed the presence of a cementitious material skim coat at multiple locations that pulled off with CFRP (Figure 121). This coat was most likely used to level the surface after the repair forms were removed.

Figure 121—Evidence of skim coat at the bond

On both girders, a primer was used at the interface between old and new concrete. The primer was recognizable by a distinct light brown color that bled through (Figure 122). Marks from the primer were detected on the stripped CFRP.

A few areas on each girder were found to be repaired with a cementitious repair material. Two such areas were identified on Girder #1, and were surrounded by severely debonded CFRP. The debonding occurred at the CFRP-epoxy interface (Figure 123), which is unusual; the most common type of debonding occurs at the concrete-epoxy interface.

(a)

(b)

(c)
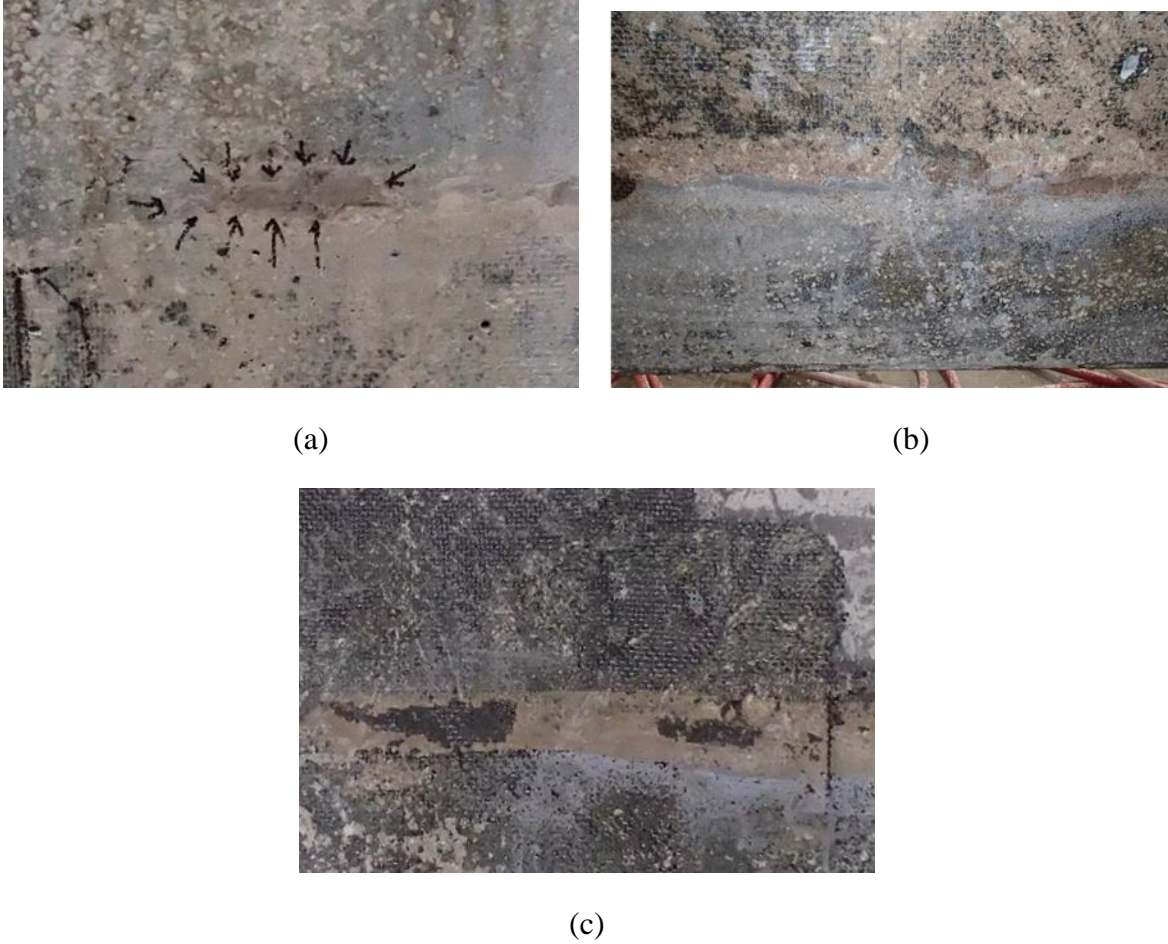
Figure 122—Evidence of primer at the new–old concrete interface

(a)

(b)

Figure 123—Evidence of delaminated bond surface along the CFRP-epoxy interface on: (a) the girder and (b) CFRP wrap

5.8.2 Steel Reinforcement

Steel reinforcement was inspected following the structural test. To expose the reinforcement, a concrete chain saw, and a chisel were used (Figure 124). Both girders were inverted to give access to the tension zone during demolition.

(a)	(b)

Figure 124—(a) Chiseling of concrete surrounding the reinforcing bars and (b) bridge girder in upside-down position

Care was taken not to damage the reinforcement during the process. Specific locations of interest were chosen along the span (Figure 125) to determine the possible presence of corrosion:

1. Splash zone at abutment: This region is thought to be the most affected by splash of brackish water. CFRP wrap starts in this region. Concrete was removed at the edge of the CFRP wrap to reveal the reinforcement on both sides of CFRP. No signs of corrosion were observed.
2. Old/new concrete interface (towards the abutment): An "anode-ring effect" takes place when new concrete is installed adjacent to chloride-contaminated concrete. The potential difference between the repair concrete and surrounding salt-contaminated concrete creates a corrosion cell where the anodic reaction occurs in the reinforcement adjacent to the repaired area; this reinforcement is also surrounded by chloride-contaminated concrete. No significant corrosion was observed on the reinforcement surrounding the repair, indicating that the anode ring effect did not strongly promote corrosion.
3. Repaired region: This region was initially the most severely damaged by corrosion, and consequently most of the repair efforts took place in this region. Corroded reinforcement was coated with a protective polymer coating. Average section losses of approximately 5% and 12% were observed in Girders #1 and #2, respectively; however, it is believed that no substantial corrosion processes have occurred following the CFRP repair. Close-up images of corroded reinforcement are shown in Figure 126.
4. Old/new concrete interface (towards the pier support): This area was revealed to determine possible evidence of ring anode effect. It should be noted that this region was entirely wrapped with CFRP.
5. Old concrete (towards the pier support) and end of CFRP wrap: Reinforcement in this region was examined to evaluate the advancement of corrosion following the

most recent repair on the bridge. Moreover, steel reinforcement adjacent to the end of CFRP wrap was examined to determine what effect CFRP wrap had on corrosion of existing reinforcement. No significant signs of corrosion were observed.

Concrete screws were observed at multiple locations during the concrete chiseling process (Figure 127). It was later confirmed from repair procedure photos that the screws served the purpose of enhancing the bond between the old and new repair concrete.
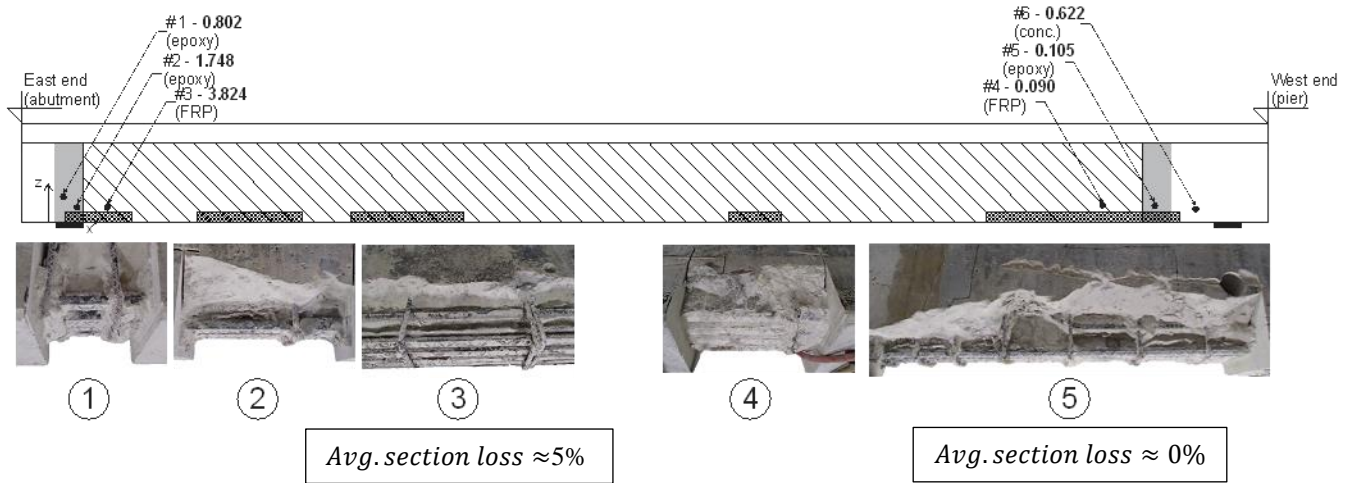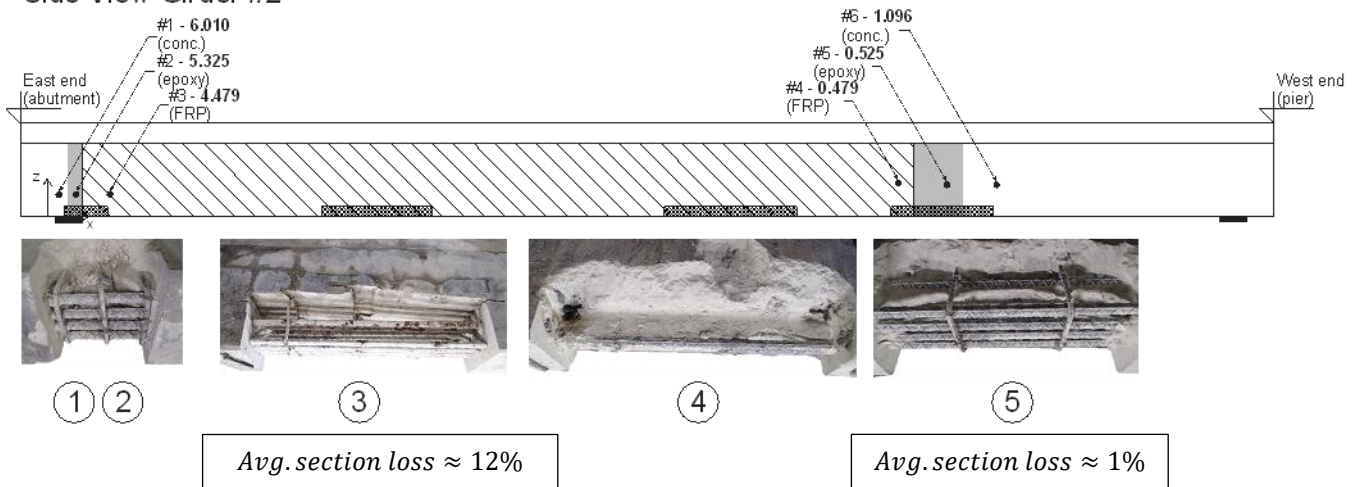
Figure 125—State of reinforcement and chloride contents (pcy) at specified locations along the north face of Girders #1 and #2

Figure 126—Close-up images of corroded reinforcement

Figure 127—Concrete screw at the interface between new and old concrete

5.9   Chlorides and Corrosion

Chloride concentrations are shown in Figure 125, at the corresponding locations along the girders. Complete Cl⁻ penetration profiles for specified cores are shown in Figure 128.

Chloride ion (Cl⁻) concentrations vary on girders #1 and #2 (Figure 125). This variation is particularly acute in the splash zone (near the abutment support). Inconsistent exposure of each location to wind and wave action was likely the cause of the differences in Cl- concentrations (Figure 129). Both girders were interior, with girder #1 situated further away from the exterior girder, thus placing it further away from the wind and wave action approaching from the North. Exposure to wave action was particularly severe at the east end of each girder, due to the configuration of abutment support and the diaphragm (Figure 130).

Lower Cl⁻ concentrations were expected in concrete that was wrapped with CFRP, as it is assumed that CFRP acts as a barrier that prevents diffusion of Cl⁻ into concrete. In girder #1, however, a significantly higher concentration of Cl⁻ was observed in concrete under CFRP (core #3) when compared to two coring locations adjacent to CFRP wrap (cores #1 and #2). Figure 130 shows the non-uniform exposure of concrete near abutment is evident; the two locations with lower concentrations were less severely exposed to splash water, while the location under CFRP likely had higher residual Cl⁻ concentration (prior to CFRP repair), in addition to more

severe exposure following the repair. Differing exposure histories of the concrete near the abutment support explain the anomalously high Cl⁻ concentration under the CFRP.
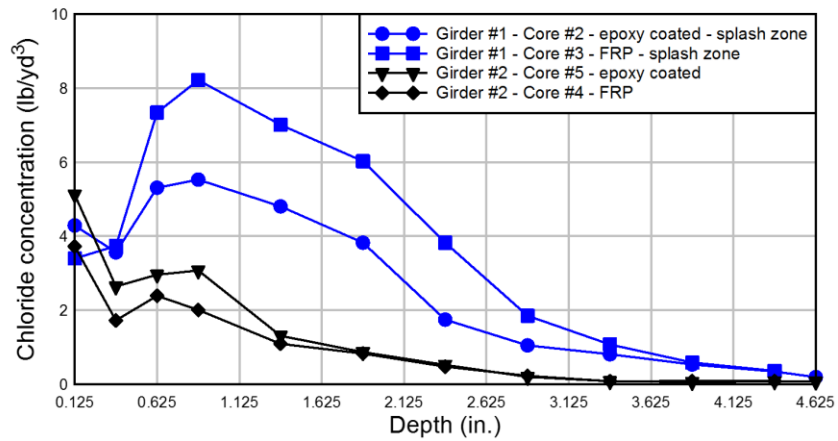
Figure 128—Chloride penetration profiles at specified locations

On the other hand, cores #4, #5, and #6 were situated at locations with a uniform exposure to the splashing due to wind and wave action; therefore, this location is likely more indicative of the effects of CFRP on the rate of diffusion of Cl- into the concrete. According to the chloride concentrations obtained from these locations, it is apparent that CFRP has had significant effect on the diffusion of chlorides throughout the service life of the repair. Reduction in chloride concentration under CFRP ranged from 0.53 lb/yd³ to 0.62 lb/yd³ (85% and 56%) in Girders #1 and #2, respectively. Furthermore, concrete with the epoxy coating only exhibited a reduction in chloride concentration of 0.52 lb/yd³ and 0.57 lb/yd³ in Girders #1 and #2, respectively. Similar reductions between chloride concentrations measured under CFRP and epoxy, indicate that epoxy adhesive may have been the major contributing factor to retarding chloride intrusion into the concrete.
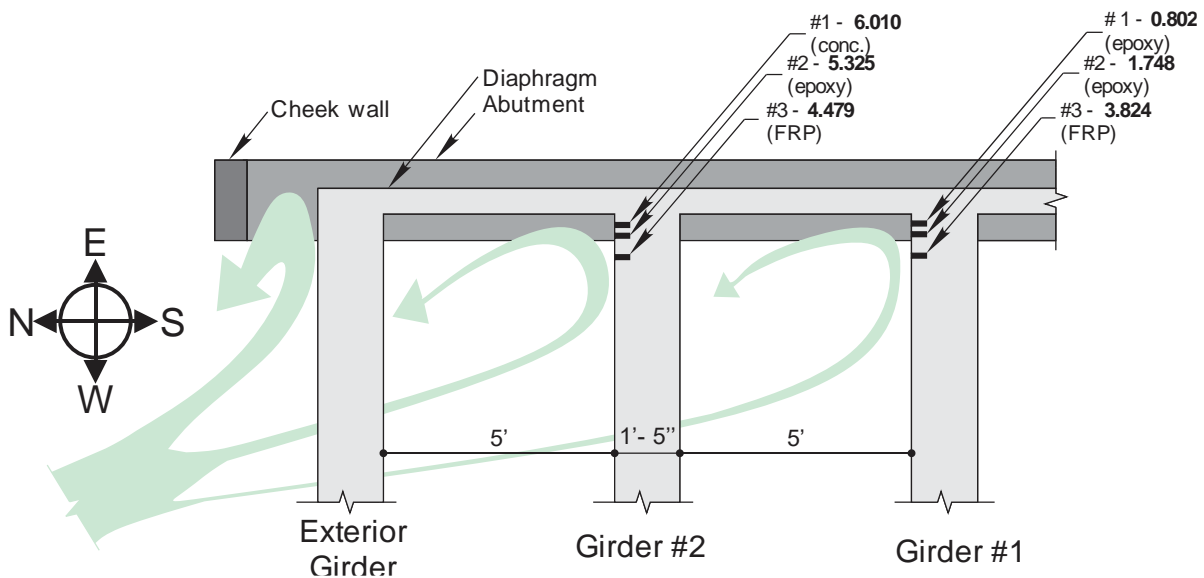
Figure 129—Wind and wave action on bridge girders near abutment (plan view)

Figure 130—Example of wetting caused by wind and wave action

5.10 Findings

Two concrete bridge girders were salvaged from a bridge originally constructed in the 1960s and located over salt water. The girders were repaired with bonded, wet layup CFRP in 1999, and taken out of service in 2010. A set of tests were performed to assess the efficacy of the CFRP repair in terms of added strength, as well as its effects on the corrosion activity and the diffusion of chloride ions. The following are findings and observations from the testing and analysis:

1. Bond between CFRP and concrete had passed the strength criterion (>200 psi) prescribed by ACI 440.2R and NCHRP (2010); possible signs of bond degradation manifested through adhesive failure mode in two of the pull-off tests.

2. Effects of CFRP wrapping on the girder ultimate strength were relatively minor; added strength from CFRP wraps were 8% and 12% for Girders #1 and #2, respectively.

3. Results of a theoretical moment-curvature analysis was in good agreement with experimental moment-curvature on each girder.

4. Only 28% of full elongation capacity of CFRP was developed. This is likely due to evolution of localized strains in CFRP at flexural crack locations, fiber misalignment, and size effects; additional research is required to characterize the behavior.

5. Comparison of data between field and laboratory load tests indicated that AASHTO load distribution factors gave girder loads that were significantly higher than those measured during the load test. The discrepancy between the observed distribution factors, and

those calculated based on AASHTO is accredited primarily to added stiffness from non-structural components, and frictional horizontal reaction at the supports.

6. No significant corrosion had occurred following the CFRP repair in 1999; no signs of anode ring effect were observed either. Based on the results from this study, CFRP provided a satisfactory corrosion protection to internal steel reinforcement. Bonded CFRP appeared to have acted as a barrier that lowered the rate of diffusion of chloride ions in to the underlying concrete substrate; a reduction in chloride contents of 85 and 56% were observed in regions with CFRP overlays located adjacent to exposed concrete in Girder #1 and Girder #2, respectively.

6   University Blvd

6.1   Bridge History

The University Boulevard Bridge (Figure 131) is a reinforced concrete cast-in-place T-girder bridge that spans the Arlington River in Jacksonville, Florida and was built in 1957 (bridge #724214). The bridge was strengthened with FRP composites in 2005 as part of an Innovative Bridge Research and Construction grant from the Federal Highway Administration. This was a joint effort undertaken by the University of Florida (UF) and the Florida Department of Transportation (FDOT). The girders were salvaged from the bridge in 2015.

Figure 131—University Boulevard Bridge

Two spans were selected for repair based on the inspection reports available for this bridge. Span 3 was selected because it was the most severely deteriorated of the spans (Figure 132). Span 4 was selected due to its proximity to Span 3, and to serve as a control. Eight beams, four in each span, were repaired and strengthened. Spans were numbered from south to north while the beams in each span were numbered from west to east. The girders tested in this study were salvaged from Spans 3, 4 and 5.

Prior to the application of the FRP composite reinforcement, some preparatory work was conducted, which included cleaning and patching areas with spalled concrete and sandblasting areas of the beams on which the FRP composite reinforcement was to be installed. The preparatory work was conducted separately from installation of the FRP composite reinforcement. A hybrid FRP composite reinforcement system was installed that included

1.   Externally bonded carbon FRP (CFRP) laminates for flexural strengthening
2.   Glass FRP (GFRP) spray-up for shear strengthening.

After installation of the FRP composite reinforcement, the bridge was instrumented with Fiber Optic Strain (FOS) gages, temperature gages, and corrosion probes that enabled data collection and storage over time.
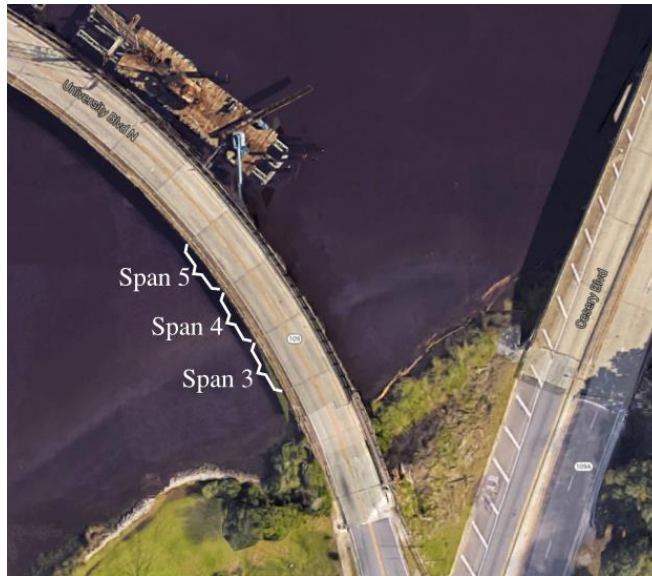
Figure 132—Aerial view of the University Boulevard bridge

Two field load tests were conducted on the bridge, one prior to the installation of the FRP reinforcement and one afterwards. Results from both tests are discussed in this report.

Girders were extracted from the bridge by saw-cutting the deck. Figure 133 shows a partial framing plan that identifies the girders salvaged for testing with a grey shading; GFRP spray-up regions are shown in blue. Curvature of the horizontal bridge alignment resulted in girders with lengths that varied moderately across the width of the bridge. For example, span 3 had girder lengths that varied from 34'-11" for 3-1 to 36'-10" for 3-4. Figure 134 shows cross-section geometry of the salvaged girders and Figure 135 shows a partial section that indicates the FRP locations and dimensions. The GFRP had a thickness of approximately 3/8".
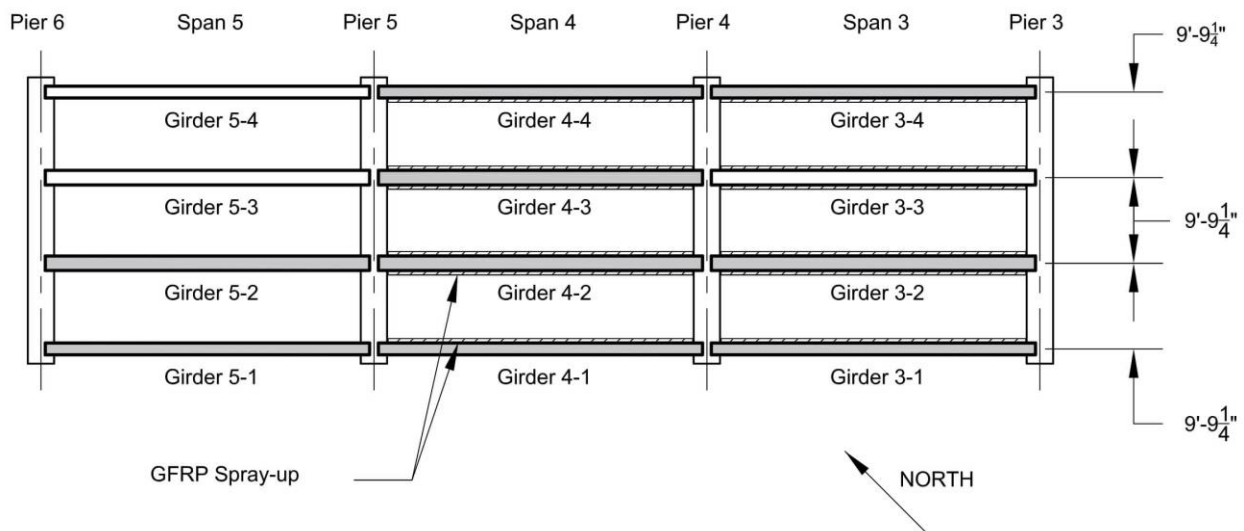
Figure 133—Plan view of spans 3, 4, and 5 chosen for evaluation
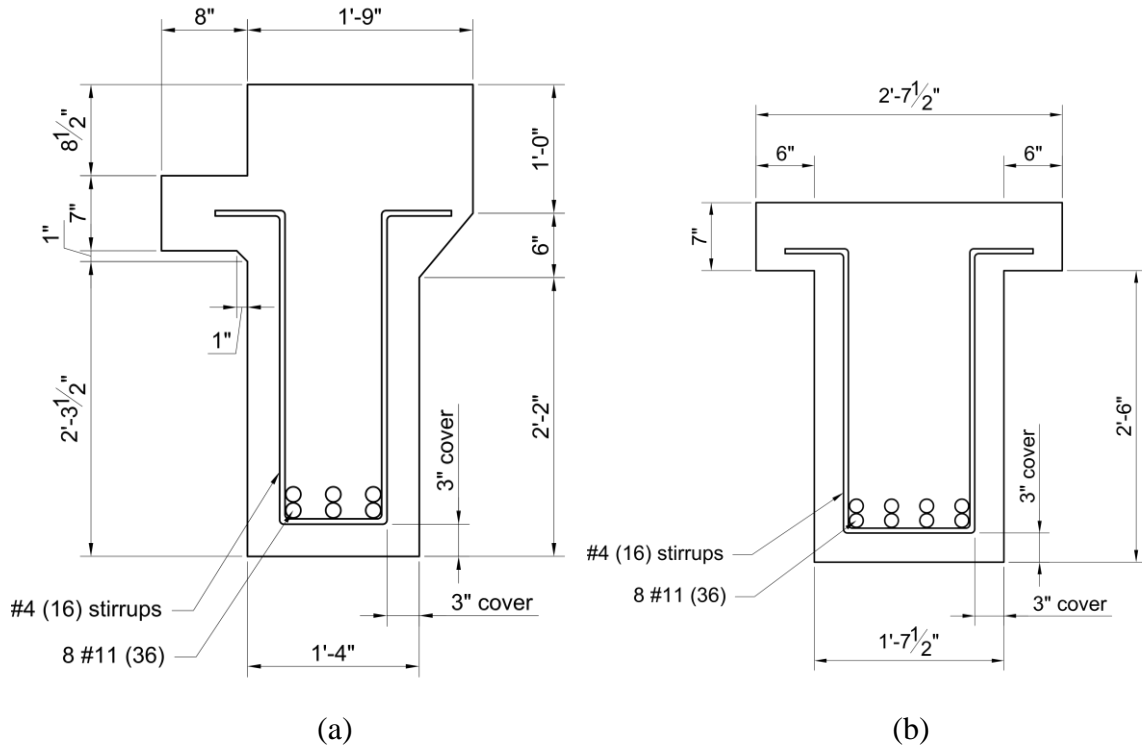
Figure 134—Typical cross-section for (a) Girders 3-1, 3-4, 4-1, 4-4, and 5-1 and (b) Girders 3-2, 4-2, 4-3 and 5-2
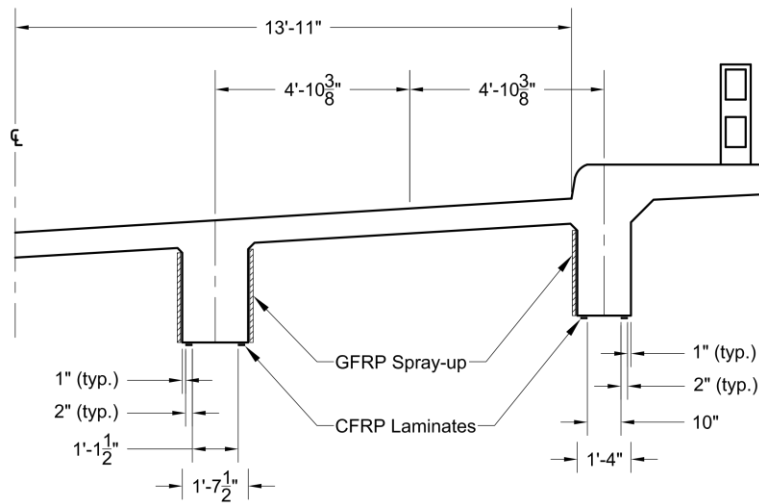
Figure 135—Typical partial cross-section of the bridge span with FRP installed

Figure 136 shows the proximity of spans 3, 4 and 5 to the water level during high tide. Prior to FRP installation, the regular inundation of span three had resulted in corrosion damage that had to be repaired prior to application of FRP composites.

(a)   (b)

Figure 136—High tide inundation of (a) spans 3, 4, and 5, and (b) Girder 3-1 during low tide

6.2 Material Properties

The processes used for measuring compressive strength, chloride content, carbonation, steel reinforcement, and CFRP reinforcement were similar to those used for the Indian River bridge. The following sections will only provide information that varies from the procedures used in materials testing of the Indian River bridge.

6.2.1 Concrete: Compressive Strength

Figure 137 shows the three compression core locations obtained from Girder 3-1 and Girder 5-2. Results from the compressive strength tests are summarized in Table 19.
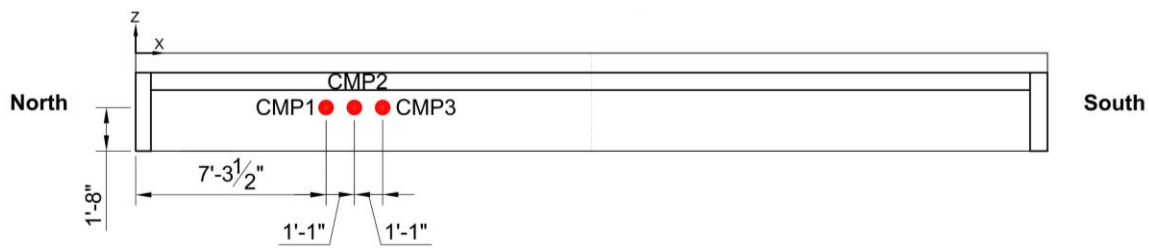
Figure 137—Typical coring locations for compression cores

Table 19—Summary of compression test results

Girder	Core #	x (in.)	y (in.)	z (in.)	Strength (psi)	Failure mode (ASTM C39)	Average strength (psi)
3-1	CMP1	87.5	8	20	2,709	Type 4	2,890
	CMP2	100.5	8	20	2.942	Type 1	
	CMP3	113.5	8	20	3,031	Type 1	
5-2	CMP1	87.5	9.5	20	3,617	Type 1	3,710
	CMP2	100.5	9.5	20	3,507	Type 1	
	CMP3	113.5	9.5	20	3,991	Type 1	

6.2.2   Concrete: Chloride Content

Twelve cores (2-in. dia. by 4-in. min. length) were taken for chloride ion content after structural testing. Core locations were chosen to examine the effects of GFRP wrapping on Cl⁻ contents (Figure 138). Chloride content measurements were performed by FDOT SMO. The results are summarized in Table 20 and Table 21.
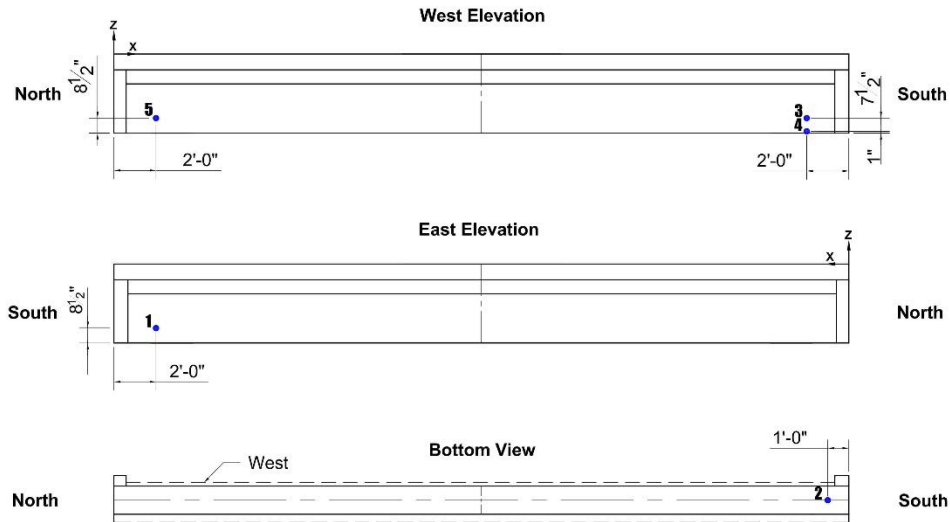
Figure 138—Typical Cl⁻ penetration coring locations indicated in blue

Table 20—Cl⁻ content

Girder	Location	Description	Cl⁻ Content (pcy)
3-2	1	Splash zone - GFRP applied	0.127
3-4	1	Splash zone - concrete	0.248
4-1	1	GFRP applied	0.232
4-2	1	GFRP applied	0.595
4-3	1	GFRP applied	1.681
4-4	1	Concrete	0.118
5-1	1	Concrete	0.106
5-2	1	Concrete	0.338

Table 21—Cl⁻ content in Girder 3-1

Location	Description	Cl⁻ Content (pcy)
1	Splash zone - GFRP applied	2.991
2	Splash zone - concrete	6.632
3	Concrete	4.382
4	Concrete	14.008

6.2.3 Concrete: Carbonation

Six cores for chloride ion penetration were tested for depth of carbonation. These samples were not ground for compression tests, as done for the Indian River samples. Two samples within a few inches apart were taken from Girder 5-2 to check for consistency in the results.

Higher depths of carbonation were noted in specimens with no GFRP on the exterior surface compared to specimens with GFRP (Table 22). The carbonation depths of the samples with and without externally bonded GFRP are compared in Figure 139.

Table 22—Maximum carbonation depths

Girder	Location	Surface	d_k (in)
3-1	5	Concrete	1
3-2	5	GFRP	0
4-2	5	GFRP	0
4-3	5	GFRP	0
5-2 (Sample 1)	5	Concrete	0.5
5-2 (Sample 2)	5	Concrete	0.25
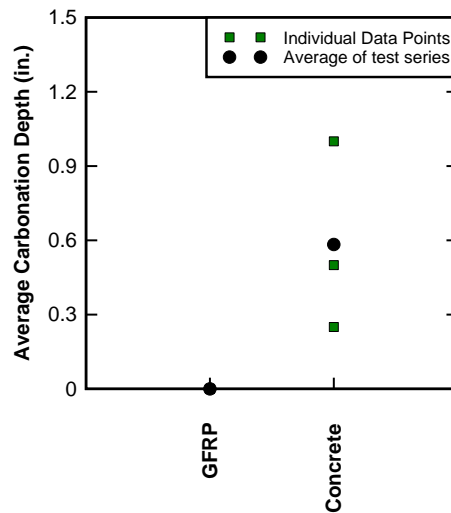
Figure 139—Carbonation depth measurements

6.2.4 Concrete: Corrosion Potential Testing

Corrosion potential testing was conducted on exterior girders (Girder 3-4, 4-1, and 4-4) and control girders (Girder 5-1 and 5-2) in accordance with ASTM C876. The probability of corrosion as given by ASTM C876 is shown in Table 23.

Locations were chosen to examine the effects of GFRP wrapping on corrosion. The locations and results of the potential tests are documented in figures and tables as follows:

- Corrosion potential reading locations for 3-4, 4-1, 4-4, 5-1, and 5-2 are documented in Figure 140
- Girder 3-4 is documented in Table 24
- Girder 4-1 and 4-4 are documented in Table 25
- Girder 5-1 and 5-2 are documented in Table 26
- Corrosion potential reading locations for 3-2, 4-2, and 4-3 are documented in Figure 141
- Girder 3-2, 4-2, and 4-3 are documented in Table 27
- Corrosion potential reading locations for 3-1 is documented in Figure 142
- Girder 3-1 is documented in Table 28

Table 23—Probability of corrosion based on corrosion potential readings

Probability Identification	Voltmeter Reading (V)	Probability
N	Greater than -0.2	Greater than 90% probability that no reinforcing steel corrosion is occurring
U	-0.2 to -0.35	Corrosion activity of the reinforcing steel in that area is uncertain
Y	Lower than -0.35	Greater than 90% probability that reinforcing steel corrosion is occurring
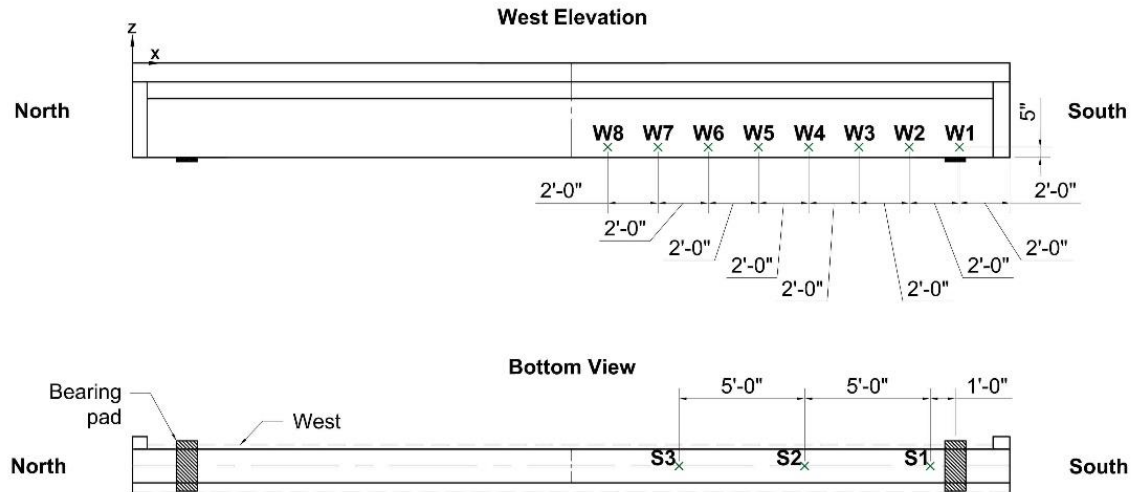
Figure 140—Typical potential testing locations for exterior girders and control

Table 24—Corrosion potential results for Girder 3-4

Location	GFRP (Y/N)	Voltmeter reading (V)	Probability Identification
W1	Y	-0.09	N
W2	Y	-0.10	N
W3	Y	-0.07	N
W4	Y	-0.10	N
W5	Y	-0.13	N
W6	Y	-0.17	N
W7	Y	-0.32	U
W8	Y	-0.36	Y
S1	N	-0.06	N
S2	N	-0.10	N
S3	N	-0.20	U

Table 25—Corrosion potential results for girders in Span 4

Girder	GFRP (Y/N)	Location	Voltmeter reading (V)	Probability Identification
4-1	N	W1	-0.20	U
	N	W2	-0.18	N
	N	W3	-0.14	N
	N	W4	-0.15	N
	N	W5	-0.11	N
	N	W6	-0.24	U
	N	W7	-0.03	N
	N	W8	-0.05	N
	N	S1	-0.51	Y
	N	S2	-0.19	N
	N	S3	-0.03	N
4-4	Y	W1	-0.11	N
	Y	W2	-0.11	N
	Y	W3	-0.12	N
	Y	W4	-0.13	N
	Y	W5	-0.13	N
	Y	W6	-0.15	N
	Y	W7	-0.20	U
	Y	W8	-0.23	U
	N	S1	-0.12	N
	N	S2	-0.13	N
	N	S3	-0.19	N

Table 26—Corrosion potential results for girders in Span 5

Girder	GFRP (Y/N)	Location	Voltmeter reading (V)	Probability Identification
5-1	N	W1	-0.08	N
	N	W2	-0.09	N
	N	W3	-0.07	N
	N	W4	-0.07	N
	N	W5	-0.09	N
	N	W6	-0.11	N
	N	W7	-0.16	N
	N	W8	-0.14	N
	N	S1	-0.03	N
	N	S2	-0.07	N
	N	S3	-0.03	N
5-2	N	W1	-0.11	N
	N	W2	-0.17	N
	N	W3	-0.18	N
	N	W4	-0.15	N
	N	W5	-0.14	N
	N	W6	-0.25	U
	N	W7	-0.18	N
	N	W8	-0.23	U
	N	S1	-0.14	N
	N	S2	-0.13	N
	N	S3	-0.14	N
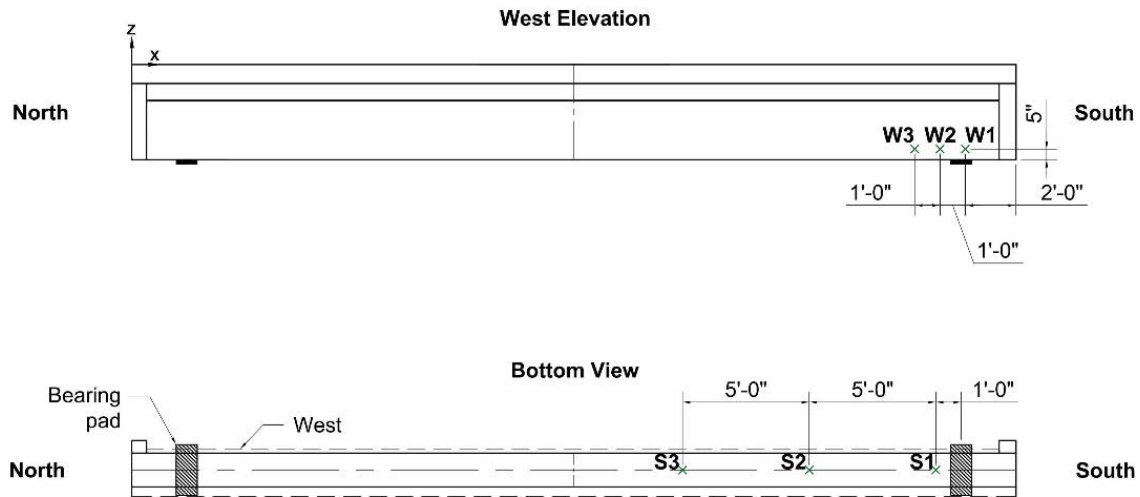
Figure 141—Typical potential testing locations for interior girders

Table 27—Corrosion potential results for interior girders with GFRP

Girder	GFRP (Y/N)	Location	Voltmeter reading (V)	Probability Identification
3-2	Y	W1	-0.09	N
	Y	W2	-0.12	N
	Y	W3	-0.11	N
	N	S1	-0.10	N
	N	S2	-0.11	N
	N	S3	-0.11	N
4-2	Y	W1	-0.22	U
	Y	W2	-0.21	U
	Y	W3	-0.18	N
	N	S1	-0.19	N
	N	S2	-0.19	N
	N	S3	-0.28	U
4-3	Y	W1	-0.36	Y
	Y	W2	-0.36	Y
	Y	W3	-0.24	U
	N	S1	-0.40	Y
	N	S2	-0.42	Y
	N	S3	-0.49	Y
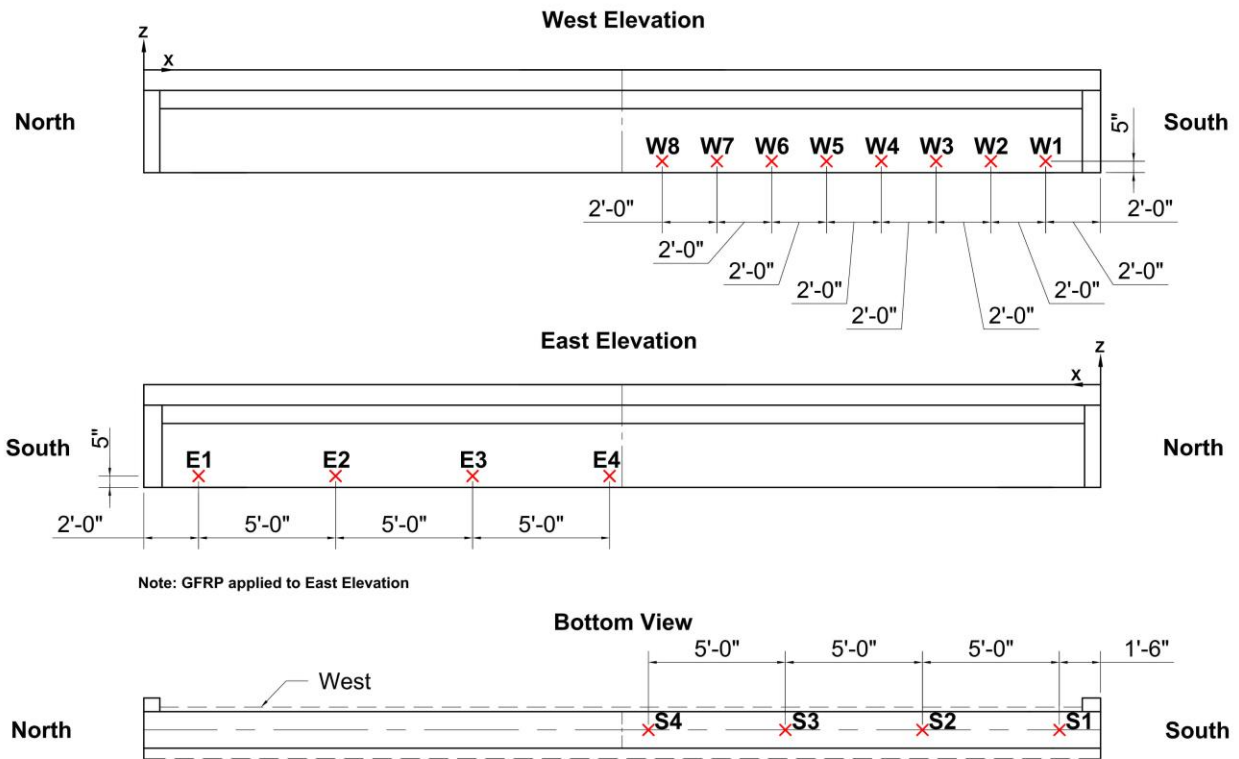
Figure 142—Potential testing locations for Girder 3-1

Table 28—Corrosion potential results for Girder 3-1

Location	GFRP (Y/N)	Voltmeter reading (V)	Probability Identification
E1	Y	-0.81	Y
E2	Y	-0.69	Y
E3	Y	-0.23	U
E4	Y	-0.65	Y
E5	Y	-0.31	U
W1	N	-0.63	Y
W2	N	-0.70	Y
W3	N	-0.62	Y
W4	N	-0.55	Y
W5	N	-0.61	Y
W6	N	-0.57	Y
W7	N	-0.54	Y
W8	N	-0.60	Y
S1	N	-0.64	Y
S2	N	-0.50	Y
S3	N	-0.47	Y
S4	N	-0.69	Y

Girder 3-1 was predicted to have heavier levels of corrosion than the remaining tested girders because of its close proximity to the tidal fluctuations and due to a horizontal crack at approximately 5 in. from the bottom of the girder (Figure 143); girder 3-1 was not structurally tested due to this crack. This provided the opportunity to conduct additional material tests on Girder 3-1. All of the readings on the west elevation of 3-1 had a potential of -0.54V or lower, indicating a high probability of corrosion. Two of the voltmeter readings on the east elevation fall into the category where reinforcing steel in that area is uncertain. This may indicate that GFRP has some effect on the corrosion behavior of the steel reinforcement closest to the east elevation.

Figure 143—Horizontal crack on Girder 3-1 indicated by red arrow

6.2.5 Steel Reinforcement

Steel reinforcement samples for tension testing were taken from the south ends of Girders 3-1, 4-1, 4-3 and 5-1. Girders in Span 3 were more prone to chloride intrusion compared to Span 5 due to the difference in elevation above high tide (Figure 136).

Samples were wire brushed to bare metal to avoid slipping in the grip during tension testing (Figure 144); grip length was 8 in. Wire brushed regions were also used to measure the cross-sectional dimensions so that section loss could be determined. After each sample was tested, approximately 6 in. of the steel reinforcement along the grip region was cut then weighed and measured with a caliper. The grip region was chosen because these regions had already been wire brushed for the corroded samples. Section loss was calculated by normalizing the cross-sectional area of corroded reinforcement to an average cross-sectional area of uncorroded reinforcement. The results from tensile testing the steel reinforcement can be found in Table 29. It was discovered during sampling that stirrups were welded to longitudinal reinforcement in some locations (Figure 145). These samples typically fractured at the spot weld (Figure 146).

Figure 148 shows that there is a positive correlation between the weight and section loss. The regression line, however, does not fit the data as well as it did in the steel reinforcement samples from the Indian River Bridge (R^2=0.92). Indian River bridge data had more data points with higher levels of corrosion. This lack of data points on corroded samples may result in an uncertainty for the University Boulevard samples due to lack of data on the corroded samples.

The method used to measure weight loss for these steel reinforcement samples was slightly different than done for Indian River bridge girders.

Figure 144—Reinforcement with bare metal exposed

Table 29—Results of tests on steel reinforcement

Beam	Location	Yield Strength (ksi)	Tensile Strength (ksi)	Elongation (%)	Section Loss (%)	Weight Loss (%)	Fail at Weld (Y/N)	Flat Failure Surface
3-1	S1	37	67	6.5	20	34	Y	Y
	SE1[S]	34	57	5	26	10	Y	Y
	SE2	38	73	15.5	15	12	N	Y
	SW1	37	69	18.5	18	10	N	N
4-1	S1	42	78	**	12	2	Y	Y
	SE1	42	80	13.5	12	3	N	Y
	SE2	38	66	25.5*	12	4	Y	N
	SW1[S]	38	71	**	12	6	Y	Y
4-3	SE1[S]	42	78	10	7	3	Y	Y
	SE2	40	74	**	7	1	Y	Y
	SW1	42	66	5.5	7	0	Y	Y
	SW2	42	81	12	6	7	Y	Y
5-1	S1	41	78	8*	8	1	N	Y
	SE1[S]	41	76	**	9	4	Y	Y
	SE2	42	71	4.5	12	1	Y	Y
	SW1	41	79	**	7	2	Y	Y

** fracture occurred outside gage region
[S] stirrup not removed from sample
* outlier as determined per ASTM E178

Figure 145—Steel reinforcement welded together with stirrups

Figure 146—Typical hackle pattern pointing to the origin of fracture surface, which in this case is the spot weld

Figure 147—Stirrup remaining on steel reinforcement sample
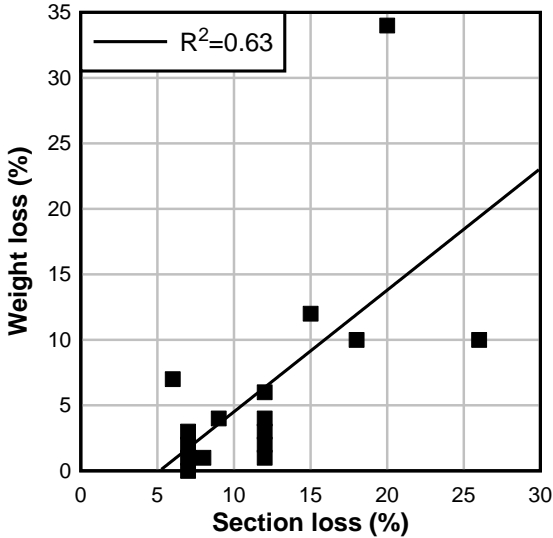
Figure 148—Correlation between weight loss and section loss

6.2.6 CFRP Reinforcement

To determine the mechanical properties of the CFRP material, tensile tests were performed on 23 carbon fiber laminate coupons that were cut out of the CFRP strips that debonded after the beams were tested in flexure. These samples consist of carbon fibers that are impregnated into an epoxy resin matrix. The precured CFRP laminate used to reinforce the beams was Sika CarboDur Type S512. The carbon fiber system, as specified by the manufacturer, has a tensile strength of 406 ksi, a maximum elongation at break of 1.69% and a MOE of 23900 ksi.

One CFRP sample was tested with three strain gages to determine if bending was affecting the results. The remaining samples used a single gage. The tests were performed on a Tinius Olsen testing machine, as per ASTM D3039 (Figure 149). Load data were acquired from the built-in 90-kip load cell, and the displacement data were collected with a 350Ω Omega strain gage with a gage length of 6 mm. Typical failure mode of the test coupon is shown in Figure 149b.

Tensile properties of the samples were compared to the manufacturer's specifications (Table 30). In interpretation of test results, it should be noted that the composite had experienced significant stress prior to tensile testing - during the structural test, and debonding from the concrete surface. A slight case of bending also occurred while testing the samples, which could affect the results.

(a)   (b)

Figure 149—(a) CFRP coupon tension test setup (b) typical failure mode of test coupon

The data in Table 30 represent tensile stress values and elongation values similar to the manufacturer's specifications. Plots comparing the experimental and theoretical values of ultimate stress and elongation are shown in Figure 151.

Table 30—CFRP coupon tension test results

Specimen Number	Tensile Strength (ksi)	Elongation	Modulus of Elasticity (ksi)
3-4E(1)	420	–	–
3-4E(2)	390	–	–
3-4E(3)	321	–	–
3-4E(4)	397	–	–
3-4W(1)	431	0.0177	26700
3-4W(2)	488	0.0170	29600
3-4W(3)	444	0.0176	29200
3-4W(4)	487	0.0169	30800
3-4W(5)	392	0.0174*	18400
4-1W(1)	440	0.0151*	28200
4-1W(2)	450	0.0158*	27300
4-1W(3)	413	0.0162	26200
4-1W(4)	405	0.0173	25800
4-1W(5)	386	0.0142*	26900
4-3E(1)	464	0.0177*	26900
4-3E(2)	277	0.0170*	27800
4-3E(3)	282	0.0176*	38400
4-3E(4)	441	0.0169	25900
4-3E(5)	444	0.0174*	29600
4-4W(1)	453	0.0132*	25500
4-4W(2)	477	0.0140*	26000
4-4W(3)	312	0.0164	24800
4-4W(4)	324	0.0163	25800
Average:	406	0.0169	27400
COV:	0.16	0.03	0.14

* strain gage detached from sample before rupture occurred; actual elongation may be larger

(a)   (b)
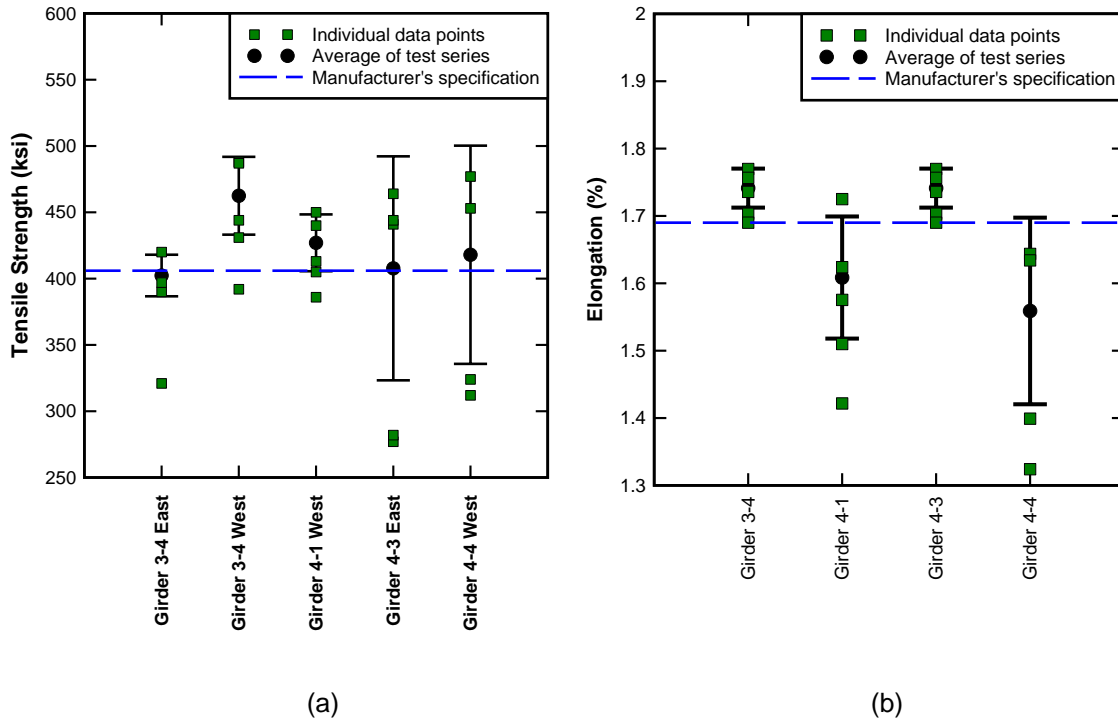
Figure 150—Correlation between the theoretical and experimental (a) tensile strength and (b) elongation

6.2.7   FRP Reinforcement: Pull-off Tests for Girder 3-1

Direct pull-off testing locations were chosen to examine the quality control of the external FRP repairs (Figure 151). Sixteen tests were performed on Girder 3-1, three of which were additional samples due to failure at the interface between the loading fixture and the FRP (failure mode A) to determine whether or not a cohesive or adhesive failure would occur. Pull-off tests were positioned down the middle of each bonded precured CFRP strip.
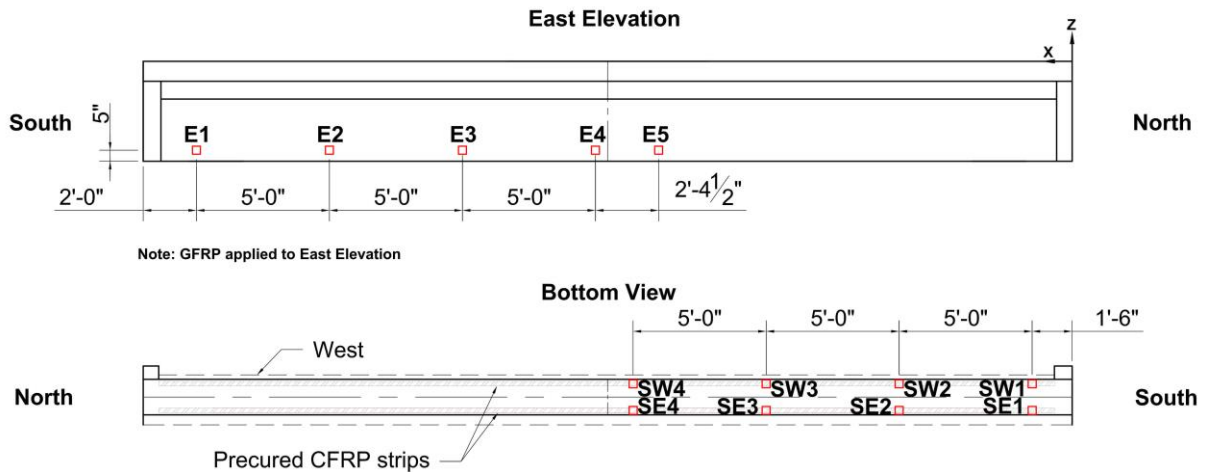
Figure 151—Direct pull-off testing locations for Girder 3-1

Direct pull-off test results are summarized in Table 31. The percent of adhesive failure mode was determined on each sample by a visual approximation. Approximately 63% of the pull-off tests passed the tensile pull-off strength criterion. In addition, 54% of the samples failed cohesively; however, an adhesive and a mixed failure mode were also observed. Samples with failure mode A were not considered.

Table 31—Summary of direct pull-off test results for Girder 3-1

Location	GFRP (Y/N)	CFRP (Y/N)	Stress at failure (psi)	Failure mode (% adhesive)	ASTM D7522 failure mode	Note
E1	Y	N	409.3	0	G	–
E2	Y	N	69.1	95	E	–
E3	Y	N	99.3	95	F	–
E4	Y	N	169.0	95	F	–
E5	Y	N	112.4	95	F	Failure in darker repair concrete substrate
SE1	N	Y	43.0	5	B	–
SE2 (1)	N	Y	146.1	–	A	–
SE2 (2)	N	Y	280.4	0	G	Failure in darker repair concrete substrate
SE3	N	Y	261.0	0	F	Failure in darker repair concrete substrate
SE4	N	Y	243.5	0	G	Failure in darker repair concrete substrate
SW1 (1)	N	Y	261.0	–	A	–
SW1 (2)	N	Y	241.3	0	G	–
SW2	N	Y	260.1	0	G	–
SW3	N	Y	297.3	0	G	–
SW4 (1)	N	Y	357.1	–	A	–
SW4 (2)	N	Y	257.8	0	G	–

6.2.8 FRP Reinforcement: Pull-off Tests for Exterior Girders

Figure 152 shows the locations of direct pull-off testing for exterior girders (3-1, 4-1, and 4-4). Direct pull-off test results for Girder 3-4 are summarized in Table 32. Approximately 83% of the pull-off tests passed the tensile pull-off strength criterion. One of the two samples that failed the tensile test had a crack in the testing location that most likely affected the tensile strength results. In addition, 50% of the samples failed cohesively; however, an adhesive and a mixed failure mode were also observed.

Direct pull-off test results for Girder 4-1 are summarized in Table 33. Approximately 83% of the pull-off tests passed the tensile pull-off strength criterion. One of the two samples, however, that did not exceed the strength criterion failed in mode A, which is considered neither an adhesive nor a cohesive failure mode. All but one sample failed cohesively; samples with failure mode A were not considered. The one sample that failed adhesively also failed at the interface between the loading fixture and the FRP, which may have had an effect on the failure mode.

Direct pull-off test results for Girder 4-4 are summarized in Table 34. All tests passed the tensile pull-off strength criterion. In addition, 33% of the samples failed cohesively; adhesive and mixed failure modes, however, were also observed. Some voids in the concrete were noted during testing (Figure 153).
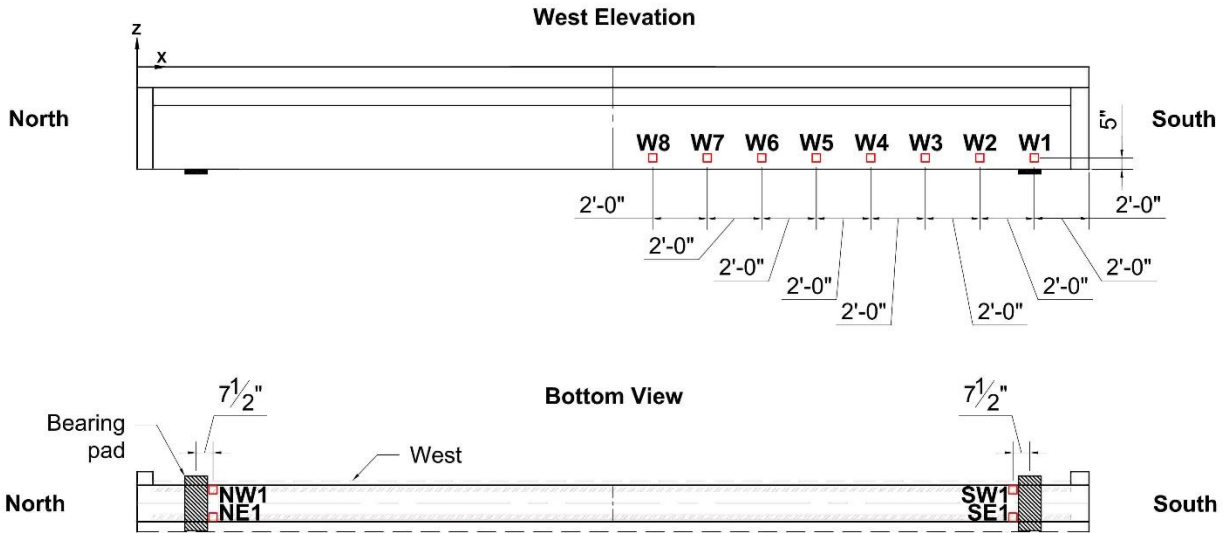
Figure 152—Direct pull-off testing locations for exterior girders

Table 32—Summary of direct pull-off test results for Girder 3-4

Location	GFRP (Y/N)	CFRP (Y/N)	Stress at failure (psi)	Failure mode (% adhesive)	ASTM D7522 failure mode	Note
W1	Y	N	322.8	0	G	–
W2	Y	N	81.5	65	E	–
W3	Y	N	459.6	0	G	–
W4	Y	N	570.7	0	G	–
W5	Y	N	446.9	30	F	–
W6	Y	N	513.1	5	F	–
W7	Y	N	326.6	0	G	Two cracks present in testing area
W8	Y	N	6.4	3	F	Two cracks run through the test location; relocated 4' north of W8 location
NE1	N	Y	293.2	80	E	–
SE1	N	Y	493.4	0	G	–
NW1	N	Y	433.9	0	G	–
SW1	N	Y	241.6	30	F	–

Table 33—Summary of direct pull-off test results for Girder 4-1

Location	GFRP (Y/N)	CFRP (Y/N)	Stress at failure (psi)	Failure mode (% adhesive)	ASTM D7522 failure mode	Note
NE1	N	Y	274.1	–	A	–
SE1	N	Y	221.5	0	G	Two cracks present in testing area
NW1	N	Y	335.5	0	G	–
SW1	N	Y	81.5	–	A and C	Adhesive on interface between the loading fixture and FRP was still tacky
NE2	N	Y	230.5	0	G	Relocated 9" south of W8 location

Table 34—Summary of direct pull-off test results for Girder 4-4

Location	GFRP (Y/N)	CFRP (Y/N)	Stress at failure (psi)	Failure mode (% adhesive)	ASTM D7522 failure mode	Note
W1	Y	N	433.9	0	G	Small void on tested area
W2	Y	N	335.5	35	F	Presence of 3 small voids
W3	Y	N	–	–	–	–
W4	Y	N	488.9	60	F	–
W5	Y	N	481.3	80	F	–
W6	Y	N	327.5	100	C	–
W7	Y	N	276.0	50	F	Presence of a few small voids
W9	Y	N	277.9	5	F	Relocated 2" below W8 location
NE1	N	Y	380.1	0	G	–
SE1	N	Y	393.4	100	C	–
NW1	N	Y	243.8	0	G	–
SW1	N	Y	479.1	0	G	–

Figure 153—Pull-off testing sample from Girder 4-4 with multiple voids in concrete

6.2.9   FRP Reinforcement: Pull-off Tests for Interior Girders with FRP

Figure 154 shows the locations of direct pull-off testing for interior girders (3-2, 4-2, and 4-3). Some of the pull-off tests failed at the dolly to FRP interface (Failure mode A), either from the adhesive not being completely cured or from the set of smooth dollies which were used on 11 pull-off testing locations (Figure 155). The same bond tester used in the Indian River report was used after these 11 locations to avoid more samples from failing in Failure mode A.

Direct pull-off test results for Girder 3-2 and 4-2 are summarized in Table 35 and Table 36, respectively. All tests passed the tensile pull-off strength criterion, and failed cohesively (excluding samples that had failure mode A). Direct pull-off test results for Girder 4-3 are summarized in Table 37. Six of nine tests passed the tensile pull-off strength criterion. Samples that failed the tensile test were noted to either have a crack or void in the testing area, which may have reduced the tensile strength results.
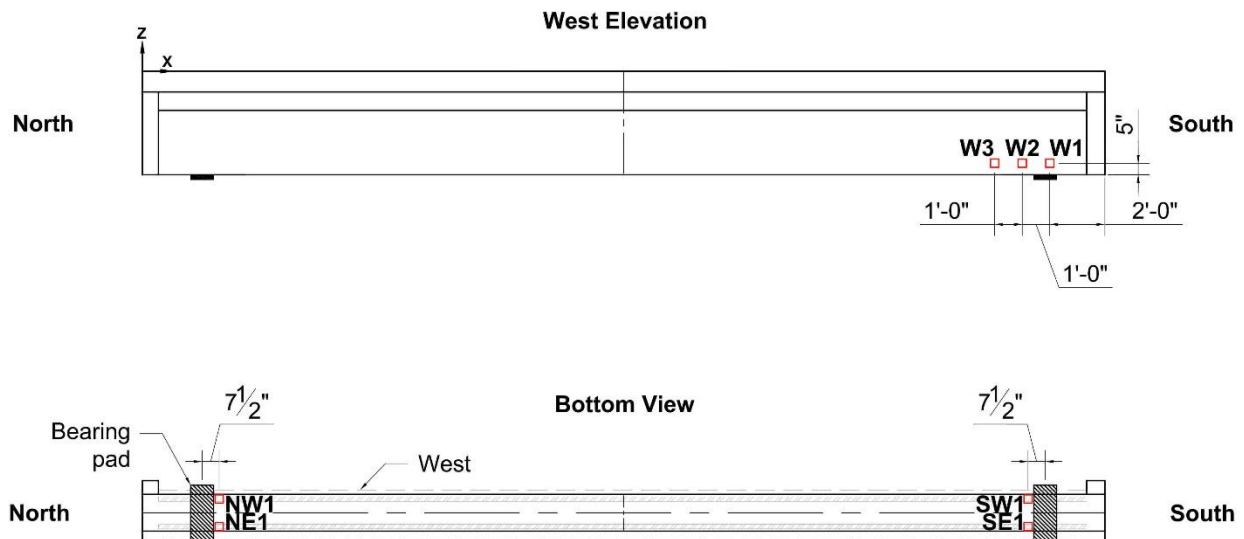
Figure 154—Direct pull-off testing locations for interior girders

Figure 155—Smooth dolly that failed at the dolly-to-FRP interface

Table 35—Summary of direct pull-off test results for Girder 3-2

Location	GFRP (Y/N)	CFRP (Y/N)	Stress at failure (psi)	Failure mode (% adhesive)	ASTM D7522 failure mode
W1	Y	N	469.2	0	G
W2	Y	N	313.9	0	G
W3	Y	N	550.7	0	G
NE1*	N	Y	467.0	–	A
SE1*	N	Y	438.0	0	G
NW1*	N	Y	499.0	0	G
SW1*	N	Y	604.8	0	G

*results were determined by DeFlesko Positest AT-M adhesion tester bond tester

Table 36—Summary of direct pull-off test results for Girder 4-2

Location	GFRP (Y/N)	CFRP (Y/N)	Stress at failure (psi)	Failure mode (% adhesive)	ASTM D7522 failure mode
W1*	Y	N	476.5	–	A
W2*	Y	N	392.8	0	G
W3*	Y	N	366.1	0	G
NE1*	N	Y	375.0	0	G
SE1*	N	Y	384.2	0	G
NW1*	N	Y	426.0	–	A
SW1*	N	Y	402.3	0	G

*results were determined by DeFlesko Positest AT-M adhesion tester bond tester

Table 37—Summary of direct pull-off test results for Girder 4-3

Location	GFRP (Y/N)	CFRP (Y/N)	Stress at failure (psi)	Failure mode (% adhesive)	ASTM D7522 failure mode	Note
W1	Y	N	368.6	100	E	–
W2	Y	N	405.5	–	A	–
W3	Y	N	399.2	0	G	–
NE1	N	Y	268.3	0	G	–
SE1	N	Y	75.1	0	G	Test location compromised from cracks
NW1	N	Y	435.4	–	A	–
SW1	N	Y	15.0	0	G	Test location compromised from cracks
SE2	N	Y	496.6	0	G	Test site 14" N of original location
NW2	N	Y	–	–	–	–
SW2	N	Y	58.9	0	G	Relocated 17.5" north of original location; deeper fracture due to the presence of a void

6.2.10 GFRP Reinforcement

To determine the mechanical properties of the GFRP, tensile tests were performed on 20 GFRP samples extracted from Girders 3-1, 4-1, 4-2 and 4-3. The GFRP was initially installed using a spray-up system by Magnum Venus Products (MVP). The GFRP used to strengthen the beams was a PPG Industries Hybon 6400. The glass fiber system, as specified by the manufacturer, has a dry tensile strength of 14.1 ksi and a wet tensile strength of 13.4 ksi.

The average thickness in each set of samples from a specific girder dictated the sample size based on ASTM D638. Samples from Girder 3-1, 4-1 and 4-2 had an average thickness (T) between 0.28 in. and 0.55 in., which categorized them as Type III specimens. Samples from Girder 4-3 had an average thickness (T) of 0.28 in. or less, which categorized these samples as Type I. After determining the classification, the samples were shaped to meet ASTM D638 dimensions for each type (Figure 156 and Table 38).

Tension tests were performed on a Tinius Olsen testing machine, as per ASTM D638 (Figure 157). Load data were acquired by the built-in 90-kip load cell. Typical failure mode of the test coupon is shown in Figure 157b. Dimensions and tensile properties of the samples are documented in Table 39. Figure 158 shows a comparison of the tensile strength determined by the manufacturer using dry tensile strength criteria.

Figure 156—Specimen dimensions based on thickness T as per ASTM D638

Table 38—Dimensions of specimen as per ASTM D638

Dimensions (see Figure 158)	Type I (in.)	Type III (in.)
W – Width of narrow section	0.50	0.75
L – Length of narrow section	2.25	2.25
WO – Width overall, min	0.75	1.13
LO – Length overall, min	6.50	9.70
G – Gage length	2.00	2.00
D – Distance between grips	4.50	4.50
R – Radius of fillet	3.00	3.00

(a)   (b)

Figure 157—(a) GFRP coupon tension test setup (b) typical failure mode of test coupon

Table 39—GFRP coupon tensile test results

Specimen Number	Type	Thickness T (in.)	Width W (in.)	Tensile Strength (ksi)	Modulus of Elasticity (ksi)
3-1(1)	III	0.303	0.773	11.3	88.6
3-1(2)		0.321	0.729	11.8	87.9
3-1(3)		0.309	0.683	14.3	111.0
3-1(4)		0.342	0.729	14.0	125.0
3-1(5)		0.353	0.775	11.5*	81.4*
4-1(1)		0.330	0.745	13.8	102.0
4-1(2)		0.294	0.727	14.4	90.7
4-1(3)		0.268	0.671	14.6	146.0
4-1(4)		0.295	0.781	16.5	125.0
4-1(5)		0.303	0.724	13.5	121.0
4-2(1)		0.238	0.713	13.6	106.0
4-2(2)		0.252	0.694	11.6	134.0
4-2(3)		0.245	0.694	11.3	120.0
4-2(4)		0.235	0.723	13.5	129.0
4-2(5)		0.241	0.699	10.8	95.7
4-3(1)	I	0.120	0.495	15.1	167.0
4-3(2)		0.136	0.475	13.3	162.0
4-3(3)		0.100	0.498	11.9	207.0
4-3(4)		0.144	0.468	13.7	220.0
4-3(5)		0.096	0.473	11.5	263.0
			Average:	13.2	134.1
			COV:	0.12	0.36

* specimen failed outside the gage region, and was excluded from average values of ultimate stress
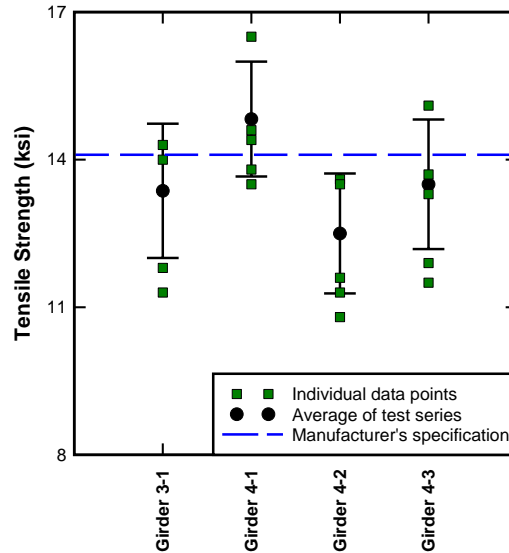
Figure 158—Comparison of experimental tensile strength and manufacturer's specified tensile strength (error bars represent one standard deviation)

6.2.11 CFRP Reinforcement: Materials Testing of Bond Specimens

Rectangular (1/2 in. × 1/2 in.) samples of CFRP were taken from the debonded regions. Some of the samples were extracted from the regions on the girders where CFRP debonded cohesively and had intact concrete substrate on one side. Both the surface of the debonded CFRP and the bonded concrete substrate were imaged at a high magnification in the SEM.

Due to its high viscosity and high silica sand content, the paste epoxy used to bond CFRP laminate to the girders had large number of voids present within its microstructure (Figure 159a). Additionally, possibly due to the environmental degradation, microcracks were observed at the interface between silica-sand filler particles and the epoxy adhesive (Figure 159b). No defects were observed at the CFRP-epoxy interface (Figure 159a). Many voids were found, however, along the interface between epoxy and concrete (Figure 160) which likely occurred during the installation of the composite. CFRP composite, similarly to the wet-layup system used in the Indian River Bridge, exhibited damage within the matrix and matrix-fiber interface (Figure 161). It is not clear whether the damage was due to the environmental degradation, specimen manipulation and handling, or the installation defects.
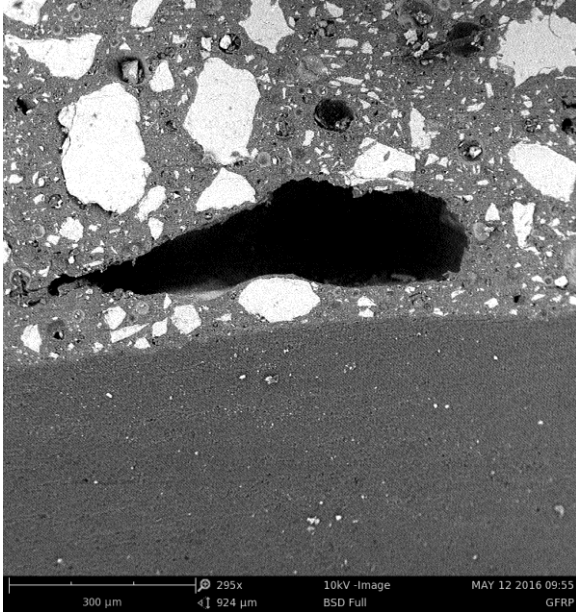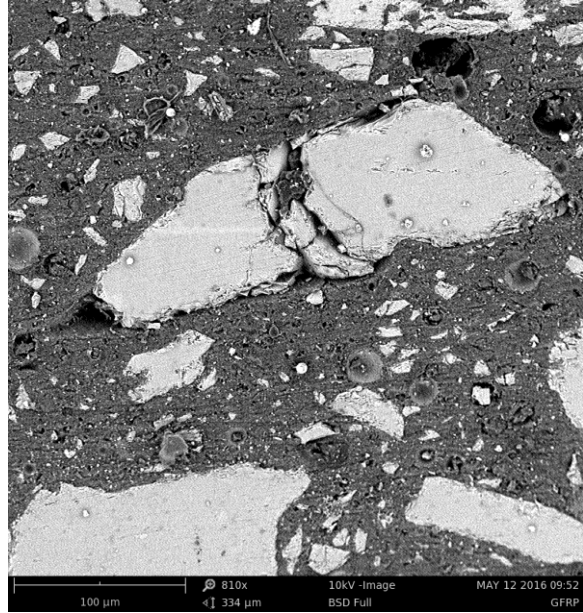
(a)   (b)

Figure 159—SEM images of: (a) interface between CFRP (bottom) and epoxy (top) (b) magnified image of a single silica sand grain in the epoxy matrix.
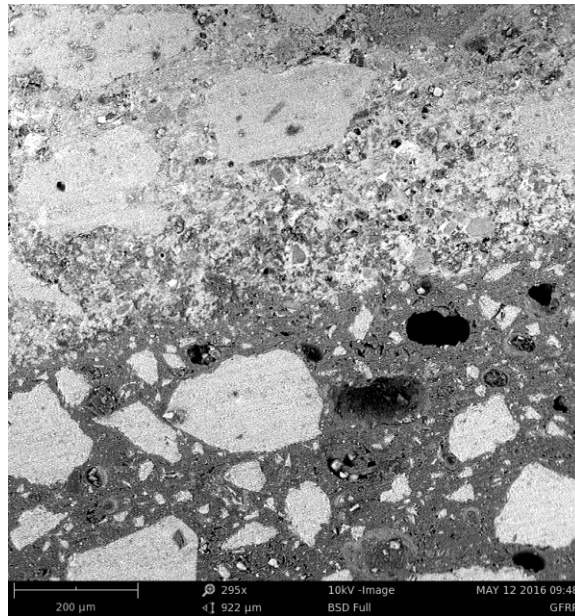
Figure 160—SEM image of interface between concrete (top) and epoxy (bottom).
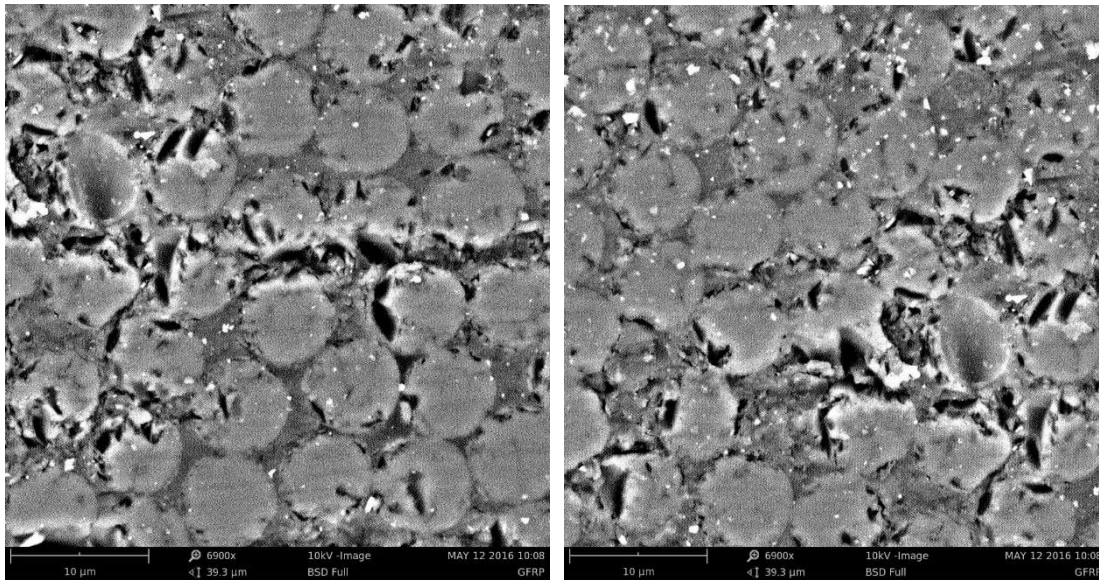
Figure 161—Examples of damage distributed within the CFRP

6.2.12 GFRP Reinforcement: Flexural Testing

Flexural tests were performed on 20 glass fiber coupons that were extracted from Girder 3-1, 4-1, 4-2 and 4-3. The glass fiber system, as specified by the manufacturer, has a dry flexural strength of 26.9 ksi, and a dry modulus of elasticity of 1050 ksi. The glass fiber system is also rated to have a wet flexural strength of 24.7 ksi and a wet flexural modulus of 780 ksi.

The cross-sectional dimensions varied among the samples, so an average thickness was taken for each set of samples from a specific girder and a span was determined based on that average (Table 40). This approach was taken to to avoid variability in test results.

Testing was performed on a Tinius Olsen testing machine, as per ASTM D790 using the test setup shown in Figure 162. Load data were acquired using the built-in 90-kip load cell, and the displacement data were collected with an LVDT setup using two RDP D5/400AG LVDTs with a range of 19 mm. Typical failure mode of the test coupon is shown in Figure 162b. Test results are shown in Table 40.

Figure 163 and Figure 168 compare, respectively, the results of the flexural strength and flexural modulus of elasticity determined using the manufacturer's dry flexural strength specifications.

Table 40—GFRP coupon flexural test results

Specimen Number	Thickness (in.)	Width (in.)	Flexural Strength (ksi)	Displacement (in)	Modulus of Elasticity (ksi)
3-1(1)	0.255	1.105	25.7	0.41	1340
3-1(2)	0.279	1.123	28.8	0.33	1500
3-1(3)	0.311	1.146	24.4	0.31	1290
3-1(4)	0.290	1.165	22.2	0.27	1550
3-1(5)	0.252	1.154	24.9	0.41	1340
4-1(1)	0.347	1.316	20.9	0.38	1250
4-1(2)	0.357	1.291	23.9	0.34	1240
4-1(3)	0.329	1.299	22.7	0.34	1240
4-1(4)	0.267	1.265	24.4	0.38	1430
4-1(5)	0.299	1.278	23.2	0.32	1210
4-2(1)	0.190	0.825	27.0	0.29	1470
4-2(2)	0.189	0.803	20.0	0.27	1280
4-2(3)	0.210	0.805	23.8	0.24	1130
4-2(4)	0.214	0.788	24.2	0.24	1250
4-2(5)	0.203	0.817	24.3	0.28	1300
4-3(1)	0.156	0.480	28.8	0.18	1400
4-3(2)	0.138	0.528	22.6	0.24	1170
4-3(3)	0.138	0.535	22.2	0.21	1240
4-3(4)	0.116	0.532	27.4	0.19	1440
4-3(5)	0.134	0.520	26.4	0.18	1430
		Average:	24.4	0.29	1330
		COV:	0.10	0.25	0.09

(a)   (b)
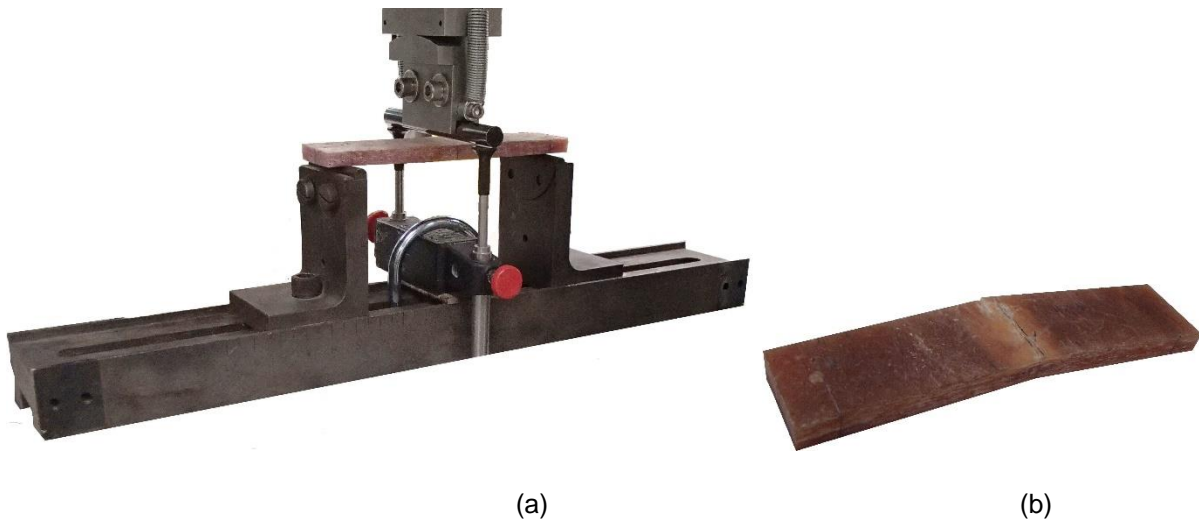
Figure 162—(a) GFRP coupon flexural test setup (b) typical failure mode of test coupon
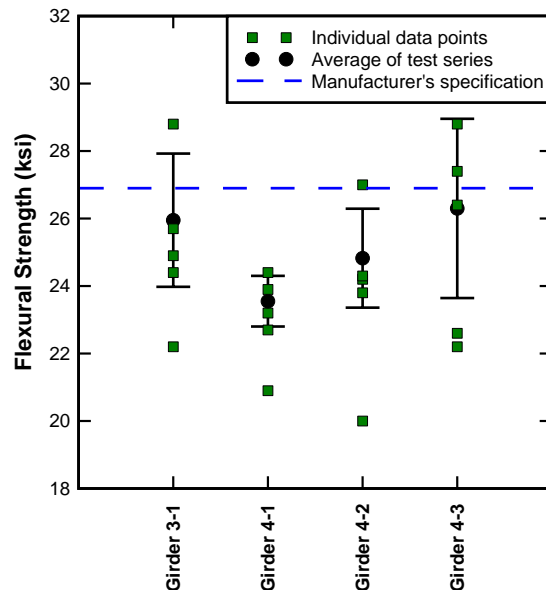
Figure 163—Comparison of the experimental flexural strength and manufacturer's specified flexural strength (error bars represent one standard deviation)

6.2.13 GFRP Reinforcement: Materials Testing of Bond Specimens

Rectangular (1/2 in. × 1/2 in.) samples of GFRP with bonded concrete were extracted with an angle grinder subsequent to collecting GFRP coupons for tensile and flexural testing. Similar procedures to those described in chapter 5 were used to prepare and image the samples in the SEM.

Inspection of the GFRP composite indicated that fibers were oriented in preferential directions. Additionally, it was apparent that fibers were also not uniformly distributed within the matrix. Regions with very high volume fractions of fibers were contrasted by the regions without any fiber content. Large defects (Figure 164) in the regions without fibers do not fully benefit from the fibers' crack-bridging effect, which can possibly improve the macroscale mechanical properties of the composite. Magnified images of the fibers embedded in the polyester matrix did not show any signs of matrix or interfacial damage (Figure 165); the fibers, however, appear to be packed very tightly, which could result in significant stress concentrations when stresses acting perpendicular to the fiber direction are applied.

Figure 166 shows a backscatter electron image of the adhesive interface between GFRP and concrete. Dark regions in the image are representative of low average atomic number (low backscatter electron yield) and correspond to the adhesive; relatively brighter regions on the image represent concrete. Even though mechanical interlocking due to concrete surface irregularities is apparent, the collected SEM images reveal separation between the adhesive and concrete indicating potentially poor adhesion.
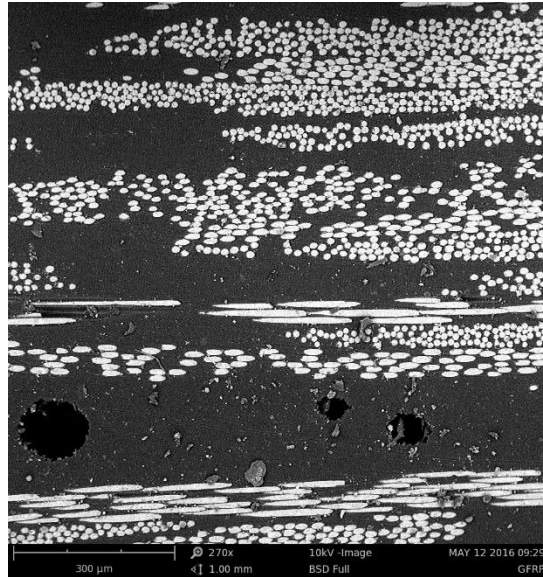
Figure 164—SEM image showing non-uniform distribution and preferential orientation of fibers within the GFRP composite matrix
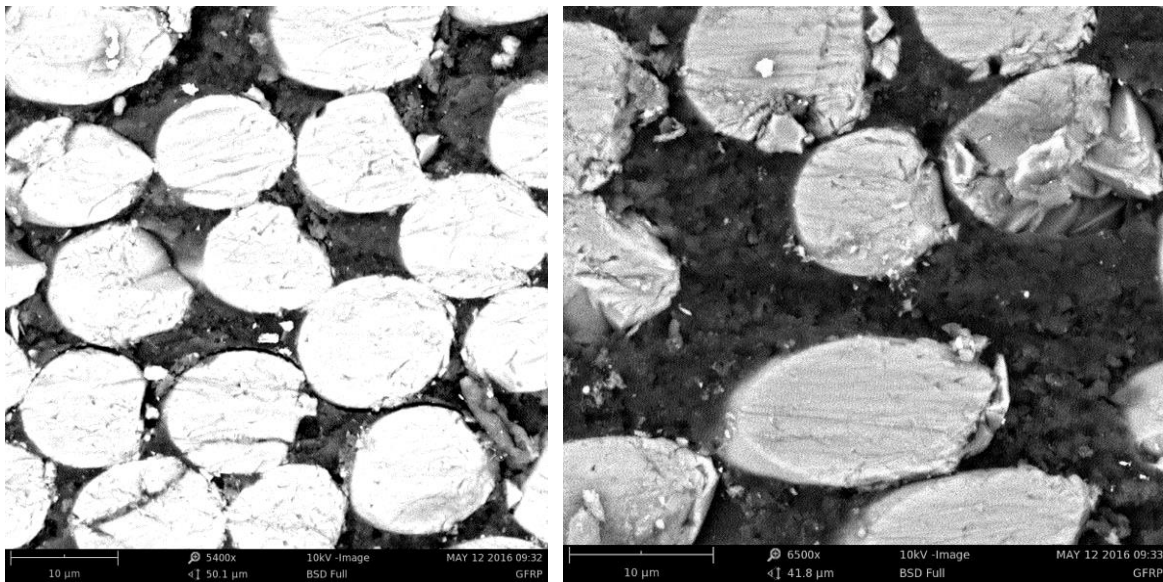
Figure 165—Magnified SEM images of fiber-matrix interface
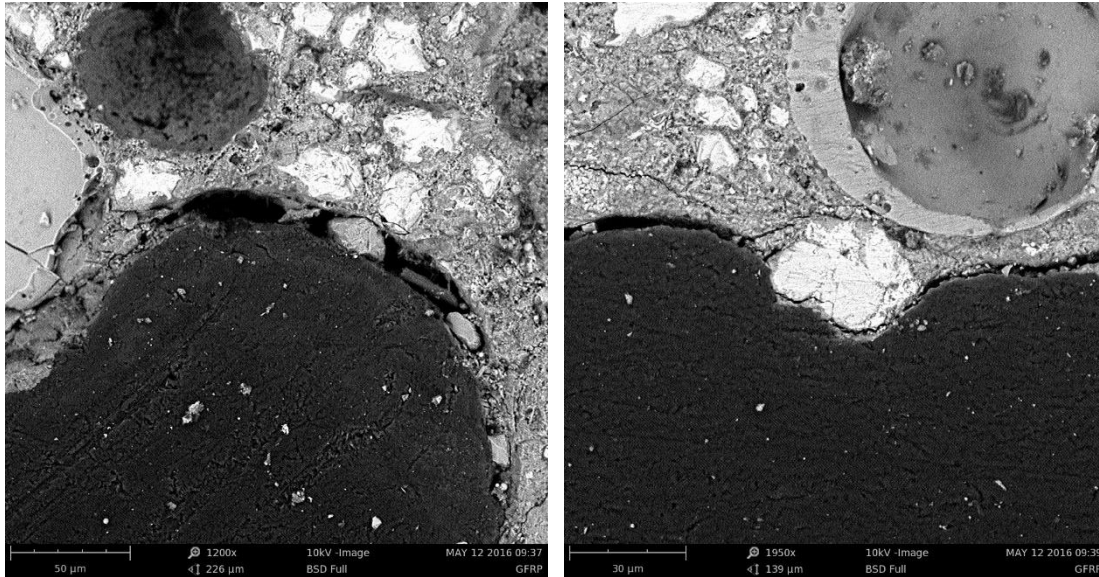
Figure 166—SEM image of interface between concrete (top) and GFRP composite (bottom)

6.3 Flexural Test Setup and Instrumentation

The preparation procedures used for flexural testing were identical to those used for the Indian River bridge girders. The following sections provide information that varies from the chapter covering Indian River bridge (Section 5.4). Eight of nine girders were tested in flexure using a four-point bending test setup to determine their behavior in flexure (Figure 167 through Figure 170). Girder 3-1 was not tested in flexure to preserve it so that in-depth materials testing could be conducted.

Figure 167—Girder loaded in test frame

Top View

West Elevation
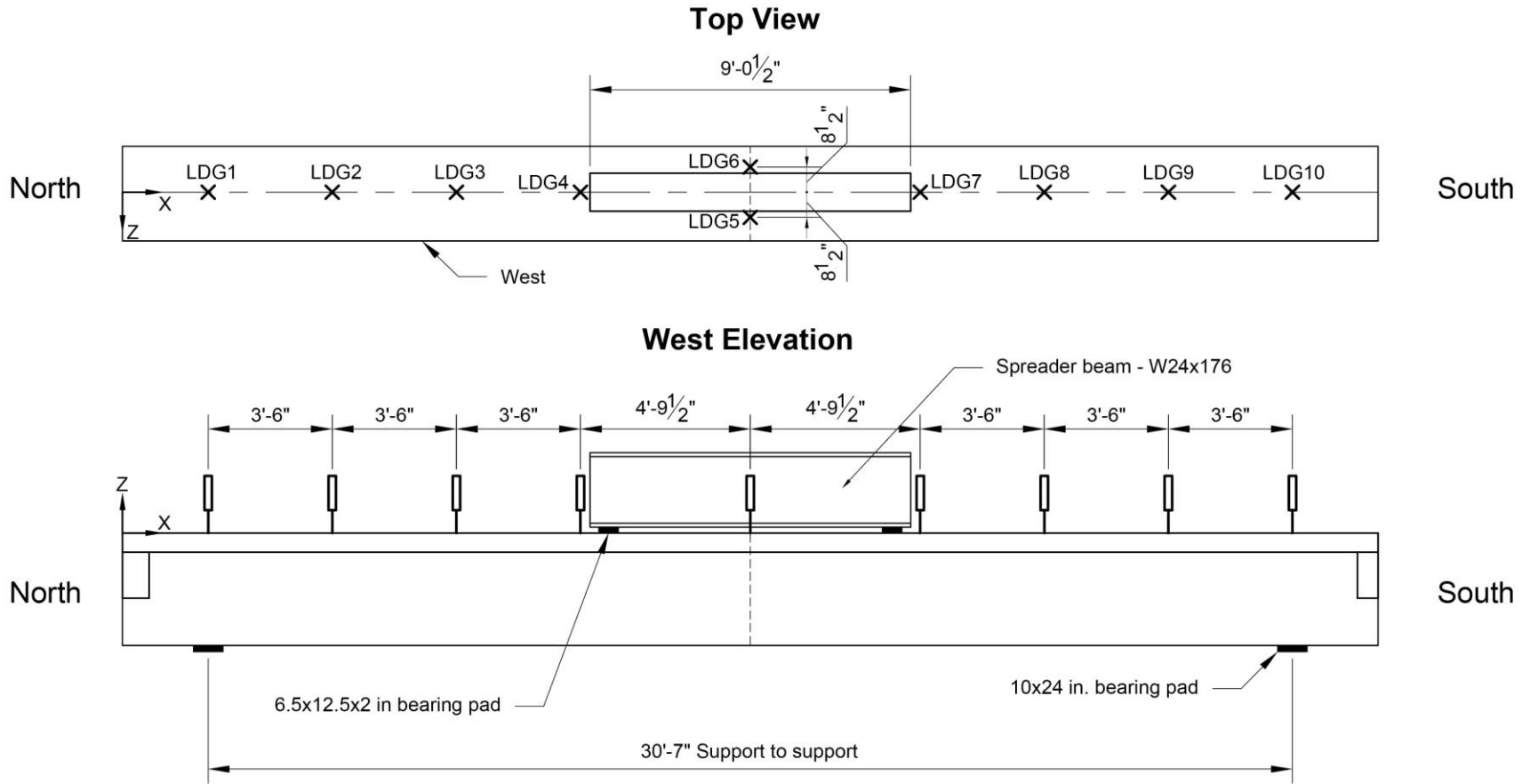
Figure 168—Typical instrumentation plan representing the locations for the laser displacement transducers
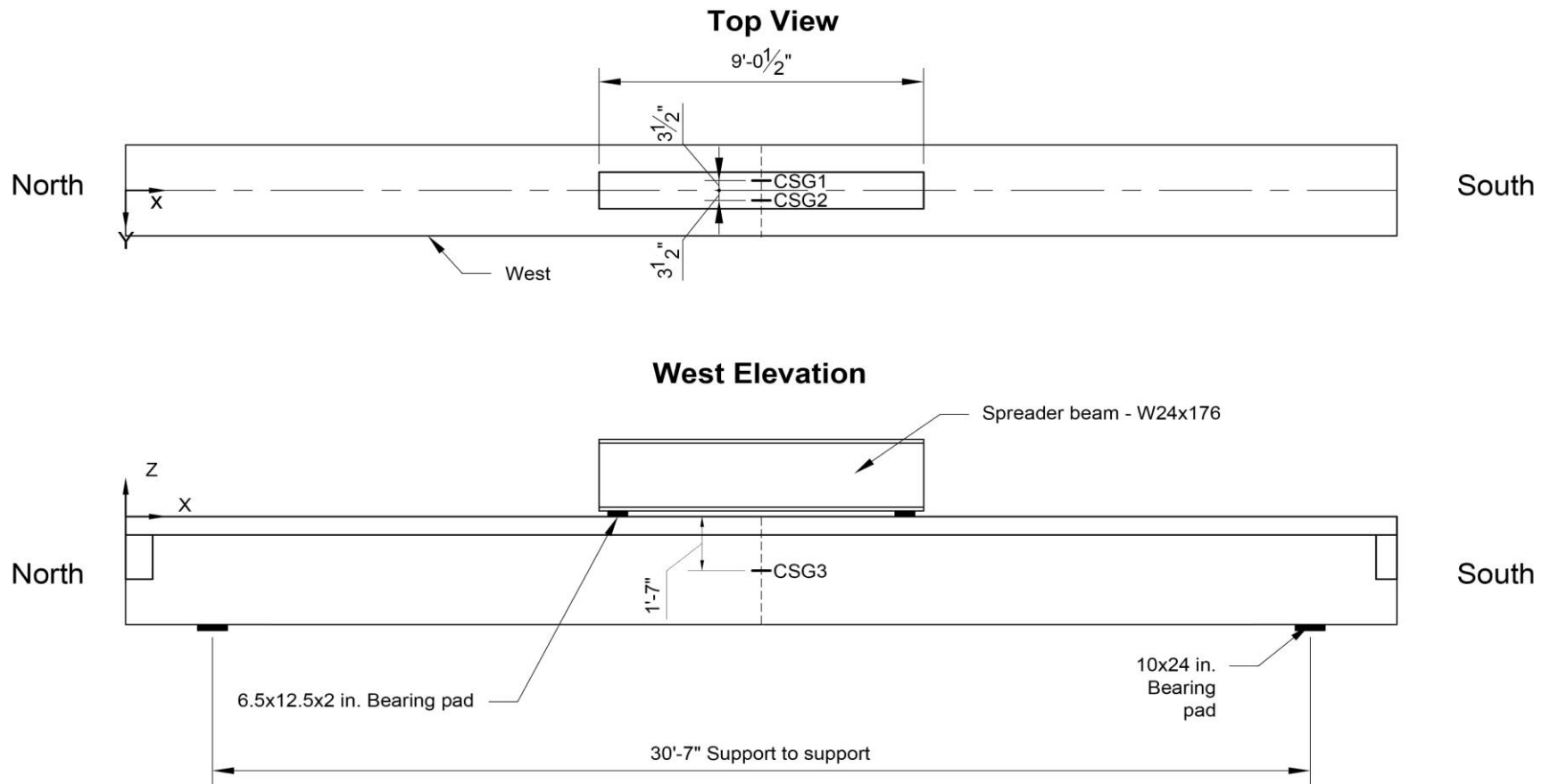
Figure 169—Instrumentation plan indicating the strain gage locations for girders without FRP
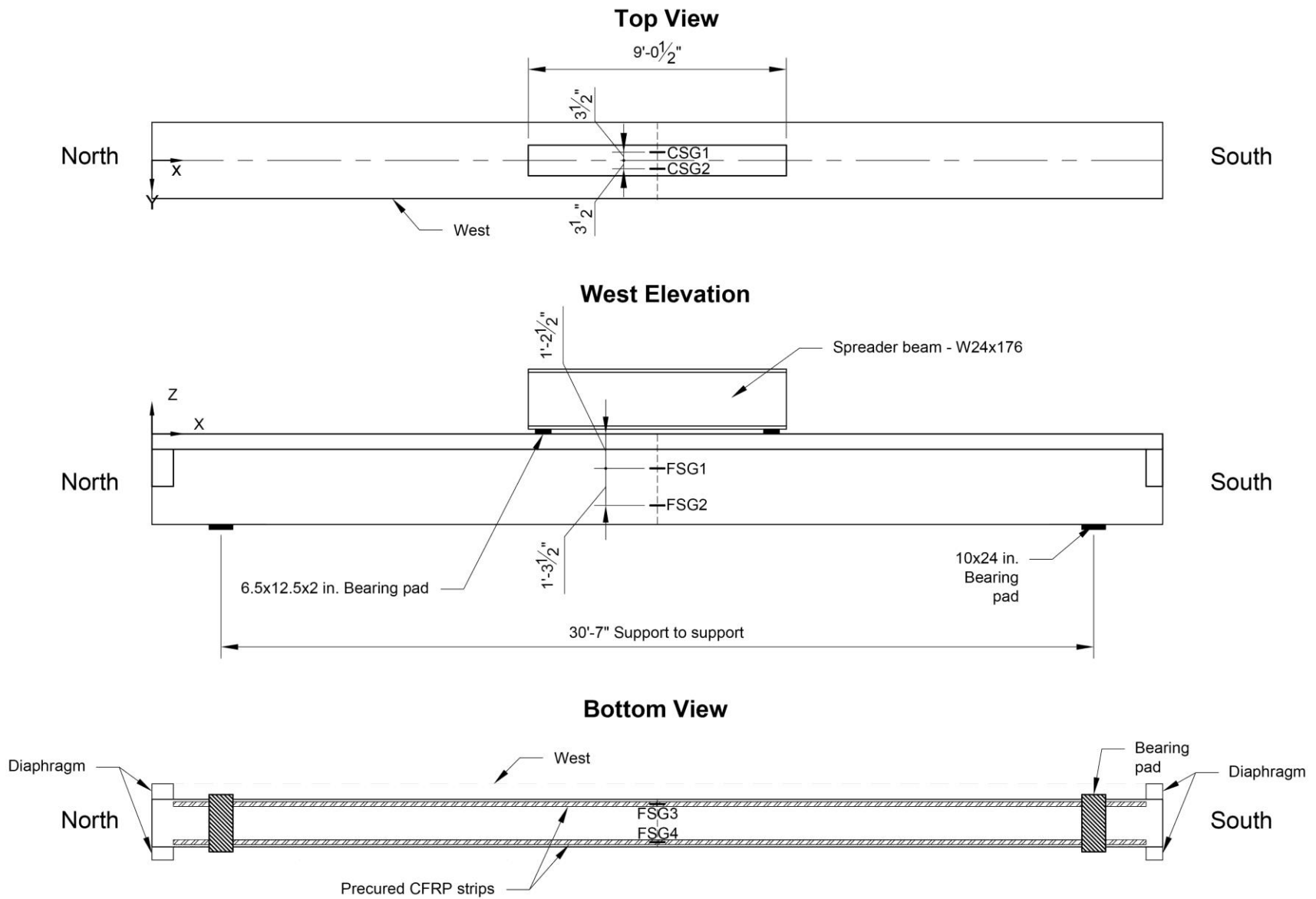
Figure 170—Instrumentation plan indicating the strain gage locations for girders with FRP

6.4 Flexural Test Procedures

Girders 3-2 and 4-3 were loaded monotonically to the incremental service load levels shown in Table 41 for two cycles. Girder 4-2 and 5-2 were loaded monotonically to the incremental service load levels shown in Table 41 for one cycle. This initial load level is based on the load caused by the LRFD HL-93 notional truck load under service conditions. A second service load level was added to determine if any further cracking and debonding had occurred at a load above service load levels for the remainder of the tests (Table 42).

The final cycle for all tests consisted of monotonic loading up to the full flexural strength. The remaining girders were loaded monotonically to the incremental service load levels shown in Table 42.

Table 41—Girder loading scheme

Cycle	Step	Description
	1	Load to 56 kip
1	2	Hold to mark cracks/cointap
	3	Unload
2	n/a	Load to full strength capacity

Table 42—Girder loading scheme

Cycle	Step	Description
1	1	Load to 56 kip
	2	Hold to mark cracks/cointap
2	1	Load to 85 kip
	2	Hold to mark cracks/cointap
3	n/a	Load to full strength capacity

6.5 Flexural Test Results and Discussion

This section is divided into two sub-sections to cover the exterior girder and interior girder flexural testing results separately. The exterior girders had less steel reinforcement and larger depth than the interior girders, so this approach was done for a more direct comparison for load and displacement values.

6.5.1 Flexural Test Results and Discussion: Exterior Girders

Load-displacement plots for the girders are presented in Figure 171. Girders with FRP installed exhibited similar behavior in the laboratory test. Girder 3-4, 4-1, 4-4 were exterior girders which had GFRP installed on one web face and CFRP strips externally bonded on the bottom of the beam. Girder 5-1 is an exterior girder without FRP. All of the exterior girders with FRP experienced FRP rupture failure prior to concrete crushing in the compression zone.

No significant change in stiffness was noted up until approximately 190 kip where the steel reinforcement began to yield. Girder 4-1 and 4-4 had a slightly higher stiffness than Girder 3-4 and 5-1 immediately after yielding, possibly due to the added stiffness from externally bonded

GFRP. Cracking noise occurred more frequently and became more audible as the load approached the yield load.

All of the exterior girders had relatively similar values for ultimate strength. Each of the girders, both with and without FRP, had reached their calculated nominal flexural strength. Refer to Section 6.6.1 for a comparison between the experimental and theoretical capacities.

A gradual drop in load after reaching ultimate strength occurred in Girder 4-1 and 4-4 that may indicate that the GFRP may have ruptured before the CFRP because of the GFRP's lower ultimate strength. Girder 3-4 had a much larger sudden drop in load immediately before failure. Having the GFRP on one side may be the reason that the GFRP ruptured at a lower ultimate strength than predicted.

Girder 3-4 had the highest ductility of all four exterior girders, which was also the only girder with FRP to have a higher ductility than a girder without FRP. This may be the case because Girder 3-4 was the only girder to have the CFRP strips debond and rupture prior to the GFRP rupture, before any crushing of concrete in the compression zone had occurred. The other two girders with FRP had the GFRP rupture first, which may have resulted in a sudden increase in strain for the CFRP strip that may have led to the CFRP strip rupture and debond earlier than anticipated.

When comparing the results on Figure 171, Girder 3-4 had a notably higher ductility than the other girders with FRP. CFRP strips in Girder 3-4, 4-1, and 4-4 reached 61%, 49%, and 42% of the ultimate design rupture strain, respectively. Having the CFRP strips in Girder 3-4 reach closer to the ultimate design rupture strain may have resulted in Girder 3-4 in reaching a higher ultimate strength and ductility than the other girders. All of the CFRP laminate strips on the exterior girders had met the ACI 440 strain level at which debonding may occur.
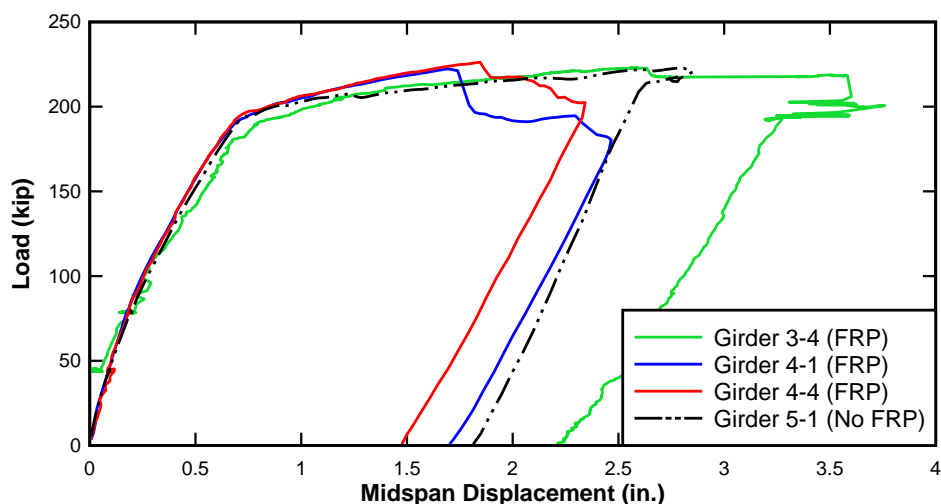
Figure 171—Load-displacement of exterior test girders

Girder 3-4 bearing was not perpendicular to the vertical beam axis, which required the use of tapered plates to ensure loading was in line with the vertical axis. The cross-section of this

girder was asymmetric due to a curb that made an even loading distribution more difficult to achieve.

During flexural testing of 3-4, FSG3 indicated approximately 1000 microstrain more than FSG4. This difference in strain increased to approximately 3000 microstrain as the CFRP strips as the load approached ultimate strength. This difference in strain may be an indicator that lateral deformations were occurring since GFRP was only applied to the west face. Another possibility is that strain gages may have been in varying proximity to flexural cracks, which produced differing strains near ultimate strength. While the west CFRP strip debonded at a load of 217 kip, there was no indication on the load-displacement plot (Figure 172). The east CFRP debonded at ultimate strength (223 kip), which resulted in a small loss in load. The GFRP ruptured at 218.3 kip. At this point, both CFRP strips had debonded (Figure 173), and the GFRP had ruptured (Figure 174), resulting in a load decrease to approximately 200 kip residual strength. The GFRP rupture occurred simultaneously with a crack that formed in a formwork joint on the opposite face (east elevation) (Figure 175). The crack then lengthened into the compression zone (Figure 175b) where crushing occurred (Figure 175c).
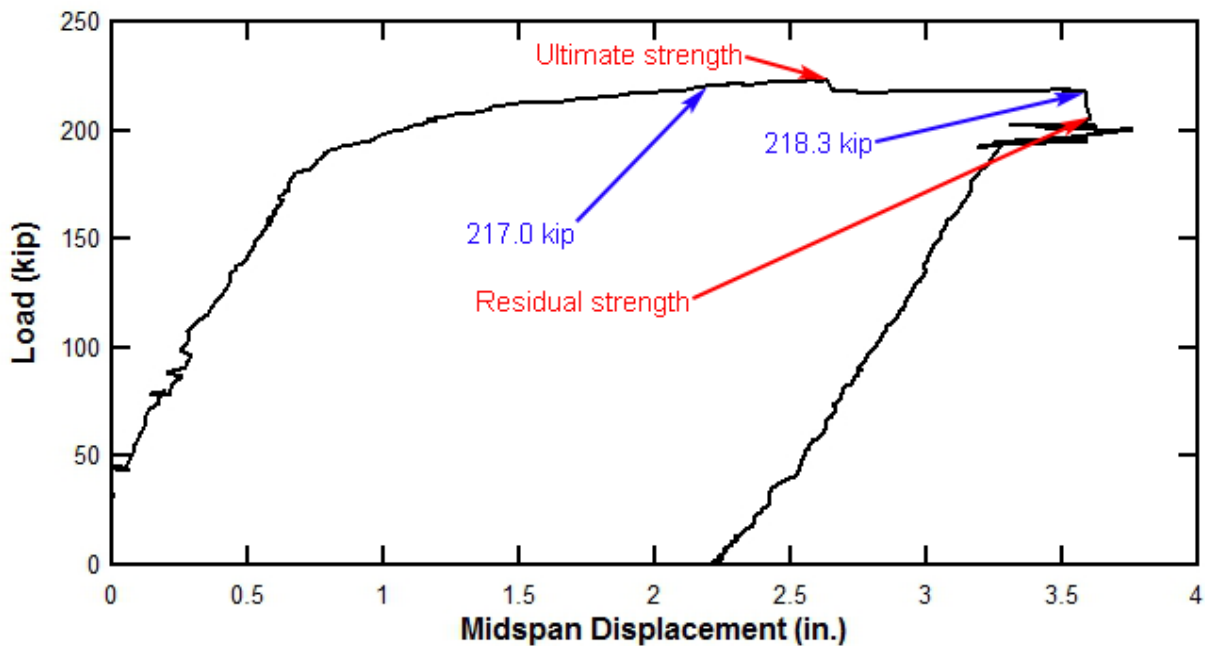
Figure 172—Load vs. displacement plot for Girder 3-4

Figure 173—CFRP debonding (Girder 3-4)

Figure 174—GFRP rupture (Girder 3-4)

| (a) | (b) | (c) |

Figure 175—Concrete damage to Girder 3-4 including (a) cracking near formwork joint (b) concrete crushing in compression zone in east elevation (c) crushing of concrete in west elevation

The cross-section of Girder 4-1 was slightly asymmetric. During testing of the CFRP strips, the strain gage readings on the CFRP strip on the west half of the girder (FSG3) varied from a few hundred to 1000 microstrain from the readings on the CFRP strip on the east half of the girder (FSG4). The GFRP ruptured first at the ultimate strength (222 kip), which resulted in a decrease in load to 195.7 kip (Figure 176). The CFRP strips debonded shortly after the GFRP ruptured. FSG3 indicated that a strain release occurred at 198 kip, followed by another strain release detected by FSG4 at 194.3 kip, indicated CFRP debonding. CFRP debonding was also detected by FSG3 at a load of 189.1 kip. Following CFRP debonding (Figure 177) and rupture (Figure 178), and GFRP rupture (Figure 179) the beam resisted a residual load of 181 kip. The debonding crack front was visible on the west CFRP strip (Figure 180). Crushing of concrete in the compression zone had also occurred at failure (Figure 181).
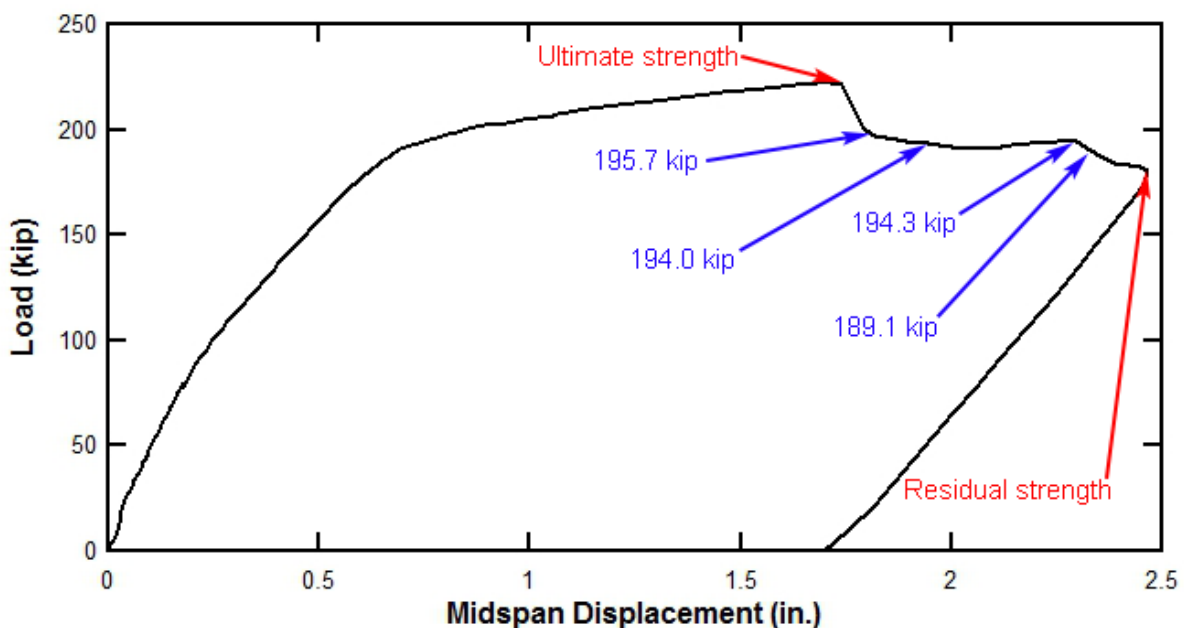
Figure 176—Load vs displacement plot for Girder 4-1

Figure 177—Debonded CFRP strips (Girder 4-1)
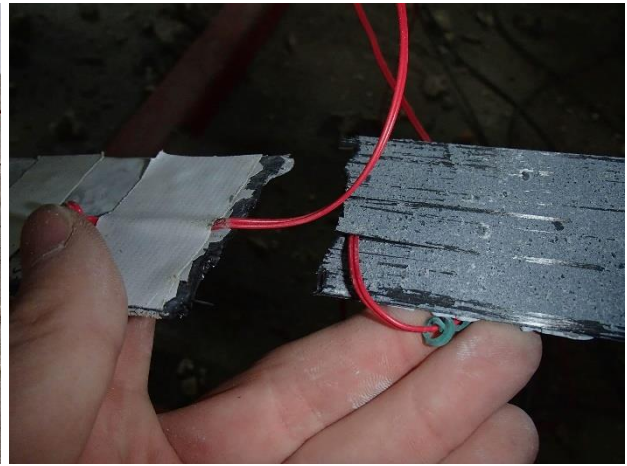
| (a) | (b) |

Figure 178—CFRP rupture (Girder 4-1): (a) one strip breaks apart (b) close-up image

Figure 179—GFRP rupture (Girder 4-1) with debonded GFRP region outlined in red
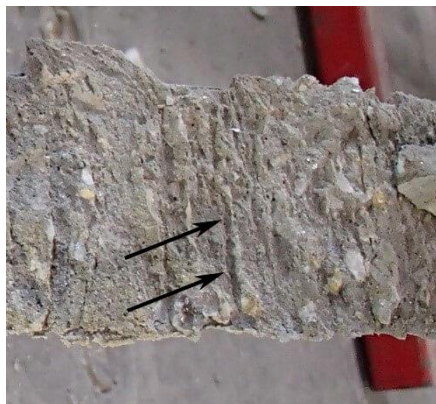
Figure 180—Crack front appearing on concrete substrate of debonded CFRP (Girder 4-1)

| (a) | (b) |

Figure 181—Damage to Girder 4-1 including (a) compression failure on east elevation (b) compression failure on west elevation

Girder 4-4 bearing was not perpendicular to the vertical beam axis (similar to Girder 3-4), which required the use of tapered plates to ensure loading was in line with the vertical axis. The cross-section of this girder was asymmetric due to a curb that made an even loading distribution more difficult to achieve.

During flexural testing of 4-4, FSG3 indicated approximately 1000 microstrain more than FSG4. This difference in strain grew to approximately 3000 microstrain as the load approached ultimate strength. This difference in strain may be an indicator that lateral deformations were occurring since GFRP was only applied to the west face. GFRP ruptured first at the ultimate strength (226 kip), which resulted in a slight loss in load Figure 182. FSG4 indicated that a strain release occurred at 217.2 kip, followed by another strain release detected by FSG3 at 212.3 kip, then resulting in debonding detected by FSG4 at 210.7 kip, and by FSG3 at 206 kip. The residual strength was 202 kip following FRP rupture and debonding. Both CFRP strips have debonded (Figure 183) and GFRP rupture occurred on the west elevation (Figure 184) as well. Similar to Girder 3-4, cracking formed at a formwork joint on the east elevation (Figure 185). The crack

then expanded into the compression zone (Figure 185b). Crushing of concrete in the compression zone in the west elevation also occurred (Figure 185c).
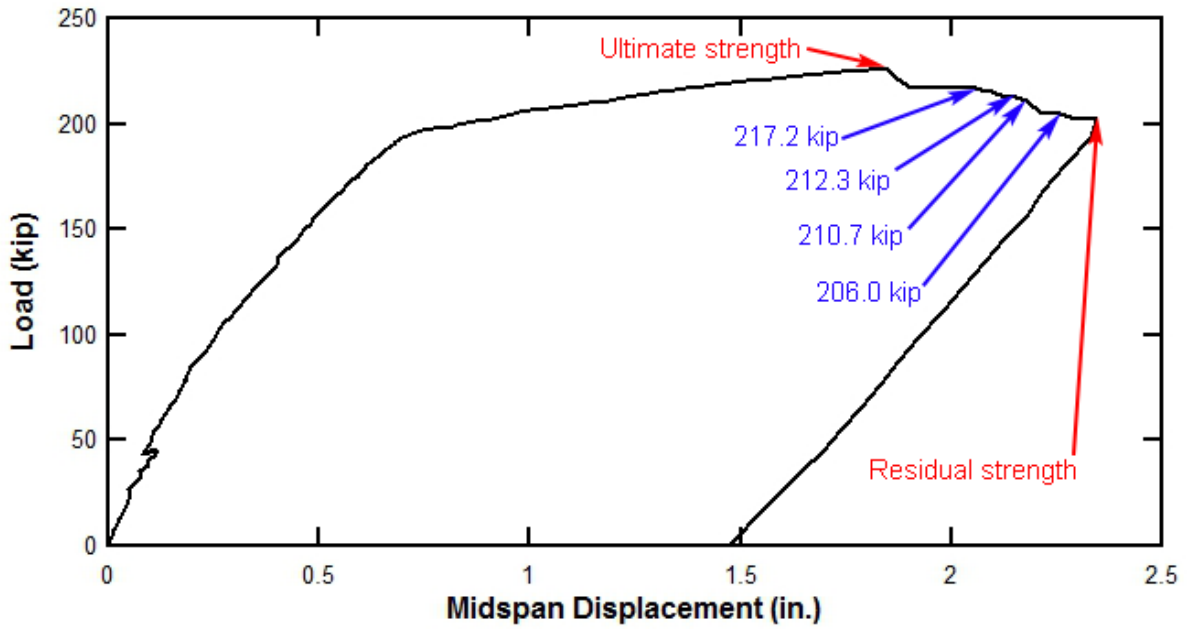
Figure 182—Load vs Displacement plot for Girder 4-4
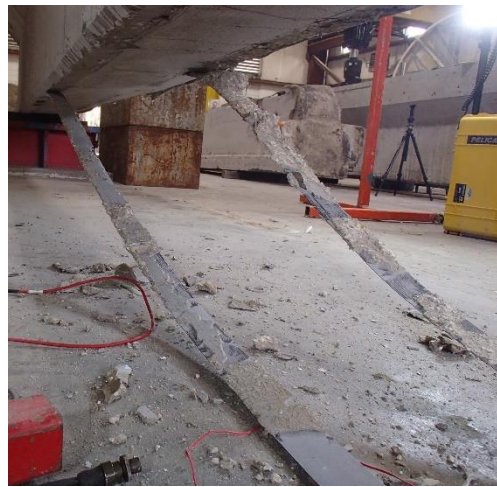
(a)   (b)

Figure 183—CFRP strip debonded (Girder 4-4): (a) single strip up close (b) both strips from a distance

Figure 184—GFRP rupture (Girder 4-4)

| (a) | (b) | (c) |
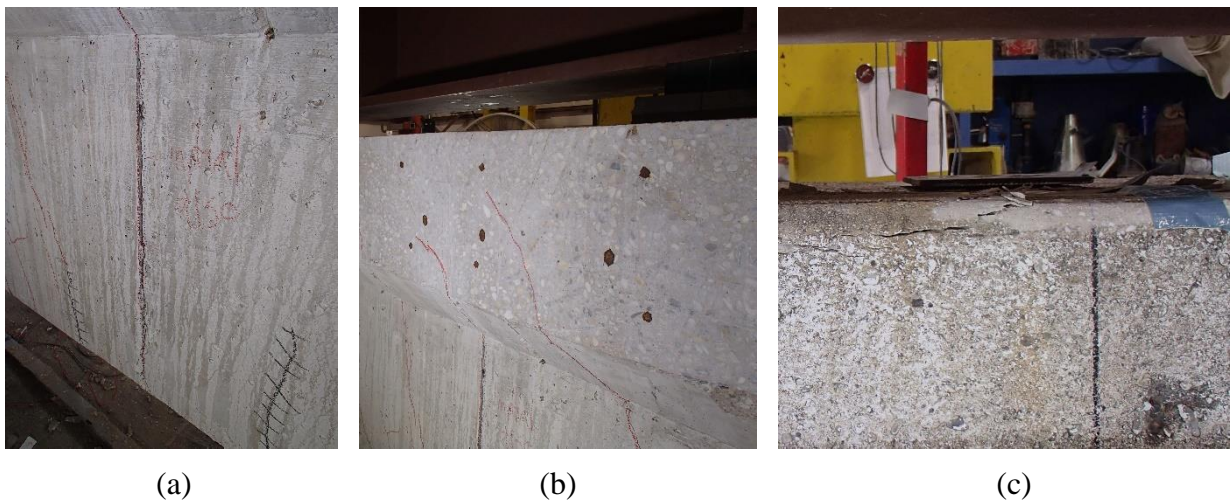
Figure 185—Damage to Girder 4-4 including (a) cracking at formwork joint (b) crack at formwork joint extended to compression zone in east elevation (c) crushing of concrete in west elevation

Girder 5-1 had a reduced cross-section at the midspan (Figure 186) with initial cracks located at about 12 in. away from the midspan. The contractors that extracted the girders from the University Boulevard bridge had attempted to ease removing girders 5-1 and 5-2 by coring both sides of the flange, which resulted in a reduced cross-section. During load testing, the service load cycles caused cracks to develop closer to the midspan. At ultimate strength, the girder failed by crushing of concrete in the compression zone (Figure 187). The failure occurred once the beam cracked at a formwork joint on the east elevation (Figure 188), after cracks developed in the compression zone and expanded to the joint.

(a)	(b)

Figure 186—Reduced cross-section at the midspan (Girder 5-1): (a) west elevation (b) east elevation

(a)	(b)

Figure 187—Crushing of concrete in compression zone (Girder 5-1): (a) west elevation (b) east elevation

Figure 188—Formwork joint on the east elevation (Girder 5-1)

6.5.2 Flexural Test Results and Discussion: Interior Girders

Load-displacement plots for the interior girders are presented in Figure 189. Girder 3-2, 4-2, and 4-3 were interior girders that had GFRP installed on both elevations, and CFRP strips externally bonded to the tension face. Girder 5-2 was the only interior girder without externally bonded FRP. All interior girders with FRP had a notably higher stiffness before and after yielding occurred when compared to Girder 5-2. Girder 5-2, however, had a much lower ultimate strength than the other girders due to the reduced cross-section caused by coring (Section 6.5.1).

Loss of initial stiffness occurred at a lower load in Girder 5-2 compared to the other interior girders, likely because it did not have externally bonded FRP. The interior beams with FRP had a notable increase in stiffness over Girder 5-2. Two girders with FRP, Girder 3-2 and 4-2, had slightly less ductility than Girder 5-2. Girder 4-3 had the highest ductility of all four interior girders, which was also the only girder with FRP to have a higher ductility than a girder without FRP. Ultimate strength for the girders with FRP was about 250 kip and unstrengthened was approximately 200 kip. Girder 3-2 and 5-2 exhibited a compression failure mode and Girder 4-2 and 4-3 exhibited FRP rupture.

ACI 440.2R-08 controls debonding by limiting the FRP effective strain to ε_{fd}:

$$\varepsilon_{fd} = 0.083 \sqrt{\frac{f_c'}{n E_f t_f}} \leq 0.9 \varepsilon_{fu} \qquad\qquad\qquad \text{Eq. 4}$$

where f_c' is the specified concrete compressive strength, n is the number of plies of FRP, E_f is the FRP tensile modulus of elasticity, t_f is the nominal thickness per ply of FRP, and ε_{fu} is the FRP design rupture strain. Computing the limit of the test specimens results in $\varepsilon_{fd} = 0.004623$ and $0.9\varepsilon_{fu} = 0.01521$. The measured strains for the CFRP laminate strips on the interior girders were less than the limiting strain criteria (ε_{fd}).

Girder 4-3 had a notably higher ultimate strength and ductility than the other girders with FRP (Figure 189). The CFRP strips in Girder 3-2 and 4-3 had reached 60% and 59% of $0.9\varepsilon_{fu}$, respectively; Girder 4-3, however, most likely had more strength due to less section loss in the steel reinforcement. Girder 5-2 had a much lower ultimate strength than the other girders due to a reduced cross-section, as mentioned earlier.
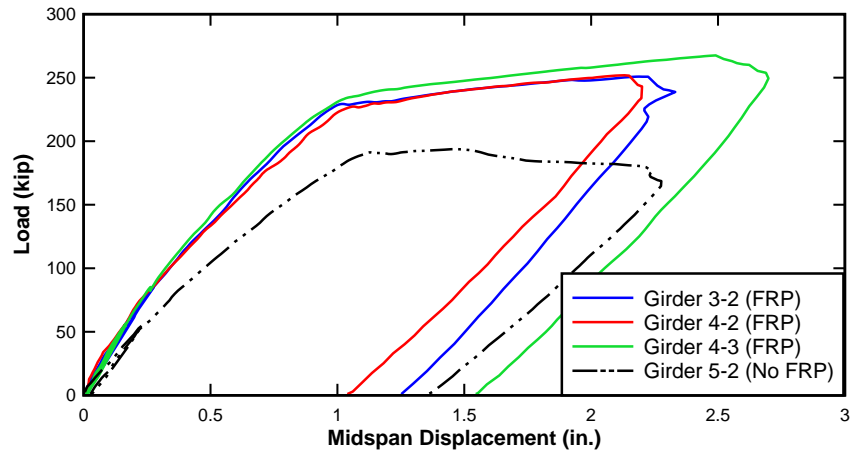
Figure 189—Load-midspan displacement of interior test girders

Girder 3-2 had considerable audible GFRP cracking at midspan when the load reached approximately 220 kip. This was likely the result of nearing the yield point, which was at approximately 229 kip. The girder reached ultimate strength when the GFRP ruptured; crushing of concrete in compression was observed as well (Figure 190). Debonding of CFRP closest to the east face occurred around midspan. The span of the debonded CFRP strip is indicated by red arrows (Figure 191) and the GFRP on the midspan of the east face has blue hatching to indicate the debonded region around the GFRP rupture (Figure 192).

Figure 190—Crushing of concrete in compression (east elevation view of Girder 3-2)

Figure 191—Red arrows indicate the span of debonded CFRP strip (Girder 3-2)

Figure 192—GFRP rupture and GFRP debonding indicated in hatch (Girder 3-2)

Girder 4-2 had considerable audible GFRP cracking at midspan when the load reached approximately 200 kip, which is approximately 27 kip before a change in stiffness occurred. At ultimate strength, the girder failed by crushing of concrete in compression (Figure 193). Although cracks formed in the web near midspan (Figure 194), they did not seem to expand (Figure 195), or appear to affect the failure mode. Although some debonding occurred at midspan on the west face (Figure 195), the debonding did not result in GFRP rupture.

(a)   (b)

Figure 193—Crushing of concrete in compression (Girder 4-2): (a) west elevation (b) east elevation

(a)   (b)

Figure 194—Girder 4-2 cracking on bottom and side (a) at initial and (b) after failure

Figure 195—GFRP debonding by midspan on west elevation (Girder 4-2)

Girder 4-3 had considerable audible GFRP cracking at midspan when the load reached approximately 230 kip, which is a relatively close to yield (at approximately 232 kip). At ultimate strength, the girder failed by rupture of GFRP and CFRP; concrete crushing occurred

(Figure 196) followed the FRP rupture. GFRP rupture occurred on the east elevation (Figure 197), followed by debonding (Figure 198b) and rupture (Figure 198a) of the CFRP strip on the beam web closest to the east elevation. Longitudinal cracking found on the bottom face of the web may have been due to corrosion (Figure 199).

| (a) | (b) |
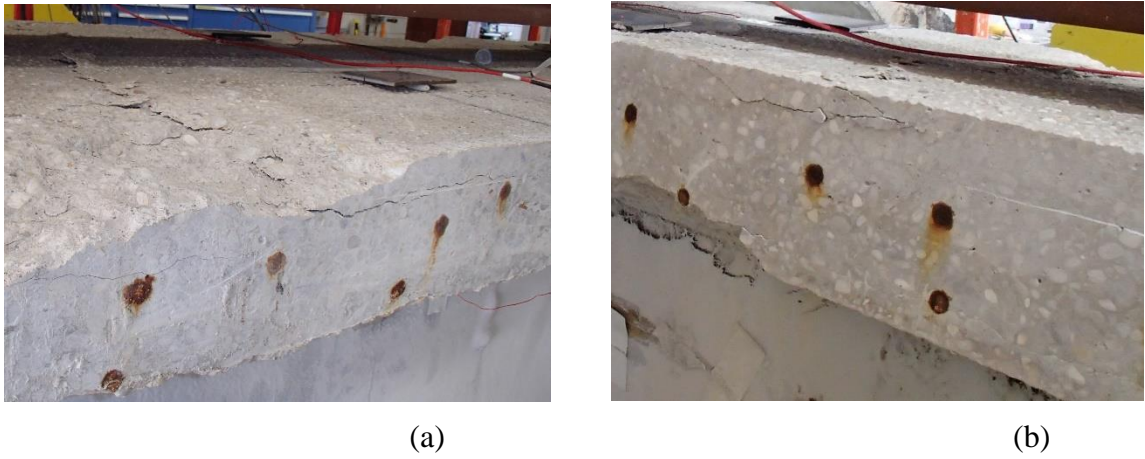
Figure 196—Crushing of concrete in compression (Girder 4-3): (a) west elevation (b) east elevation

Figure 197—GFRP rupture on east elevation (Girder 4-3)

(a)	(b)

Figure 198—CFRP on east elevation (Girder 4-3): (a) ruptured (b) debonded

Figure 199—Longitudinal cracking on the tension face of Girder 4-3

Girder 5-2 had a reduced cross-section at the midspan (Figure 200) with initial cracks on the reduced cross-section and nearby regions. At ultimate strength, the girder failed by crushing of concrete in compression (Figure 201).

(a)	(b)
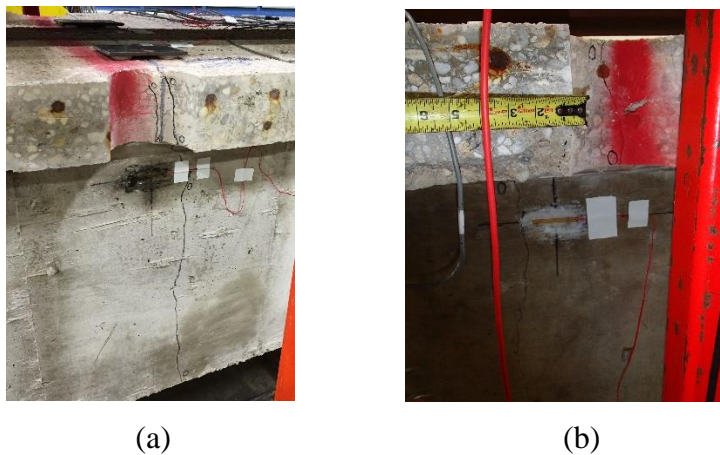
Figure 200—Reduced cross-section at midspan (Girder 5-2): (a) west elevation (b) east elevation

<center>(a)   (b)</center>
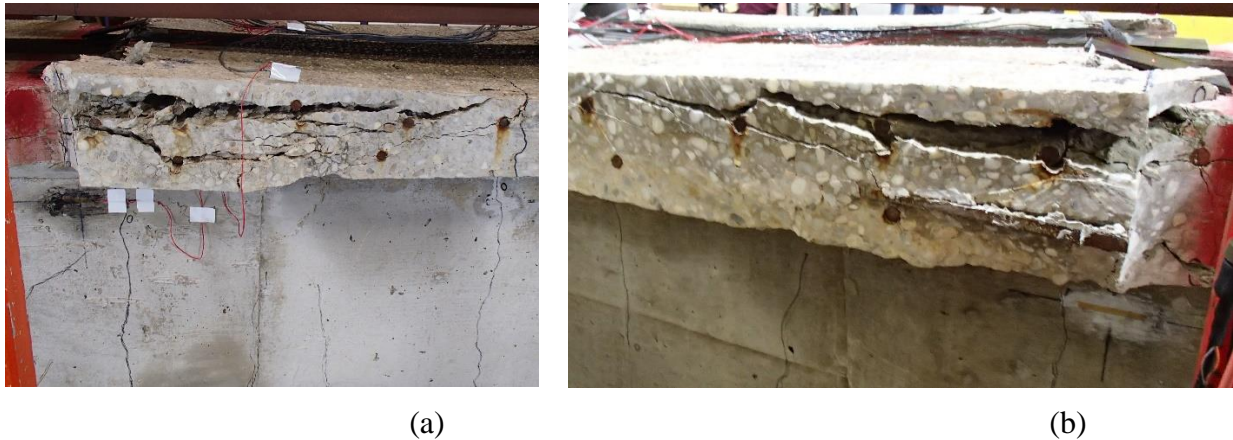
<center>Figure 201—Crushing of concrete (Girder 5-2): (a) west elevation and (b) east elevation</center>

6.6   Moment Curvature Analysis

The processes used for moment curvature analysis was identical to those used for the Indian River bridge (Section 5.7). The following sections will only provide information that varies from the Indian River chapter. Concrete compressive strength of 3,500 psi was assumed based on the compressive strength data for these girders (Table 19). FRP material properties obtained from tensile tests (Table 30 and Table 39) were used in the analysis. Girder 5-1 and 5-2 had strain gages at the top and bottom only, so the experimental strain moment-curvature was not determined due to a limited amount of data to determine the curvature.

As discussed in (Section 5.7), an ultimate strain of 0.003 for both CFRP and GFRP was assumed in modeling the theoretical moment curvatures. This strain value used for the CFRP in the model corresponds to only 18% of measured (Table 30) elongation at rupture of CFRP. The elongation for the GFRP was neither measured nor specified by the manufacturer.

6.6.1   Moment Curvature Analysis: Exterior Girders

Figure 202 through Figure 205 show comparisons of experimental moment curvatures to theoretical moment curvatures for Girders 3-4, 4-1, 4-4, and 5-1. Table 43 shows a comparison of theoretical moment strength with measured strength. The theoretical moment curvature for Girder 5-1 was determined based on the original cross-section before the reduction had occurred. In all cases, the theoretical ultimate moment was within 5% of the measured flexural strength.

<center>Table 43—Theoretical versus experimental strength of girders</center>

Girder	Theoretical Strength (kip-ft.)	Experimental Strength (kip-ft.)	Ratio of Experimental to Theoretical Strength
3-4	1,363	1,372	1.01
4-1	1,367	1,391	1.02
4-4	1,363	1,391	1.02
5-1	1,333	1,378	1.03
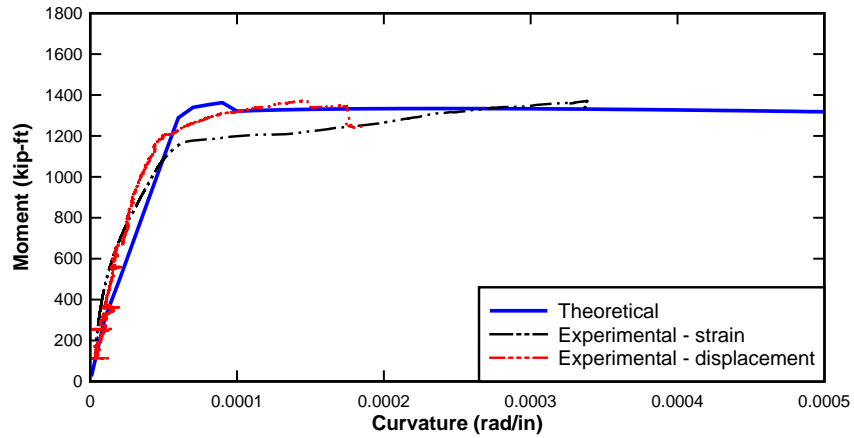
Figure 202—Moment curvature for Girder 3-4
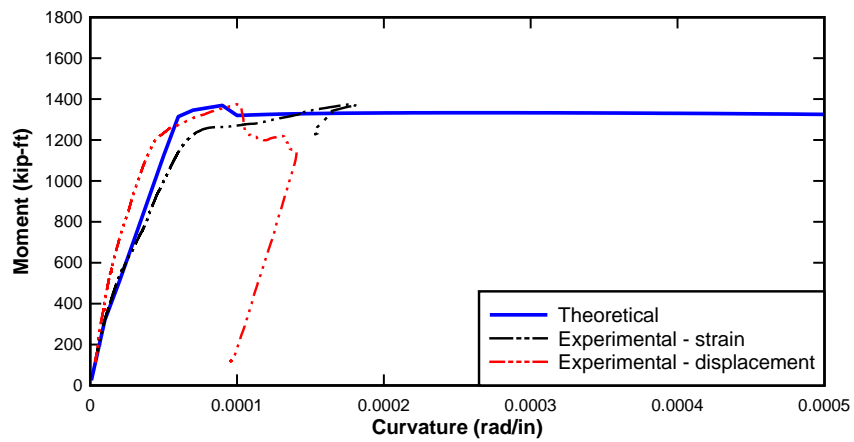
Figure 203—Moment curvature of Girder 4-1
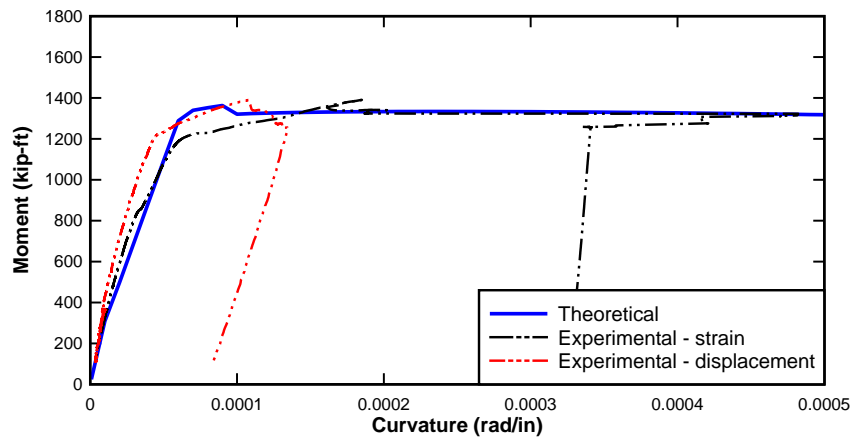
Figure 204—Moment curvature of Girder 4-4
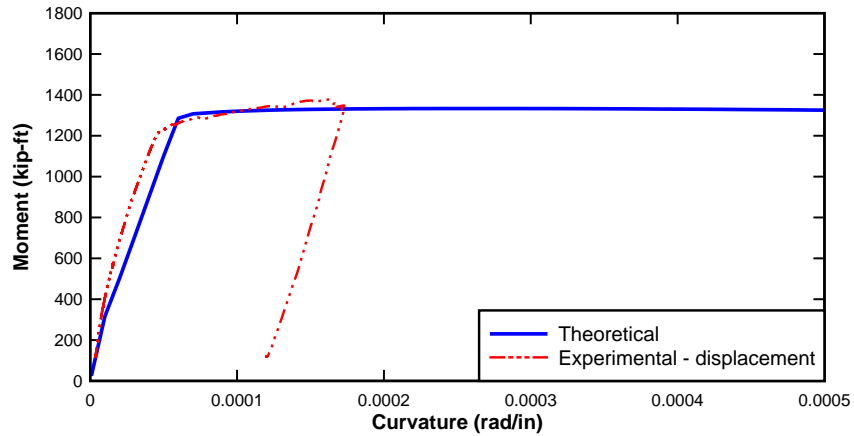
Figure 205—Moment curvature of Girder 5-1

6.6.2 Moment Curvature Analysis: Interior Girders

Figure 206 through Figure 209 show comparisons of experimental moment curvatures to theoretical moment curvatures for Girders 3-2, 4-2, 4-3, and 5-2. Table 44 shows comparison of measured strength with theoretical strength. The theoretical moment curvature for Girder 5-2 was determined based on the original cross-section before the reduction had occurred.

Table 44—Theoretical versus experimental strength of girders

Girder	Theoretical Strength (kip-ft.)	Experimental Strength (kip-ft.)	Ratio of Experimental to Theoretical Strength
3-2	1,483	1,530	1.03
4-2	1,535	1,539	1.00
4-3	1,483	1,625	1.10
5-2	1,513	1,211	0.80

Generally, the experimental moment curvature showed yielding at a lower moment than the theoretical. According to the data in Table 29, Girder 4-3 had the lowest level of steel reinforcement section loss. This may be an indicator why the experimental moment capacity was much higher for this girder compared to the other girders analyzed in this section. The reduced cross-section of Girder 5-2 may explain why the tested flexural strength is significantly lower than the theoretical; the original cross-sectional dimensions were used to generate the theoretical moment curvature.
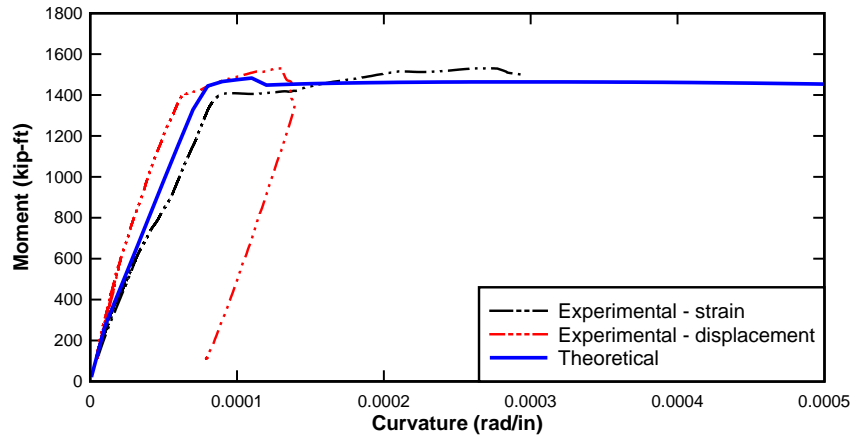
Figure 206—Moment curvature of Girder 3-2
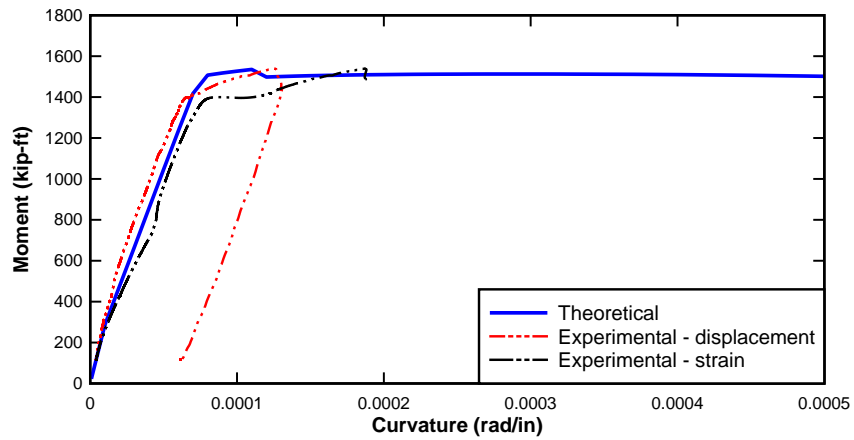
Figure 207—Moment curvature of Girder 4-2
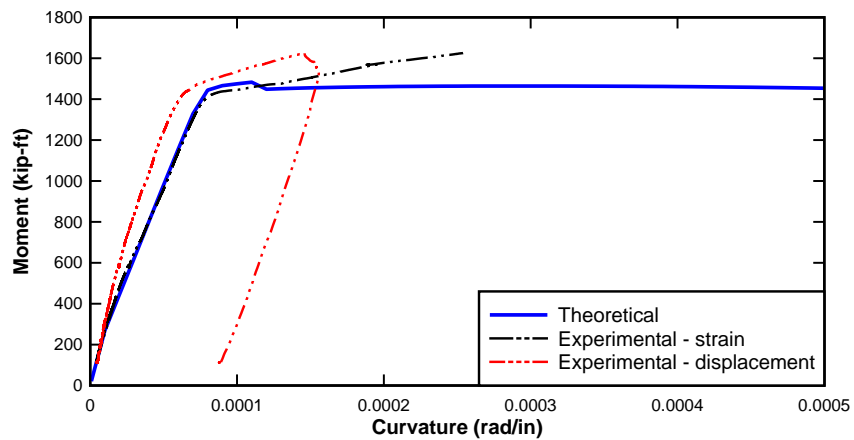
Figure 208—Moment curvature of Girder 4-3
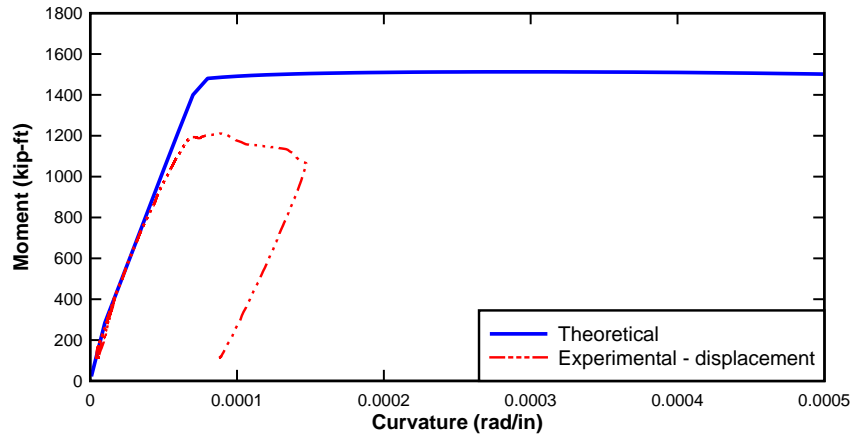
Figure 209—Moment curvature of Girder 5-2

6.7 Girder Dissection

Following the structural test, an autopsy was performed on five girders. FRP was recovered from the southeast end of the girders and the steel reinforcement was extracted from the south end of the girders. The south end of the girders was closest to the tidal fluctuations, so these locations were chosen because of the highest level of exposure to the brackish water. After FRP was removed, the girders were placed upside-down to allow cover concrete to be removed for inspection and sampling of steel reinforcement at desired locations (Figure 210).

Figure 210—Steel reinforcement exposed

6.7.1 FRP Condition

CFRP samples were extracted from the precured CFRP laminate strips that have either debonded or ruptured from the girders after flexural testing. The samples that were determined for use in tensile testing had no signs of cohesive debonding (Figure 211). Figure 211 represents a typical sample surface, which primarily debonded at the CFRP-epoxy interface. Although Figure 212 signifies some samples had a similar failure mode, some regions had debonding at the concrete-epoxy interface. The failure modes on these regions may represent bond degradation or inadequate installation. Cohesive failure modes, however, were noted on all the laminate strips. Figure 213 shows the white coating finish that was applied externally to some of the CFRP.

Figure 211—Debonding only occurred at the CFRP-epoxy interface surface prior to tensile testing

Figure 212—Some debonding occurred on the CFRP at the concrete-epoxy interface surface prior to tensile testing

Figure 213—Exterior face of CFRP samples with white coating

GFRP coupons were saw cut from the east face approximately 3 feet from the south end of four beams, and manually peeled from the concrete surface. In some cases, concrete remained adhered to the surface (Figure 214a) and in other cases the sample came away clean (Figure 214b) Prior to sanding the GFRP samples to uniform dimensions, the surface condition of each sample was characterized as having a light, medium, or heavy concrete concentration. This was done to determine the effect of the residual concrete on the flexural strength of the samples (Figure 215). Although there may be a slight indication of a higher than average flexural strength on the cohesively debonded samples, no firm conclusions can be drawn.

(a)

(b)

Figure 214—GFRP samples with (a) residual concrete adhered and (b) free of concrete
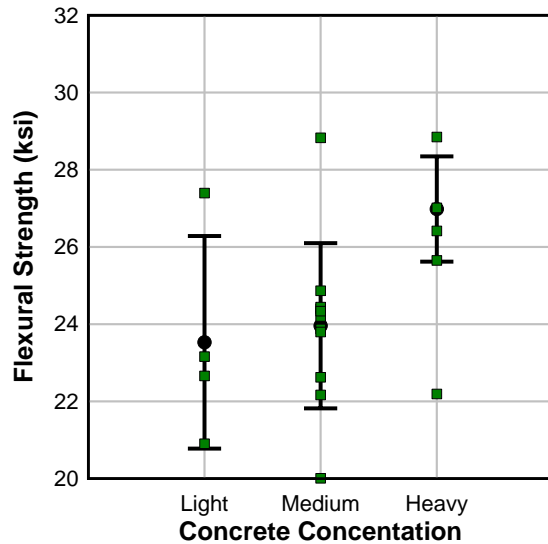
Figure 215—Comparison between debonded concrete concentration and flexural strength

6.7.2   Steel Reinforcement

Girder 3-1, 4-1, 4-3, and 5-1 were selected for reinforcing steel sampling. Jackhammers and chisels were used to expose the reinforcement for inspection and sampling (Figure 216). The steel reinforcement samples were extracted using an acetylene torch. All girders were inverted to give access to the tension zone during demolition.

(a)   (b)
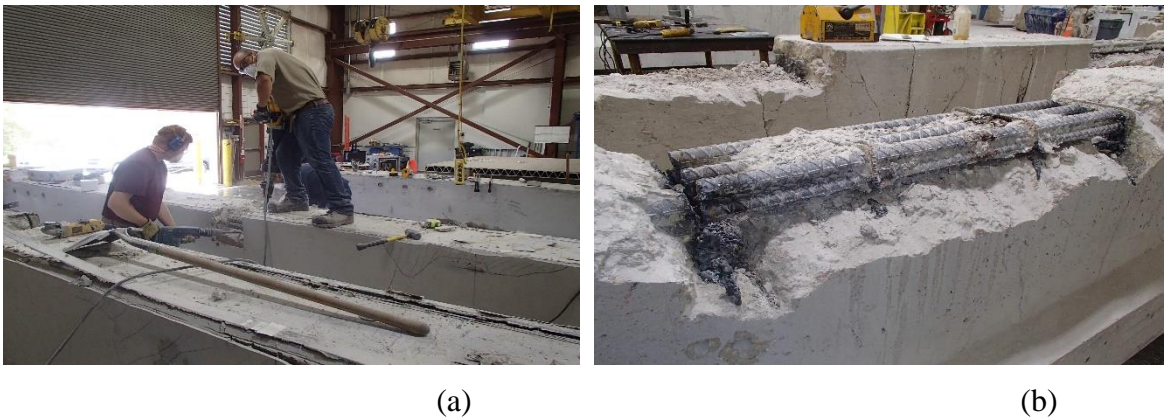
Figure 216—(a) Jackhammering concrete surrounding the reinforcing bars and (b) bridge girder in upside-down position with steel reinforcement exposed

Care was taken not to damage the reinforcement during the process. Girder 3-1 was chosen because when inspected in 2005, this girder had the most severe levels of corrosion and concrete spalling of Span 3 and 4. Girder 4-1 and 5-1 were chosen because although Girder 4-1 had externally bonded FRP, it had a lower ultimate strength than the other exterior girder (Girder 5-

1). Girder 4-3 was chosen due to a horizontal crack noticed on the bottom face of the web after failing in flexure.

The south ends of the four selected girders were compared because higher levels of corrosion were expected in the regions closest to the tidal fluctuations (Figure 217). Girders were divided into thirds so the locations of steel reinforcement extraction remained consistent within all of the girders. Figure 218 and Figure 219 are images of steel reinforcement with the highest levels of corrosion of four samples.
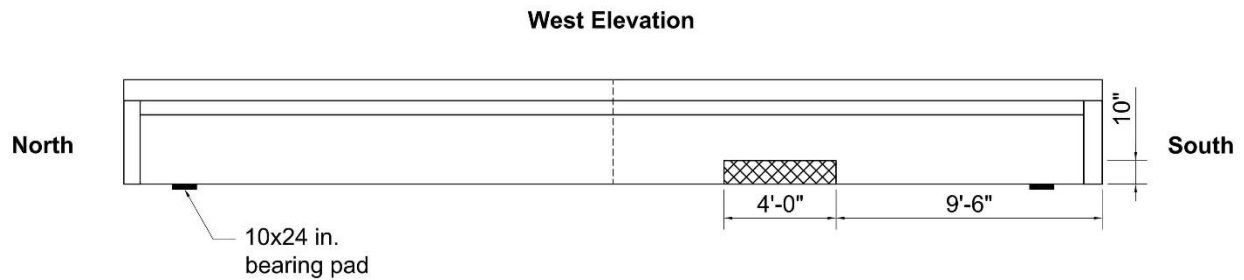
Figure 217—Typical steel reinforcement extraction location

(a)

(b)

Figure 218—Corroded reinforcement samples from (a) Girder 3-1 and (b) Girder 4-1

(a)

(b)

Figure 219—Corroded reinforcement samples from (a) Girder 4-3 and (b) Girder 5-1

The steel reinforcement at the north end of Girder 3-1 was uncovered due to the swelling and cracking noted there (Figure 220). This location was the most severe, with reinforcement section losses of up to 34% (Table 29). The severe corrosion uncovered at this location had likely occurred prior to FRP application. Furthermore, GFRP was applied to the inside face, but not the outside face of Girder 3-1. Consequently, it is not possible to determine if the corrosion was deterred by the presence of the FRP.

Figure 220—Corroded steel reinforcement in the north end of Girder 3-1

6.8 Chlorides, Potential, and Corrosion

Complete Cl⁻ penetration profiles for specified cores are shown in Figure 221. Five samples were sliced in 13 locations to determine the chloride concentration throughout the depth.
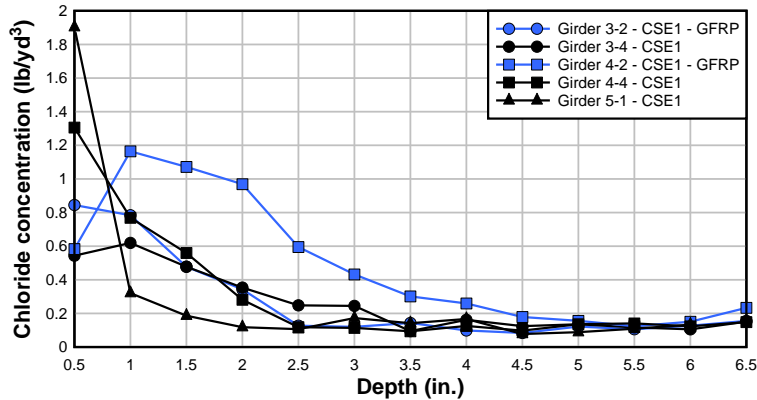
Figure 221—Chloride penetration profiles at specified locations

Cl⁻ concentrations varied among all of the girders. At a depth of about 2.5 in., the Cl⁻ concentrations became more consistent for all samples except Girder 4-2. Although the results from samples with GFRP do not indicate lower Cl⁻ levels than the samples without GFRP, the samples with GFRP were extracted from interior girders, so a direct comparison cannot be made because inconsistent exposure of each location to wind and wave action was likely the cause of the differences in Cl⁻ concentrations. It is not clear from these results if the FRP had a significant impact on mitigating the Cl⁻ intrusion, because samples with and without GFRP in a particular region of each girder with identical exposure would have to be compared.

Girder 3-1 had the most severe Cl⁻ content ranging from 2.99 pcy (GFRP applied) to 14.00 pcy (concrete exposed). Girder 3-1 also had the highest levels of corrosion on the steel reinforcement among all of the tested girders, with a maximum level of section loss and weight loss of 26% and 34%, respectively. Girder 4-3 had the second highest levels of Cl⁻ content with 1.68 pcy (GFRP applied), with a maximum level of steel reinforcement section loss and weight loss of 7% and 3%, respectively. The remaining seven girders had a Cl⁻ content of 0.595 pcy and lower.

Girder 4-1 and 5-1, however, had slightly more steel reinforcement section loss and weight loss than Girder 4-3 despite lower levels of Cl⁻ content, with values of 0.23 pcy (GFRP applied) and 0.11 pcy (concrete exposed), respectively. Girder 4-1 had a maximum steel reinforcement section loss and weight loss of 12% and 6%, whereas Girder 5-1 had 12% and 4%, respectively. One Cl⁻ core was taken per each of the girders (except for Girder 3-1), so other regions of Girder 4-1 and 5-1 may have had higher levels of Cl⁻ content.

Lower Cl⁻ concentrations were expected in concrete with externally bonded FRP, as it is assumed that FRP acts as a barrier that prevents diffusion of Cl⁻ into concrete. In Span 4, however, higher Cl⁻ concentrations are noted under GFRP (Girder 4-2, 4-3 and 4-4) when compared to the coring location without FRP (Girder 4-1) (Figure 222). Figure 223 shows lower Cl⁻ levels under GFRP (Girder 3-2 and 3-4) than the location without GFRP wrap (Girder 3-1).

In the span without FRP, Span 5, Figure 224 shows that the interior girder has higher Cl⁻ levels. The higher levels of Cl⁻ on the interior girders is consistent with that in Span 4, which might indicate that the interior girders have more exposure to wave action.

Steel reinforcement section loss was higher in Span 3 than the other two spans, which was expected since Span 3 was the lowest elevation and was inundated during high tide (Figure 222). Span 4 had more section loss on the exterior girder (Girder 4-1) than the interior girder (Girder 4-3). It is not clear why the Cl$^-$ concentration does not relate to the levels of section loss due to corrosion
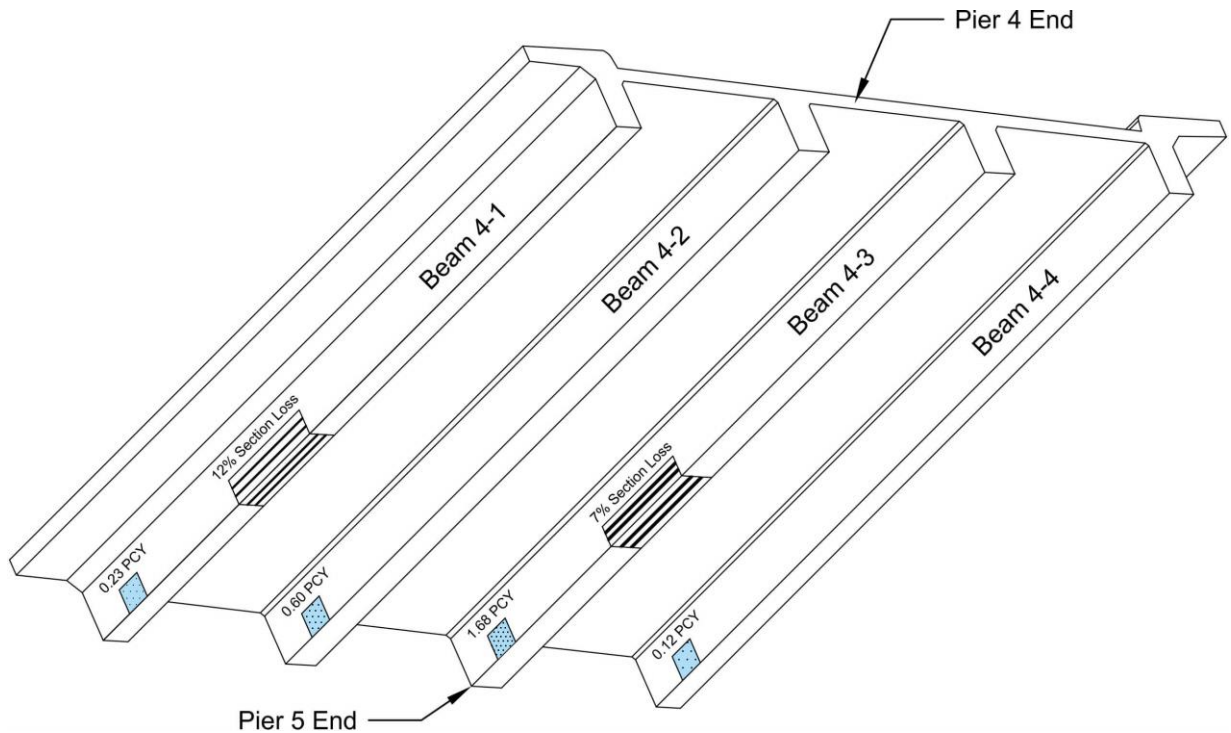
Figure 222—Chloride ion contamination levels and section loss in steel reinforcement in Span 4
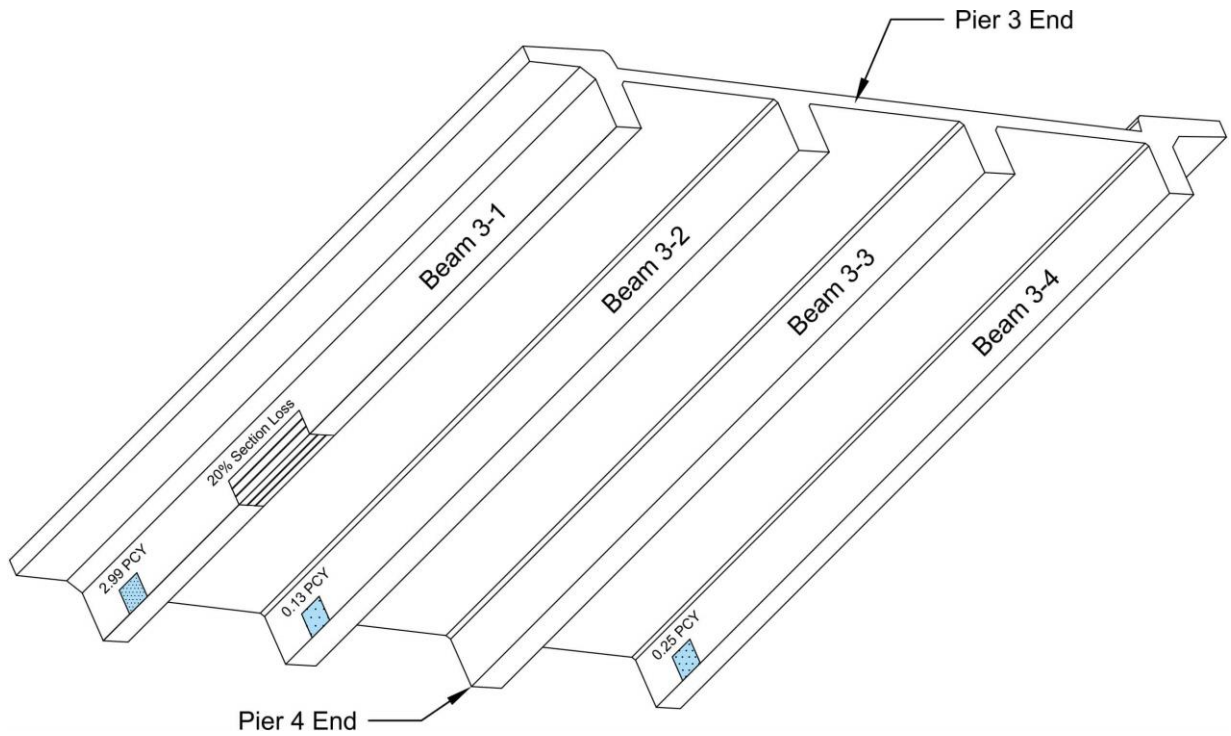
Figure 223—Chloride ion contamination levels and section loss in steel reinforcement in Span 3
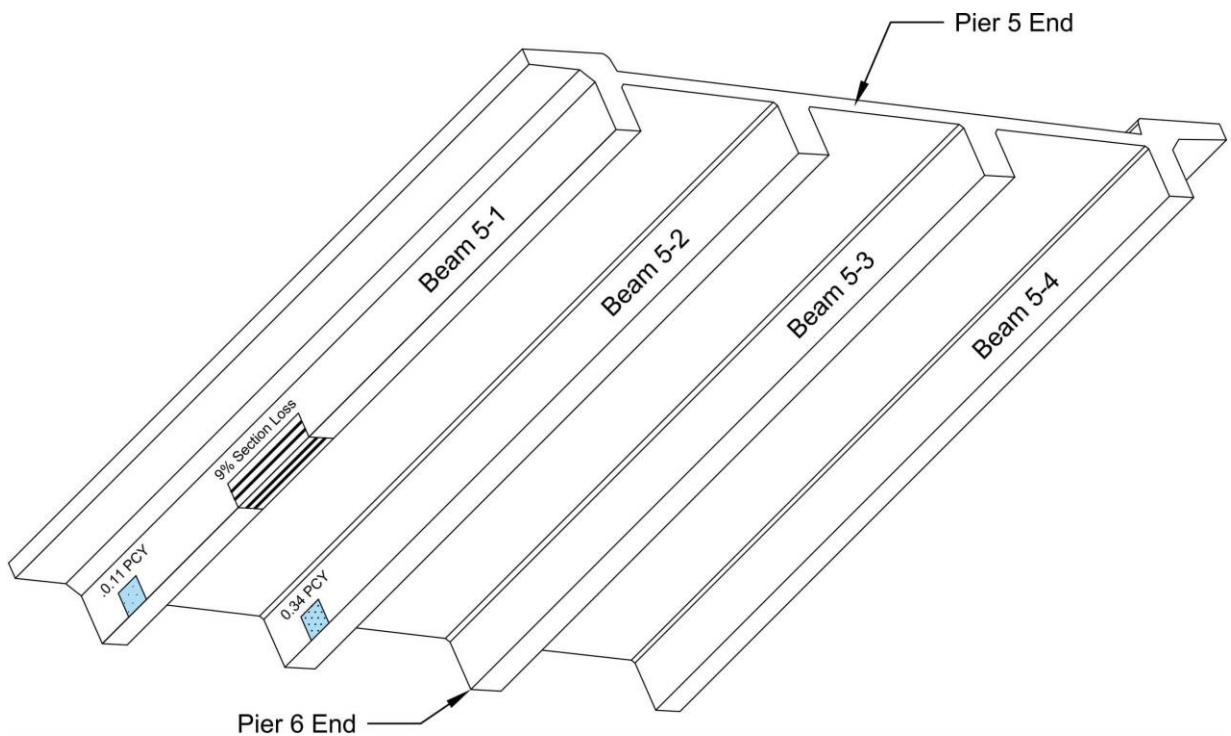
Figure 224—Chloride ion contamination levels and section loss in steel reinforcement in Span 5

Figure 225 shows the probability of corrosion mapped onto the girders. Based on the figure, a higher likelihood of corrosion would be expected for Girder 4-3 than Girder 4-1 and 5-1. Higher Cl⁻ content found in Girder 4-3 would also increase susceptibility to corrosion over that of Girder 4-1 and Girder 5-1. These results also tend to reflect the exposure conditions; girders in Span 4 had higher exposure to wetting and drying than Span 5, due to the height above water levels and high tide inundation.

Steel reinforcement section loss was highest in Girder 3-1 and diminished in the following order: Girder 4-1, 5-1 and 4-3. This may indicate that the west-most exterior girders had higher levels of corrosion due to more exposure to wetting and drying. Indeed, girders along line 1 were the closest to the water due to the superelevation, which may explain this trend.

Another possibility for the apparent discrepancy between chloride content and section loss in Girder 4-3 is that cores for Cl⁻ content were extracted at different locations from the steel reinforcement samples. Steel samples were taken at about 12 ft. from the south end of the girders, where levels of corrosion may have been lower.
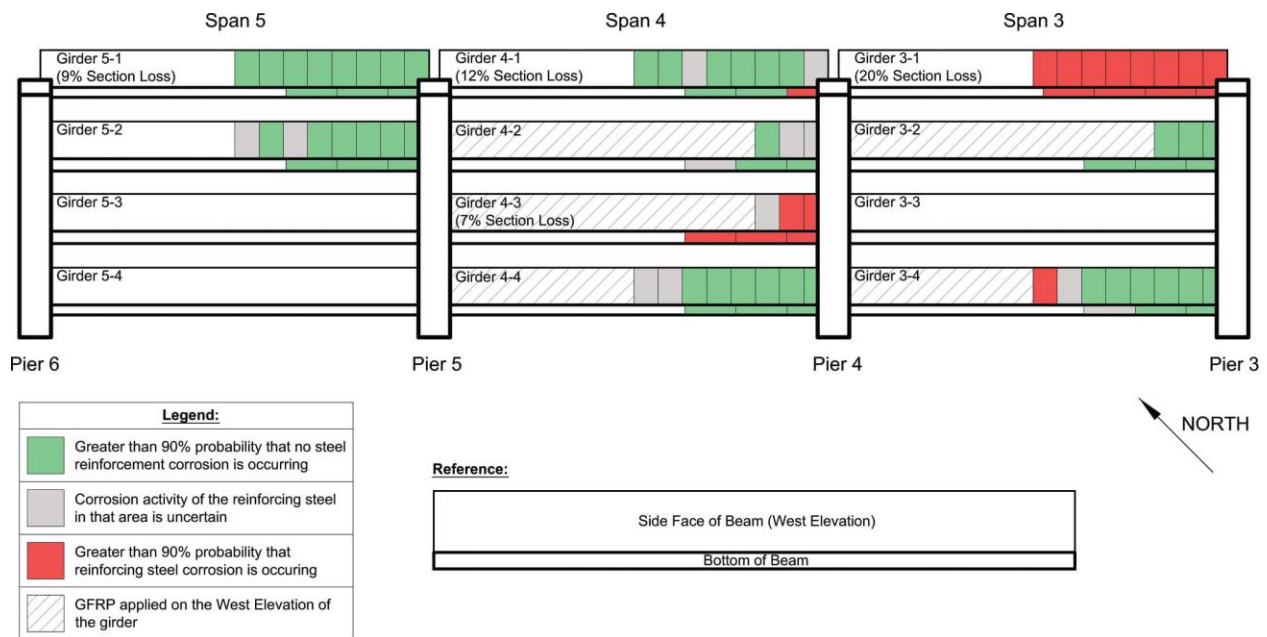
Figure 225—Corrosion potential mapping on girders in spans 3, 4, and 5

6.9 Findings

Nine concrete bridge girders were salvaged from a bridge originally constructed in 1957 and located over brackish water. In 2005, these girders were strengthened with spray-up GFRP and bonded CFRP precured laminates. Structural and materials testing were conducted to determine the efficacy of the system. The following are findings and observations from the testing and analysis:

1. Over 82% of bond tests exceeded the minimum strength criterion (>200 psi) prescribed by ACI 440.2R and NCHRP (2010)
2. In 19 of 57 pull-off tests, an adhesive or mixed failure mode occurred, indicating either installation issues or that some bond degradation may have occurred.
3. Effects of CFRP laminate strips on the girder ultimate strength were relatively minor; added strength from CFRP wraps ranged from 6.7% to 18.4%.
4. Higher depths of carbonation were noted in specimens with no externally bonded GFRP than the specimens with GFRP.
5. Ninety-five percent of CFRP composite samples exceeded the tensile modulus of elasticity as specified by the manufacturer.
6. All GFRP samples exceeded the flexural modulus of elasticity as specified by the manufacturer.
7. Corrosion of reinforcement was found in numerous locations, all of which was likely to be present prior to the application of the FRP repair. Because there was very little concrete repair conducted, it was impossible to distinguish between corrosion that occurred prior to the repair and that following the repair. Nevertheless, no signs of anode ring effect were observed during materials sampling or exploratory concrete demolition.
8. Results of a theoretical moment-curvature analysis was in good agreement with experimental moment-curvature on each girder.

7 Chaffee Road

7.1 Bridge History

The Chaffee Road Bridge is an overpass of Interstate 10 located near Jacksonville, Florida (bridge # 720206). The bridge was constructed in 1960 with a 15ft-6in. clearance height. For many years, this bridge had the lowest clearance height westbound out of Jacksonville, which resulted in multiple truck impacts with varying degrees of damage sustained. Figure 226 shows a plan view that identifies the girders salvaged for testing. The girders were salvaged from the bridge in 2010.

On July 7th, 2001, two over-height vehicles struck the Chaffee Road Bridge, which damaged concrete and cut some prestressing strands on two of the five type III AASHTO girders (Figure 227). SDR Engineering Consultants, Inc., restored the girders by repairing the damaged portions of concrete, and installing an externally bonded CFRP system (Figure 228). This system was a wet layup multiple layer bidirectional carbon fiber fabric and an epoxy matrix, which completely wrapped the middle 30 ft section of both exterior girders that were damaged. According to Fallaha and Rambo-Roddenberry (2013), the repairs cost approximately $20,000 and took approximately a week from impact for the bridge to be returned to service.

In June of 2003, another over-height vehicle impacted the Chaffee Road Bridge, which damaged one of the girders previously repaired with FRP (Figure 229). The FDOT decided to restore the damaged girders once more using the same repair process as before. The bridge was eventually replaced in 2012 by the FDOT, due to old age and condition of the girders after multiple impacts.
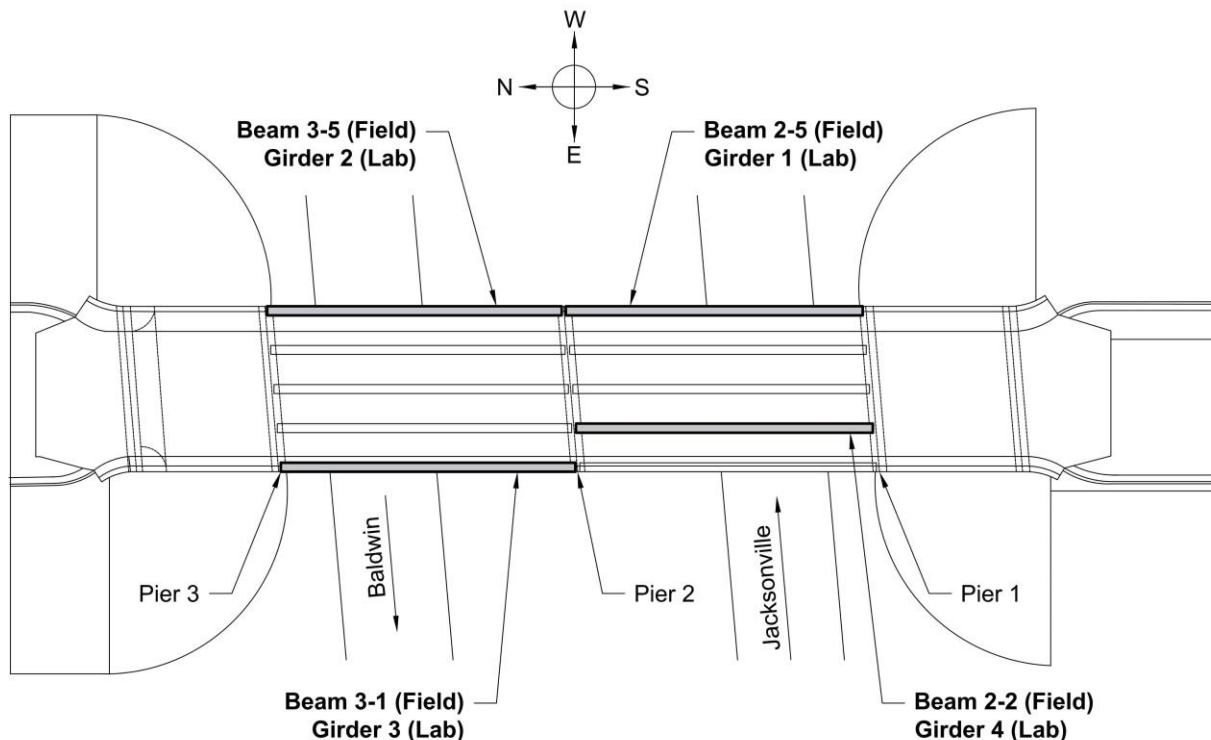
Figure 226—Plan view of Chaffee Road Bridge with salvaged girders identified

---

Figure 227—Girder damage from vehicle impact in July of 2001
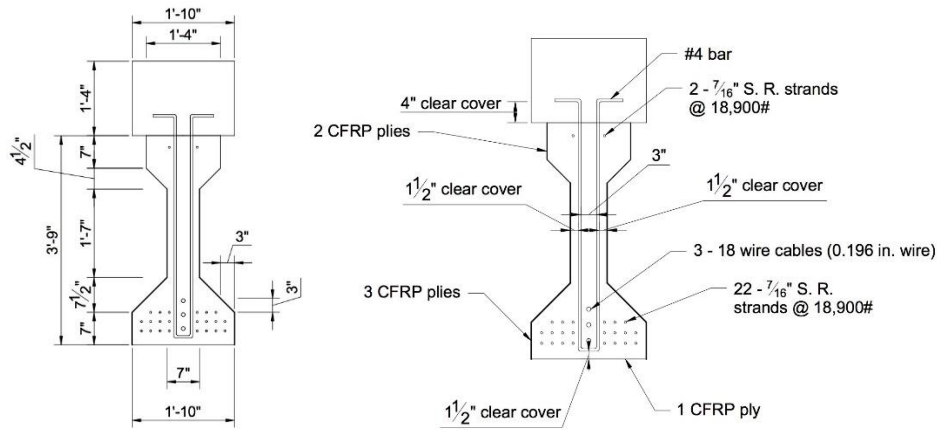
Figure 228—Typical beam section (a) original and (b) with CFRP repair
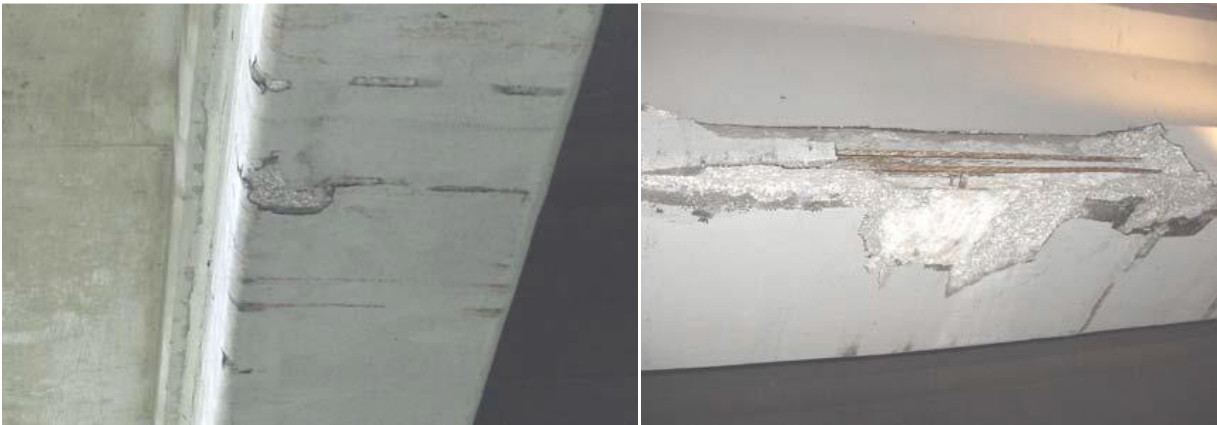
Figure 229—Condition of girder before and after vehicle impact in June of 2003

7.2 Material Properties

The processes used for assessing material properties of concrete, steel reinforcement, and CFRP reinforcement are covered in Chapter 4. The following sections provide information that varies from that chapter.

7.2.1 Concrete: Compressive Strength

Concrete cores for compression test were taken from locations near the supports that were not affected by the structural test. Care was taken to inspect each core and make sure their quality and size conformed to ASTM C42/AASHTO T24. Nine satisfactory cores from all four tested girders were obtained and results are shown in Table 45. Figure 230 shows the two typical compression core locations obtained from the four girders. Any modifications to these dimensions are listed in Table 45. Girder depths varied due to varying deck thickness.
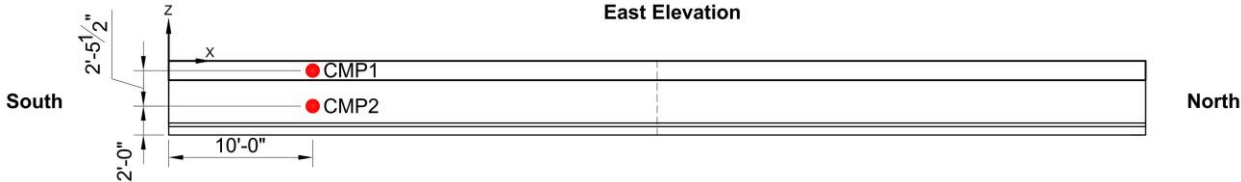
Figure 230—Typical coring locations for compression cores

Table 45—Summary of compression test results

Girder	Core	x (in.)	y (in.)	z (in.)	Strength (psi)	Failure mode (ASTM C39)	Average strength (psi)
1	CMP1	120	11	-8	5,390	Type 1	5,575
2		54	11	-8	5,130	Type 1	
3		120	21.5	-12.5	5,800	Type 1	
4		120	11	-5.5	5,980	Type 1	
1	CMP2	120	3.5	-37.5	7,710	Type 1	7,192
3		120	3.5	-37	7,180	Type 1	
3		120	3.5	-37	6,360	Type 1	
4		120	3.5	-30	7,540	Type 1	
4		120	3.5	-30	7,170	Type 1	

7.2.2 Prestressing Steel

Prestressing strand samples for tension testing were taken away from the damaged area from Girder 1. It was assumed that the girders were all constructed with similar prestressing strand. Strands measuring approximately 60 in. were collected using a saw. Six specimens were collected from the south end of Girder 1. Prestressing strands were specified to be 7/16 in. dia. seven-wire stress-relieved strands grade 250 (ASTM A416) in the original construction drawings.

All steel reinforcement specimens were tested in tension at FDOT SMO (Figure 231), as per ASTM A416. Strands were cut to 50 in. length to meet the ASTM standard requirements. Silicon carbide was adhered with glue to 8 in. on each end (Figure 232) for additional grip. Results from the tensile test are listed in Table 46.

(a)   (b)
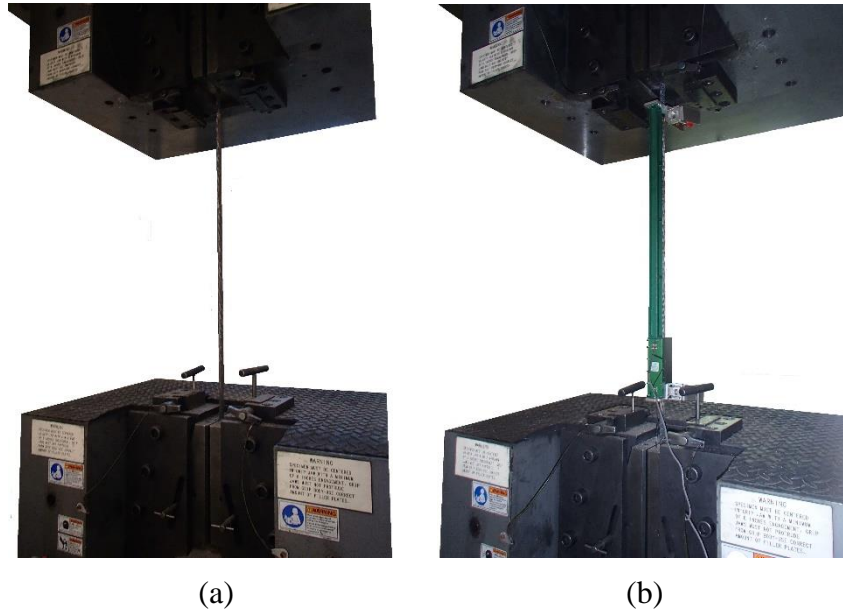
Figure 231—(a) Strand in tensile test setup (b) strand in tensile test setup with extensometer

Figure 232—Silicon carbide applied to the ends of each sample

Table 46—Results of tests on steel reinforcement

Specimen Identification	Elongation (%)	Yield Strength (lbf)	Load at 1% Extension (lbf)	Breaking Strength of Strand (lbf)
1SE1	6.59	26,370	26,990	29,620
1SE2	strand slipped-invalid			
1SE3	6.49	26,030	26,571	29,360
1SW1	strand slipped-invalid			
1SW2	6.29	26,510	27,089	29,630
1SW3	6.72	26,490	27,051	29,750
ASTM A416 - 16	3.5		24,300	27,000

Samples in Table 46 except for 1SE2 and 1SW1 (slipped in grips during testing) meet ASTM A416 – 16 requirements. All of the strands met the minimum dimensional requirements of per ASTM A416. Figure 233 compares the load versus strain values of the strands.
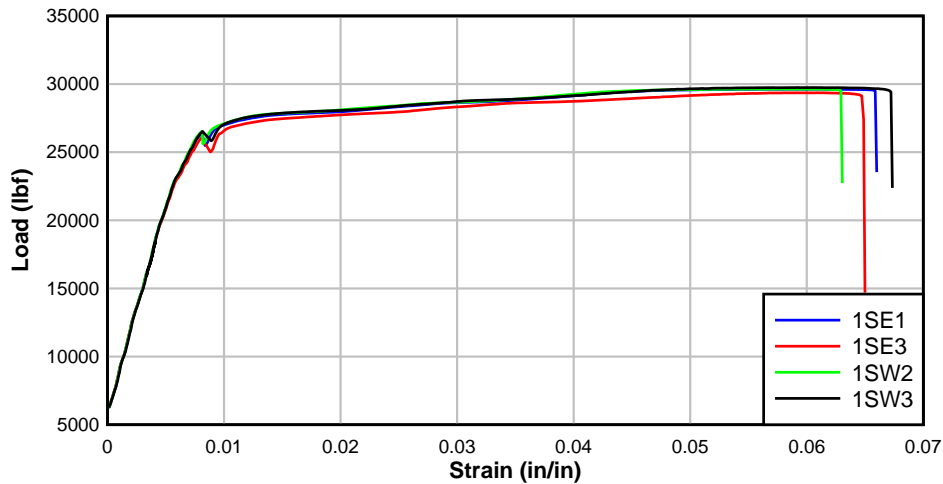
Figure 233—Typical load vs. strain plot

7.2.3 CFRP Reinforcement

To determine the mechanical properties of the CFRP material, tensile tests were performed on 10 CFRP coupons that were cut out of the CFRP strips pulled from Girder 3 after testing in flexure. The manufacturer of the carbon fiber system was unknown. Table 47 shows test results and Figure 234 shows a comparison of the tension test results.

Table 47—CFRP coupon tension test results

Specimen Number	Tensile Strength (ksi)	Elongation (in/in)	Modulus of Elasticity (ksi)
3-E(1)	13	0.003	5970
3-E(2)	39	0.011	6100
3-E(3)	33	0.006	6330
3-E(4)	29	0.005	5640
3-E(5)	17	0.002	7070
3-W(1)	24*	–	–
3-W(2)	24*	–	–
3-W(3)	22	0.006	4490
3-W(4)	22	0.004	5010
Average:	25	0.005	5800
COV:	0.37	0.55	0.15

*excluded from average values of CFRP-concrete bond; strain gage detached from sample before reaching strength
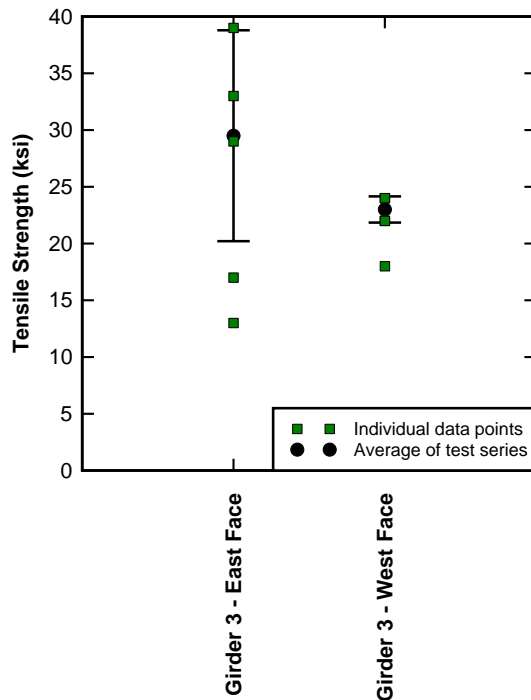
Figure 234—Comparison of tensile strength of the tested samples (error bars represent one standard deviation)

7.2.4 CFRP Reinforcement: Pull-off Tests

Direct pull-off test locations were chosen to examine the quality control of the external FRP repairs (Figure 235 and Figure 236). Eleven tests were performed on Girder 2 and 10 were performed on Girder 3. Direct pull-off test results are summarized in Table 48. All tests passed the tensile pull-off strength criterion. Seven of the 11 samples failed cohesively for Girder 2, the remaining samples had an adhesive failure mode. Only four of the 10 samples failed cohesively for Girder 3, while the remaining samples had an adhesive and mixed failure mode.

Overall, direct tension pull-off tests between Girder 2 and 3, showed that all of the samples (excluding samples which had failure mode A) met the specified strength of over 200 psi (Figure 237). Over 42% did show an adhesive or mixed failure mode, however, indicating that there may have been some bond degradation.
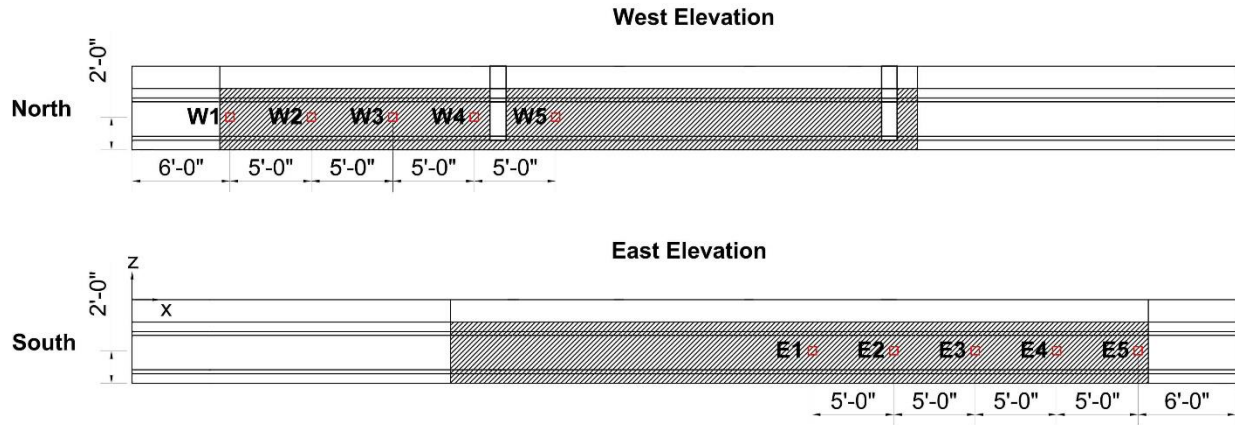
Figure 235—Direct pull-off testing locations for Girder 2
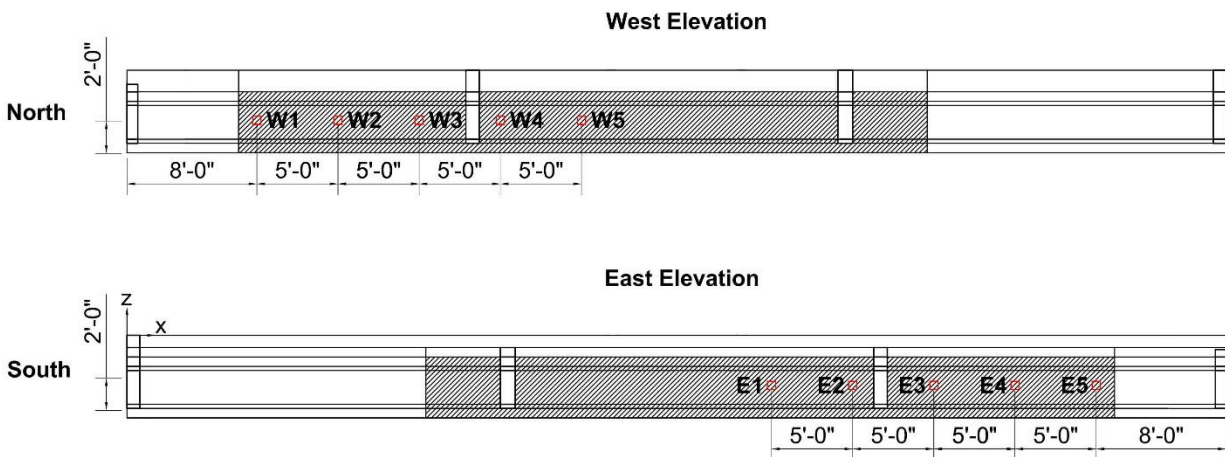
Figure 236—Direct pull-off testing locations for Girder 3

Table 48—Summary of direct pull-off test results

Girder	Location	Stress at failure (psi)	Failure mode (% adhesive)	ASTM D7522 failure mode	Note
2	E1	390	0	G	Result from second attempt, the apparatus was not seating properly in first attempt
	E2	290	0	G	Failure occurred at a location containing a void in concrete
	E3	-	-	A	
	E4	363	100	E	Presence of small voids in epoxy
	E5	407	0	G	Brownish color around fractured aggregate in concrete substrate
	E6	217	100	E	Presence of voids in concrete. Three visible layers of FRP; the exterior layer is delaminating
	W1	420	0	G	
	W2	227	0	G	
	W3	356	100	E	Two voids in concrete were initially filled with epoxy
	W4	118	0	G	Epoxy interface can be seen thru a void in concrete substrate, possible damaged location in concrete
	W5	178	0	G	Presence of 2 different concrete colors (light brown and grey) , possible damaged location
3	E1	197	30	F	
	E2	402	0	G	
	E3	267	5	F	
	E4	368	65	F	
	E5	265	5	F	
	W1	203	95	F	
	W2	108	-	A	
	W3	488	0	G	
	W4	296	0	G	Small void in concrete substrate
	W5	640	0	G	Concrete substrate color is darker than previous samples

(a)   (b)
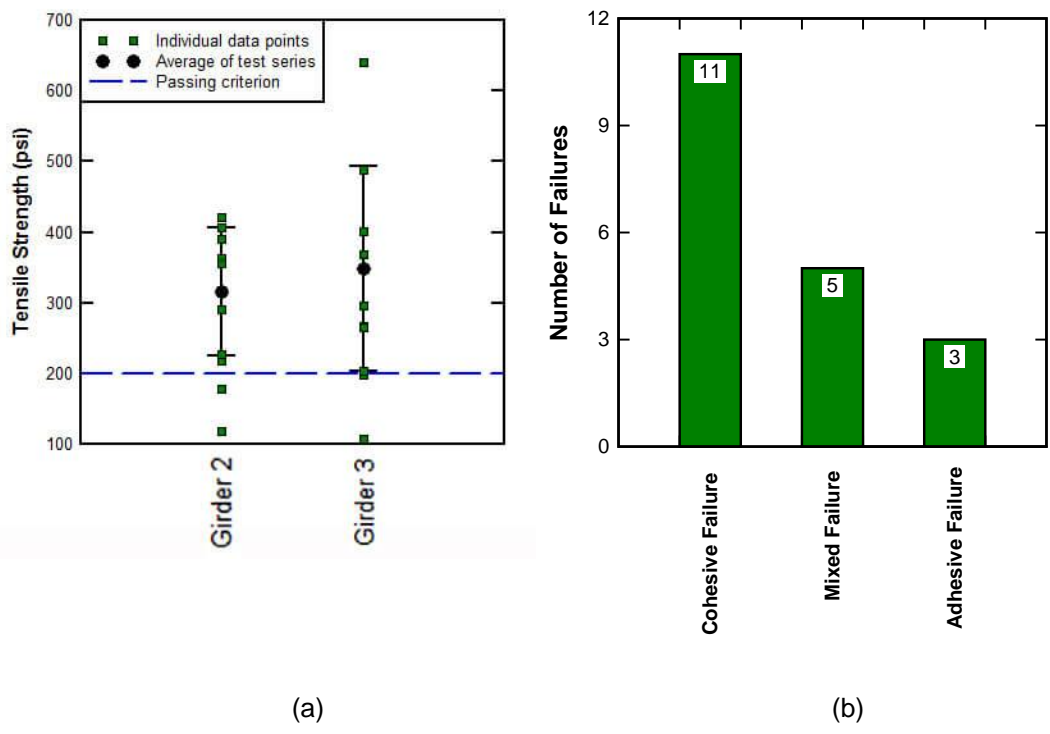
Figure 237—Direct pull-off testing: (a) tensile strength comparison and (b) failure modes

7.3 Flexural Test Setup and Instrumentation

The procedure used for flexural testing was identical to those used for the Indian River bridge girders (see chapter 5). The following sections will only provide information that varies from the chapter covering Indian River bridge.

All four girders were tested in flexure using a four-point bending test setup to determine their behavior in flexure. Girder ends were supported on 2-in. thick neoprene pads measuring 7 in. × 18 in. at the base, placed on top of concrete blocks to provide sufficient clearance under the girder (Figure 238). Test setup and instrumentation is shown in Figure 239 through Figure 243.

Figure 238—Girder loaded in test frame

Top View

West Elevation
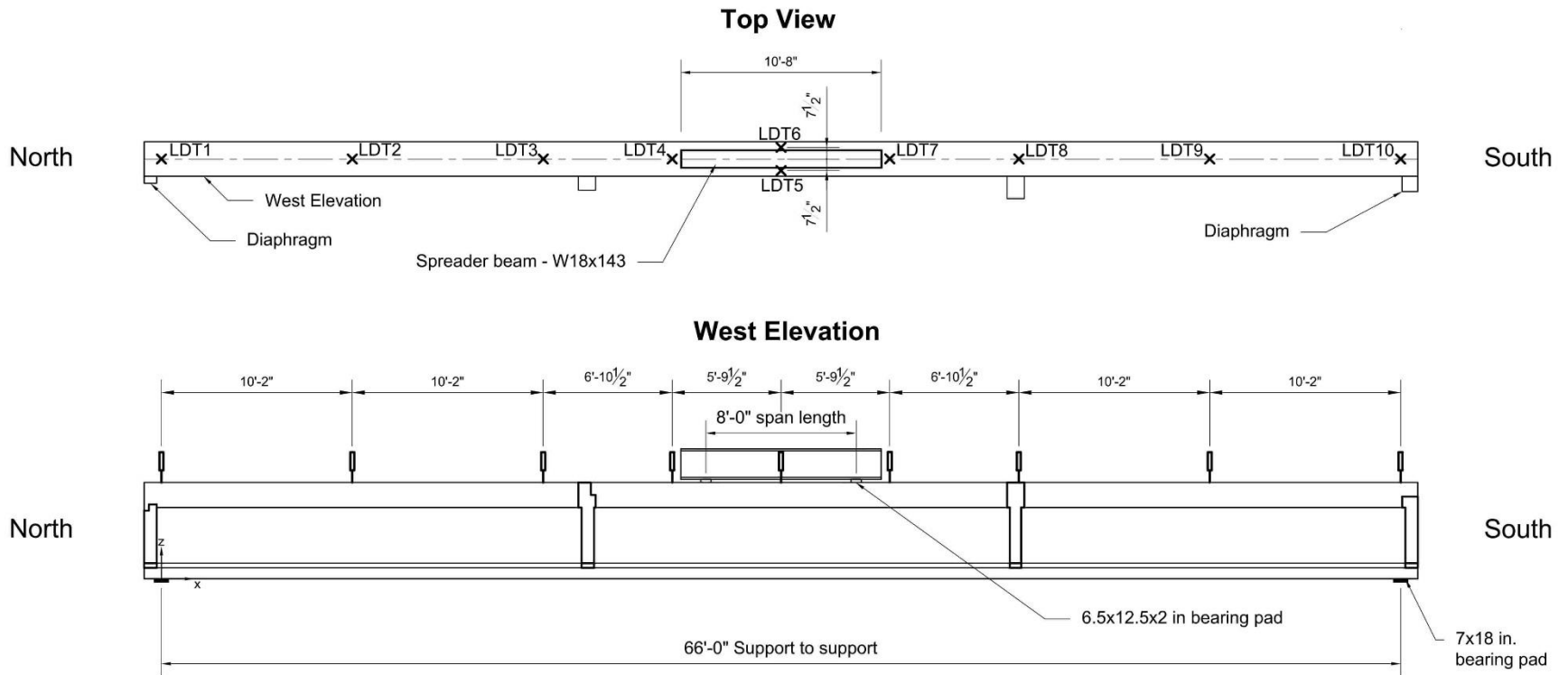
Figure 239—Typical instrumentation plan representing the locations for the laser displacement transducers
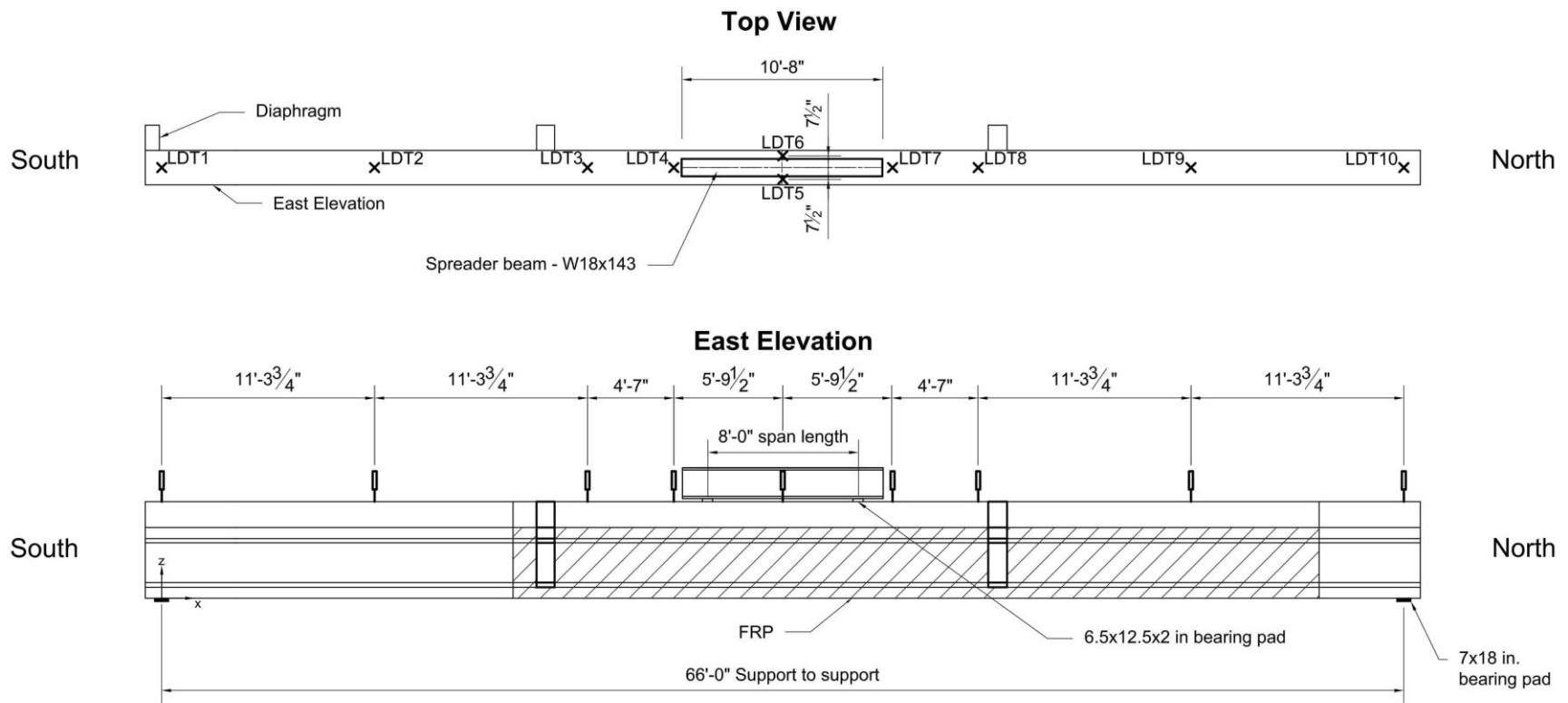
Figure 240—Instrumentation plan representing the locations for the laser displacement transducers on Girder 2
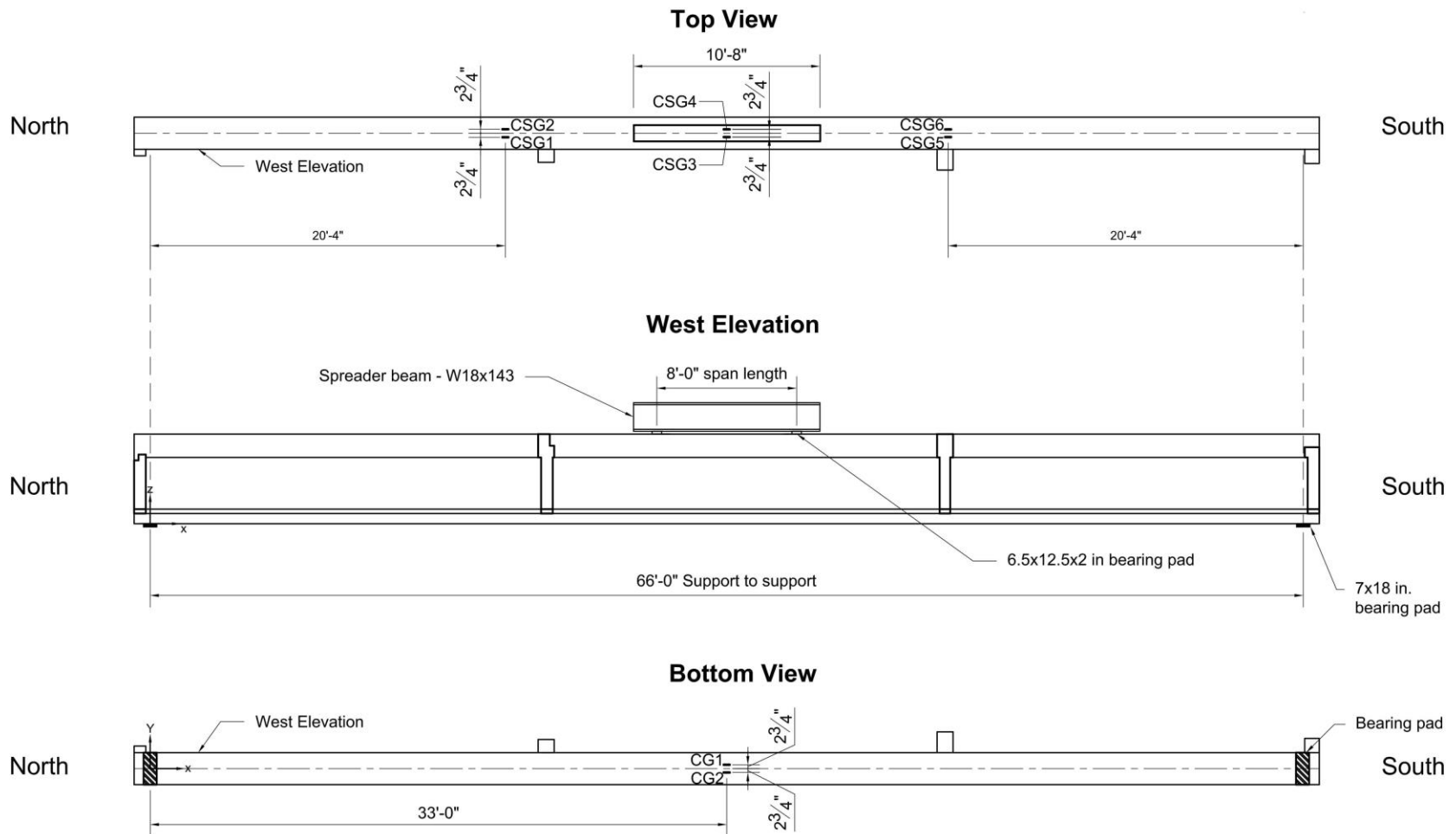
Figure 241—Typical instrumentation plan indicating the strain gage locations for girders without FRP
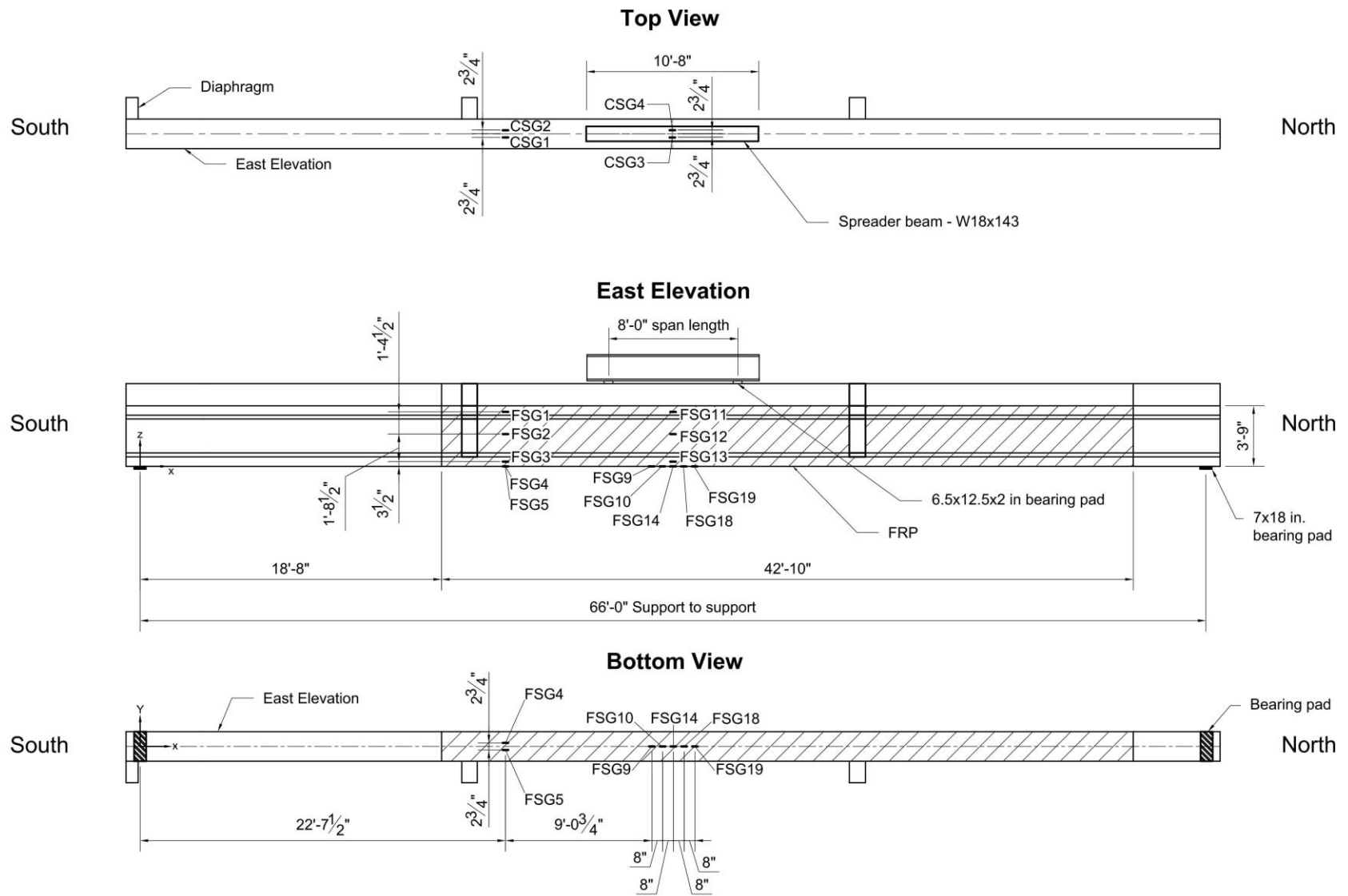
Figure 242—Instrumentation plan indicating the strain gage locations for Girder 2
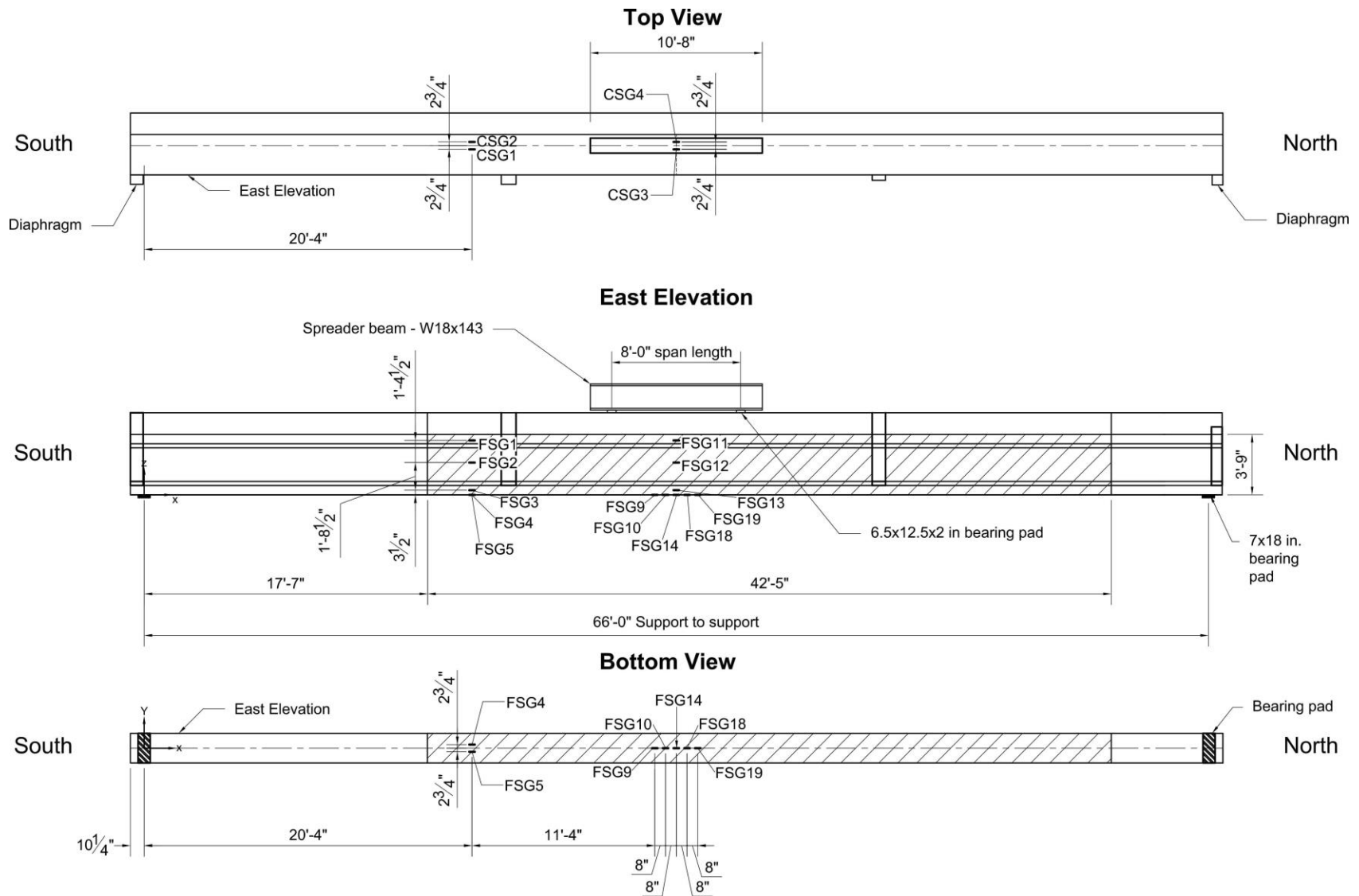
Figure 243—Instrumentation plan indicating the strain gage locations for Girder 3

7.4 Flexural Test Procedures

Girder 1 and 4 were loaded monotonically to the incremental service load levels shown in Table 49 for one cycle. Girders 2 and 3 were loaded monotonically to the incremental service load levels shown in Table 50 for two cycles. The final cycle consisted of monotonic loading up to the full flexural strength. The load value of cycle 1 was determined per AASHTO to be the maximum service load of each beam while it was part of the bridge structure. The load value of cycle 2 (Table 50) was arbitrarily selected as a secondary checkpoint to determine cracking and debonding of the FRP before failure.

Table 49—Girder loading scheme

Cycle	Step	Description
	1	Load to 50 kip
1	2	Hold to mark cracks/cointap
	3	Unload
2	n/a	Load to full strength capacity

Table 50—Girder loading scheme

Cycle	Step	Description
1	1	Load to 50 kip
	2	Hold to mark cracks/cointap
2	1	Load to 90 kip
	2	Hold to mark cracks/cointap
3	n/a	Load to full strength capacity

7.5 Flexural Test Results and Discussion

Load-displacement plots for all four girders are presented in Figure 244. Girders with FRP installed exhibited similar behavior in the laboratory test. Girder 1 had notably higher uncracked stiffness than the other three, and slightly higher strength. It is not clear why. Girders 2, 3, and 4 all had similar uncracked behavior. Their behavior diverged upon cracking, with the two CFRP-repaired girders indicating a higher stiffness than the unrepaired girder. The ultimate strength of the repaired girders was proportionally higher than that of the unrepaired.
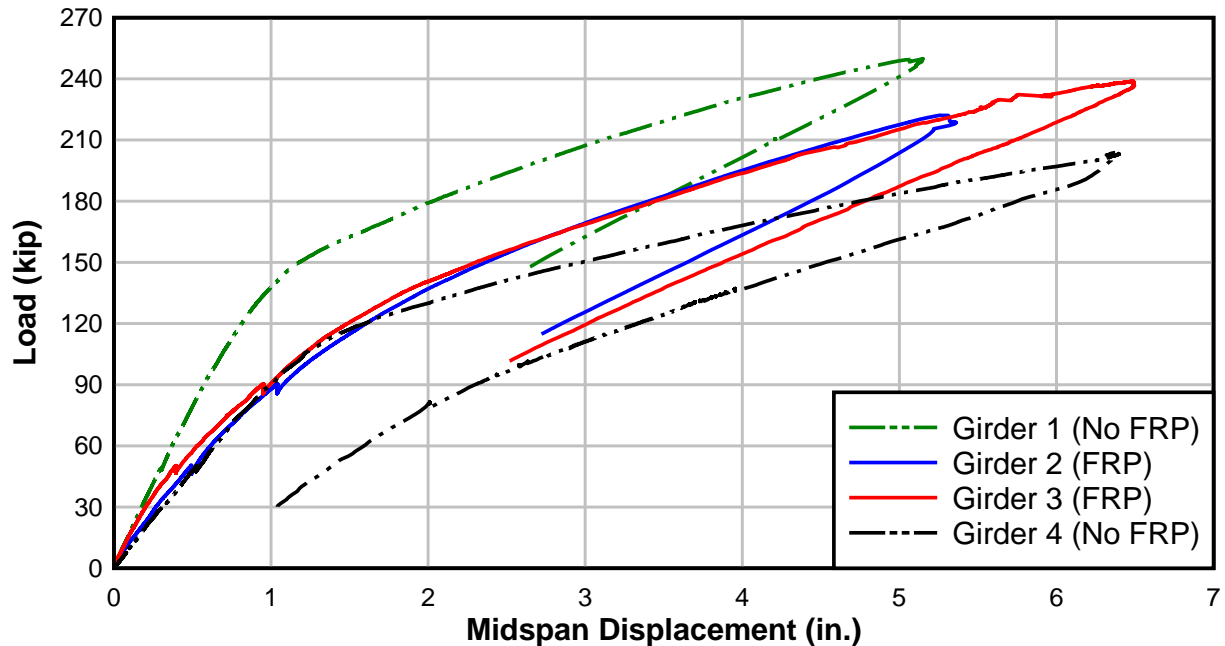
Figure 244—Load-midspan displacement of test girders

Girder 1 was the easternmost exterior girder over the eastbound lane, and its repair did not include FRP (Figure 245). This was most likely the case because the damage may have not been as severe as Girder 2 and Girder 3. Girder 1 and Girder 2 had identical cross-section geometry. The failure mode only consisted of the concrete crushing in the compression zone (Figure 246), as expected. When loading the girder past its ultimate strength, Girder 1 failed at the end of the repaired region (Figure 247), which may indicate that the repair had a minor effect on the ultimate strength.

Figure 245—Region of concrete repair indicated in hatched area

Figure 246—Concrete crushing in compression zone

Figure 247—Girder 1 failed at the end of the repaired region

An FDOT inspection report by Cheshire (2001) indicates that Girder 2 (Beam 3-5) had the most severe damage in Span 3, because of four severed strands from an impact (Figure 248). This girder was the easternmost exterior girder over the westbound lane, which is why it had the most severe damage. Girder 2 failed at the center of the repaired region that had only repair mortar without FRP, which was likely due to multiple repairs to multiple impacts (Figure 249). The repair originally had FRP in this location, but it was removed during a more recent impact event and the section was restored without application of FRP; FRP, however, was still on the web. Although Girder 1 and Girder 2 had an identical cross-section (Figure 228), Girder 2 had four severed strands. The location of failure may indicate that the repair had affected the ultimate strength, resulting in Girder 2 having a lower ultimate strength than the other exterior girder. The failure mode consisted of the concrete crushing in the compression zone (Figure 250), instead of FRP rupture prior to a concrete crushing failure mode. This may indicate that the FRP was not able to provide as much supplemental reinforcement as intended when designed.
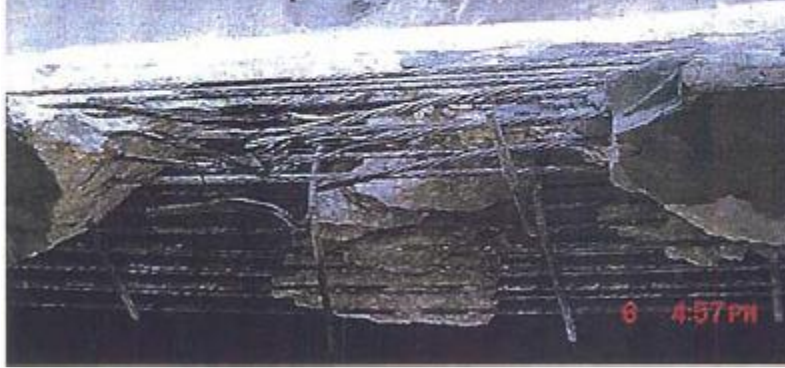
Figure 248—Severed strands on Girder 2 after impact in 2001 (Green et al., 2004)

| (a) | (b) | (c) |
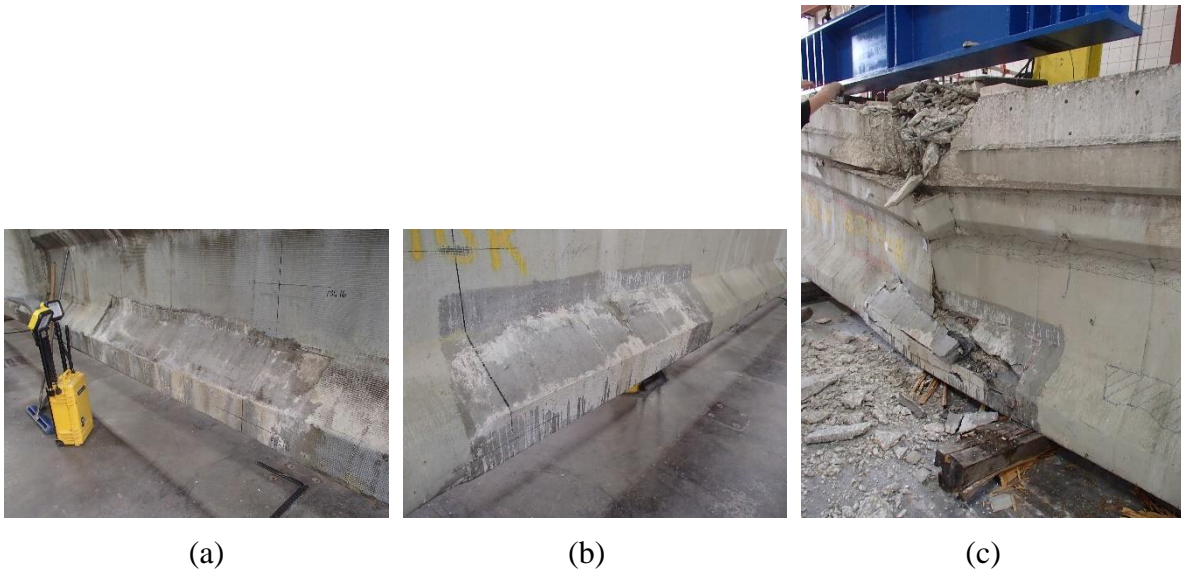
Figure 249—Repaired region of Girder 2: (a) west face initially before testing (b) east face initially before testing (c) east face after failure

Figure 250—Concrete crushing in the compression zone

Girder 3 was the westernmost exterior girder over the westbound lane. At failure, the FRP ruptured on the west elevation (Figure 251a) and on the east elevation (Figure 251b), which was in a highly debonded region directly below the north end of the spreader beam bearing pad (Figure 251c). The cross-section for Girder 3 was different from Girder 1 and Girder 2. Additional depth was provided by the deck in Girder 1 and Girder 2, which may explain why Girder 1 had a higher ultimate strength than Girder 3. Although Girder 3 had a number of debonded regions after loading, Girder 2 had larger amounts of debonded regions and the FRP may have not been as effective in increasing the ultimate strength and ductility because of the repaired region without FRP, which included four severed prestressing strands.

| (a) | (b) | (c) |
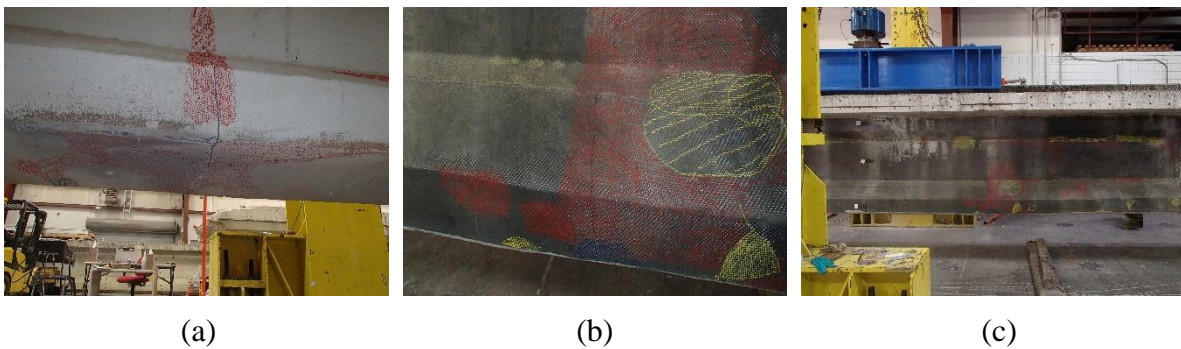
Figure 251—FRP damage on Girder 3: (a) close-up of rupture on east face (b) close-up of rupture on west face (c) rupture location on west face

Girder 4 was a westernmost interior girder facing eastbound traffic, which did not have any apparent repairs in the midspan region. This girder had a shallower overall depth than the exterior girders due to the smaller deck thickness than that of the exterior girders. This resulted in the girder having the lowest ultimate strength of the tested girders. The failure mode consisted of the concrete crushing in the compression zone (Figure 252).

Figure 252—Concrete crushing in the compression zone

7.6 Moment Curvature Analysis

Moment curvature analysis presented here was conducted similar to that of the Indian River bridge specimens with the following exceptions. Concrete compressive strength of 7,000 psi was assumed based on the compressive strength data for these girders (Table 45). FRP material properties obtained from material testing (Section 7.2.3) were used in the analysis. Each cross-section had 40 prestressing strands with material properties as listed in this section, with a modulus of elasticity of 28,500 ksi.

As explained in Section 5.7, an ultimate strain of 0.003 for CFRP was assumed in modeling the theoretical moment curvatures. This strain value used for the CFRP in the model corresponds to only 60% of measured (Table 47 and Table 30) elongation at rupture of CFRP.

Figure 253 through Figure 256 show comparisons of experimental moment curvatures to theoretical moment curvatures for Girders 1, 2, 3 and 4. Girder 2 and 3 had externally bonded FRP. Girder 1 and 4 had strain gages at the top and bottom only, so the experimental strain moment-curvature was not determined due to a limited amount of data to determine the curvature. Table 51 shows a comparison of theoretical strength with measured strength.

Table 51—Theoretical versus experimental strength of girders

Girder	Theoretical Strength (kip-ft.)	Experimental Strength (kip-ft.)	Ratio of Experimental to Theoretical Strength
1	4855	4166	0.86
2	4811	3813	0.79
3	4215	4210	1
4	3799	3436	0.90
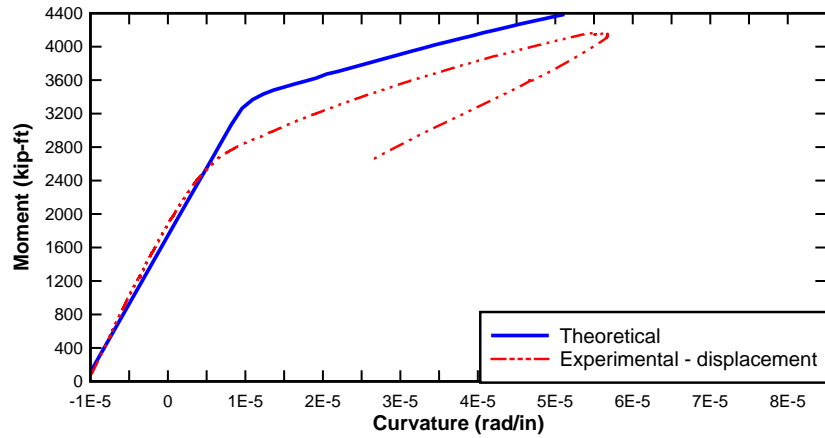
Figure 253—Moment curvature for Girder 1
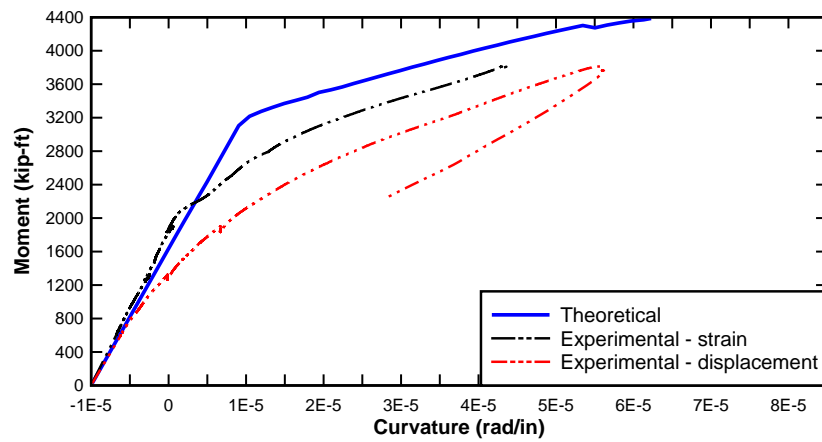
Figure 254—Moment curvature of Girder 2
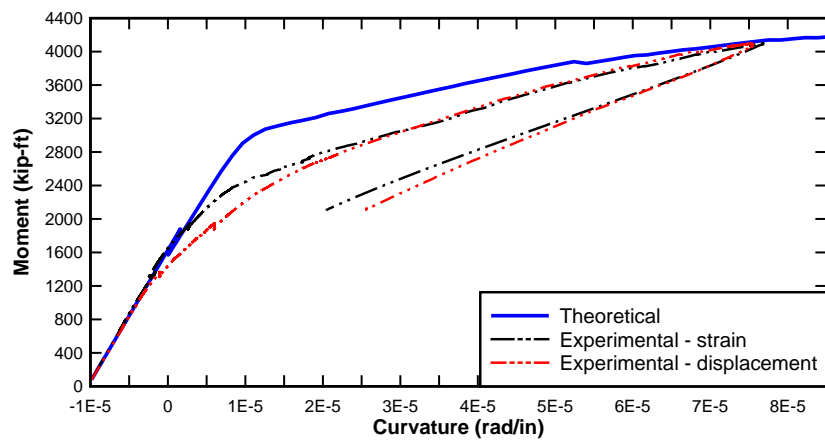
Figure 255—Moment curvature of Girder 3
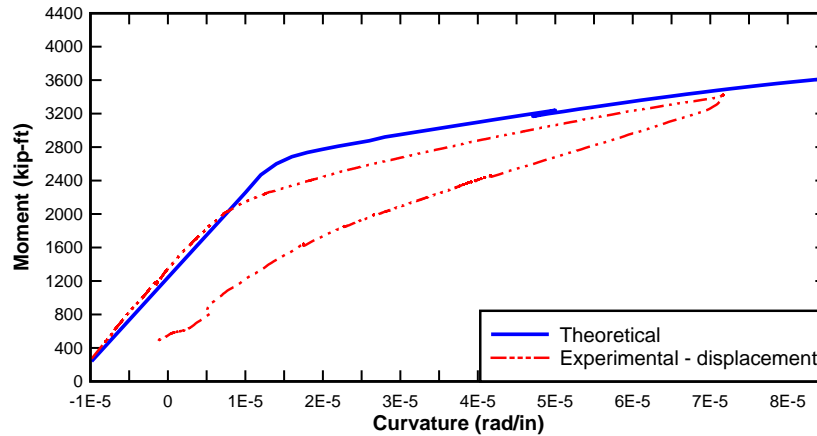
Figure 256—Moment curvature of Girder 4

Girder 1 had a lower experimental moment capacity than the theoretical moment curvature, most likely due to prior damage from a collision. Girder 2 had four severed strands, which greatly affected the moment capacity of the girder. Although it had been repaired with FRP, a majority of debonded regions were determined by a coin tap prior to testing the girder in flexure ().

Prior to loading Girder 2 in flexure, debonded regions were identified through coin tap inspection (Figure 257a). Some additional debonding had occurred when loading the girder to 90 kips, primarily in areas within the constant moment region that most likely did not have a critical effect on the ultimate capacity, with the exception of the debonded region near the repair. Figure 257b shows the proximity of the repaired region to the constant moment region. Failure had occurred in this repaired region, which most likely was the cause of failure at a load notably lower than the theoretical ultimate capacity.

Based on inspection through coin tap prior to testing the girders in flexure, the total debonded area on Girder 3 was less than that of Girder 2 prior to loading (Figure 258a) and after loading the girder to 90 kips in flexure (Figure 258b). Girder 3, however, did not have a repair region within the constant moment region, which most likely was the reason why Girder 3 had a much higher ultimate capacity than Girder 2.

Further information on the conditions of the girders can be found in Section 7.5.
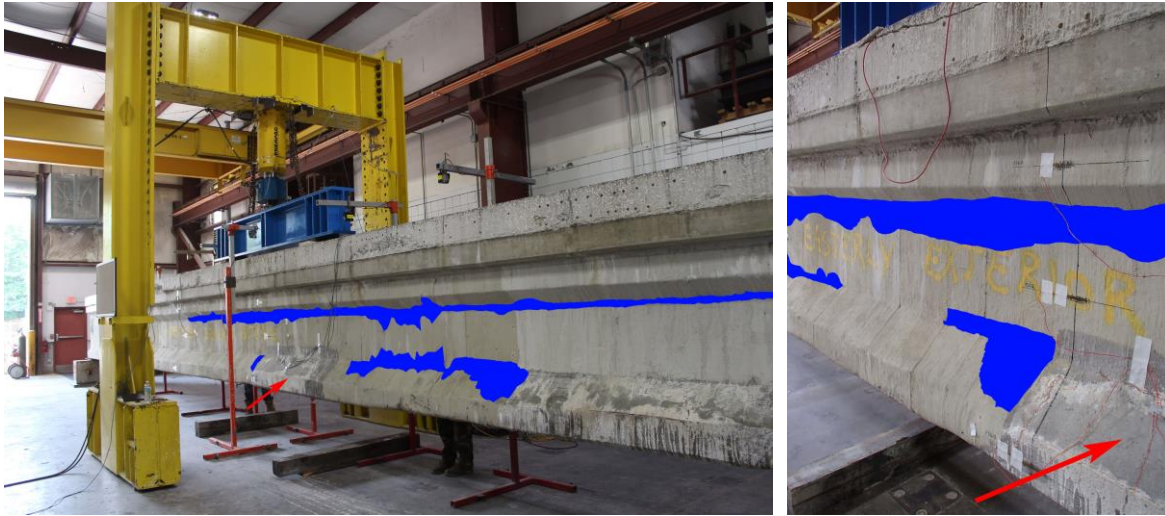
Figure 257—FRP debonding on Girder 2; repaired region is identified with a red arrow, and debonding is identified in blue: (a) prior to loading in flexure (b) after loading Girder 2 to 90 kips

Figure 258—FRP debonding on Girder 3; repaired region is identified with a red arrow, and debonding is identified in blue: (a) prior to loading in flexure (b) after loading Girder 3 to 90 kips

An additional theoretical moment curvature analysis was also performed for Girder 2 (Figure 259) and Girder 3 (Figure 260) using the numerical model developed by Consolazio et al. (2004), with an assumed FRP strain of 0.003. This additional analysis provided a comparison of the theoretical ultimate capacity with and without FRP. Aside from an increase in stiffness, the comparison between both models shows very little difference in ultimate capacity for both cases when considering externally bonded FRP. A more substantial amount of FRP would most likely be necessary to see a significant improvement in a prestressed girder with high strength capacities.
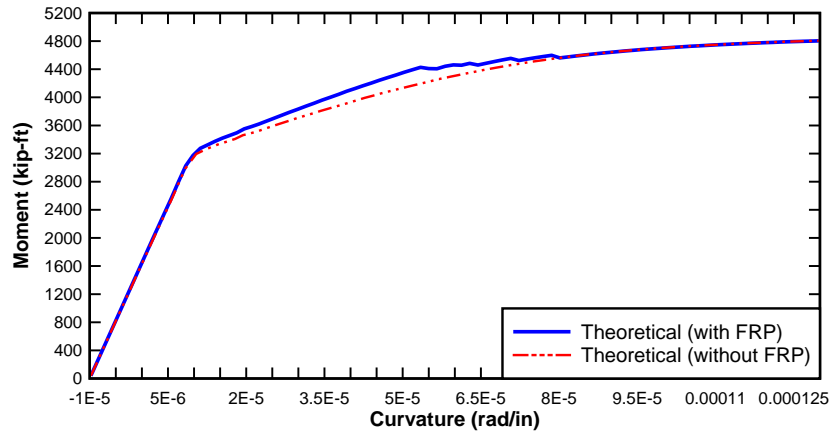
Figure 259—Girder 2 comparison of the theoretical ultimate capacity with and without FRP
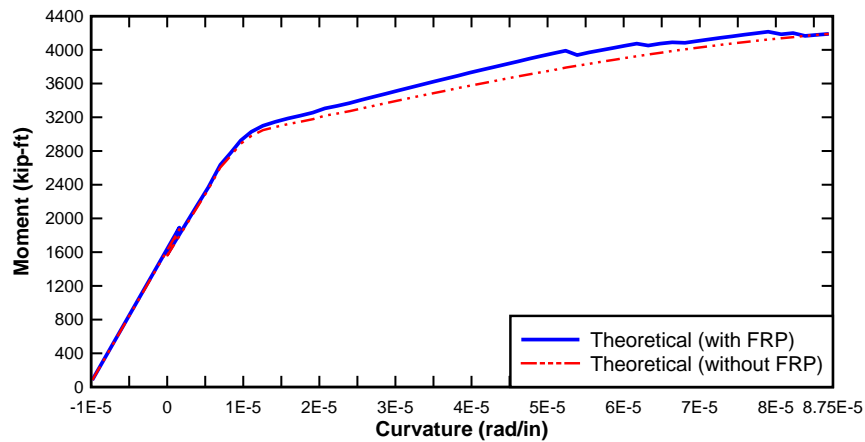
Figure 260—Girder 3 comparison of the theoretical ultimate capacity with and without FRP

7.7 Girder Dissection

Following the structural test, materials test samples were taken and inspections were performed on Girder 1 and 3. Prestressing strands were taken from Girder 1 and CFRP samples were pulled from Girder 3. No deterioration of the concrete or steel was noted during the sampling.

7.7.1 CFRP Condition

CFRP samples were extracted from the concrete surface by the use of a cutting wheel combined with hand prying and peeling. The process revealed that large portions of CFRP on the east face was debonded at the CFRP-epoxy interface. Figure 261 illustrates the lack of concrete substrate that remained adhered to the CFRP laminate when removed from the surface. Removal of the CFRP on the west face also revealed poor bonding at the concrete-epoxy interface (Figure 262). The CFRP on the east face was painted (Figure 263a). The CFRP on the west was not painted and may not have been completely saturated in resin prior to installation based on the voids visible in the weaves (Figure 263b).

Figure 261—CFRP sample with most of debonding at the CFRP-epoxy interface

Figure 262—CFRP sample with most of its debonding at the concrete-epoxy interface

(a)   (b)
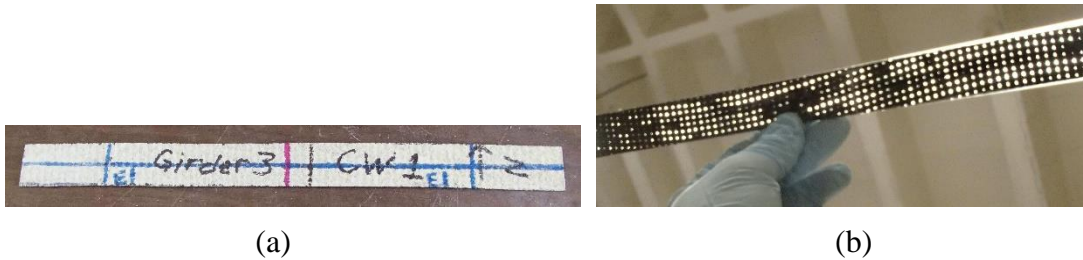
Figure 263—CFRP samples: (a) from east face with coating (b) from west face without coating

7.7.2   Steel Reinforcement

Prestressing strand samples were extracted from the South end of Girder 1 by the use of a jackhammer and were saw cut to approximately 60". Visual inspection of the strands indicated no signs of corrosion.

7.8 Findings

Two prestressed concrete AASHTO Type III girders were salvaged from an I-10 overpass bridge. In 2001, following a truck impact, these girders were repaired and strengthened with wet layup CFRP composites. Structural and materials testing were conducted to determine the efficacy of the system. The following are findings and observations from the testing and analysis:

1. Over 80% of bond between CFRP and concrete exceeded the minimum strength criterion (>200 psi) prescribed by ACI 440.2R and NCHRP (2010)
2. Over 42% showed an adhesive or mixed failure mode, indicating either installation issues or that some bond degradation may have occurred
3. The theoretical strength increase provided by CFRP composite was less than 5%. Actual increase in strength is difficult to determine because the girders were damaged by impact
4. Results of a theoretical moment-curvature analysis was in good agreement with experimental moment-curvature on each girder
5. No corrosion or other signs of deterioration were noted during post-test examination of test specimen

8 Outcomes

This research project aimed to evaluate existing bridges repaired or strengthened with bonded FRP composites. Repair or strengthening of a bridge can delay the need for replacement and thus lower the life-cycle cost of that bridge as well as delay the need for funds to construct a replacement bridge.

The service life of the repairs was in the 10 to 15 year range. Overall bond performance was good. Most of the bond tests exceeded the minimum 200-psi requirement with some evidence of bond deterioration based on the failure modes in the pull-off testing (both lab and field-testing). In some cases, the deterioration could possibly be attributed to inadequate surface preparation or insufficient wetting of FRP fabric.

Evidence from Indian River repair indicated that the CFRP was providing modest protection of underlying reinforcement from further serious corrosion. No ring-anode effect was apparent in the areas surrounding the concrete repair made under the bonded CFRP composite. Even in severe conditions for approximately 13 years, the bonded CFRP system ruptured at the ultimate flexural strength, thus utilizing the full tensile strength of the repair system. Similar results were obtained in the other girder tests.

In this study, the quantity of CFRP composite material used in the repairs would be considered modest in that they did not increase the strength of the girders much beyond 10% of their in situ strength. A word of caution is offered here in that heavier strengthening (more CFRP plies or higher fiber counts) that may generate higher bond stresses, could be more sensitive to bond degradation.

The results of the testing conducted herein indicate that bonded CFRP repairs with a good quality system on a well-prepared surface using good installation techniques can last upwards of 15 years and perhaps beyond. This is particularly true when a bridge is located away from the coast and is not exposed to continuous moisture or other harsh conditions.

9 Future Research

FRP repairs have been in somewhat regular use over the past twenty years in the repair and retrofit of bridges as engineers and owners have become more comfortable with the use of the material. In addition, laboratory work has continued using accelerated conditioning techniques to evaluate the durability of such systems. It is imperative to combine these laboratory techniques with the evaluation of actual field installed systems to help calibrate laboratory models and techniques, but also to better understand their behavior under real exposure conditions for longer service lives.

Although a difficult topic to research, it is still important that we strive to better understand the effect that application of bonded systems has on the underlying reinforcing steel, particularly when dealing with chloride contaminated concrete and concrete repair.

Finally, as mentioned previously, the girders studied in this research were repaired with relatively light systems. As these systems are more widely used, it is likely that they will be relied upon to carry a larger portion of the loads (up to that limited by design specifications). Research should also focus on better understanding the performance of these stronger FRP systems.

References

AASHTO (2011). *Manual for Bridge Evaluation,* 2nd edition. American Association of State Highway and Transportation Officials, Washington, D.C.

AASHTO (2015). *AASHTO LRFD Bridge Design Specifications*. American Association of State Highway and Transportation Officials (AASHTO), Washington, D.C.

AASHTO M 235 (2009). *Standard Method of Test for Testing Epoxy Resin Adhesive*. American Association of State Highway and Transportation Officials (AASHTO), Washington, D.C.

AASHTO T24 (2007). *Standard Test Method for Obtaining and Testing Drilled Cores and Sawed Beams of Concrete*. American Association of State Highway and Transportation Officials (AASHTO), Washington, D.C.

AASHTO T24 (2007). *Standard Test Method for Test for Sampling and Testing for Chloride Ion in Concrete and Concrete Raw Materials*. American Association of State Highway and Transportation Officials (AASHTO), Washington, D.C.

AASHTO T24 (2013). *Standard Method of Test for Obtaining and Testing Drilled Cores and Sawed Beams of Concrete*. American Association of State Highway and Transportation Officials (AASHTO), Washington, D.C.

AASHTO T260 (1997). *Standard Method of Test for Sampling and Testing for Chloride Ion in Concrete and Concrete Raw Materials*. American Association of State Highway and Transportation Officials (AASHTO), Washington, D.C.

ACI 355.4-11 (2011). *Qualification of Post-Installed Adhesive Anchors in Concrete and Commentary*. American Concrete Institute Committee 355.

ACI 440.2R-08 (2008). *Guide for the Design and Construction of Externally bonded FRP Systems for Strengthening Concrete Structures*. American Concrete institute Committee 440.

ACI 440R-07 (2007). *Report on Fiber-Reinforced Polymer (FRP) Reinforcement for Concrete Structures*. American Concrete Institute Committee 440.

ACI Committee 214 (2010). *Guide for Obtaining Cores and Interpreting Compressive Strength Results*. ACI 214.4R-10, American Concrete Institute, Farmington Hills, MI.

ACI Committee 222 (2010). *Protection of Metals in Concrete against Corrosion*. ACI 222R-10, American Concrete Institute, Farmington Hills, MI.

ACI Committee 318 (2014). *Building Code Requirements for Structural Concrete (ACI 318-14) and Commentary*. ACI 318-14, American Concrete Institute, Farmington Hills, MI.

ACI Committee 440 (2008). *Guide for the Design and Construction of Externally bonded FRP Systems for Strengthening Concrete Structures*. ACI 440.2R-08, *American Concrete Institute*, Farmington Hills, MI.

ACI Committee 440 (2008). *Guide for the Design and Construction of Externally Bonded FRP Systems for Strengthening Concrete Structures*. ACI 440.2R-08, *American Concrete Institute*, Farmington Hills, MI.

Alfar, A. (2006). *Durability of Reinforced Concrete Members Strengthened with CFRP Plates and Subjected to Moisture and Salts*. PhD Dissertation, Technische Universität Carolo - Wilhelmina zu Braunschweig.

ASTM A370 (2013). *Standard Test Methods and Definitions for Mechanical Testing of Steel Products*. West Conshohocken, PA, ASTM International, 2013.

ASTM A615 (2015). *Standard Specification for Deformed and Plain Carbon-Steel Bars for Concrete Reinforcement*. West Conshohocken, PA, ASTM International, 2015.

ASTM C 39 (2012). *Standard Test Method for Compressive Strength of Cylindrical Concrete Specimens*. West Conshohocken, PA, ASTM International, 2012.

ASTM C 42 (2013). *Standard Test Method for Obtaining and Testing Drilled Cores and Sawed Beams of Concrete*. West Conshohocken, PA, ASTM International, 2013.

ASTM C 457 (2012). *Standard Test Method for Microscopical Determination of Parameters of the Air-Void System in Hardened Concrete*. West Conshohocken, PA, ASTM International, 2012.

ASTM C143 (2012). *Standard Test Method for Slump of Hydraulic-Cement Concrete*. West Conshohocken, PA, ASTM International, 2012.

ASTM C231 (2010). *Standard Test Method for Air Content of Freshly Mixed Concrete by the Pressure Method*. West Conshohocken, PA, ASTM International, 2010.

ASTM C39 (2015). *Standard Test Method for Compressive Strength of Cylindrical Concrete Specimens*. West Conshohocken, PA, ASTM International, 2015.

ASTM C42 (2013). *Standard Test Method for Obtaining and Testing Drilled Cores and Sawed Beams of Concrete*. West Conshohocken, PA, ASTM International, 2013.

ASTM C469 (2010). *Standard Test Method for Static Modulus of Elasticity and Poisson's Ratio of Concrete in Compression*. West Conshohocken, PA, ASTM International, 2010.

ASTM C566 (2013). *Standard Test Method for Total Evaporable Moisture Content of Aggregate by Drying*. West Conshohocken, PA, ASTM International, 2013.

ASTM C581-03 (2003). *Standard practice for determining chemical resistance of thermosetting resins used in glass-fiber-reinforced structures intended for liquid service*. West Conshohocken, PA, ASTM International, 2008, p. 5.

ASTM C881 (2010). *Standard Specification for Epoxy-Resin-Base Bonding Systems for Concrete*. West Conshohocken, PA, ASTM International, 2010.

ASTM C882-91 (1991). *Standard test method for bond strength of epoxy resin system used with concrete by slant shear*. West Conshohocken, PA, ASTM International, 1991.

ASTM D1141-98 (1998). *Standard practice for the preparation of substitute ocean water*. West Conshohocken, PA, ASTM International, 2008, p. 3.

ASTM D2247-02 (2002). *Standard practice for testing water resistance of coatings in 100% relative humidity*. West Conshohocken, PA, ASTM International, p. 5.

ASTM D3039 (2008). *Standard Test Method for Tensile Properties of Polymer Matrix Composite Materials*. West Conshohocken, PA, ASTM International, 2008.

ASTM D3039-08 (2008). *Standard test method for tensile properties of polymer matrix composite materials*. West Conshohocken, PA, ASTM International, p. 13.

ASTM D3045-92 (1992). *Standard practice for heat aging of plastics without load*, West Conshohocken, PA, ASTM International, p. 5.

ASTM D4065 (2012). *Standard Practice for Plastics: Dynamic Mechanical Properties: Determination and Report of Procedures*. West Conshohocken, PA, ASTM International, 2012.

ASTM D638 (2010). *Standard Test Method for Tensile Properties of Plastics*. West Conshohocken, PA, ASTM International, 2010.

ASTM D695 (2010). *Standard Test Method for Compressive Properties of Rigid Plastics*. West Conshohocken, PA, ASTM International, 2010.

ASTM D7522 (2009). *Standard Test Method for Pull-Off Strength for FRP Bonded to Concrete Substrate*. *ASTM International*, West Conshohocken, PA, 2009.

ASTM D7522-09 (2009). *Standard Test Method for Pull-Off Strength for FRP Bonded to Concrete Substrate*. West Conshohocken, PA, ASTM International, 2009.

ASTM D7565 (2010). *Standard Test Method for Determining Tensile Properties of Fiber-reinforced Polymer Matrix Composites Used for Strengthening of Civil Structures*. West Conshohocken, PA, ASTM International, 2010.

Atadero, R. A., Allen, D. G., Mata, O. R. (2013). *Long-term Monitoring of Mechanical Properties of FRP Repair Materials*. Colorado Department of Transportation Report No. CDOT-2013-13.

Au, C. (2005). *Moisture Degradation in FRP Bonded Concrete Systems: An Interface Fracture Approach*. Massachusetts Institute of Technology PhD Dissertation.

Au, C., and Buyukozturk, O. (2006). "Peel and Shear Fracture Characterization of Debonding in FRP Plated Concrete Affected by Moisture," *ASCE Journal of Composites for Construction*, 10(1), pp 35-47.

Au, C., and Buyukozturk, O. (2006). "Debonding of FRP-Plated Concrete: A Tri-layer Fracture Treatment". *Engineering Fracture Mechanics*, No. 73, pp. 348-365.

Bae, S., Belarbi, A. (2009). "Effects of Corrosion of Steel Reinforcement on RC Columns Wrapped with FRP Sheets". *Journal of Performance of Constructed Facilities*, pp. 20-31.

Banthia, N., Abdolrahimzadeh, A., Demers, M., Mufti, A., Sheikh, S. (2010). "Durability of FRP-Concrete Bond in FRP Strengthened Bridges". *Concrete International*, vol. 32, issue 08, pp. 45-51.

Beaudoin, Y., Labossiere, P., Neale, K. W. (1998). "Wet-dry Action on the Bond Between Composite Materials and Reinforced Concrete Beams". *Proceedings of The First International Conference on Durability of Fiber-reinforced Polymer (FRP) Composites for Construction (CDCC 98)*, Sherbrooke (Quebec), Canada, August 5-7, 1998, pp. 537-546.

Belarbi, A., Hsu, T. C. (1994). "Constitutive Laws of Concrete in Tension and Reinforcing Bars Stiffened by Concrete". *ACI Structural Journal*, 91 (4), pp. 465-474.

Benjeddou, O., Ouezdou, M. B., and Bedday, A. (2007). "Damaged RC Beams Repaired by Bonding of CFRP Laminates". *Construction and Building Materials*, Vol. 21, No. 6, pp 1301-1310.

Blackburn, B. P., Tatar, J., Douglas E. P., and Hamilton, H. R., (2015). "Effects of Hygrothermal Conditioning on Epoxy Adhesives Used in FRP Composites," *Construction & Building Materials*, Vol. 96, pp. 679-689.

Blackburn, B. P. (2013). "Effects of Hydrothermal Conditioning on Epoxy Used in FRP Composites". *University of Florida Master's Thesis*.

Barnes, R. W. and Carmichael, B. M. (2005). *Repair of The Uphapee Creek Bridge With FRP* Alabama Dept. of Trans. Research Report RP-930-466-2, 111 pp.

Chajes, M. J., Thomson, T. A. Jr, Farschman, C. A. (1995). "Durability of Concrete Beams Externally Reinforced With Composite Fabric". *Construction and Building Materials*, Vol. 9, No. 3, pp. 141-148.

Cheok, G. S., Phan, L. T. (1998). "Post-Installed Anchors – A Literature Review", *National Institute of Standards and Technology*, NISTIR 6096.

Cheshire, R. W. (2001). "Florida Department of Transportation Bridge Management System Accident Inspection Report". FDOT Report INSP002.

Collins, M. P., and Mitchell, D. (1991). "Prestressed Concrete Structures", Prentice-Hall, Englewood Cliffs, N. J., pp. 766.

Colombi, P., Fava, G., Poggi, C. (2010). "Bond Strength of CFRP-Concrete Elements Under Freeze-Thaw Cycles". *Composite Structures 2010*, 92, pp. 973-983.

Conner,S., Huo, X. S. (2006). "Influence of Parapets and Aspect Ratio on Live-Load Distribution". *ASCE Journal of Bridge Engineering*, 11 (2), pp. 188-196.

Consolazio, G.R., Fung, J., Ansley, M. (2004). "M-f-P Diagrams for Concrete Sections Under Biaxial Flexure and Axial Compression", *ACI Structural Journal*, Vol. 101, No. 1, pp. 114-123.

Cromwell, J. R., Harries, K. A., Shahrooz, B. M. (2011). "Environmental Durability of Externally Bonded FRP Materials Intended for Repair of Concrete Structures". *Construction and Building Materials*, 25, pp. 2528-2539.

Dai, J., Yokota, H., Iwanami, M., and Kato, E. (2010). "Experimental Investigation of the Influence of Moisture on the Bond Behavior of FRP to Concrete Interfaces". *Journal of Composites in Construction*, 14(6), pp. 834–844

Davalos, J. F., Chen, A., Ray, I., Levan, J. R., (2012). "Comprehensive Study on Using Externally Bonded FRP Composites for the Rehabilitation of Reinforced Concrete T-Beam Bridges," *Journal of Infrastructure Systems*, 18(2), p 89-102.

David, E., Neuner, J. D. (2001). "Environmental Durability Studies for FRP Systems: Definition of Normal Conditions of Use of FRP for Structural Strengthening Applications". *Proceedings of the International Conference on Composites in Civil Engineering*, vol. 2, pp 1551-1558.

Dolan, C.W., Tanner, J., Mukai, D., Hamilton, H. R., Douglas, E. (2010). "Design Guidelines for Durability of Bonded CFRP Repair/Strengthening of Concrete Beams". *NCHRP Web-Only Document 155,* National Cooperative Highway Research Program, Transportation Research Board of the National Academies, Washington, DC.

Douglas, E.P., Hamilton, H.R., Nino, J., Stewart, A., Tatar, J. (2013). "Highly Accelerated Lifetime for Externally Applied Bond Critical Fiber-reinforced Polymer (FRP) Infrastructure Materials". FDOT Report BDK75-977-45.

Eamon, C.D., Nowak, A. S. (2002). "Effects of Edge-Stiffening Elements and Diaphragms on Bridge Resistance and Load Distribution". *ASCE Journal of Bridge Engineering*, 7 (5), pp. 258-266.

Hag-Elsafi, O., Kunin, J., Alampalli, S., and Conway, T. (2001). *Strengthening of Route 378 Bridge Over Wynantskill Creek in New York Using FRP Laminates,* New York Dept. of Trans. Special Report 135, 57 pp.

Hag-Elsafi, O., Lund, R., and Alampalli, S. (2002). *Strengthening of Church Street Bridge Pier Capbeam Using Bonded FRP Composite Plates: Strengthening and Load Testing,* New York Dept. of Trans. Special Report 138, 57 pp.

Eveslage, T., Aidoo, J., Harries, K.A., and Bro, W. (2010). "Towards a Standard Test Method for Assessing FRP-to-concrete Bond Characteristics". *Proceedings of the 5th International Conference on FRP Composites in Civil Engineering* (CICE 2010) Beijing, September 2010.

Fallaha, S., Rambo-Roddenberry, M. (2013). "Spring 2013 Research Showcase". FDOT Research Center, Tallahassee, pp. 1-16.

Fava, G., Mazzotti, C., Poggi, C., Savioia, M. (2007). "Durability of FRP-Concrete Bonding Exposed to Aggressive Environment". *Proceedings of 8th International Symposium on Fiber-reinforced Polymer Reinforcement for Concrete Structures – FRPRCS-8*, University of Patras, Patras, Greece, July 16-18, 2007.

Frigione, M., Aiello, M. A., Naddeo, C. (2006). "Water Effects of the Bond Strength of Concrete/Concrete Adhesive Joints". *Construction and Building Materials*, No, 20, pp. 957-970.

Gadve, S, Mukherjee, A., Malhotra, S.N. (2009). "Corrosion of steel reinforcements embedded in FRP wrapped concrete". *Construction and Building Materials*, 23, pp. 153-161.

Garmage, J. C. P. H., Al-Mahaidi, R., Wong, M. B. (2009). "Durability of CFRP-strengthened Concrete Members Under Extreme Temperature and Humidity". *Australian Journal of Structural Engineering*, Vol. 9, no. 2 (2009), pp. 111-118.

Gartner, A. L. (2007). *Development of a Flexural Bond Strength Test to Determine Environmental Degradation of Carbon Fiber-Reinforced Polymer (CFRP) Composites Bonded to Concrete*. M. Eng. Thesis, University of Florida.

Gartner, A. L., Douglas, E. P., Dolan, C. W., Hamilton, H. R. (2009). "Small Beam Bond Test Method for CFRP Composites Applied to Concrete". *J. Compos. Constr., 15(1)*, pp. 52-61.

Grace, N. F., Singh, S. B. (2005). "Durability Evaluation of Carbon Fiber-Reinforced Polymer Strengthened Concrete Beams: Experimental Study and Design". *ACI Structural Journal*, vo. 102, no. 1, January-February 2005, pp 40-53.

Green, M. F., Bisby, L. A., Fam, A. Z., Kodur, V. K. R. (2006). "FRP confined concrete columns: Behaviour under extreme conditions". *Cement & Concrete Composites*, 28, 2006, pp. 928-937.

Green, P. S., Boyd, A. J., Lammert, K. (2004). *CFRP Repair of Impact-Damaged Bridge Girders Volume I – Structural Evaluation of Impact Damaged Prestressed Concrete I Girders Repaired With FRP Materials*, FDOT Report 4910-45-04-922.

Hadve, S., Mukherjee, A., Malhotra, S. N. (2009). "Corrosion of steel reinforcement embedded in FRP wrapped concrete". *Construction and Building Materials*, 23, 2009, pp. 153-161.

Hahn, G. J., Meeker, W. Q. (1991). "Statistical Intervals: A Guide for Practitioners", *John Wiley & Sons, Inc.*

Halstead, J. P., O'Connor, J. S., Luu, K., Alampalli, S, Minser, A. (2000). "Fiber-Reinforced Polymer Wrapping of Deteriorated Concrete Columns". *Transportation Research Record*, 1696, Paper No. 5B0001, 2000.

Harries, K. A., Hamilton, H. R., Kasan, J., Tatar, J. (2012). "Development of Standard Bond Capacity Test for FRP Bonded to Concrete". *Proceedings of 6th International Conference on FRP Composites in Civil Engineering (CICE 2012)*, Rome, Italy, 13-15 June 2012.

Harries, K.A., Reeve, B. and Zorn, A. (2007). "Experimental Evaluation of Factors Affecting the Monotonic and Fatigue Behavior of FRP-to-Concrete Bond". *ACI Structural Journal,* Vol. 104, No. 6, pp 667-674.

Higgins, C., Dawson, M. R., Mitchell, M. M., Sopal, G., Senturk, A. E. (2009). *Environmental Durability of Reinforced Concrete Deck Girders Strengthened for Shear with Surface-Bonded Carbon Fiber-Reinforced Polymer*, Oregon Dept. of Trans. Research Report FHWA-OR-RD-09-17, pp. 208.

Hindo, K. R. and Bergstrom, W. R. (1985). "Statistical Evaluation of the In-Place Compressive Strength of Concrete". *Concrete International*, 7 (2), pp. 44-48.

Immergut, E. H., Mark, H. F. (1965). "Principles of Plasticization". *Plasticization and Plasticizer Processes, Advances in Chemistry*, vol. 48, pp. 1-26.

ISO 22768 (2006). "Rubber, raw – Determination of the glass transition temperature by differential scanning calorimetry (DSC)". *International Organization for Standardization*, 2006

Jiangang, D. (2008). *Durability of Carbon Fiber-reinforced Polymer (CFRP) Repair/Strengthening Concrete Beams*. *PhD Dissertation*, University of Wyoming, August, 2008.

Kachlakev, D. and McCurry, D. D. (2000). "Behavior of full-scale reinforced concrete beams retrofitted for shear and flexural with FRP laminates," *Composites Part B: Engineering*, 31(6-7), pp. 445-452.

Karbhari, V.M. and Engineer, M. (1996). "Effect of Environmental Exposure on the External Strengthening of Concrete with Composites – Short Term Bond Durability". *Journal of Reinforced Plastics and Composites*, Vol. 15, pp. 194-1215.

Karbhari, V.M., Engineer, M., Eckell, D. A. (1997). "On the Durability of Composite Rehabilitation Schemes for Concrete: Use of a Peel Test". *Journal of Materials Science*, No. 32, pp. 147-156.

Klamer, E. L., Hordijk, D. A., Janssen, H. J. M. (2005). "The Influence of Temperature on the Debonding of Externally Bonded CFRP". *ACI Special Publications*, vol. 230, October 1, 2005, pp 1551-1570.

Kharkovsky, S., Stephen, V., Ryley, A. C., Robbins, J.T., Zoughi, R. (2008) *Preservation of Missouri Transportation Infrastructures: Life-Cycle Inspection and Monitoring of FRP-Strengthened Concrete Structures using Near-Field Microwave Nondestructive Testing Methods*. MoDOT Report OR09-008.

Labossière, P., Neale, K.W., Rochette, P., Demers, M., Lamothe, P., Lapierre, P., Desgagné, G. (2000). "Fibre reinforced polymer strengthening of the Sainte-Emelie-de-l'Energie bridge: Design, instrumentation, and field testing," *Canadian Journal of Civil Engineering*, 27(5), p 916-927.

Lai, W. L., Kou, S. C., Poon, C. S., Tsang, W. F., Lee, K. K. (2013). "A Durability Study of Externally Bonded FRP-Concrete Beams via Full-Field Infrared Thermography (IRT) and Quasi-Static Shear Test". *Construction and Building Materials*, 40, pp. 481-491.

Lai, W. L., Kou, S. C., Poon, C. S., Tsang, W. F., Lai, C. C. (2009). "Effects of elevated water temperatures on interfacial delaminations, failure modes and shear strength in externally-bonded CFRP-concrete beams using infrared thermography, gray-scale images and direct shear test". *Construction and Building Materials*, 23(10), pp. 3152–3160.

Leone, M., Matthys, S., and Aiello, M. A. (2009). "Effect of elevated service temperature on bond between FRP EBR systems and concrete" *Composites Part B: Engineering*, 40(1), 85–93.

Leung, H. Y., Balendran, R. V., Lim, C. W. (2001). "Flexural Capacity of Strenghtened Concrete Beam exposed to Different Environmental Conditions". *Proceedings of the International Conference on Composites in Civil Engineering*, vol. 2, pp 1597-1606.

Lian, C., Zhuge, Y., Beecham, S. (2011). "The relationship between porosity and strength for porous concrete". *Construction and Building Materials*, Vol. 25, issue 11, pp. 4294-4298.

Lundqvist, J., Nordin, H., Taljsten, B. and Olofsson, T. (2005). "Numerical Analysis of Concrete Beams Strengthened with CFRP – A Study of Anchorage Lengths". *Proceedings of the International Symposium on Bond Behaviour of FRP in Structures*, December 7-9, 2005, Hong Kong. pp 239-246.

Maaddawy, T. E., Chahrour, A., Soudki, K. (2006). "Effects of Fiber-Reinforced Polymer Wraps on Corrosion Activity and Concrete Cracking in Chloride-Contaminated Concrete Cylinders". *Journal of Composites for Construction*, 10, 2006, pp. 139-147.

Maerz, N. H., Galecki, G. (2008) *Preservation of Missouri Transportation Infrastructures: Non-Destructive Testing of FRP Materials and Installation, Gold Bridge*. MoDOT Report OR09-009.

Masoud, S. and Soudki, K. (2006). "Evaluation of Corrosion Activity in FRP repaired RC beams". *Cement & Concrete Composites*, 28, 2006, pp. 969-977.

Myers, J. J., Ekenel, M. (2005). "Effects of Environmental Conditions on Bond Strength between CFRP Laminate and Concrete Substrate". *ACI Special Publications*, vol. 230, pp 1571-1592.

Myers, J. J., Holdener, D., Merkle, W., Hernandez, E. (2008) *Preservation of Missouri Transportation Infrastructures: Validation of FRP Composite: Volume I – In situ load testing of Bridges P-962, T-530, X-495, X-596 and Y-298*. MoDOT Report OR09-007.

Myers, J. J., Sawant, A. V. (2008) *Preservation of Missouri Transportation Infrastructures: Life Expectancy Modeling for FRP Strengthened Concrete Bridges*. MoDOT Report OR09-011.

NCHRP (2010). *Recommended Guide Specification for the Design of Externally Bonded FRP Systems for Repair and Strengthening of Concrete Bridge Elements*. National Cooperative Highway Research Program, Report 655, Transportation Research Board, Washington, DC.

NCHRP Report 655 (2010). *Recommended Guide Specification for the Design of Externally Bonded FRP Systems for Repair and Strengthening of Concrete Bridge Elements*. National Cooperative Highway Research Program, Transportation Research Board.

Nossoni, G., Harichandran, R. S. (2010). "Improved Repair of Concrete Structures Using Polymer Concrete Patch and FRP Overlay". *Journal of Materials in Civil Engineering*, 22, 2010, pp. 314-322.

Pan, J., Huang, Y., Xing, F. (2010). "Effect of Chloride Content on Bond Behavior Between FRP and Concrete". *Transactions of Tianjin University (2010)*, No. 116, pp. 405-410.

Pantelides, C. P., Gibbons, M. E. and Reaveley, L. D. (2011). *Non-Destructive and Destructive Investigation of Aged-in-the Field Carbon FRP-Wrapped Columns*, Utah Dept. of Transportation Report, Report No. UT-11.16, 105 pp.

Pantazopoulou, S. J., Bonacci, J. F., Sheikh, S., Thomas, M. D. A., Hearn, N. (2001). "Repair of Corrosion-Damaged Columns with FRP Wraps". *Journal of Composites for Construction*, 5(1), 2001, pp. 3-11.

Pessiki, S., Harries, K. A., Kestner, J. T., Sause, R., Ricles, J. M. (2001). "Axial Behavior of Reinforced Concrete Columns Confined with FRP Jackets". *ASCE Journal of Composites for Construction*, 5(4), pp. 237-245.

Powers, T.C. (1949). "The air requirement of frost-resistant concrete". *Proc. Highway Res. Board 29*, pp. 184-202.

Reay, J. T. and Pantelides, C. P., (2006). "Long-Term Durability of State Street Bridge on Interstate 80," *Journal of Bridge Engineering*, 11(2), pp. 205-216.

Riggs, H.R., Park, S.H., Robertson, I.N., and Fischer G., (2004). "Use of Advanced Composites for Hawaii Bridges," Hawaii Dept. of Trans. Report HWY-L-2001-01, 39 pp.

RILEM CPC-18 (1994). "Measurement of hardened concrete carbonation depth". RILEM Recommendations for the Testing and Use of Constructions Materials, pp. 56-58.

Saadatmanesh, H., Ehsani, M. R. (1990). "Fiber Composite Plates Can Strengthen Beams". *Concrete International*, March 1990, pp 65-71.

Sebastian, W. M. (2001). "Significance of Midspan Debonding Failure in FRP-Plated Concrete Beams". *Journal of Structural Engineering*, 127(7), pp. 792-798.

Sen, R., Shahawy, M., Mullins, G., Spain, J. (1999). "Durability of Carbon Fiber-Reinforced Polymer/Epoxy/Concrete Bond in Marine Environment". *ACI Structural Journal*, vol. 96, pp. 906-914.

Shahrooz, B. M. and Boy, S. (2004). "Retrofit of a three-span slab bridge with fiber reinforced polymer systems-testing and rating," *Journal of Composites for Construction*, 8(3), p 241-247.

Shrestha, J., Ueda, T., Zhang, D., Kitami, A., Komori, A. (2013). "Investigation of Moisture Behavior of High Strength Concrete and FRP Bond by Accelerated Durability Test". *Proceedings of 11th International Symposium on Fiber-reinforced Polymer Reinforcement for Concrete Structures*, FRPRCS-11, University of Minho, Guimaraes, Portugal, June 26-28, 2013.

Silva, M. A. G., Biscaia, H. (2008). "Degradation of bond between FRP and RC beams". *Composite Structures*, 25, pp. 164-174.

Silverman, B. W. (1986). "Density estimation for statistics and data analysis". *Chapman & Hall, London, UK*.

Sim, J., Oh, H., Meyer, C. (2006). "Structural assessment of externally strengthened bridge deck panels," *Applied Composite Materials*, v 13, n 2, p 99-114.

Smith, S. T., Teng, J. G. (2002). "FRP-strengthened RC beams. I: review of debonding strength models". *Engineering Structures 2002*, 24(4), pp. 385-395.

Soudki, K. El-Salakawy, E., Craig, B. (2007). "Behavior of CFRP Strengthened Reinforced Beams in Corrosive Environment". *Journal of Composites for Construction*, vol. 11, no. 3, pp. 291-298.

Spainhour, L. K., Wootton, I. A. (2008). "Corrosion process and abatement in reinforced concrete rapped by fiber-reinforced polymer". *Cement & Concrete Composites*, 30, 2008, pp. 535-543.

Stallings, J. M., Tedesco, J. W., El-Mihilmy, M., McCauley, M. W. (2000) "Field performance of FRP bridge repairs," *Journal of Bridge Engineering*, 5(2), pp. 107-113.

Standard test method for scaling resistance of concrete surfaces exposed to deicing chemicals. *Annual Book of ASTM Standards*, Designation C672-84, ASTM, Philadelphia, PA, 1990, Vol. 04.02.

Stephens, M. A. (1974). "EDF Statistics for Goodness of Fit and Some Comparisons". *Journal of American Statistical Association*, no. 69, pp. 730-737.

Stewart, A. (2012). *Study of Cement-Epoxy Interfaces, Accelerated Testing, and Surface Modification*. Ph.D. Dissertation, University of Florida.

Stockdale, G., Riggs, H. R., and Robertson, I. N., (2012) *Generalized Processing of FBG/FRP Strain Data for Structural Health Monitoring*, Research Report UHM/CEE/12-01.

Taljsten, B. (1996). "Strengthening of Concrete Prisms Using the Plate-Bonding Technique". *International Journal of Fracture*, Vol. 82, 1996, pp. 253-266.

Tatar, J. and Hamilton, H. R., (2016) "Implementation of Bond Durability in the Design of Flexural Members with Externally Bonded FRP," J. Compos. Constr, Volume 20, Issue 3, 10 pp.

Thomson Reuters, Web of Knowledge, http://apps.worldofknowledge.com (accessed 10/17/2013).

Toutanji, H. A., Gomez, W. (1997). "Durability Characteristics of Concrete Beams Externally Bonded with FRP Composite Sheets". *Cement and Concrete Composites*, No. 19, pp 351-358.

Tuakta, C., Buyukozturk O. (2010). "Deterioration of FRP/concrete bond system under variable moisture conditions quantified by fracture mechanics". *Composites Part B: Engineering* 42 (2): 145-154.

Watkins, S. E. (2008) "Preservation of Missouri Transportation Infrastructures: Strain Determination by Fiber Optics". MoDOT Report OR09-010.

Wan, B., Petrou, M. F., Harries, K. A. (2006). "The Effect of Presence of Water on the Durability of Bond between CFRP and Concrete". *Journal of Reinforced Plastics and Composites*, May 2006 25, pp. 875-890

Wan, B., Sutton, M., Petrou, M.F., Harries, K.A., Li, N. "Investigation of Bond between FRP and Concrete Undergoing Global Mixed Mode I/II Loading", *ASCE Journal of Engineering Mechanics,* Vol. 130 No. 12, Dec. 2004, pp 1467-1475.

Wu, L., Hoa, S. V., Ton-That, M. (2004). "Effects of Water on the Curing and Properties of Epoxy Adhesive Used for Bonding FRP Composite Sheet to Concrete". *Journal of Applied Polymer Science*, 92, 2004, pp. 2261-2268.

Wu, Z., Yuan, H., Yoshizawa, H., Kanakubo, T. (2001). "Experimental/Analytical Study on Interfacial Fracture Energy and Fracture Propagation Along FRP-Concrete Interface". *ACI international*, SP-201-8, pp. 133–152.

Xie, M., Hoa, S. V., Xiao, X. R. (1995). "Bonding Steel Reinforced Concrete with Composites". *Journal of Reinforced Plastics and Composites*, September 1995, Vol. 14, pp. 949-964.

Yang, X., Nanni, A., Haug, S., Sun, C. L. (2002). "Strength and Modulus Degradation of Carbon Fiber-Reinforced Polymer Laminates from Fiber Misalignment". *ASCE Journal of Materials in Civil Engineering*, 14(4), pp. 320-326.

Appendix A—Test Specimens for Marine Environment
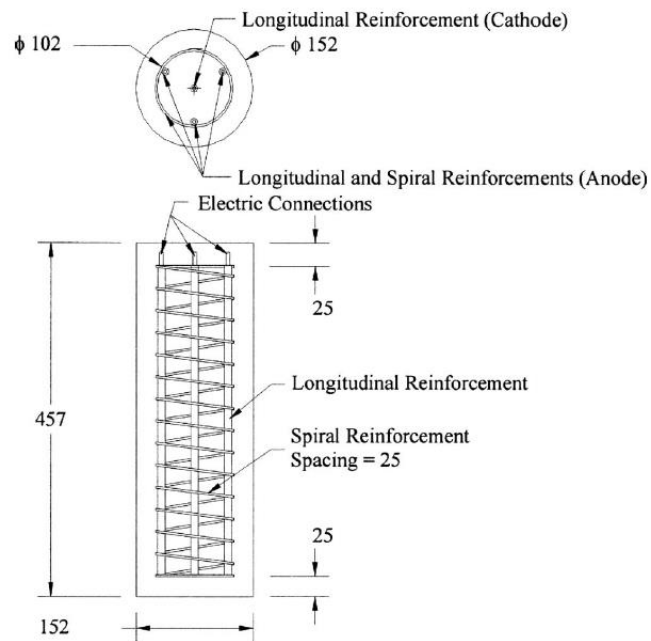
Figure 264—Small-scale columns (Bae and Belarbi, 2009): Specimen details of small-scale RC columns (dimensions in mm)

Figure 265—Small-scale columns (Bae and Belarbi, 2009): reinforcement cage used for small-scale RC columns (left) and small scale RC columns after CFRP sheet wrapping
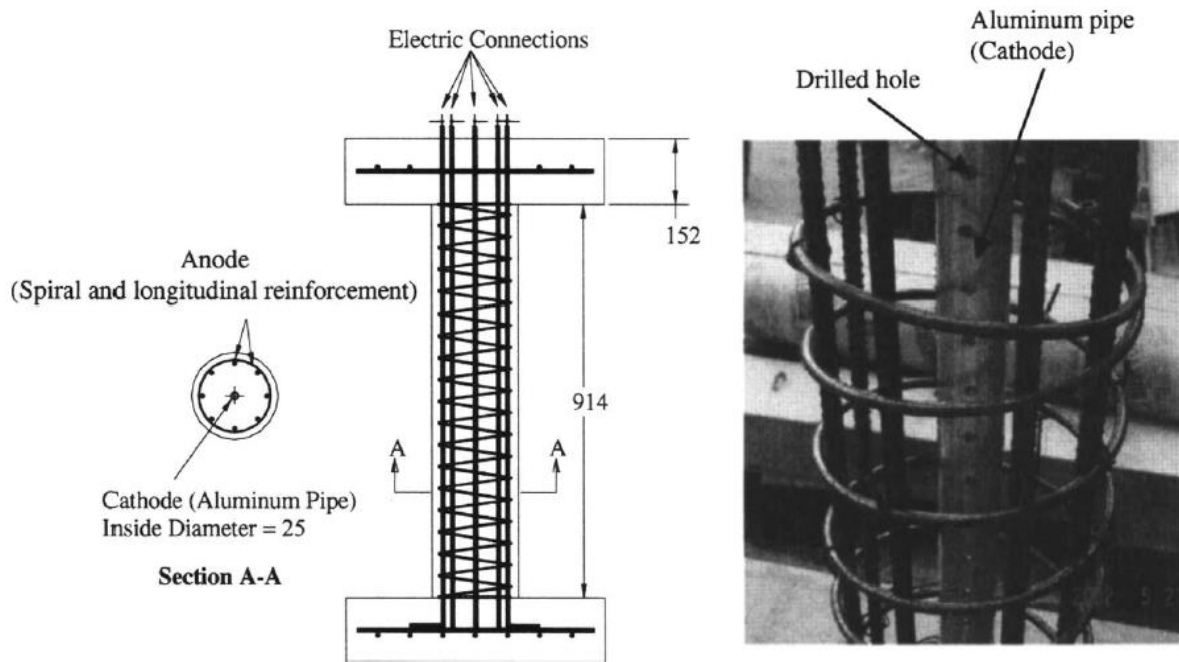
Figure 266—Bae and Belarbi (2009): Midscale RC columns
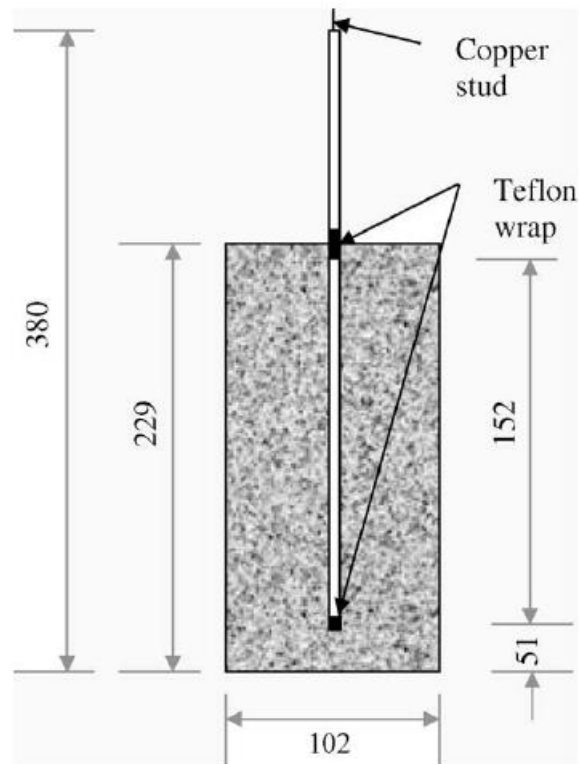
Figure 267—Gadve et al. (2009): Cylindrical reinforced concrete specimen
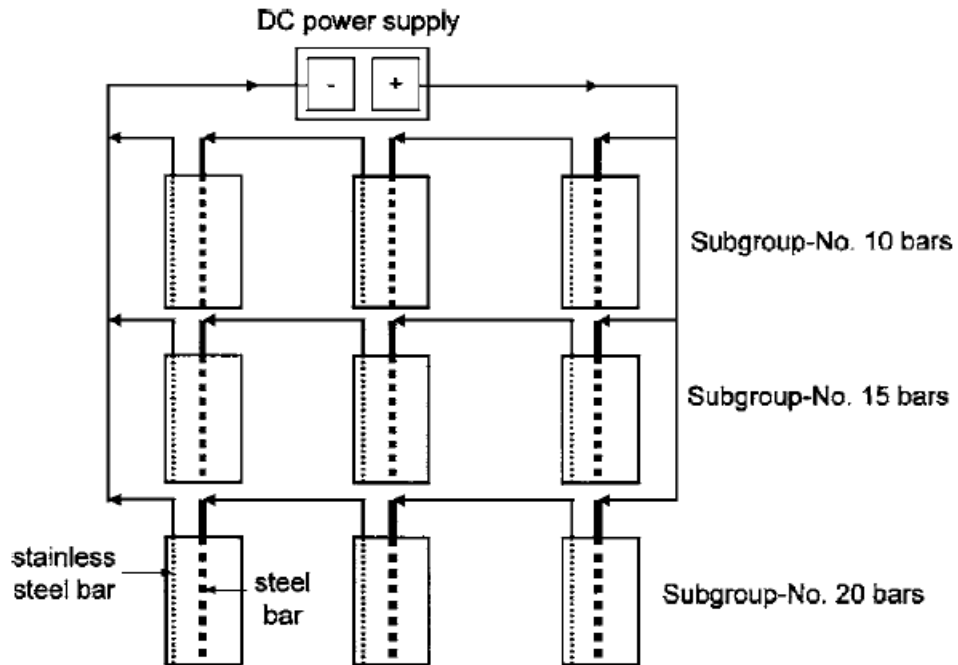
Figure 268—Maaddawy et al. (2006): typical electrical circuit for group of specimens
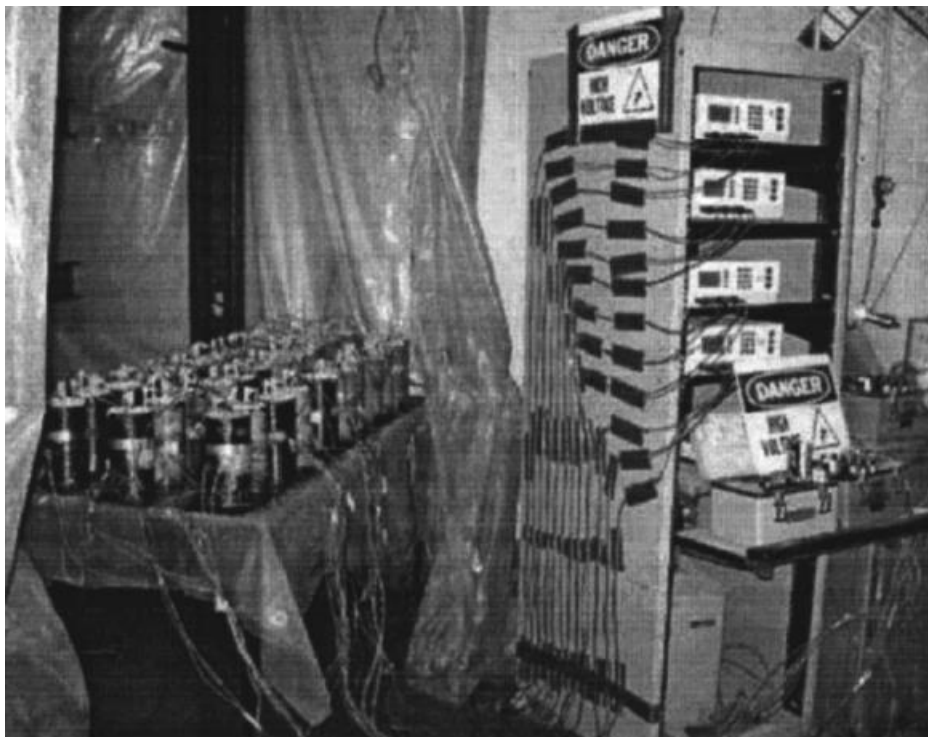
Figure 269—Maaddawy et al. (2006): view of specimens and power supply
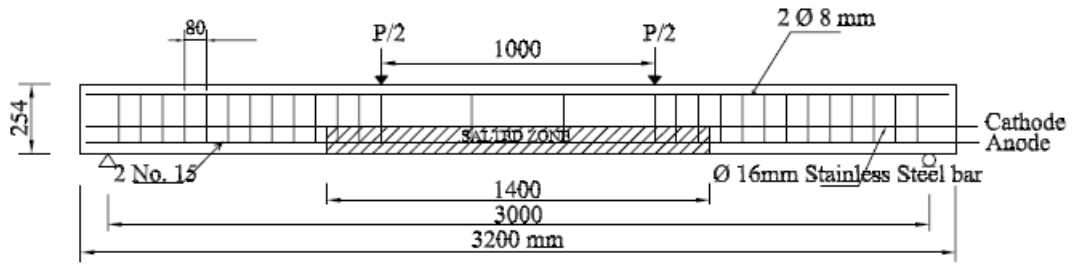
Figure 270—Masoud and Soudki (2006): Typical dimension and reinforcement details of the test specimen
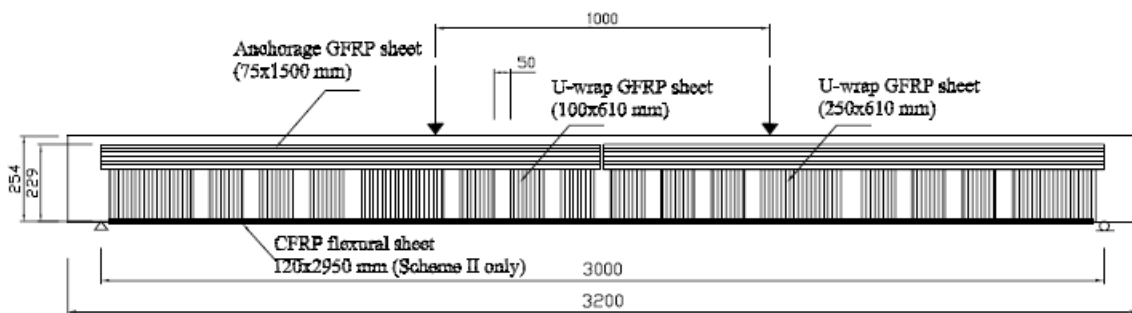
Figure 271—Masoud and Suodki (2006): A schematic for FRP repair schemes I and II
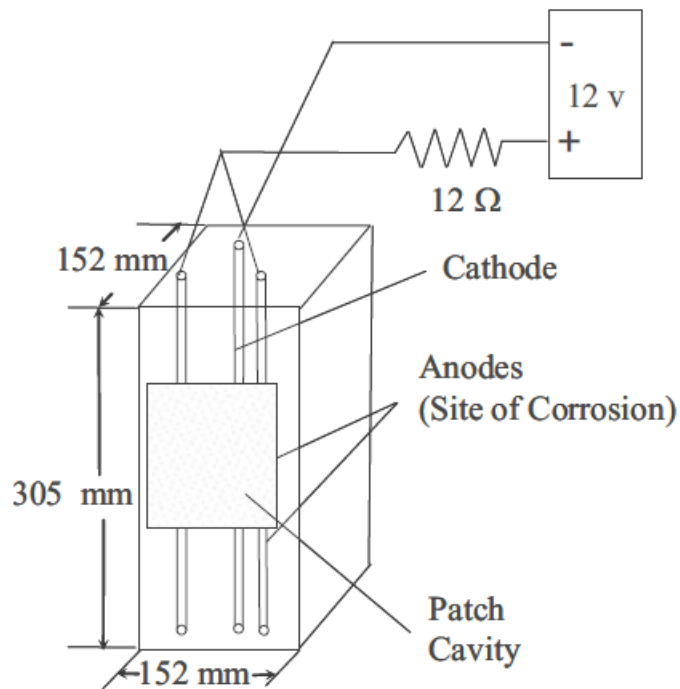
Figure 272—Nossoni and Harichandran (2010): Specimen design
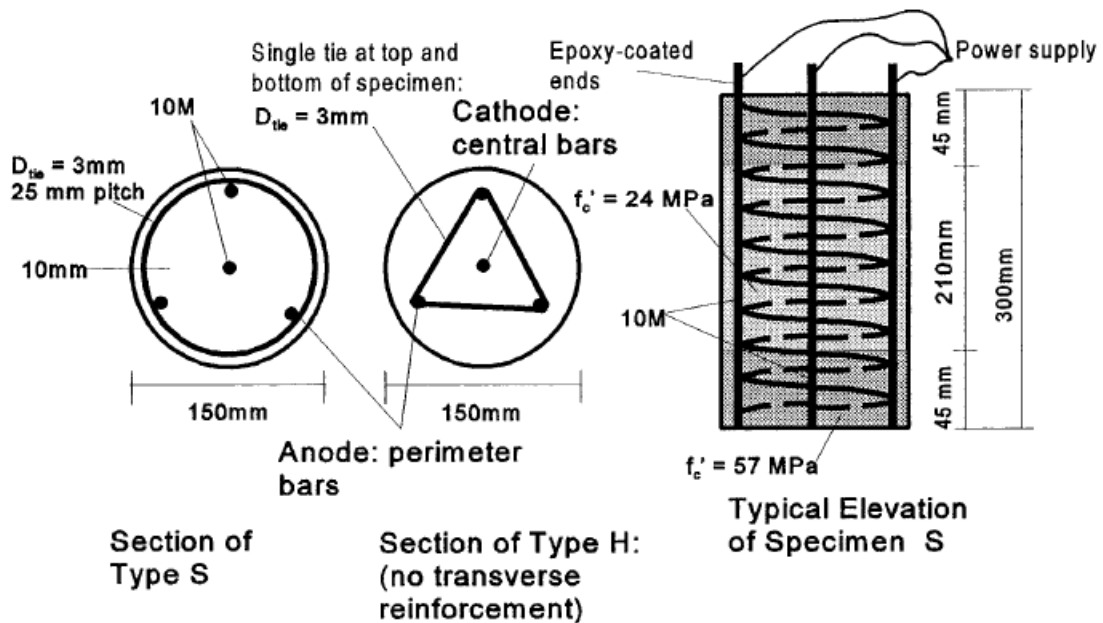
Figure 273—Pantazopoulou et al. (2001): typical specimen geometry
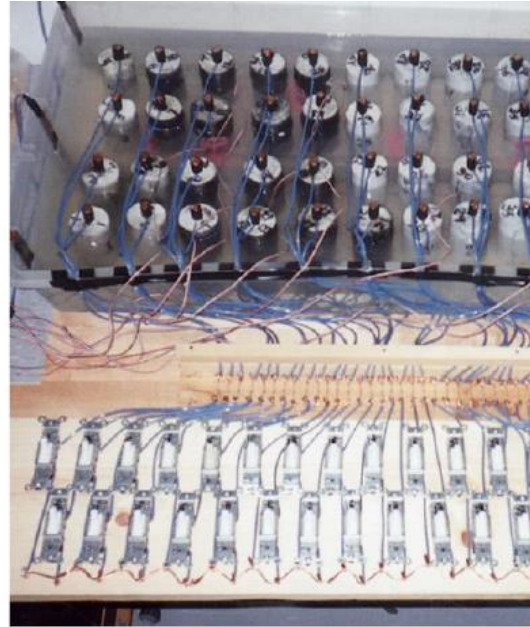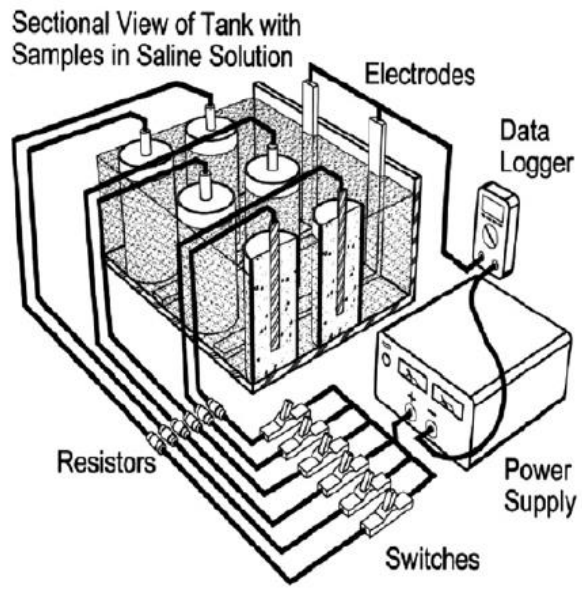
Figure 274—Spainhour and Wootton (2008): Test configuration

Appendix B—Grenada Bridge

Figure 275—Grenada Bridge plan and elevation drawings

Pier	Pier figure	Core Locations
7	 (a)	Taken on 11-03-2014 C7-1: West face of Pier 7 (middle foundation) – above the high tide water line C7-2: West face of Pier 7 (middle foundation) – below the high tide water line
8	 (b)	Taken on 11-03-2014 CN1: North side of Pier 8 – West face – above the high tide (HT) water line CN2: North side of Pier 8 – West face – below the high tide (HT) water line CS1: South side of Pier 8 – West face – above the high tide (HT) water line CS2: South side of Pier 8 – West face – below the high tide (HT) water line CD1: east face – debonded region – above the high tide (HT) water line CD2: east face – debonded region – below the high tide (HT) water line

| 9 | Pier 9 West Face

(c) | Taken on 11-03-2014
C9-1: West face of Pier 9 – above the high tide water line
C9-2: West face of Pier 9 – below the high tide water line |
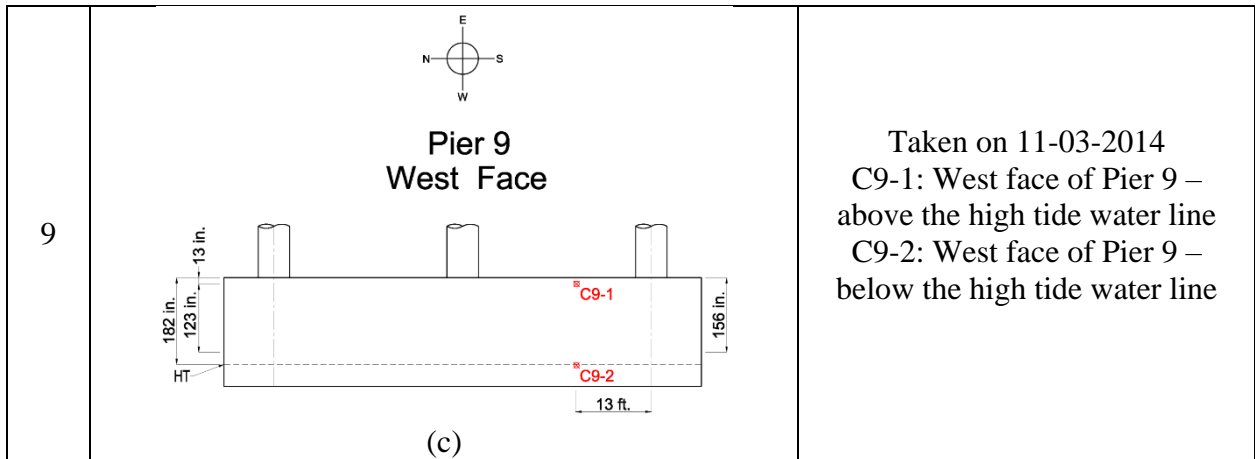
Figure 276—Grenada Bridge coring locations: (a) Pier 7 (b) Pier 8 (c) Pier 9
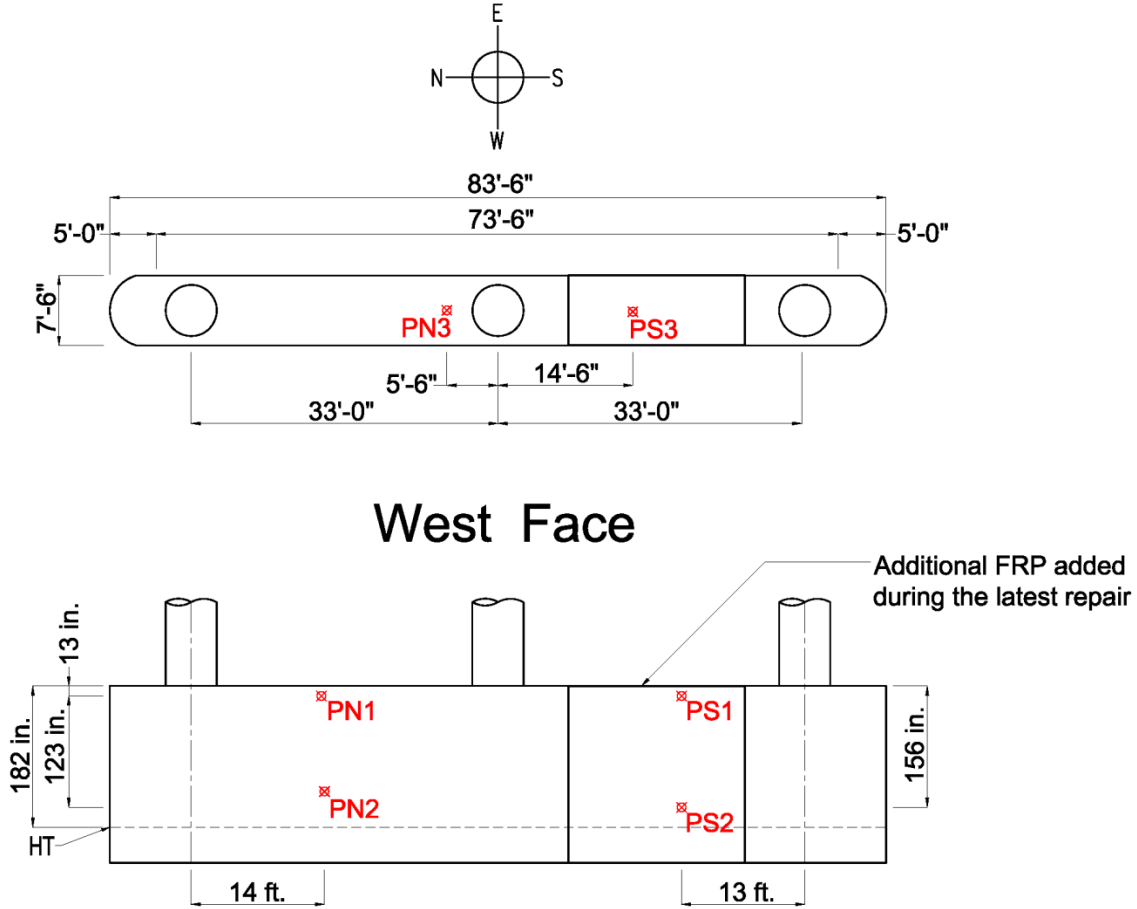
Figure 277—Pull-off test locations on Pier 8

A total of six pull-off tests were performed on Pier 8 crash wall, as per ASTM D7522. Test disks were installed on Monday, November 3rd 2014; the testing was performed on Tuesday, November 4th 2014. Tests were executed at the following locations:

1. **PN1**: North side of Pier 8 – West face – above the high tide water line
2. **PN2**: North side of Pier 8 – West face – below the high tide water line
3. **PS1**: South side of Pier 8 – West face – above the high tide water line
4. **PS2**: South side of Pier 8 – West face – below the high tide water line
5. **PN3**: North side of Pier 8 – Top face
6. **PS3**: South side of Pier 8 – Top face

B.3 Chloride Penetration Profile Test Results

Table 52—Cl⁻ content test results for Granada Bridge; sample CN1

Date Tested: January 6, 2014

Test Performed By: Jason Burchfield

Unit Weight: 3800 lb/yd³   LIMS #: _____   Lab #: 2014-12-011

Description			Results (lb/yd³)				Average	
			A	B	C	Range	ppm	lb/yd³
Standard Solution	**Date:** 1/6/2014	**Expected Value:** 3.0					3.0	
Sample: CN1, District 5, Volusia County, SR 40 over Halifax River,								
Grenada Bridge # 790132. 2" Core taken from the North side of Pier 8,								
West Face, Above the High Tide water line; Length: ~3.5".								
A 0-0.5"			0.790	0.802	0.806	0.0160	210.4	0.799
B 0.5-1.0"			0.623	0.608	0.619	0.0150	162.3	0.617
C 1.0-1.5"			0.650	0.638	0.646	0.0120	169.6	0.645
D 1.5-2.0"			0.627	0.642	0.631	0.0150	166.7	0.633
E 2.0-2.5"			0.635	0.623	0.616	0.0190	164.4	0.625
F 2.5-3.0"			0.536	0.536	0.532	0.0040	140.7	0.535
G 3.0-3.5"			0.547	0.540	0.616	0.0760	149.4	0.568

Table 53—Cl⁻ content test results for Granada Bridge; sample CN2

Date Tested: December 30, 2014

Test Performed By: Jason Burchfield

Unit Weight: 3800 lb/yd³   LIMS #: _____   Lab #: 2014-12-012

Description			Results (lb/yd³)				Average	
			A	B	C	Range	ppm	lb/yd³
Standard Solution	**Date:** 12/30/2014	**Expected Value:** 3.0					3.0	
Sample: CN2, District 5, Volusia County, SR 40 over Halifax River,								
Grenada Bridge # 790132. 2" Core taken from the North side of Pier 8,								
West Face, Below the High Tide water line; Length: ~2.5".								
A 0-0.5"			13.593	13.490	13.748	0.2580	3581.7	13.610
B 0.5-1.0"			13.809	14.022	13.908	0.2130	3661.3	13.913
C 1.0-1.5"			15.310	15.781	15.610	0.4710	4096.6	15.567
D 1.5-2.0"			13.357	13.178	13.224	0.1790	3487.6	13.253
E 2.0-2.5"			10.503	10.416	10.530	0.1140	2758.7	10.483

Table 54—Cl⁻ content test results for Granada Bridge; sample CS1

Date Tested: January 14, 2014

Test Performed By: Jason Burchfield

Unit Weight: 3800 lb/yd^3 LIMS #: _____   Lab #: 2014-12-013

Description			Results (lb/yd^3)				Average	
			A	**B**	**C**	**Range**	**ppm**	**lb/yd^3**
Standard Solution	**Date:** 1/14/2014	**Expected Value:** 3.0					3.0	
Sample: CS1, District 5, Volusia County, SR 40 over Halifax River,								
Grenada Bridge # 790132. 2" Core taken from the South side of Pier 8,								
West Face, Above the High Tide water line; Length: ~5.0". Core to be								
Sliced in 1/2" increments the entire length of core								
A 0-0.5"			0.631	0.623	0.635	0.0120	165.7	0.630
B 0.5-1.0"			0.699	0.692	0.695	0.0070	183.0	0.695
C 1.0-1.5"			0.699	0.692	0.707	0.0150	184.0	0.699
D 1.5-2.0"			0.551	0.547	0.547	0.0040	144.3	0.548
E 2.0-2.5"			0.490	0.494	0.505	0.0150	130.6	0.496
F 2.5-3.0"			0.445	0.445	0.448	0.0030	117.4	0.446
G 3.0-3.5"			0.410	0.410	0.426	0.0160	109.3	0.415
H 3.5-4.0"			0.353	0.365	0.353	0.0120	93.9	0.357
I 4.0-4.5"			0.391	0.399	0.399	0.0080	104.3	0.396
J 4.5-5.0"			0.353	0.357	0.357	0.0040	93.6	0.356

Table 55—Cl⁻ content test results for Granada Bridge; sample CS2

Date Tested: December 25, 2014
Test Performed By: Jason Burchfield

Unit Weight: 3800 lb/yd³   LIMS #:   Lab #: 2014-12-014

Description		Results (lb/yd³)				Average	
		A	**B**	**C**	**Range**	**ppm**	**lb/yd³**
Standard Solution | **Date:** 12/25/2014 | **Expected Value:** 3.0						3.0	
Sample: CS2, District 5, Volusia County, SR 40 over Halifax River,							
Grenada Bridge # 790132. 2" Core taken from the South side of Pier 8,							
West Face, Above the High Tide water line; Length: ~4.5". Core to be							
Sliced in 1/2" increments the entire length of core.							
A 0-0.5"		5.924	5.578	5.829	0.3460	1520.3	5.777
B 0.5-1.0"		5.928	5.951	5.966	0.0380	1565.4	5.948
C 1.0-1.5"		4.579	4.465	4.495	0.1140	1187.6	4.513
D 1.5-2.0"		4.853	4.948	4.777	0.1710	1278.8	4.859
E 2.0-2.5"		4.492	4.617	4.674	0.1820	1209.0	4.594
F 2.5-3.0"		4.803	4.765	4.853	0.0880	1265.0	4.807
G 3.0-3.5"		4.917	4.982	4.883	0.0990	1296.7	4.927
H 3.5-4.0"		4.400	4.328	4.431	0.1030	1154.3	4.386
I 4.0-4.5"		4.256	4.370	4.378	0.1220	1140.7	4.335

Table 56—Cl⁻ content test results for Granada Bridge; sample CD1

Date Tested: January 12, 2014

Test Performed By: Jason Burchfield

Unit Weight: 3800 lb/yd³   LIMS #: _____   Lab #: 2014-12-015

Description			Results (lb/yd³)				Average	
			A	B	C	Range	ppm	lb/yd³
Standard Solution	**Date:** 1/12/2015	**Expected Value:** 3.0					3.0	
Sample: CD1, District 5, Volusia County, SR 40 over Halifax River,								
Grenada Bridge # 790132. 2" Core taken from the East Face of Pier 8,								
Debonded Region, Above the High Tide water line; Length: ~4.25".								
A 0-0.5"			0.806	0.806	0.806	0.0000	212.1	0.806
B 0.5-1.0"			0.692	0.684	0.684	0.0080	180.7	0.687
C 1.0-1.5"			0.452	0.441	0.441	0.0110	117.0	0.445
D 1.5-2.0"			0.437	0.445	0.433	0.0120	115.4	0.438
E 2.0-2.5"			0.342	0.331	0.361	0.0300	90.7	0.345
F 2.5-3.0"			0.289	0.274	0.277	0.0150	73.7	0.280
G 3.0-3.5"			0.236	0.243	0.247	0.0110	63.7	0.242
H 3.5-4.0"			0.171	0.190	0.179	0.0190	47.4	0.180
I 4.0-4.25"			0.190	0.182	0.194	0.0120	49.6	0.189

Table 57—Cl⁻ content test results for Granada Bridge; sample CD2

Date Tested: December 30, 2014

Test Performed By: Jason Burchfield

Unit Weight: 3800 lb/yd³   LIMS #: _____   Lab #: 2014-12-016

Description			Results (lb/yd³)				Average	
			A	B	C	Range	ppm	lb/yd³
Standard Solution	**Date:** 12/30/2014	**Expected Value:** 3.0					3.0	
Sample: CD2, District 5, Volusia County, SR 40 over Halifax River,								
Grenada Bridge # 790132. 2" Core taken from the East Face of Pier 8,								
Debonded Region, Below the High Tide water line; Length: ~4.0".								
A 0-0.5"			6.228	6.160	6.563	0.4030	1662.4	6.317
B 0.5-1.0"			7.129	7.098	7.129	0.0310	1873.3	7.119
C 1.0-1.5"			7.167	7.171	7.159	0.0120	1885.7	7.166
D 1.5-2.0"			7.311	7.159	7.076	0.2350	1890.0	7.182
E 2.0-2.5"			5.639	5.647	5.681	0.0420	1488.3	5.656
F 2.5-3.0"			5.955	5.947	6.061	0.1140	1575.7	5.988
G 3.0-3.5"			5.396	5.320	5.400	0.0800	1413.7	5.372
H 3.5-4.0"			5.495	5.723	5.449	0.2740	1462.0	5.556

Table 58—Cl⁻ content test results for Granada Bridge; sample C7-1

Date Tested: January 5, 2014

Test Performed By: Jason Burchfield

Unit Weight: 3800 lb/yd³   LIMS #: _____   Lab #: 2014-12-017

Description			Results (lb/yd³)				Average	
			A	B	C	Range	ppm	lb/yd³
Standard Solution	**Date:** 1/5/2015	**Expected Value:** 3.0					3.0	
Sample: C7-1, District 5, Volusia County, SR 40 over Halifax River,								
Grenada Bridge # 790132. 2" Core taken from the West Face of Pier 7,								
Middle Foundation, Above the High Tide water line; Length: ~5.75".								
Core to be Sliced in 1/2" increments the entire length of core								
A 0-0.5"			10.461	10.503	10.515	0.0540	2761.3	10.493
B 0.5-1.0"			7.015	7.178	7.148	0.1630	1872.0	7.114
C 1.0-1.5"			5.236	5.301	5.244	0.0650	1384.3	5.260
D 1.5-2.0"			2.010	2.041	2.029	0.0310	533.3	2.027
E 2.0-2.5"			1.250	1.239	1.246	0.0110	327.6	1.245
F 2.5-3.0"			0.783	0.771	0.787	0.0160	205.4	0.780
G 3.0-3.5"			0.331	0.312	0.331	0.0190	85.4	0.325
H 3.5-4.0"			0.186	0.190	0.179	0.0110	48.7	0.185
I 4.0-4.5"			0.171	0.148	0.160	0.0230	42.0	0.160
J 4.5-5.0"			0.179	0.171	0.171	0.0080	45.7	0.174
K 5.0-5.5"			0.171	0.163	0.160	0.0110	43.3	0.165
L 5.5-5.75"			0.274	0.266	0.274	0.0080	71.4	0.271

Table 59—Cl⁻ content test results for Granada Bridge; sample C7-2

Date Tested: December 24, 2014

Test Performed By: Jason Burchfield

Unit Weight: 3800 lb/yd³   LIMS #: _____   Lab #: 2014-12-018

Description		Results (lb/yd³)				Average	
		A	**B**	**C**	**Range**	**ppm**	**lb/yd³**
Standard Solution | **Date:** 12/24/2014 | **Expected Value:** 3.0						3.0	
Sample: C7-2, District 5, Volusia County, SR 40 over Halifax River,							
Grenada Bridge # 790132. 2" Core taken from the West Face of Pier 7,							
Middle Foundation, Below the High Tide water line; Length: ~5.50".							
Core to be Sliced in 1/2" increments the entire length of core							
A 0-0.5"		31.981	31.947	31.973	0.0340	8412.4	31.967
B 0.5-1.0"		17.279	17.225	17.237	0.0540	4538.7	17.247
C 1.0-1.5"		15.865	15.546	15.595	0.3190	4123.3	15.669
D 1.5-2.0"		11.575	11.377	11.408	0.1980	3014.0	11.453
E 2.0-2.5"		7.220	7.068	7.049	0.1710	1871.7	7.112
F 2.5-3.0"		9.722	6.737	6.802	2.9850	2040.4	7.754
G 3.0-3.5"		3.724	3.333	3.504	0.3910	926.4	3.520
H 3.5-4.0"		2.447	2.352	2.246	0.2010	618.0	2.348
I 4.0-4.5"		0.977	1.474	1.170	0.4970	317.6	1.207
J 4.5-5.0"		0.999	1.007	0.996	0.0110	263.3	1.001
K 5.0-5.5"		1.011	1.018	1.011	0.0070	266.7	1.013

Table 60—Cl⁻ content test results for Granada Bridge; sample C9-1

Date Tested: January 15, 2014

Test Performed By: Jason Burchfield

Unit Weight: 3800 lb/yd³   LIMS #: _____   Lab #: 2014-12-019

Description			Results (lb/yd³)				Average	
			A	B	C	Range	ppm	lb/yd³
Standard Solution	**Date:** 1/15/2014	**Expected Value:** 3.0					3.0	
Sample: C9-1, District 5, Volusia County, SR 40 over Halifax River,								
Grenada Bridge # 790132. 2" Core taken from the West Face of Pier 9,								
Above the High Tide water line, Recently removed FRP wrap; Length:								
~4.0". Core to be Sliced in 1/2" increments the entire length of core								
A 0-0.5"			3.082	2.561	2.968	0.5210	755.4	2.870
B 0.5-1.0"			0.376	0.391	0.399	0.0230	102.3	0.389
C 1.0-1.5"			0.289	0.304	0.274	0.0300	76.1	0.289
D 1.5-2.0"			0.262	0.296	0.289	0.0340	74.3	0.282
E 2.0-2.5"			0.281	0.258	0.270	0.0230	71.0	0.270
F 2.5-3.0"			0.315	0.285	0.304	0.0300	79.3	0.301
G 3.0-3.5"			0.274	0.262	0.274	0.0120	71.1	0.270
H 3.5-4.0"			0.312	0.334	0.350	0.0380	87.4	0.332

Table 61—Cl⁻ content test results for Granada Bridge; sample C9-2

Date Tested: December 22, 2014

Test Performed By: Jason Burchfield

Unit Weight: 3800 lb/yd³   LIMS #:   Lab #: 2014-12-020

Description		Results (lb/yd³)				Average	
		A	B	C	Range	ppm	lb/yd³
Standard Solution	**Date:** 12/17/2014 **Expected Value:** 3.0					3.0	
Sample: C9-2, District 5, Volusia County, SR 40 over Halifax River,							
Grenada Bridge # 790132. 2" Core taken from the West Face of Pier 9,							
Below the High Tide water line, Recently removed FRP wrap; Length:							
~6.0". Core to be Sliced in 1/2" increments the entire length of core							
A 0-0.5"		5.198	5.487	5.217	0.2890	1394.9	5.301
B 0.5-1.0"		0.555	0.559	0.562	0.0070	147.0	0.559
C 1.0-1.5"		0.323	0.323	0.312	0.0110	84.0	0.319
D 1.5-2.0"		0.308	0.327	0.308	0.0190	82.7	0.314
E 2.0-2.5"		0.338	0.346	0.365	0.0270	92.0	0.350
F 2.5-3.0"		0.239	0.274	0.312	0.0730	72.4	0.275
G 3.0-3.5"		0.300	0.315	0.308	0.0150	81.0	0.308
H 3.5-4.0"		0.315	0.308	0.308	0.0070	81.7	0.310
I 4.0-4.5"		0.289	0.289	0.319	0.0300	78.7	0.299
J 4.5-5.0"		0.315	0.327	0.346	0.0310	86.7	0.329
K 5.0-5.5"		0.285	0.293	0.285	0.0080	75.7	0.288
L 5.5-6.0"		0.315	0.308	0.331	0.0230	83.7	0.318

Appendix C—Additional Information

C.1 Questionnaire

The purpose of the survey is to create a database of FRP repaired bridges. Collected information may be used to conduct quality control measurements to assess the current state of the FRP repairs. The survey targets FDOT officials and engineers across the state of Florida.

Initial Survey

1. First name: _____
2. Last name: _____
3. FDOT district: _____
4. Position: _____
5. E-mail address: _____
6. Phone number: _____
7. Are you aware of any fiber-reinforced polymer composite repairs that have been used on a bridge or bridges in your district?
   a) None.
   b) I am aware of _____ repairs.
8. If you answered "None" to the previous question, is there anyone in your office who might know?_____

Follow-up survey.

1. Location of the bridge:_____
2. Bridge number:_____
3. Current traffic volume of the bridge:_____
4. What was the increase in traffic volume over the past 10 years?

   _____

5. What was the increase in traffic volume over the past 20 years?

   _____

6. What was/were the date/s of repair/s?

   _____

7. Does inspection report prior to repair exist?

a) Yes.

b) No.

c) I am not sure.

8. Who was the design engineer on the project (name and contact information)?

_____

9. Was the design of FRP repair properly documented?

a) Yes.

b) No.

c) I am not sure.

10. Was the actual repair documented?

a) Yes.

b) No.

c) I am not sure.

11. How was the quality control performed after the repair (check all that apply)?

a) Pull-off testing.

b) Coin tap.

c) Other, please specify:_____

d) Quality control was not performed.

12. What was the condition of concrete substrate prior to repair?

a) Poor (severely cracked, spalled, or both).

b) Moderate (moderate amount of cracks, some spalling, or both)

c) Good (hairline cracks or no cracking at all, no spalling)

13. Was new concrete used as substrate for FRP?

a) Yes.

b) No.

14. How was the substrate prepared?

a) Sandblasting.

b) Other, please specify:_____

15. Which type of FRP reinforcement was used?

a) Wet layup CFRP.

b) Wet layup GFRP.

     c) Near surface mounted CFRP.

     d) Near surface mounted GFRP.

     e) CFRP procured laminate.

     f) Other, please specify:_____

16. What FRP material was used (manufacturer and product name, or material properties)?

_____

17. Was primer used?

     a) Yes.

     b) No.

     c) I am not sure.

18. Was paste epoxy used to level the substrate prior to applying the FRP?

     a) Yes.

     b) No.

     c) I am not sure.

19. Were overlap shear splices utilized in the repair?

     a) Yes.

     b) No.

     c) I am not sure.

20. If you answered "Yes" to the previous question, what was the primary motivation for incorporating the overlap shear splice? In other words, why not use a single saturated sheet that spans the entire length of the repair region?

_____

21. Were any evaluations of applied FRP reinforcement conducted after the repair?

     a) Yes.

     b) No.

     c) I am not sure.

22. Are there any bridge inspection reports post repair available?

     a) Yes.

     b) No.

     c) I am not sure.

C.2 CFRP Samples – Tab Installation

A copper circuit board was used as grips on both sides of the CFRP samples to avoid damaging the FRP during testing and as a relatively flat surface. The circuit board was cut into a dimension of 1 in. × 2 in., and sanded with 80-grit sandpaper on both sides for a rough finish to better adhere to the samples and to the serrated grips used in testing. BASF Concresive 2200 was used as the epoxy to adhere the grips to the samples. The CFRP was also lightly sanded for better adherence between the grips and samples. The area of the CFRP samples that was to be adhered to the grips (1 in. × 2 in. on both sides) were sanded with 240-grit sandpaper for five strokes in the same orientation as the fibers that were completely in tension.

C.3 Chloride Penetration Profile Test Results – University Blvd Bridge

Table 62—Cl⁻ content test results for University Blvd Bridge; Beam 3-1 sample CS1

Date Tested: May 9, 2016

Test Performed By: Elizabeth Weber

Unit Weight: 3800 lb/yd³   **LIMS #:** N/A   **Lab #:** 2016-04-024

Description	Results (lb/yd³)				Average	
	A	B	C	Range	ppm	lb/yd³
Sample: Beam 3-1 CS1, UF Research Project Cores. 2" core taken from						
Beam 3-1, CS1. Core Length: 5.5". Core to be sliced at steel depth and						
tested between 1.5" - 2.0", 2.0" - 2.5" and 2.5" - 3.0".						
1.5-2.0"	13.467	13.156	13.235	0.3110	3496.3	13.286
2.0-2.5" (steel depth)	6.452	6.707	6.737	0.2850	1745.3	6.632
2.5-3.0"	11.320	11.313	11.176	0.1440	2965.7	11.270

Table 63—Cl⁻ content test results for University Blvd Bridge; Beam 3-1 sample CSE1

Date Tested: May 9, 2016

Test Performed By: Elizabeth Weber

Unit Weight: 3800 lb/yd³   **LIMS #:** N/A   **Lab #:** 2016-04-025

Description	Results (lb/yd³)				Average	
	A	B	C	Range	ppm	lb/yd³
Sample: Beam 3-1 CSE1, UF Research Project Cores. 2" core taken from						
Beam 3-1, CSE1 with Wrap. Core Length: 5.0". Core to be sliced at steel						
depth and tested between 1.5" - 2.0", 2.0" - 2.5" and 2.5" - 2.0".						
1.5-2.0"	4.104	4.484	4.108	0.3800	1113.7	4.232
2.0-2.5" (steel depth)	2.991	2.991	2.991	0.0000	787.1	2.991
2.5-3.0"	3.477	3.450	3.298	0.1790	896.9	3.408

Table 64—Cl⁻ content test results for University Blvd Bridge; Beam 3-1 sample CSW1

Date Tested: May 9, 2016

Test Performed By: Elizabeth Weber

Unit Weight: 3800 lb/yd³   **LIMS #:** N/A   **Lab #:** 2016-04-026

Description	Results (lb/yd³)				Average	
	A	B	C	Range	ppm	lb/yd³
Sample: Beam 3-1 CSW1, UF Research Project Cores. 2" core taken from						
Beam 3-1, CSW1. Core Length: 4.5". Core to be sliced at steel depth and						
tested between 2.0" - 2.5".						
	4.378	4.408	4.359	0.0490	1153.1	4.382

Table 65—Cl⁻ content test results for University Blvd Bridge; Beam 3-1 sample CSW2

Date Tested: May 9, 2016

Test Performed By: Elizabeth Weber

Unit Weight: 3800 lb/yd³   **LIMS #:** N/A   **Lab #:** 2016-04-027

Description	Results (lb/yd³)				Average	
	A	B	C	Range	ppm	lb/yd³
Sample: Beam 3-1 CSW2, UF Research Project Cores. 2" core taken from						
Beam 3-1, CSW2. Core Length: 6.5". Core to be sliced at steel depth and						
tested between 2.0" - 2.5".						
	14.201	14.052	13.771	0.4300	3686.3	14.008

Table 66—Cl⁻ content test results for University Blvd Bridge; Beam 3-2 sample CSE1

Date Tested: April 25, 2016

Test Performed By: Elizabeth Weber

Unit Weight: 3800 lb/yd³   LIMS #: N/A   Lab #: 2016-04-019

Description	Results (lb/yd³)				Average	
	A	B	C	Range	ppm	lb/yd³
Sample: Beam 3-2, UF Research Project Cores. 2" core taken from Beam						
3-2, CSE1 with Wrap. Core Length: 6.5". Core to be sliced in 1/2"						
increments the entire length. Slices A-M.						
A 0-0.5"	0.787	0.893	0.855	0.1060	222.4	0.845
B 0.5-1.0"	0.794	0.779	0.779	0.0150	206.3	0.784
C 1.0-1.5"	0.490	0.483	0.460	0.0300	125.7	0.478
D 1.5-2.0"	0.331	0.342	0.357	0.0260	90.4	0.343
E 2.0-2.5"	0.125	0.133	0.122	0.0110	33.3	0.127
F 2.5-3.0"	0.118	0.125	0.118	0.0070	31.7	0.120
G 3.0-3.5"	0.144	0.156	0.129	0.0270	37.6	0.143
H 3.5-4.0"	0.095	0.095	0.106	0.0110	26.0	0.099
I 4.0-4.5"	0.091	0.084	0.076	0.0150	22.0	0.084
J 4.5-5.0"	0.118	0.110	0.137	0.0270	32.0	0.122
K 5.0-5.5"	0.106	0.106	0.106	0.0000	27.9	0.106
L 5.5-6.0"	0.118	0.125	0.137	0.0190	33.3	0.127
M 6.0-6.5"	0.144	0.144	0.179	0.0350	41.0	0.156

Table 67—Cl⁻ content test results for University Blvd Bridge; Beam 3-4 sample CSE1

Date Tested: April 27, 2016

Test Performed By: Elizabeth Weber

Unit Weight: 3800 lb/yd³   **LIMS #:** N/A   **Lab #:** 2016-04-020

Description	Results (lb/yd³)				Average	
	A	B	C	Range	ppm	lb/yd³
Sample: Beam 3-4, UF Research Project Cores. 2" core taken from Beam						
3-4, CSE1. Core Length: 6.5". Core to be sliced in 1/2" increments the						
entire length. Slices A-M.						
A 0-0.5"	0.540	0.543	0.547	0.0070	143.0	0.543
B 0.5-1.0"	0.612	0.623	0.623	0.0110	163.0	0.619
C 1.0-1.5"	0.479	0.475	0.479	0.0040	125.7	0.478
D 1.5-2.0"	0.350	0.361	0.350	0.0110	93.1	0.354
E 2.0-2.5"	0.247	0.239	0.258	0.0190	65.3	0.248
F 2.5-3.0"	0.243	0.236	0.255	0.0190	64.4	0.245
G 3.0-3.5"	0.091	0.087	0.106	0.0190	24.9	0.095
H 3.5-4.0"	0.163	0.163	0.160	0.0030	42.6	0.162
I 4.0-4.5"	0.137	0.118	0.118	0.0190	32.7	0.124
J 4.5-5.0"	0.148	0.133	0.125	0.0230	35.6	0.135
K 5.0-5.5"	0.118	0.118	0.114	0.0040	30.7	0.117
L 5.5-6.0"	0.122	0.095	0.099	0.0270	27.7	0.105
M 6.0-6.5"	0.160	0.152	0.141	0.0190	39.7	0.151

Table 68—Cl⁻ content test results for University Blvd Bridge; Beam 4-1 sample CSE1 (Core 1)

Date Tested: May 9, 2016

Test Performed By: Elizabeth Weber

Unit Weight: 3800 lb/yd³   **LIMS #:** N/A   **Lab #:** 2016-04-028

Description	Results (lb/yd³)				Average	
	A	B	C	Range	ppm	lb/yd³
Sample: Beam 4-1 Core 1, UF Research Project Cores. 2" core taken from						
Beam 4-1, CSE1 with Wrap, Core 1. Core Length: 3.0". Core to be sliced						
at steel depth and tested between 2.0" - 2.5".						
	0.277	0.236	0.236	0.0410	65.7	0.250

Table 69—Cl⁻ content test results for University Blvd Bridge; Beam 4-1 sample CSE1 (Core 2)

Date Tested: May 9, 2016

Test Performed By: Elizabeth Weber

Unit Weight: 3800 lb/yd³   LIMS #: N/A   Lab #: 2016-04-029

Description	Results (lb/yd³)				Average	
	A	B	C	Range	ppm	lb/yd³
Sample: Beam 4-1 Core 2, UF Research Project Cores. 2" core taken from						
Beam 4-1, CSE1 with Wrap, Core 2. Core Length: 6.5". Core to be sliced						
at steel depth and tested between 2.0" - 2.5".						
	0.217	0.213	0.209	0.0080	56.1	0.213

Table 70—Cl⁻ content test results for University Blvd Bridge; Beam 4-2 sample CSE1

Date Tested: May 3, 2016

Test Performed By: Elizabeth Weber

Unit Weight: 3800 lb/yd^3 **LIMS #:** N/A **Lab #:** 2016-04-021

Description	Results (lb/yd^3)				Average	
	A	B	C	Range	ppm	lb/yd^3
Sample: Beam 4-2 CSE1 with Wrap, UF Research Project Cores. 2" core						
taken from Beam 4-2, CSE1 with Wrap. Core Length: 6.5". Core to be						
sliced in 1/2" increments the entire length. Slices A-M.						
A 0-0.5"	0.559	0.578	0.612	0.0530	153.4	0.583
B 0.5-1.0"	1.167	1.167	1.159	0.0080	306.4	1.164
C 1.0-1.5"	1.060	1.064	1.091	0.0310	282.0	1.072
D 1.5-2.0"	0.961	0.965	0.980	0.0190	254.9	0.969
E 2.0-2.5"	0.581	0.585	0.619	0.0380	156.6	0.595
F 2.5-3.0"	0.437	0.426	0.433	0.0110	113.7	0.432
G 3.0-3.5"	0.304	0.300	0.300	0.0040	79.3	0.301
H 3.5-4.0"	0.258	0.258	0.262	0.0040	68.2	0.259
I 4.0-4.5"	0.182	0.179	0.175	0.0070	47.0	0.179
J 4.5-5.0"	0.152	0.156	0.160	0.0080	41.1	0.156
K 5.0-5.5"	0.122	0.125	0.125	0.0030	32.6	0.124
L 5.5-6.0"	0.148	0.141	0.163	0.0220	39.6	0.151
M 6.0-6.5"	0.236	0.236	0.228	0.0080	61.4	0.233

Table 71—Cl⁻ content test results for University Blvd Bridge; Beam 3-2 sample CSE1 (Core 1)

Date Tested: May 9, 2016

Test Performed By: Elizabeth Weber

Unit Weight: 3800 lb/yd³   LIMS #: N/A   Lab #: 2016-04-030

Description	Results (lb/yd³)				Average	
	A	B	C	Range	ppm	lb/yd³
Sample: Beam 4-3 Core 1, UF Research Project Cores. 2" core taken from						
Beam 4-3, CSE1 with Wrap, Core 1. Core Length: 4.0". Core to be sliced						
at steel depth and tested between 2.0" - 2.5".						
	1.672	1.672	1.672	0.0000	440.0	1.672

Table 72—Cl⁻ content test results for University Blvd Bridge; Beam 4-3 sample CSE1 (Core 2)

Date Tested: May 9, 2016

Test Performed By: Elizabeth Weber

Unit Weight: 3800 lb/yd^3 **LIMS #:** N/A   **Lab #:** 2016-04-031

Description	Results (lb/yd^3)				Average	
	A	B	C	Range	ppm	lb/yd^3
Sample: Beam 4-3 Core 2, UF Research Project Cores. 2" core taken from						
Beam 4-3, CSE1 with Wrap, Core 2. Core Length: 4.0". Core to be sliced						
at steel depth and tested between 1.5" - 2.0", 2.0" - 2.5" and 2.5" - 3.0".						
1.5-2.0"	2.105	1.744	1.645	0.4600	481.9	1.831
2.0-2.5" (steel depth)	1.683	1.683	1.702	0.0190	444.6	1.689
2.5-3.0"	1.303	1.281	1.170	0.1330	329.3	1.251

Table 73—Cl⁻ content test results for University Blvd Bridge; Beam 4-4 sample CSE1

Date Tested: May 4, 2016

Test Performed By: Elizabeth Weber

Unit Weight: 3800 lb/yd³   **LIMS #:** N/A   **Lab #:** 2016-04-022

Description	Results (lb/yd³)				Average	
	A	B	C	Range	ppm	lb/yd³
Sample: Beam 4-4, UF Research Project Cores. 2" core taken from Beam						
4-4, CSE1. Core Length: 6.5". Core to be sliced in 1/2" increments the						
entire length. Slices A-M.						
A 0-0.5"	1.311	1.303	1.303	0.0080	343.6	1.306
B 0.5-1.0"	0.775	0.775	0.756	0.0190	202.3	0.769
C 1.0-1.5"	0.562	0.555	0.562	0.0070	147.3	0.560
D 1.5-2.0"	0.289	0.281	0.274	0.0150	74.0	0.281
E 2.0-2.5"	0.118	0.118	0.118	0.0000	31.1	0.118
F 2.5-3.0"	0.114	0.106	0.122	0.0160	30.0	0.114
G 3.0-3.5"	0.087	0.091	0.103	0.0160	24.6	0.094
H 3.5-4.0"	0.125	0.118	0.133	0.0150	33.0	0.125
I 4.0-4.5"	0.099	0.114	0.080	0.0340	25.7	0.098
J 4.5-5.0"	0.141	0.137	0.129	0.0120	35.7	0.136
K 5.0-5.5"	0.141	0.137	0.144	0.0070	37.0	0.141
L 5.5-6.0"	0.125	0.122	0.122	0.0030	32.4	0.123
M 6.0-6.5"	0.160	0.144	0.141	0.0190	39.0	0.148

Table 74—Cl⁻ content test results for University Blvd Bridge; Beam 5-1 sample CSE1

Date Tested: May 5, 2016

Test Performed By: Elizabeth Weber

Unit Weight: 3800 lb/yd³ **LIMS #:** N/A **Lab #:** 2016-04-023

Description	Results (lb/yd³)				Average	
	A	B	C	Range	ppm	lb/yd³
Sample: Beam 5-1, UF Research Project Cores. 2" core taken from Beam						
5-1, CSE1. Core Length: 6.0". Core to be sliced in 1/2" increments the						
entire length. Slices A-L.						
A 0-0.5"	1.900	1.908	1.900	0.0080	500.7	1.903
B 0.5-1.0"	0.312	0.319	0.331	0.0190	84.4	0.321
C 1.0-1.5"	0.194	0.179	0.186	0.0150	49.0	0.186
D 1.5-2.0"	0.114	0.118	0.122	0.0080	31.1	0.118
E 2.0-2.5"	0.103	0.110	0.106	0.0070	28.0	0.106
F 2.5-3.0"	0.179	0.171	0.167	0.0120	45.4	0.172
G 3.0-3.5"	0.129	0.144	0.152	0.0230	37.3	0.142
H 3.5-4.0"	0.171	0.167	0.163	0.0080	43.9	0.167
I 4.0-4.5"	0.076	0.072	0.084	0.0120	20.4	0.077
J 4.5-5.0"	0.087	0.087	0.091	0.0040	23.2	0.088
K 5.0-5.5"	0.118	0.091	0.118	0.0270	28.7	0.109
L 5.5-6.0"	0.129	0.133	0.137	0.0080	35.0	0.133

Table 75—Cl⁻ content test results for University Blvd Bridge; Beam 5-2 sample CSE1

Date Tested: May 9, 2016

Test Performed By: Elizabeth Weber

Unit Weight: 3800 lb/yd³ **LIMS #:** N/A **Lab #:** 2016-04-032

Description	Results (lb/yd³)				Average	
	A	B	C	Range	ppm	lb/yd³
Sample: Beam 5-2, UF Research Project Cores. 2" core taken from Beam						
5-2, CSE1. Core Length: 7.0". Core to be sliced at steel depth and tested						
between 2.0" - 2.5".						
	0.342	0.338	0.334	0.0080	88.9	0.338